Pollution aerosol across Northern Europe: Assessing properties, processes and effects on regional climate

A thesis submitted to the University of Manchester for the degree of Doctor of Philosophy in the Faculty of Engineering and Physical Sciences

2010

WILLIAM T. MORGAN

SCHOOL OF EARTH, ATMOSPHERIC AND ENVIRONMENTAL SCIENCES

Contents

Word count: 51,519

Abstract

Atmospheric aerosols are the major component in the shorter-term variability governing the radiative balance of the climate system, particularly on regional scales. However, knowledge of the myriad of properties and processes associated with aerosols is often limited, which results in major uncertainties when assessing their climate effects. One such aspect is the chemical make-up of the atmospheric aerosol burden.

Airborne measurements of aerosol properties across Northern Europe are presented here in order to facilitate constraint of the properties, processes and effects of aerosols in this highly populated and industrialised region. An Aerodyne Aerosol Mass Spectrometer (AMS) delivered highly time-resolved measurements of aerosol chemical components, which included organic matter, sulphate, nitrate and ammonium.

The chemical composition of the aerosol burden was strongly determined by the dominant meteorological conditions in Northern Europe. Pollution loadings in North-Western Europe were strongly enhanced when air masses originated from Continental Europe. Conversely, much cleaner conditions were associated with air masses from the Atlantic Ocean.

Organic matter was found to be ubiquitous across Northern Europe and predominantly secondary in nature, which is consistent with other analyses in polluted regions of the Northern Hemisphere. Furthermore, its concentration was generally comparable to, or exceeded that of, sulphate. Significant chemical processing of the organic aerosol component was observed. Highly oxidised secondary organic aerosol dominated, as the distance from source and photochemical processing increased.

Ammonium nitrate was found to be a major component of the aerosol burden in Northern Europe, with peak contributions occurring in North-Western Europe, due to the co-location of its emission precursors (NH_3 and NO_x) in the region. Ammonium nitrate was found to be the dominant sub-micron chemical constituent during periods associated with enhanced pollution episodes. Its concentration was shown to be modulated by the thermodynamic structure of the lower troposphere, with enhanced concentrations prevalent at the top of the boundary layer. This phenomenon greatly enhanced the radiative impact of the aerosol burden; the increased mass and water uptake by the aerosol significantly amplified the aerosol optical depth in the region.

The results presented in this thesis highlight a highly dynamic region, where major changes in emissions have played a significant role in determining the chemical composition of the aerosol burden. As substantial reductions in sulphur dioxide emissions have occurred over the past two decades in Northern Europe, the relative contribution of sulphate aerosols to the regional aerosol burden has decreased. Consequently, it is more pertinent to consider the roles of organic matter and ammonium nitrate, as their influence becomes more pronounced than sulphate on regional and global climate.

No portion of the work referred to in this thesis has been submitted in support of an application for another degree or qualification of this or any other university or other institute of learning.

Copyright

Acknowledgements

I am eternally grateful to my fiancée Ayşe, without whom this thesis would not have been possible. Her patience, support, belief and encouragement have been crucial throughout. I would also like to thank my family for their help and support.

Many thanks go to my supervisor Hugh Coe for his encouragement, enthusiasm and humour, which has been evident since the first email I sent regarding a potential PhD in Manchester. Huge thanks to my co-supervisor James for being the font of AMS and Igor knowledge, as well as being a lot of fun to work with. Many people have been involved in the serious work of fieldwork and data analysis but Jonny, Gavin, Paul and Keith deserve lots of thanks for making it a lot of fun along the way.

I was supported by a Natural Environment Research Council (NERC) studentship NER/S/A/2006/14040 and a CASE sponsorship from Aerodyne Research Inc. The fieldwork was funded by NERC ADIENT project NE/E011101/1 and EUCAARI project 036833-2.

Chapter 1

Introduction

1.1 Motivation & Scope

The complexity surrounding anthropogenic perturbation of global climate is vast and far-reaching. The many inter-related processes and mechanisms at work make quantification of both past and future changes extremely challenging. The huge range of spatial scales involved, which encompasses the microscopic world through to changes in solar output is one of the most challenging aspects. Detailed knowledge of the processes involved at all of these scales is paramount if we are to accurately judge the impact of close to two centuries of fossil fuel dependence. The question of scale is particularly relevant at present as a result of the advent of sophisticated numerical models capable of resolving atmospheric processes at the regional level. Such techniques are capable of representing atmospheric phenomena on the scale of cities through to individual countries, which is the scale of key relevance to both legislators and the general public. Consequently, accurate knowledge of atmospheric processes that govern the radiative balance of the climate system at the regional scale is required. While rising levels of greenhouse gases dominate changes on the long-term global scale, the atmospheric aerosol burden is the major component in shorter-term variability on regional scales. Thus accurate representation of the processes governing the life cycle of atmospheric aerosol and its impact upon the climate system at this scale is required.

The impact of atmospheric aerosols on the Earth's climate, specifically its radiative effect, has historically received much interest. This is a result of the evidence that human activity has increased the atmospheric aerosol concentration (Haywood and Boucher, 2000). Furthermore, changes in land use and climate may also have altered the natural aerosol fraction (e.g. Denman et al., 2007). Such activity is of particular interest when attempting to unravel the complex issue of anthropogenic-induced climate change. Greenhouse gases act to warm the climate system via the retention of longwave radiation by the atmospheric greenhouse effect. Human activity has also led

to a substantial increase in their concentrations (e.g. Penner et al., 2001; Forster et al., 2007). As a result, it is 'extremely likely' that humans have exerted a substantial warming influence on the Earth's climate since the pre-industrial era (Forster et al., 2007). Aerosols are of particular interest as they act in opposition to this warming influence via a myriad of processes.

Atmospheric aerosols exhibit a highly heterogeneous distribution both temporally and spatially on a global scale due to their relatively short lifetime when compared to greenhouse gases. Consequently, their impacts are often most keenly felt on regional scales. On such scales, aerosols are capable of reducing the radiative impact of greenhouse gases due to their respective cooling and warming effects (Forster et al., 2007). Essentially, anthropogenic activities have increased the aerosol burden to such an extent that the flux of shortwave radiation reaching the Earth's surface is reduced over extensive areas of the globe. One such region is Northern Europe where the aerosol chemical composition is known to be extremely complex (Putaud et al., 2004). Furthermore, the radiative effect of aerosols in this region is uncertain (Myhre et al., 2009). The measurements presented here provide vital elucidation of the complex processes governing the aerosol chemical composition, which plays a direct role in the regional radiative impact of the European aerosol burden. Aerosol chemical composition measurements using the Aerodyne Aerosol Mass Spectrometer (AMS, Jayne et al., 2000; Canagaratna et al., 2007) in combination with other measurements of aerosol properties will form the major part of this work. Such measurements will concentrate upon the spatial distribution and evolution of aerosol chemical composition in Northern Europe and its role in perturbing the so-called direct radiative forcing by aerosols, which will be discussed in the following sections.

1.2 Atmospheric aerosols and climate

1.2.1 Background

Aerosols are defined as the suspension of a solid or liquid particle within a gaseous medium and may be derived from both natural and man-made sources. They may be emitted directly to the atmosphere in particulate form or they may form in the atmosphere itself, via gas-to-particle conversion processes. Aerosols act as an essential ingredient in transitions between the gas and particulate phase in the ambient atmosphere. Furthermore, they are fundamental in the formation of clouds and ultimately precipitation. This is a result of their ability to act as the surface area upon which water is able to transfer from the vapour to liquid phase. Consequently, categorisation of their form and subsequent assessments of their impacts often proves complex. Such impacts include, but are not limited to, adverse effects upon human health (e.g. Dockery et al., 1993), disruption of natural ecosystems (e.g. Andreae and Crutzen, 1997), visibility

levels (e.g. White and Roberts, 1977) and the degradation of buildings (e.g. Grossi and Brimblecombe, 2002). Additionally, aerosols are of intrinsic importance for future climate projections and when assessing historical climate change, especially during the 20th Century (e.g. Charlson et al., 1992; Haywood and Boucher, 2000). Consequently, understanding the processes governing the formation, transformation and deposition of atmospheric aerosols are of fundamental importance. The current discussion will focus upon properties of atmospheric aerosol and their role in perturbing the radiative balance of the climate system, specifically via the scattering and absorption of solar radiation.

Aerosols are known to significantly alter the Earth's climate on regional to global scales (e.g. Charlson et al., 1992; Haywood and Boucher, 2000; Penner et al., 2001; Forster et al., 2007). Aerosols can scatter and absorb solar and longwave radiation, inducing changes in the atmosphere's radiative balance. This perturbation is known as the direct radiative effect of aerosols (Charlson et al., 1992). Aerosols may also perturb the hydrological cycle via the modification of the microphysical properties of clouds. Consequently, the amount, lifetime and radiative properties of clouds may be modified. This is known as the indirect effect of aerosols (e.g. Haywood and Boucher, 2000; Penner et al., 2001; Forster et al., 2007). Absorbing aerosol species, such as Black Carbon (BC), may also exhibit an effect on clouds. A local warming of the atmosphere, induced by absorption of shortwave radiation by aerosols, can result in an alteration of the relative humidity and stability of the atmosphere. Such changes may alter cloud formation processes and lifetimes which is known as the semi-direct effect of aerosols (e.g. Hansen et al., 1997; Ackerman et al., 2000; Cook and Highwood, 2004; Johnson et al., 2004). Aerosols arise from both anthropogenic and biogenic sources, which makes elucidation of their impacts particularly difficult. Furthermore, aerosol emission sources, subsequent processes in the atmosphere and their removal from it, are a function of meteorological parameters such as temperature, wind and moisture content. Consequently, perturbation of such parameters under both past and future climate change scenarios may stimulate potentially significant alterations in aerosol concentrations (e.g. Denman et al., 2007). Additionally, aerosols themselves may perturb meteorological conditions such as circulation patterns (e.g. Denman et al., 2007). Aerosols are thus a considerable component in the issue of anthropogenically-induced climate change.

The effect of aerosol upon the Earth's climate can be represented via several metrics. One such metric is the concept of radiative forcing. This is defined as 'the change in net (down minus up) irradiance (solar plus longwave; in Wm^{-2}) at the tropopause after allowing for stratospheric temperatures to readjust to radiative equilibrium, but with surface and tropospheric temperatures and state held fixed at the unperturbed values' (Ramaswamy et al., 2001). Essentially, the Earth system's energy balance in an unperturbed state is held in an equilibrium between the flux of incoming solar energy

and the outgoing flux of longwave radiation. Changes within the climate system introduce a perturbation to this equilibrium by altering the balance between the incoming and outgoing flux. In terms of the direct effect, aerosols act to reflect incoming solar radiation back to space. This reduces the amount of solar (incoming) radiation incident upon the surface, causing a negative radiative forcing resulting in a cooling of the climate system. This is in contrast to the radiative forcing of greenhouse gases, which act to increase the equilibrium temperature of the Earth via retention of outgoing longwave radiation. The concept of radiative forcing is used as a means of comparing and quantifying the relative impacts of both anthropogenic and natural climate perturbations. Conceptually it is an attractive metric as it can be related to a global mean equilibrium temperature change at the surface, ΔT_s^{eq}, by the following relation:

$$\Delta T_s^{eq} = \lambda \Delta F \tag{1.1}$$

where ΔF is a change in radiative forcing and λ is the climate sensitivity parameter (e.g. Ramaswamy et al., 2001). However, calculation of the climate sensitivity parameter is challenging as a result of the uncertainty surrounding calculation and representation of various climate feedbacks (e.g. Ramaswamy et al., 2001; Forster et al., 2007). The effects of aerosols on the radiative balance of the Earth make up a component of the radiative forcing term in equation 1.1.

Atmospheric aerosols exhibit a highly inhomogeneous distribution on a global scale. Consequently, their impact reflects this distribution. This is particularly evident over industrialized regions of the Northern Hemisphere such as North America, Europe and South-East Asia. Regions in the tropics, for example in Indonesia, South America and Central Africa, where significant seasonal biomass burning occurs, have a similar effect. These spatial patterns are illustrated in Figure 1.1. Thus, the concept of a 'surface forcing' is a particularly useful metric for assessing the impact of aerosols on climate. Surface forcing refers to the 'instantaneous perturbation of the surface radiative balance by a forcing agent' (Forster et al., 2007). Such a perturbation will induce changes in the latent and sensible heat fluxes in addition to changes in solar and longwave irradiance. Consequently, its properties, magnitude and spatial variability will be distinct from those pertaining to radiative forcing (Forster et al., 2007). Forster et al. (2007) concluded that 'wherever aerosol presence is considerable (namely the Northern Hemisphere), the surface forcing is negative, relative to pre-industrial times'.

The spatial distribution and properties of atmospheric aerosols have a major impact upon the climate system. In particular, the life cycle of aerosols is often poorly represented in global and regional aerosol models (Textor et al., 2006). Consequently, accurate knowledge regarding its properties and the spatial distribution of such properties represents a key area of uncertainty regarding the impact of atmospheric aerosols.

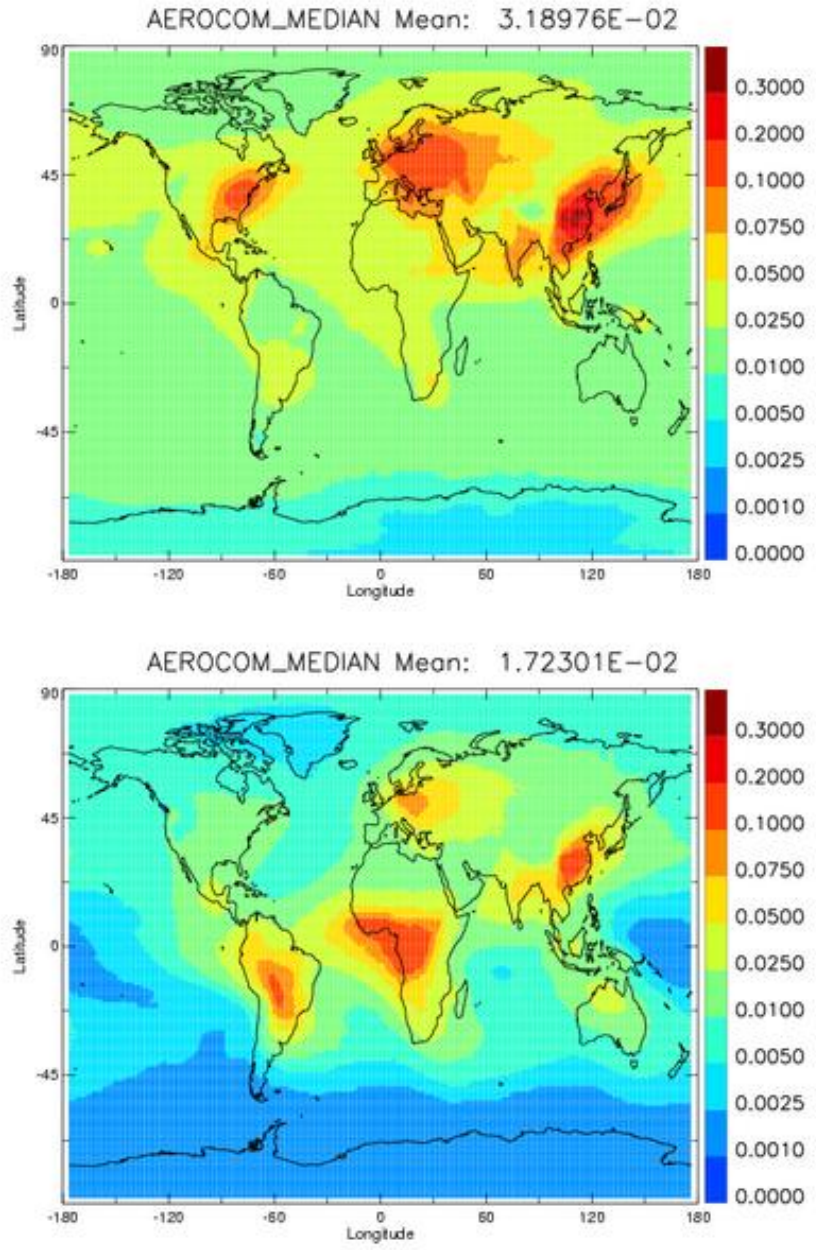

Figure 1.1: Global maps of aerosol optical depth at 550 nm for the year 2000 for sulphate (top) and particulate organic matter (bottom) derived from the AeroCom exercise (Kinne et al., 2006; Textor et al., 2006). The data is the median value across 10 global aerosol models operating in their standard configurations. Images were downloaded from the AEROCOM website (`http://nansen.ipsl.jussieu.fr/AEROCOM/`).

1.2.2 Life cycle and properties of atmospheric aerosol

The myriad of processes that govern the sources, formation pathways and removal mechanisms of atmospheric aerosols lead to substantial complexity when determining their properties. This complexity is particularly important when attempting to ascertain the potential impact of the aerosol burden, particularly on the Earth's climate. Studies of the perturbation of the Earth's radiative balance usually aim to distinguish the anthropogenic impact that is superimposed upon the natural background. Thus the fact that aerosol particles arise both from natural and anthropogenic sources presents a significant challenge. For example, sulphate aerosol may be formed from both natural sources from sea surface emissions of dimethyl sulphide (DMS) or from subsequent oxidation of SO_2 emitted from fossil fuel combustion in power stations. Thus such source profiles need to be constrained in order to establish the anthropogenic contribution. Other examples of natural sources include wind blown mineral dust, sea spray from the ocean's surface and volcanoes. The combustion of fossil fuels, such as in power stations and motorised vehicles, contribute a substantial percentage of anthropogenic emission of aerosols. Agricultural practices, such as biomass burning and the use of fertilisers, can also contribute significantly to the aerosol burden of the atmosphere.

Figure 1.2 comprehensively illustrates the complex task inherent in attempts to constrain the impacts of atmospheric aerosols. As well as being regarded as either of anthropogenic or natural origin, aerosols are also classified according to their method of formation or emission to the atmosphere. Aerosols directly emitted in the particulate phase are known as primary aerosols (e.g. Pandis et al., 1995). Examples of primary particles include wind blown dust, BC and primary organic matter generated during combustion processes. Those formed via gas-to-particle conversion processes within the atmosphere itself are known as secondary aerosols (e.g. Pandis et al., 1995). An example of the formation of secondary aerosol is the formation of Secondary Organic Aerosol (SOA) from condensation of Volatile Organic Compounds (VOCs) which may arise from natural emissions from vegetation or anthropogenic emissions such as combustion. Generally, such transitions occur via gas-phase oxidation causing the formation of low vapour pressure products. The formation of new particles may then occur when the gaseous partial pressure of a compound exceeds its equilibrium pressure above the aerosol surface (e.g. Raes et al., 2000). Low volatility compounds will readily partition to the particle phase. Semi-volatile compounds distribute between the gas and particle phases in order to achieve thermodynamic equilibrium. Similarly to the necessity to separate anthropogenic aerosol from natural sources, it is equally desirable to characterise aerosol sources to primary and secondary sources in order to effectively regulate their emission sources.

Size distributions of aerosols in the atmosphere span several orders of magnitude

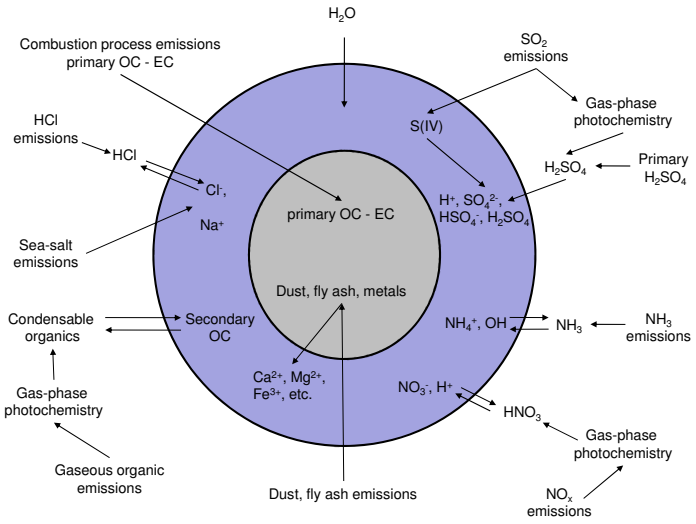

Figure 1.2: Sources of typical aerosol species. The figure is adapted from Pandis et al. (1995). OC refers to Organic Carbon and EC refers to Elemental Carbon.

(e.g. Pandis et al., 1995). An aerosol's size is of major importance when considering its potential impact; categorisation on the basis of size is therefore necessary. Generally, a distinction is made between particles larger than 2.5 μm, so called coarse mode particles and those smaller than 2.5 μm, which are known as fine mode particles.

Coarse mode particles are generally produced mechanically, whilst there are a number of formation pathways for fine mode particles. The coarse mode contains a significant fraction of the total aerosol mass, although particles in this mode are present in very low number concentrations. Furthermore, particles are efficiently removed from this mode via dry deposition due to their high sedimentation velocities (e.g. Pandis et al., 1995).

The fine mode is further sub-divided between the nucleation mode, for particles smaller than 0.01 μm, the Aitken mode, from 0.01 to 0.1 μm, and the accumulation mode, for particles between 0.1 to 2.5 μm. The accumulation mode overlaps both the fine and coarse modes at approximately 1 μm. The nucleation mode comprises freshly produced aerosol formed via the emission of gaseous precursors (Kulmala, 2003; Kulmala et al., 2004). The Aitken mode consists of relatively fresh particles often associated with combustion sources, such as vehicle exhausts, and the coagulation of smaller particles (e.g. Pandis et al., 1995). The Aitken mode dominates the aerosol number distribution; however, the small size of these particles typically results in this mode accounting for a small percentage of the mass concentration in the atmosphere (e.g.

Pandis et al., 1995). The accumulation mode accounts for the majority of the aerosol surface area and makes up a significant proportion of the number distribution (e.g. Pandis et al., 1995). The differing formation and growth processes in the atmosphere lead to preferential accumulation of particles in this mode. Coagulation and condensation processes involving existing particles are the primary sources of particles in this mode. Furthermore, particles in this mode are somewhat insusceptible to dry deposition processes. Consequently, particles in the accumulation mode reside in the atmosphere on significantly longer time scales (e.g. Pandis et al., 1995).

The removal of aerosols from the atmosphere is governed by two processes: dry and wet deposition (e.g. Pandis et al., 1995). The dry process constitutes deposition to the Earth's surface. Wet deposition occurs as a result of the scavenging of aerosol by cloud droplets and subsequent loss via precipitation. Another form of wet deposition is the capture of aerosol by falling precipitation, a process often referred to as "washout". The relatively short residence time of aerosols in the troposphere is a consequence of the efficiency of these processes. The lifetime of tropospheric aerosols ranges from less than a day up to two weeks in the boundary layer, while aerosols in the free troposphere can reside for up to a month (e.g. Pandis et al., 1995; Raes et al., 2000).Coupled with the inhomogeneities in the distribution of aerosol sources, aerosols in the troposphere vary markedly in both composition and concentration (e.g. Pandis et al., 1995). Consequently, the impacts of tropospheric aerosols are usually confined to local to regional scales.

The key parameters for determining the direct radiative effect of aerosols are the optical properties of the aerosol population. The principal optical characteristics are described by the single scattering albedo, the specific extinction coefficient and the scattering phase function (e.g. Haywood and Boucher, 2000). Such optical properties are determined by the physical and chemical characteristics of the aerosol burden. The single scattering albedo represents the absorbing nature of a particle. It is the ratio of the scattering efficiency of a particle to its extinction efficiency, where the latter is defined as the sum of the absorption and scattering efficiencies. The specific extinction coefficient relates how incident light is attenuated by an aerosol population as it interacts with it. As with the extinction efficiency, this may be defined as the combined effect of a scattering and absorption coefficient. The value of the extinction coefficient for an aerosol layer can be coupled with the depth of the layer to prescribe an Aerosol Optical Depth (AOD e.g. Haywood and Boucher, 2000). The scattering phase function relates how light scattered by an aerosol particle has an angular dependency. Particles scatter primarily in the forward direction. However, this asymmetry does not hold for small particles with diameters approximately less than 0.1 μm (e.g. Seinfeld and Pandis, 1998). The scattering phase function can be integrated in order to calculate the asymmetry parameter or the backscatter fraction (e.g. Charlson et al., 1992). Such properties are a function of the particle's size, the refractive index of the particle pop-

ulation and the wavelength of the incident light upon it. The effect of composition is important as different chemical species have different complex refractive indices. The effect of internal mixing of chemical species within an aerosol particle is particularly complicated when assessing the refractive index. Radiative impacts are also dependent upon the solar zenith angle and the nature of the surface underlying the aerosol.

The residence of aerosol species in the accumulation mode is particularly important with regard to its interaction with solar radiation. The mass scattering efficiency of ambient aerosol particles is most efficient between 0.1 and 1.0 μm (Seinfeld and Pandis, 1998). Thus, the accumulation mode covers this more efficient range. Particles residing in the accumulation mode are also adept at taking up water at a given relative humidity. Such hygroscopic aerosol particles can significantly alter the size and chemical composition of the aerosol. Water associated with the aerosol burden can greatly exacerbate the aerosol direct effect, particularly via increasing the AOD. Consequently, precise measurements of the size distributions and chemical composition of ambient aerosol, particularly of the accumulation mode particles, is required in order to assess their climate effect. Coupled with their prolonged residence in the atmosphere compared to particles in smaller or larger size ranges, accumulation mode particles are particularly important in terms of the climatic impact of atmospheric aerosol.

1.2.3 Aerosol chemical composition

The effects of chemical composition on the direct effect are particularly important in terms of attribution of climate change and have direct policy implications. Measurements of the chemical composition of the aerosol population, particularly as a function of size are required in order to constrain the estimates for the radiative impacts of individual species. Furthermore, the effects of mixing state and relative humidity upon aerosol properties is a key aspect relating to aerosol chemical composition. The following discussions will focus upon accumulation mode aerosol and the major inorganic and carbonaceous species present in this size range, namely sulphate, nitrate, organic carbon/matter and BC.

The composition of atmospheric aerosols may be broadly categorised as having an inorganic and an organic fraction. The organic fraction refers to carbon containing compounds. Conversely, the inorganic fraction refers to compounds that do not contain carbon. The variation in aerosol chemical composition is dependent upon a number of factors including location, season and source strength. The processes which govern the formation and transformation of the aerosol species are also of paramount importance. Pandis et al. (1995) state that the aerosol chemical components present in the troposphere includes “sulphate, ammonium, nitrate, sodium, chloride, trace metals, carbonaceous material, crustal elements and water”. BC and organic carbon make up the carbonaceous fraction of the aerosol population.

Sulphate aerosol particles present in the troposphere can exist in a range of particulate forms, including sulphuric acid (H_2SO_4), ammonium bisulphate ($(NH_4)HSO_4$) and ammonium sulphate ($(NH_4)_2HSO_4$). Sulphate aerosol is particularly efficient at acquiring water. This hygroscopic nature determines its ability to grow via condensational processes and also its removal from the atmosphere via its scavenging by cloud droplets. The acidity of sulphate aerosol particles in the atmosphere is governed by the presence of ammonia; ammonia either partly or completely neutralises the H_2SO_4 particles. Sulphate aerosols are formed via a number of processes, including; oxidation of sulphur dioxide (SO_2) via gas phase reactions with the hydroxyl radical, OH, aqueous phase reactions within cloud droplets and via condensational growth onto pre-existing particles. As such, it is present as either a liquid droplet or in a partly crystallised form. Sulphate aerosol sources include sulphur dioxide emissions from fossil fuel burning, volcanoes and biomass burning and DMS from oceanic biogenic sources. Sulphate scatters radiation across the solar spectrum, with some small absorption in the near infra-red spectrum (e.g. Forster et al., 2007).

Ammonium nitrate aerosol is a semi-volatile inorganic salt. Its formation is governed by the relative concentrations of nitric acid, ammonia and sulphate species. When sulphate is fully neutralised and an excess of ammonia is present, ammonium nitrate may form in the particle phase (e.g. Stelson and Seinfeld, 1982a). An alternative route for its formation is the deposition of nitric acid onto coarse mode particles such as sea-salt and alkaline mineral particles, which rather than forming ammonium nitrate, forms sodium nitrate. Nitric acid (HNO_3) is formed during the day when nitrogen oxides are oxidised by OH. Alternatively, it may form in the absence of solar radiation, when the nitrate (NO_3) radical is able to form. The NO_3 radical forms via the oxidation of oxides of nitrogen by ozone. A further reaction with NO_2 forms N_2O_5, which is then able to form nitric acid when water is present. Deposition or condensation of this gas phase nitric acid may then occur, again forming ammonium nitrate in the particle phase. Partitioning between the gas and particle regimes is strongly dependent upon temperature and relative humidity (Stelson and Seinfeld, 1982b; Mozurkewich, 1993). The partitioning is biased towards the particle phase at lower temperatures and high relative humidity. In common with sulphuric acid, nitric acid is highly soluble, resulting in ammonium nitrate aerosols displaying hygroscopic tendencies (Tang, 1996). Ammonium nitrate aerosol is essentially non-absorbing in the visible spectrum whilst exhibiting highly scattering properties across the solar spectrum (Forster et al., 2007).

Carbon-containing compounds are ubiquitous in the atmosphere. A distinction is usually made between organic carbon and BC. An organic carbon aerosol is a complex mixture of chemical compounds composed of carbon-carbon bonds. Sources include both anthropogenic, for example, from fossil fuel and bio-fuel combustion, and natural biogenic emissions. Hundreds of different organic compounds have been detected in the atmosphere (e.g. Hamilton et al., 2004; Murphy, 2005). Compounds may be

emitted in a primary form or in-situ via secondary processes, referred to as Primary Organic Aerosol (POA) and SOA respectively. Its in-situ formation occurs via condensation of semi or low volatility organic gases. Organic carbon aerosols undergo substantial chemical processing subsequent to emission (e.g. Kanakidou et al., 2005; Jimenez et al., 2009). This chemical processing by OH, O_3 and NO_3 results in substantial changes to the particle's chemical makeup. For example, such processing may alter the particle's hygroscopicity (e.g. Jimenez et al., 2009). A considerable fraction of the atmosphere's organic content is known to be soluble to some degree (McFiggans et al., 2005). At low relative humidity, water is often associated with the organic fraction rather than the inorganic fraction. At higher relative humidity, the hygroscopicity of organic compounds is considerably less than sulphate aerosol (Kotchenruther and Hobbs, 1998; Kotchenruther et al., 1999).

BC is a primary aerosol emitted directly to the atmosphere during incomplete combustion processes. BC is strongly absorbing in the solar spectrum (e.g. Forster et al., 2007). It is emitted as a complex chain structure (e.g. Posfai et al., 2003) such as long chain agglomerates. However, these structures tend to collapse as a particle ages (e.g. Abel et al., 2003). BC is assumed to exist entirely in the particle phase due to its non-volatile nature.

One of the many complicating properties of atmospheric aerosols is the distribution of their chemical components, known as the mixing state. An externally mixed aerosol is one where the components are present as pure particles. Nucleation and primary emissions result in the production of externally mixed particles. When the components are mixed within a single particle, the aerosol is said to be internally mixed. Aerosols are subjected to a myriad of processes; the majority of processes compel the aerosol to form an internal mixture. The mixing state of a particle is significant when deducing its potential impact. One example involves the coating of an absorbing aerosol, such as BC, with a relatively non-absorbing aerosol, such as sulphate or organic carbon. Such a mixing state induces an optical lensing effect whereby the absorption of the composite aerosol increases (e.g. Chylek et al., 1995; Jacobson, 2002; Schnaiter et al., 2005; Schuster et al., 2005; Bond and Bergstrom, 2006). Bond et al. (2006) showed that such a coating can theoretically increase absorption by a BC-containing particle by 50-100% for particle core and coating sizes present in the atmosphere. A further example is a coating of organic carbon around a hygroscopic aerosol such as sulphate. This may induce a suppression of the hygroscopic nature of the composite aerosol, resulting in suppressed water uptake by the aerosol (Quinn et al., 2005). Furthermore, a reduction of its probability of activating to form a cloud droplet may also occur (Xiong et al., 1998; Chuang, 2003). Consequently, quantitative understanding of a particle's mixing state is of primary importance.

The effects of composition have a substantial impact upon the resultant climate effects. As detailed in the examples in this section, the composition determines the

absorption or scattering nature of the aerosol population. Furthermore, the interaction of the aerosol population with water vapour has a substantial impact upon its size, removal and ultimately, its ability to form cloud droplets and precipitation. Its ability for water uptake in sub-saturated environments also increases its radiative scattering potential. This property, termed the hygroscopicity, is crucial as it determines effects such as deliquescence, crystallisation and hysterisis. The ambient relative humidity controls these properties, as increases in the relative humidity lead to the deliquescence point of a particle; the point at which a particle is able to take up water. If the ambient relative humidity were to then decrease, a particle may crystallise. However, this process displays a phenomenon known as hysterisis (Seinfeld and Pandis, 1998), thus the crystallisation relative humidity does not match the deliquescence relative humidity. The mixing state of the particles will also modulate these properties. Consequently, the detailed representation of the chemical composition is of central importance when assessing the climate impact of aerosol particles.

1.2.4 Quantifying the aerosol direct effect

Sophisticated methods are required to characterise the radiative forcing of anthropogenic aerosols relative to pre-industrial emissions. In addition, historical anthropogenic radiative forcing estimates are often desired in order to test climate models against past climate change. Thus knowledge of the temporal evolution of aerosol species on decadal to centennial time scales is required. Currently, remote sensing and in-situ measurements cannot provide the required temporal and spatial characteristics across the whole globe either for the present day or for past changes. Consequently, advanced aerosol modules are required in order to estimate the global forcing. Such models use information regarding the atmospheric aerosol life cycle, its optical properties and its spatial and temporal variation to derive an estimate of the radiative perturbation. The results of such models are then constrained by comparison with observations. Forster et al. (2007) reported that more complete aerosol modules are now present in a number of General Circulation Models (GCMs). Some have resolutions exceeding 2° by 2° in the horizontal direction coupled with greater than 30 vertical levels. In terms of representing the microphysical properties of aerosols and how the spatial variability in their concentrations and chemical composition changes, such a resolution is far too coarse. Consequently, many aerosol processes require parameterisation in order to represent them in such models. These are able to provide estimates of the direct radiative forcing from anthropogenic aerosol species, as well as representing natural aerosol species. Such models provide valuable assessments of the climate impact of aerosols and their gaseous precursors (Textor et al., 2006).

The development of long term remote sensing surface measurements provides detailed climatological information regarding aerosol parameters. The AErosol RObotic

NETwork (AERONET, Holben et al., 1998) of sun photometers provides more than 150 operational sites worldwide. The networks principal measurement is that of AOD as a function of wavelength. This has been supplemented recently by the development of algorithms to retrieve sky radiance as a function of scattering angle (Dubovik and King, 2000). Such a measurement allows determination of the size distribution, averaged over the column, and the single scattering albedo. During periods of enhanced aerosol loading (AOD>0.5), the refractive index for a particular wavelength may also be determined. As a result of the long term nature of the measurements, these aerosol properties may be determined on varying time scales, from daily to inter-annual time scales. Aerosol LIDAR (LIght Detection And Ranging) systems have also been established for the European Aerosol Research LIdar NETwork (EARLINET, Matthias et al., 2004), the Micro-Pulse Lidar NETwork (MPLNET, Welton et al., 2001) and the Asian Dust NETwork (ADNET Murayama et al., 2001). Of particular note is the situating of such LIDAR sites with collocated AERONET sites, which provides detailed remote sensing information on the aerosol vertical column.

Satellite-based retrievals of aerosol parameters have undergone extensive development recently. The installation of LIDAR systems on board satellites, such as the Cloud-Aerosol Lidar and Infrared Pathfinder Satellite Observation (CALIPSO), provides the possibility to probe the vertical structure of aerosol particles on previously unobtainable spatial scales. CALIPSO is part of the so-called A-train constellation of satellites, which operate in formation, providing information on several atmospheric variables with high time resolution. Measurements of AOD are also performed by several satellite instruments. These include the Advanced Very High Resolution Radiometer (AVHRR), the MOderate Resolution Imaging Spectrometer (MODIS), the POLarization and Directionality of the Earth's Reflectances (POLDER) and the Multi-angle Imaging Spectro-Radiometer (MISR). However, such measurements are often biased towards retrievals over ocean surfaces due to the complexity of changing surface characteristics over land. Furthermore, clouds are also a significant problem, thus calibration and screening for the effects of clouds is required. Despite such problems, the AOD retrieved from satellites has been shown to agree fairly well with data from AERONET sites (Myhre et al., 2005). However, this study concentrated on comparing satellite derived measurements over ocean with AERONET data on islands or near coastal areas. The MODIS and MISR instruments' performance is generally in better agreement with the AERONET data compared to the other satellite instruments highlighted. These instruments are designed with aerosol retrievals in mind and are able to resolve AOD over land, thus such an agreement is to be expected (Myhre et al., 2005).

Murphy et al. (2009) presented a purely observational-based estimate of the Earth's energy balance in order to potentially constrain the radiative forcing by tropospheric aerosols. This was based upon measured changes in surface temperature, ocean heat content and satellite observations of radiative fluxes since 1950. They estimated a

residual forcing between 1970 and 2000 mainly due to direct and indirect aerosol impacts of -1.1 $\pm$ 0.4 Wm^{-2}, which is consistent with the Inter-governmental Panel on Climate Change (IPCC) estimates given by Forster et al. (2007). A key result of this analysis was that very large negative estimates for the indirect aerosol forcing could be ruled out by such an observationally-based estimate.

While satellites have shown the capability to derive aerosol parameters pertinent to the aerosol direct effect, recent advances have allowed estimates of the radiative effect of both all aerosols and also the anthropogenic component to take place (e.g. Bellouin et al., 2005; Chung et al., 2005; Yu et al., 2006). However, such attempts currently require improvement, especially in constraining the radiative effect over land (Yu et al., 2006). Significant discrepancies also exist between different approaches (Yu et al., 2006). In this regard, satellites and models are similar, as the uncertainties are greater for estimates on a regional basis than on a global basis (Yu et al., 2006). A significant source of uncertainty for the satellite retrievals is the vertical distribution of aerosol properties and the effect of cloudy conditions (Yu et al., 2006). Consequently, observations of such properties are of great importance in attempts to constrain the direct radiative effect of aerosols estimated by satellites.

Separating the anthropogenic component of aerosol forcing from naturally occurring aerosol species presents a particularly significant challenge. SOA for instance can form as a result of the mixing of biogenic VOCs with anthropogenic pollutants. Goldstein et al. (2009) showed that such a process was prevalent in the South-Eastern United States and that it led to significant AOD values to be measured by remote sensing systems onboard satellite platforms. The seasonal AOD cycle in the region was shown to peak in summer during the period of enhanced emissions of biogenic VOCs which accompanies increased temperature. Such a result raises questions for attributing aerosol radiative forcing, which by convention is defined as being anthropogenic in origin. Furthermore, linkages between temperature and aerosol emission sources suggest possible future feedbacks arising due to future climate warming.

In order to successfully represent the global distribution of aerosol radiative impacts and also its temporal evolution since pre-industrial times, sophisticated aerosol modules are required. A particularly important advance is the representation of key anthropogenic and natural aerosol species in models. These include sulphate, BC, organic carbon/matter, nitrate, sea salt and mineral dust. Such species dominate the aerosol burden in the atmosphere on a mass basis. Consequently, explicit representation of these species is beneficial for determining the aerosol direct effect and subsequent policy implications. As a result of the complexity in representing atmospheric aerosols and their impact, numerical models often produce widely varying results. The AeroCom exercise assessed the differences between model outputs from sixteen global aerosol models (Kinne et al., 2006; Schulz et al., 2006; Textor et al., 2006). Textor et al. (2006) focused upon differences in the aerosol life cycles, as such differences will have a large

impact upon the simulated aerosol fields and thus the radiative effect. The study found several areas where there were significant deficiencies when comparing the models. The hygroscopic nature of the aerosol species showed particularly high diversity. Furthermore, the dispersal of aerosols in both the vertical and horizontal directions showed significant differences between the compared models. Such factors would benefit from constraint by observations in order to improve their representation and subsequently enhance estimation of the radiative effects.

The recent IPCC assessment of the scientific basis for climate change included a chapter on the 'Changes in Atmospheric Constituents and in Radiative Forcing' by Forster et al. (2007). This collated past results of both observational and modelling studies relevant to climate change studies in order to assess the current state of knowledge regarding anthropogenic climate change. The best estimate of the aerosol direct radiative forcing from 1750 to 2005 was given as -0.50 Wm^{-2} with an estimated error of $\pm$ 0.40 Wm^{-2}. The level of scientific understanding attributed to the direct effect of aerosols was given as medium-to-low. This reflects the large error associated with the estimate due to the spread of results indicated by both modelling and observational studies. The direct effect of sulphate aerosol was given as -0.40 $\pm$ 0.20 Wm^{-2}, where the magnitude of the forcing remained the same as previous IPCC assessments but the uncertainty was much better constrained. Organic carbon (from fossil fuel aerosols) was given as -0.05 $\pm$ 0.05 Wm^{-2}. This estimate was weaker than previous estimates by the IPCC and the uncertainty was again constrained. The evaluation of the direct effect of BC (from fossil fuel aerosols) was estimated at +0.20 $\pm$ 0.15 Wm^{-2}, which was better constrained than previous assessments. A best estimate was given for anthropogenic mineral dust aerosols of -0.10 $\pm$ 0.20 Wm^{-2}. Forster et al. (2007) also included estimates for nitrate aerosols of -0.10 $\pm$ 0.10 Wm^{-2} and for biomass burning aerosols of +0.03 $\pm$ 0.12 Wm^{-2}. Comparing the total and species/source specific estimates is difficult due to the large uncertainties in all cases coupled with the effects of aerosol mixing state. While progress has certainly been made as regards estimates of the global mean radiative forcing, large uncertainties are still attached to these estimates. Consequently, significant advancements in both measurements and modelling of atmospheric aerosol are required.

Figure 1.3 summarises estimates of the direct radiative forcing by aerosols that were detailed by Forster et al. (2007). These values include estimates based on satellite retrievals and several aerosol models. On average, the satellite derived estimates show stronger negative forcing than the model estimates. A key factor identified regarding the discrepancy was the representation of absorbing aerosol components, particularly in the presence of cloud. As well as the differences between the model and measured radiative forcing, there is also significant divergence between the models themselves. Such a divergence is due to a compendium of uncertainties regarding emission sources, aerosol properties and factors external to the aerosol burden such as surface albedo and

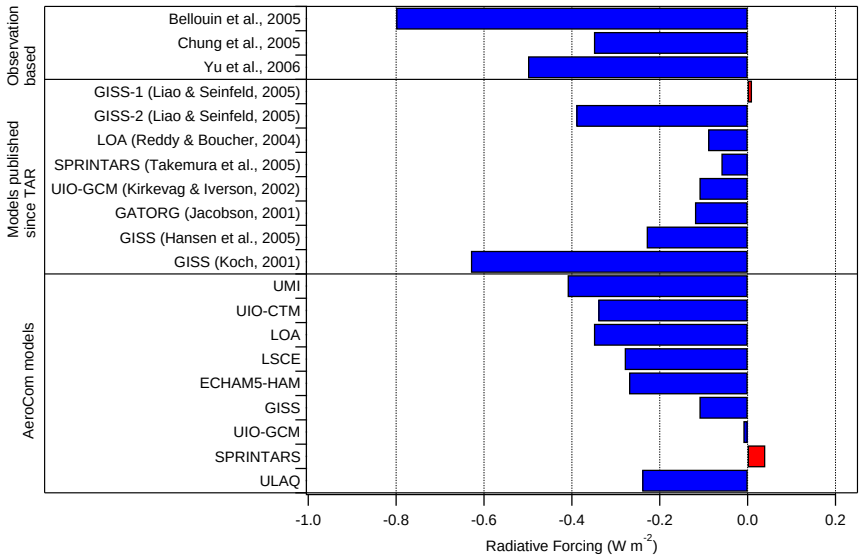

Figure 1.3: Estimates of the direct aerosol radiative forcing taken from Forster et al. (2007). The values are taken from observationally-based studies (Bellouin et al., 2005; Chung et al., 2005; Yu et al., 2006), independent modelling studies (Jacobson, 2001; Koch, 2001; Kirkevag and Iversen, 2002; Reddy and Boucher, 2004; Hansen et al., 2005; Liao and Seinfeld, 2005; Takemura et al., 2005) and AeroCom (Schulz et al., 2006). The AeroCom results are retrieved using identical aerosol and aerosol precursor emissions. The two model results provided by Liao and Seinfeld (2005) refer to different simulations using an internal mixture of aerosol (GISS-1) versus an external mixture (GISS-2). The acronyms for the models are as follows - GISS: Goddard Institute for Space Studies; LOA: Laboratoire d'Optique Atmospherique; SPRINTARS: Spectral Radiation-Transport Model for Aerosol Species; UIO-GCM: University of Oslo GCM; GATORG: Gas, Aerosol, Transport, Radiation, and General circulation model; UMI: University of Michigan; UIO-CTM: University of Oslo CTM; LSCE: Laboratoire des Sciences du Climat et de l'Environnement; ECHAM5-HAM: European Centre Hamburg with Hamburg Aerosol Module; ULAQ: University of L'Aquila.

the general state of the atmosphere. A stark example of the impact of uncertainties regarding representation of aerosol processes is the result from two simulations from the Goddard Institute for Space Studies (GISS) model presented by Liao and Seinfeld (2005). They compared the model using an internal mixture of aerosol and an external mixture, which resulted in a weakly positive and a relatively strong negative radiative forcing respectively. Such an exercise signifies how large uncertainties in aerosol processes can result not only in significant changes in the modelled magnitude of the aerosol radiative forcing but also its sign.

The distribution, makeup and magnitude of aerosol emission sources are a key uncertainty regarding efforts to model the aerosol radiative forcing. An interesting aspect of the AeroCom exercise summarised in the bottom panel of Figure 1.3 is that the included models were run using identical aerosol species (namely sulphate, BC, organic carbon/matter, sea salt and mineral dust) and aerosol precursor emissions. Such a comparison eliminates these key differences and uncertainties that are usually inherent when comparing aerosol models. However, the models still show significant divergence between their global mean radiative forcing estimates. The ensemble average of the model does show encouraging agreement with the observationally-based estimates, with the sign of the forcing reproduced although the magnitude is reduced by approximately a factor of two. A key feature of the AeroCom models was the major diversity in the regional representation of aerosol properties and radiative impact across the models (Kinne et al., 2006; Schulz et al., 2006; Textor et al., 2006). Furthermore, significant discrepancies were found when comparing to regional observations. Schulz et al. (2006) concluded that dedicated studies were required on the regional scale in order to resolve such discrepancies. The key areas highlighted were South-East Asia, African biomass burning areas, the European plume reaching out over the Eurasian continental area and the plume from Eastern North America into the Atlantic.

1.3 Thesis overview

A key theme of the previous discussion is the uncertainty governing representation of aerosol properties and impacts upon the regional scale. This is particularly pertinent as attention upon the regional scale impacts of climate change receives an increasing focus. Consequently, the diverse spatial extent of aerosol species requires characterisation of their microphysical, chemical and optical properties. Areas of uncertainty may be identified and targeted by observations in order to improve their representation in numerical models. Observations also provide important validation products to test the performance of numerical models.

Of particular relevance to this study are the properties of atmospheric aerosol on a range of scales. Aerosol measurements may be made from the microphysical scale, on the order of nanometres, up to regional scales, on the order of hundreds of kilome-

tres. Characterisation of the vertical distribution of aerosol species within the boundary layer and free troposphere require determination; there are significant deficiencies regarding these aspects. This thesis will utilise measurements from onboard the BAe-146 research aircraft, which is operated by the United Kingdom's Natural Environment Research Council (NERC) Facility for Airborne Atmospheric Measurement (FAAM). Measurements will be supported by ground-based measurements where pertinent.

No single study regarding atmospheric aerosol can possibly investigate the multitude of pathways through which it may manifest itself upon the Earth's climate. Consequently, this study will centre upon the assessment of aerosol chemical composition upon a range of spatial scales throughout Northern Europe. Such findings will then be used in tandem with measurements of aerosol optical properties in order to explore their relationship.

The instrumentation, infrastructure and methods employed in this thesis will be explored in the following section. Subsequent to this, a discussion of the evolution of aerosol microphysical and chemical properties in polluted environments, particularly in the Northern (industrialised) Hemisphere will be presented. The impact of such properties and processes relevant to the optical and radiative properties of the aerosol burden will also be highlighted.

Chapter 2

Infrastructure, instrumentation and analysis techniques

The Facility for Airborne Atmospheric Measurement (FAAM) BAe-146 houses a suite of novel aerosol related instrumentation which have been utilised throughout this study. The following chapter will discuss several of the instruments used, with particular emphasis upon the Aerodyne Aerosol Mass Spectrometer (AMS, Jayne et al., 2000; Canagaratna et al., 2007). An AMS has been operated on board the BAe-146 on a number of projects since the aircraft's inception as an atmospheric research aircraft. From July 2004 to August 2007, a quadrupole-based instrument was often part of the instrumentation fit on the aircraft. From November 2007, the mass spectrometer was upgraded to a time-of-flight variant, which greatly enhanced the sensitivity of measurements of the size-resolved chemical composition on the aircraft. Specific details regarding the AMS will be discussed in Section 2.2. Advanced factor analysis techniques regarding AMS organic aerosol data will also be discussed in Section 2.3.

2.1 The Facility for Airborne Atmospheric Measurement (FAAM)

The facility provides a BAe-146 aircraft in order to facilitate atmospheric research led by the UK research community. Significant spatial coverage is possible using the aircraft as it has a typical range of 1800 nautical miles (over 3000 km) and a height ceiling of 35,000 feet (over 10 km). The aircraft has a cruising speed of up to 796 km hr^{-1}, with a science speed of approximately 100 ms^{-1}. The maximum duration of a science flight is approximately five hours. The aircraft can accommodate a scientific payload of 4600 kg, thus it is able to house several alternative configurations of instruments. FAAM therefore provides a multi-functional platform capable of conducting studies

of a range of atmospheric phenomena. Operations are conducted all over the world, although many focus on the UK.

The FAAM BAe-146 research aircraft houses a suite of instruments capable of resolving the chemical composition, microphysical, optical and hygroscopic properties of the in-situ aerosol population. Further remote sensing instruments applicable to aerosol measurements are also included in the scientific payload. The facility also provides aircraft position information and measurements of standard atmospheric variables, such as temperature and relative humidity. Inboard aerosol instrumentation sample via stainless steel tubing from Rosemount inlets (Foltescu et al., 1995). Sub-micron particle losses have been shown to be negligible (Osborne et al., 2007). The following section will summarise some of the instrumentation utilised on the aircraft, with particular focus upon the in-situ aerosol instrumentation.

2.1.1 Aerosol chemical composition

Black Carbon (BC) mass and the number of particles containing a BC core are characterised as a function of particle size using a Droplet Measurement Technologies (DMT) Single Particle Soot Photometer (SP2, Stephens et al., 2003; Baumgardner et al., 2004). The SP2 operated onboard the BAe-146 is modified to include a four-element avalanche photodiode to improve determination of the shape of the scattering pulses of absorbing particles (Gao et al., 2007). The SP2 derives the diameter, mass and incandescence temperature of individual aerosol particles via the principles of light scattering, absorption and emission for particles between 0.15 and 1 μm diameter (Baumgardner et al., 2004). Furthermore, it can provide information on the coating of the single particles of BC, a highly important variable in terms of aerosol-climate investigations.

Bulk samples of aerosol composition are also collected using sub-micron and super-micron filters. These filter samples can be analysed post flight in order to derive additional chemical composition. Determination of the concentrations of refractory aerosol components, such as aluminium, silicon, iron, calcium and sea salt, are particularly desirable as these are not measured by the AMS. These additional measurements related to the composition of the aerosol population are particularly useful as they complement the AMS instrument and provide additional information pertinent to the study of atmospheric aerosol.

2.1.2 Aerosol microphysical properties

A Condensation Particle Counter (CPC) provides total particle counts above a given threshold size. The main principal of operation with such instruments is that particles are grown by passing them through a saturated vapour chamber prior to cooling. The resultant grown particles are consequently large enough to be detected and counted by

a laser beam. Currently, an Aerosol Dynamics Inc. Water-based Condensation Particle Counter (WCPC, Model 3786-LP, Hering et al., 2005) modified for operation at low pressure is used, which as the name suggests, uses water as the vapour in the saturation chamber. Prior to the WCPC model, a TSI 3025A CPC was operated on the aircraft as one of the core instruments since the facility's inception. The vapour used by the 3025A CPC was butanol. Both instruments had a low size cut-off of approximately 3 nm.

Number size distributions are measured via a wing-mounted Particle Measurement Systems (PMS) Passive Cavity Aerosol Spectrometer Probe 100X (PCASP, Liu et al., 1992; Strapp et al., 1992) and an inboard Scanning Mobility Particle Sizer (SMPS, Wang and Flagan, 1990). The SMPS provides size distributions between 10-350 nm. The SMPS sizes particles according to their electrical mobility, while continually ramping the classifying voltage of a Differential Mobility Analyser (DMA). Particles within the mobility range of the applied voltage are separated from the main flow and transported to a detector. Particles in each mobility bin are then counted using an identical WCPC model to the core FAAM instrument. The PCASP instrument uses the principle of light scattering intensity to measure the size of a particle and segregates these into one of fifteen size bins, which span the diameter range of 0.1-3 μm diameter. Particle size is determined via experimental calibrations using Di-Ethyl-Hexyl-Sebacate (DEHS), which is converted to a Polystyrene Latex Sphere (PSL) equivalent size. Via combination of the SMPS and PCASP measurements, size distributions from 10-3000 nm may be determined yielding significant information on the sub-Aitken and accumulation mode aerosol.

A DMT Cloud Condensation Nuclei (CCN) counter (Roberts and Nenes, 2005) has recently been added to the aircraft payload. The instrument comprises two constant flow longitudinal thermal gradient columns, which operate at a controlled supersaturated humidity in the range 0.07-2%. Particles which 'activate' at the given supersaturation are then detected by an optical particle counter, thus the number concentration of CCN is determined. The two columns allow two different super-saturations to be studied in parallel.

2.1.3 Aerosol optical properties

The Radiance Research Particle Soot Absorption Photometer (PSAP) measures the absorption intensity at 567 nm via monitoring the rate of decay of light transmission due to accumulation of absorbing particles upon a filter. Several corrections to the PSAP absorption coefficient are required (Bond et al., 1999). These include misinterpretation of scattering as absorption by purely scattering particles and overestimation of the absorption intensity as a result of multiple scattering due to external mixtures of absorbing and scattering particles.

Complementary to the measurement of absorption coefficient by the PSAP is the TSI 3563 Nephelometer (Anderson et al., 1996), which measures the total scattering and hemispheric backscattering coefficients of dry aerosol particles at 450, 550 and 700 nm. The nephelometer system onboard the BAe-146 comprises two separate instruments operating in series (Osborne et al., 2007; Haywood et al., 2008). The first nephelometer measures the sample aerosol in a 'dry' condition. The aerosol sample is then passed through a controlled humidifier, which cycles between a 20-90% Relative Humidity (RH) range prior to being sampled by the second instrument in order to measure the scattering intensity as a function of RH. This allows determination of the hygroscopic scattering enhancement, $f(RH)$. The instrument requires additional corrections as a result of angular truncation of the scattering signal and non-lambertian source errors (Anderson and Ogren, 1998).

On the BAe-146, the inlet system prior to the nephelometer and PSAP is not actively dried; instead the sample is dehydrated as a result of ram heating upon entering the inlet system. Consequently, the relative humidity of the sample is known to vary as a function of the ambient relative humidity. This has implications for the determination of accurate scattering coefficients, which is required for accurate determination of the single scattering albedo and aerosol optical depth. Furthermore, in moist ambient environments, it is necessary to parameterise the relative humidity dependence of scattering intensity in order to accurately determine and represent the ambient scattering intensity. The 'wet' nephelometer provides a means of determining this response based on in-situ measurements.

2.1.4 Trace gas species

Several instruments which resolve the concentration of atmospheric trace species are operated as part of the core instrumentation payload. Measurements of carbon monoxide (CO) are made using an Aero-laser AL5002 fast response CO monitor. The instrument uses laser induced fluorescence to detect CO. Within the planetary boundary layer, the CO concentration is an important tracer for combustion emissions. In the free troposphere, it is an important quantity when studying large-scale pollution transport due to its relatively long lifetime of approximately one month. Ozone (O_3) is detected using a Thermo Electron Corporation (TECO) 49 UV photometric instrument. The concentrations of nitrogen oxides (NO_x), the summation of Nitric Oxide (NO) and Nitrogen Dioxide (NO_2), NO and NO_2 are measured using a TECO 42 chemiluminescence monitor. The production or consumption of ozone in the atmosphere is linked to the oxidation of Volatile Organic Compounds (VOCs) in the presence of NO_x. NO_x is readily associated with anthropogenically influenced air masses.

2.2 The Aerosol Mass Spectrometer (AMS)

The Aerodyne AMS (Jayne et al., 2000; Canagaratna et al., 2007) has demonstrated the capability to quantitatively measure size-resolved chemical composition of particulate matter of widely varying volatility (Jayne et al., 2000; Allan et al., 2003b; Jimenez et al., 2003; Canagaratna et al., 2007). Furthermore, it is capable of providing such quantitative measurements with both high time resolution and in a range of environments (e.g. Canagaratna et al., 2007). Consequently, it is particularly well suited to measurements of climatically important parameters pertaining to the aerosol direct effect. Several iterations have been developed and some of these will be discussed in the following chapter.

The Quadrupole AMS (Q-AMS) introduced by Jayne et al. (2000), was the first iteration of the AMS. It was developed in response to the need to provide instrumentation which was capable of providing "real-time analysis of size resolved aerosol, mass and chemical composition". Detailed descriptions of the instrument appear in the literature (e.g. Jayne et al., 2000; Allan et al., 2003b; Jimenez et al., 2003; Canagaratna et al., 2007). A recent advancement in the development of the AMS has been the utilisation of various time-of-flight mass spectrometers in place of the traditional quadrupole mass spectrometer (Drewnick et al., 2005; DeCarlo et al., 2006; Canagaratna et al., 2007). The aim of such a development has been to further improve the sensitivity and time resolution of the AMS (Drewnick et al., 2005). The first deployment of one of these updated instruments was a version of the AMS which incorporated a compact Tofwerk AG (Thun, Switzerland) orthogonal acceleration reflectron time-of-flight mass spectrometer (Drewnick et al., 2005). This work will refer to this version of the AMS as a compact Time-of-Flight Aerosol Mass Spectrometer (cToF-AMS). A further version has since been deployed, known as a High-Resolution Time-of-Flight Aerosol Mass Spectometer (HR-ToF-AMS, DeCarlo et al., 2006). The following section will discuss the technical aspects of these iterations in more detail as well as their utilisation in the ambient environment and data analysis techniques.

2.2.1 Instrument description and operation

Conceptually, the AMS can be separated into several different sections, the majority of which are common to all of the iterations. A schematic of the Q-AMS is shown in Figure 2.1, where the AMS is separated between the different stages; ‘Particle Beam Generation’, ‘Aerodynamic Sizing’ and ‘Particle Composition’. It is only the last stage where the iterations differ markedly in terms of the mass spectrometer employed. The following section will summarise these different sections and describe the differing mass spectrometry architecture used in each AMS version.

The ‘Particle Beam Generation’ section of the AMS focuses particles into a col-

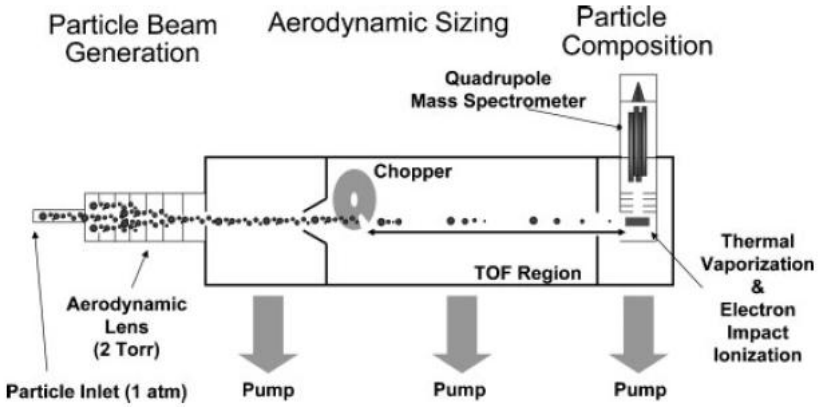

Figure 2.1: Schematic of the Q-AMS from Canagaratna et al. (2007).

limated particle beam prior to entering the detection chamber of the instrument. The particle inlet incorporates a critical orifice, which controls the flow rate into the instrument. A critical orifice of 100 μm or 120 μm is frequently used, which results in an approximate volumetric flow rate of 1.5 cm^3s^{-1} or 2.0 cm^3s^{-1} respectively. The orifice reduces the ambient atmospheric pressure to approximately 267 Pa. An aerodynamic lens system (Liu et al., 1995a,b) is used to collimate the sampled air into a narrow particle beam. The system incorporates a series of five apertures, which become progressively smaller in diameter as the flow travels through the lens. Such a system results in the focusing of the particles into a narrow beam, whilst gas phase products expand subsequent to their passage through each aperture. The AMS is differentially pumped in the vacuum chamber, further increasing the divergence of gas phase molecules upon them exiting the lens system. The overall consequence of this design is the formation of a narrow particle beam, which has undergone enrichment by a factor of approximately 10^7 compared to the gases sampled at the inlet entrance. However, the gas phase still dominates the mass of the beam compared to the mass in the particle regime.

Extensive computational fluid dynamics simulations of the inlet system have shown that the AMS inlet design has 100% transmission efficiency to the detection system for aerodynamic particle diameters between 70 nm and 500 nm (Jayne et al., 2000; Zhang et al., 2002, 2004). Furthermore, there is still significant transmission for particles in the 30-70 nm and 500-2500 nm ranges. Smaller particles (i.e. those smaller than the size cut-off) are lost as a result of them following gas streamlines in the lens system. Particles larger than the upper cut-off are lost due to deposition upon the walls of the apertures. An a priori assumption as regards the transmission efficiency is that particles are spherical or near-spherical. Highly non-spherical particles, including long chain agglomerates such as BC, are known to be inefficiently focused by the lens system

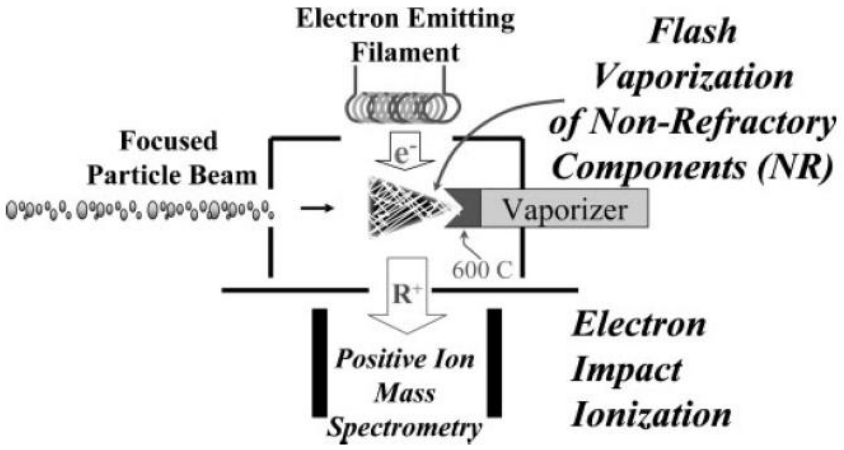

Figure 2.2: Schematic of the AMS detection scheme from Canagaratna et al. (2007).

(Liu et al., 1995b). Consequently, the AMS is ideal for the study of the majority of ambient atmospheric accumulation mode particles, the most important size range in terms of the climate effect of atmospheric aerosol.

The 'Aerodynamic Sizing' section of the AMS utilises measurement of a particle's time of flight in order to measure its size. The particle beam exits the aerodynamic lens system into a vacuum chamber. Consequently, the particle's velocity increases supersonically as a function of its vacuum aerodynamic diameter. Upon measurement of the particle time of flight through the length of the chamber, the particle's velocity and thus its size may be inferred. The mechanical chopper wheel is used to moderate the particle beam via operating it in one of three modes. The chopper has two radial 1-4% slits located 180° apart, which acts to modulate the beam by allowing packets of particles to pass through it to the detection region. This is known as the 'chopped' position. It may also operate in the 'open' position, allowing particles to pass through freely to the detection region, or in the 'closed' position, which completely blocks the beam. The use of the chopper in the 'chopped' position allows the setting of the start of the measurement of the particle's time of flight. The chopper is operated at a user definable rate, usually in the range of 100-150 Hz. Consequently, an average ensemble of the detected aerosol particles may be generated, resulting in the production of mass-size distributions.

In the 'Particle Composition' section of the AMS, shown in Figure 2.2, particles impact upon a resistively heated surface. The surface is usually operated at a temperature of 550-600°C. Upon impact, the non-refractory component of the particle beam is flash vaporised. The resultant gas is then ionized via electron impact ionisation by impacting the gas phase molecules with 70 eV electrons emitted by a Tungsten filament. Electric fields are then employed to transfer the ionized gas to the mass spectrometer.

By separating the vaporisation and ionisation steps of the detection scheme, the AMS is capable of delivering quantitative information on the chemical composition of the entrained sample. The thermal flash vaporisation stage results in minor chemical fragmentation prior to the ionisation stage. Consequently, volatile and semi-volatile chemical species are detected efficiently, including sulphate, ammonium, nitrate and organic matter. However, low volatility solid particulate matter is not desorbed upon contact with the heated surface. Species such as sea salt, metal oxides, desert dust and BC are consequently not measured by the AMS under normal operating conditions. The AMS, therefore, measures only the Non Refractory (NR) component of the sample. The NR component is operationally defined as species that rapidly vaporise (on the order of 100 μs) at the operating temperature of the AMS. Thus, the AMS measures the total NR aerosol mass loading. The ionisation method used by the AMS produces some fragmentation of the molecules sampled. However, the key advantage of this system is that known chemical products exhibit a reproducible response when subjected to electron impact ionisation. Consequently, such a response may be related to the molecular structure of the sampled molecule (McLafferty and Turecek, 1993).

The AMS typically has two modes of operation; Mass Spectrum (MS) mode and Particle Time-of-Flight (PToF) mode. The MS mode operates by alternating the chopper between the open and blocked positions. By operating the chopper in the open position, the entire particle beam, plus any gas phase species present in the system, passes through to the detection region. In order to generate a mass spectrum of the sampled species, the chopper is operated in the blocked position. This allows the detection of the background gas phase in the instrument. A complete mass spectrum of the sampled aerosol species is then derived by taking the difference between the open and blocked mass spectra. The MS mode primary outputs are qualitative information regarding the aerosol ensemble composition and the generation of quantitative chemical mass concentrations from the mass spectrum data.

The PToF mode operates by scanning through the m/z range of the instrument whilst the chopper is set to the chopped position. The passage of the aerosol beam through a chopper slit is recorded and the signal arriving at the detector is measured from this point. The particle time of flight is defined as the time taken for a particle to pass through the chopper slit and its subsequent ion detection by the mass spectrometer. Such signals are averaged over numerous chopper cycles resulting in the generation of size resolved chemical distributions. The AMS is a vacuum-based system, thus the sizing metric derived by the PToF mode is the vacuum aerodynamic diameter (d_{va}, DeCarlo et al., 2004), which is defined as the aerodynamic diameter within the free-molecular regime. Consequently, the AMS is capable of providing mass distributions for a particular chemical species as a function of the species' vacuum aerodynamic diameter.

Quadrupole Aerosol Mass Spectrometer (Q-AMS)

Quadrupole mass spectrometers are capable of scanning only one mass-to-charge ratio (m/z) at any instant. The quadrupole mass spectrometer used by the Q-AMS has a unit mass resolution up to 340 Atomic Mass Units (AMU), with a scan rate of 1 ms amu^{-1}. The selected m/z is then transferred to an electron multiplier. As a result of the relatively low ionisation efficiency of electron impact ionizers, the electron multiplier is crucial as it provides high efficiency amplification (of the order 10^6) of the ion signal. This is required in order for the signals to be detected effectively. The pre-amplifier then converts the flow of electrons into a voltage, whose signals may then be logged by the acquisition software on a local computer. By continually stepping through the mass resolution range of the instrument, a complete mass spectrum of the ensemble aerosol population can be determined in MS mode. In PToF mode, the Q-AMS only filters a few pre defined m/z in order to maximise the signal-to-noise ratio of the measurement. As a result, the sensitivity of such measurements is often limited, especially over short time periods.

As the Q-AMS is capable of scanning only one m/z at a given instant, a complete mass spectrum of an individual particle is impossible. However, quantitative data is generated regarding the entire aerosol ensemble. This has been demonstrated by laboratory studies (e.g. Alfarra, 2004), which have sought to compare chemical mass spectra derived by the AMS with those from the National Institute of Standards and Technology (NIST, Linstrom and Mallard, 2001). Such studies indicate that the AMS and NIST database compare favourably, provided that the parent molecules are resistant to thermal decomposition and fragmentation. However, for certain classes of molecules, such as long chain aliphatic organic molecules, the AMS produces a similar mass spectral fingerprint but with differing intensities to the NIST database. This effect is biased towards smaller ion fragments. This is a consequence of the vaporisation step prior to the electron impact stage in the AMS particle detection region (e.g. Canagaratna et al., 2007). The increased thermal energy obtained by particles in the vaporisation stage results in increased vaporisation. However, such spectral differences do not preclude the AMS from quantifying the total mass of organic species (Canagaratna et al., 2007).

A third mode of operation is used in the Q-AMS in order to improve the detection limits and time resolution of the instrument. This mode is known as Jump Mass Spectrum mode (JMS, Crosier et al., 2007b) and is an amalgamation of MS and PToF modes. It operates by scanning only specified m/z, instead of the whole mass spectrum. The consequence of this change is that a much greater period of time is spent obtaining information on the selected m/z. The same single mass is then scanned in PToF mode, however, only the open and closed positions of the chopper are used. The result of this is that a several fold increase in the Signal-to-Noise Ratio (SNR) of the instrument is achieved (Crosier et al., 2007b). This improvement is especially prevalent for

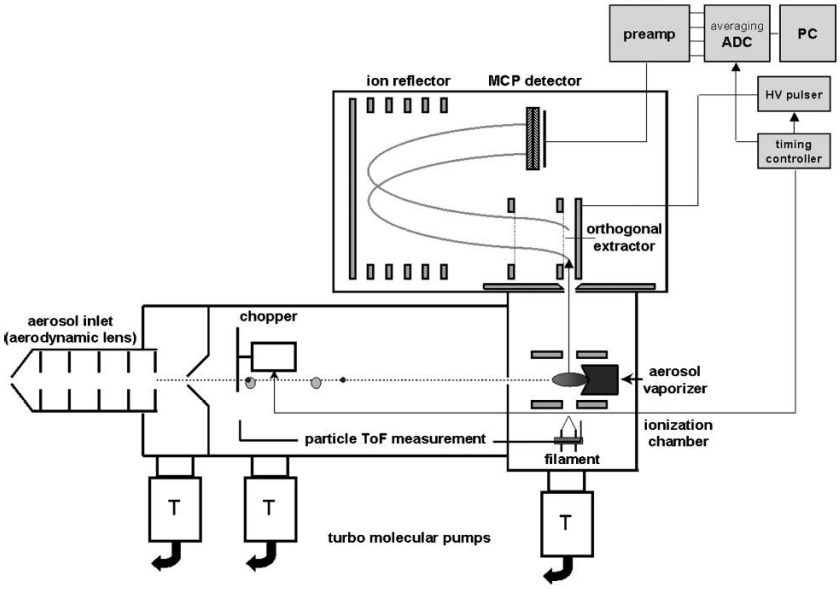

Figure 2.3: Schematic of the cToF-AMS from Drewnick et al. (2005).

inorganic masses. The improvement in the SNR for total organics is less pronounced due to the number of organic fragments present in ambient mass spectra. However, improved SNR is achievable for key organic m/z using JMS mode. The improvement in the SNR is particularly desirable when the instrument is operated in regions with small concentrations of aerosol or over short averaging periods, such as when making airborne measurements.

Compact Time-of-Flight Aerosol Mass Spectrometer (cToF-AMS)

The cToF-AMS system (shown in Figure 2.3) incorporates the standard particle focusing arrangement, particle sizing and separation of the vaporisation and ionisation steps that are utilised by the Q-AMS. The distinction between the instruments is the replacement of the quadrupole mass spectrometer and electron multiplier system with a compact time-of-flight mass spectrometer (Steiner et al., 2001). Subsequent to the vaporisation and ionisation stage, the ions are transferred to an orthogonal time-of-flight extractor via electrostatic lenses. An extraction pulse is applied in order to orthogonally transfer the ions from the extractor to the time-of-flight section. The flight path in this section is 430 mm, which is controlled by a two-stage gridded ion reflector. During the extraction and reflector stages, the ions are accelerated and then collected by the Multi-Channel Plate (MCP) detector. The output signals from the detector are detected by a data acquisition card and stored to a personal computer.

The major distinction between the Q-AMS and cToF-AMS systems is the latter's

ability to scan a complete mass spectrum at each time step during a chopper cycle (Drewnick et al., 2005; Canagaratna et al., 2007). This distinction results in a major improvement in the measurement duty cycle. The cToF-AMS completes a mass spectrum typically every 12 μs during MS mode, whilst the Q-AMS takes 300 ms to scan between m/z 1-300. Thus the cToF-AMS generates approximately 83,300 complete mass spectra every second, compared with roughly 3 generated by the Q-AMS in that time. Consequently, the sensitivity and time resolution of the instrument is improved enormously.

The cToF-AMS is typically operated using the standard MS and PToF modes. The MS and PToF modes of the cToF-AMS are conceptually similar to the equivalent modes for the Q-AMS. However, the amount of data generated by the cToF-AMS massively surpasses that produced by the Q-AMS. Consequently the data acquisition and transfer stages are optimised for the cToF-AMS in order to more efficiently operate the system (Drewnick et al., 2005).

High Resolution Time-of-Flight Aerosol Mass Spectrometer (HR-ToF-AMS)

A HR-ToF-AMS has recently been developed with the aim of further improving the resolution and sensitivity of the AMS systems (DeCarlo et al., 2006). Whilst there has been an impressive improvement in the resolution and sensitivity of the cToF-AMS (compared with the Q-AMS) it is unable to distinguish the elemental composition of ions, which have the same nominal mass. The HR-ToF-AMS is the first real time, field deployable aerosol mass spectrometer, which is able to disseminate individual mass peaks within a single unit m/z (DeCarlo et al., 2006). Consequently, it provides the capability to separate inorganic and organic mass species at the same m/z.

The HR-ToF-AMS uses the same principal modes of operation as the cToF-AMS i.e. MS and PToF. The main distinction between HR-ToF-AMS mass spectrometer and the version used in the cToF-AMS is the ion drift path. The HR-ToF-AMS incorporates a custom-designed Tofwerk AG (H-ToF platform, Thun, Switzerland) high-resolution, orthogonal time-of-flight mass spectrometer (DeCarlo et al., 2006). It is capable of switching between two different reflectron configurations. This configuration changes the effective path length within the mass spectrometer. The mass resolving power of a time-of-flight mass spectrometer increases with increasing effective path length. However, with increased path length, ion lateral broadening effects cause a reduction in detected signal. Consequently, there is a trade-off between the increased resolving power and decreased sensitivity governed by the effective path length of the mass spectrometer.

The two modes of operation of the mass spectrometer for the HR-ToF-AMS are distinguished by their ion trajectory. They are referred to as V-mode and W-mode because of the path of the ions within the mass spectrometer. In V-mode, the ions

follow the standard trajectory from the extraction region into the reflectron and back to the MCP detector. In this mode, the effective ion path length is 1.3 m, which is approximately 3 times longer than in the cToF-AMS. In W-mode, the effective path length is increased to 2.9 m, approximately 6 times longer than in the cToF-AMS. This is accomplished by directing the ions onto an ion mirror within the mass spectrometer, resulting in the ions being focused into the reflectron twice prior to detection by the MCP. Thus the most sensitive configuration for the HR-ToF-AMS is V-mode, whilst W-mode provides data with a higher mass resolution (DeCarlo et al., 2006).

AMS comparisons

The resolving power of the AMS instrument is greatly enhanced with the advent of the HR-ToF-AMS. The increase in resolution from the Q-AMS to the cTOF-AMS and subsequently the HR-ToF-AMS is substantial. The Q-AMS has a very low mass resolution compared to the subsequent versions of the AMS. The cToF-AMS has a resolution of approximately 950, whilst the HR-ToF-AMS provides a resolution of approximately 2100 or 4300 dependent upon the mode of operation (DeCarlo et al., 2006; Canagaratna et al., 2007). The consequence of this increased mass resolving power is that the HR-ToF-AMS when operating in either V-mode or W-mode is able to distinguish separate ions at the same nominal mass (DeCarlo et al., 2006).

The detection limits of the Q-AMS have been reported from several studies by Takegawa et al. (2005), Zhang et al. (2005b) and Salcedo et al. (2006). This was accomplished via sampling ambient air through a filter to remove the particle regime signal. The detection limit ranges reported were 0.02-0.09 $\mu g\,m^{-3}$ for sulphate, 0.01-0.05 $\mu g\,m^{-3}$ for nitrate, 0.11-0.49 $\mu g\,m^{-3}$ for ammonium and 0.15-0.73 $\mu g\,m^{-3}$ for organics. Such studies have displayed the quantitative capability of the Q-AMS in the ambient environment. Drewnick et al. (2009) presented a continuous method to monitor AMS detection limits and found similar detection limit values for the Q-AMS to those reported previously. Furthermore, Drewnick et al. (2009) also calculated detection limits for a cToF-AMS and found that they were reduced by an order of magnitude compared to the Q-AMS. The improvement for organics was particularly profound as cToF-AMS had a detection limit of 0.03 $\mu g\,m^{-3}$ compared with a value of 0.5 $\mu g\,m^{-3}$ for the Q-AMS. DeCarlo et al. (2006) reported detection limits for the HR-ToF-AMS of <0.04 $\mu g\,m^{-3}$ in V-mode and <0.4 $\mu g\,m^{-3}$ in W-mode. This illustrates the major advantage of the upgraded time-of-flight systems compared with the quadrupole system in terms of the sensitivity of the instrument.

The Q-AMS has previously demonstrated its capability to reliably measure ambient aerosol concentrations based on comparisons with collocated instruments (e.g. Drewnick et al., 2003; Hogrefe et al., 2004; Takegawa et al., 2005; Zhang et al., 2005b). These results indicated that the organic and inorganic mass concentrations for ambient

aerosol species from the Q-AMS are comparable to other collocated instruments to approximately 25% (Canagaratna et al., 2007). Comparisons between the cToF-AMS and the Q-AMS have been performed using the University of Manchester's Centre for Atmospheric Science instruments whilst sampling ambient concentrations in Manchester. Allan et al. (2010) included a summary of this comparison and found excellent correlations between the species ($r^2 > 0.94$ for all species). The mass concentrations for the inorganic species agreed to within 5%, while organic concentrations for the cToF-AMS were 13% greater than the Q-AMS. A speculative reason for the poorer agreement between the instruments for organics was the possible differences in lens characteristics of the two instruments. This could lead to an increase in transmission of smaller particles, which would enhance the mass of organics which tended to dominate in the urban location sampled. Furthermore, the cToF-AMS data displayed a 'smoother' version of the Q-AMS data because of the enhanced sensitivity of the instrument. The Q-AMS data displayed significant levels of noise compared with the cToF-AMS when operating downstream of a zero-particle filter in order to test the instrument sensitivity.

Hings et al. (2007) performed a comparison during a field study at the Taunus Observatory on the Kleiner Feldberg, which is a hilltop in Central Germany. When comparing time series of the cToF-AMS and Q-AMS mass concentrations, they too found very good agreement between the instruments. However, there were some noticeable divergences for the organic mass concentrations. This discrepancy was attributed to the differing mass spectrum acquisition processes of the instruments. As previously discussed, the cToF-AMS is able to scan a mass spectrum from m/z 0-300 at each time step whilst the Q-AMS is only capable of scanning one m/z at a time. The discrepancy was thus attributed to the detection of individual or very large organic particles by the cToF-AMS. Analysis of the mass spectra during these instances indicated the presence of pure hydrocarbon-like organic aerosol. Such aerosol components are likely due to a nearby contamination source. This result highlights the fact that the cToF-AMS has a much greater probability of detecting such events than the Q-AMS, especially for organic aerosol components.

Hings et al. (2007) also compared size distributions obtained by the two instruments. The instruments appeared to agree qualitatively during the experiment. However, there were some discrepancies, particularly in the intensity of the sulphate distribution. Furthermore, the cToF-AMS size distributions tended to extend to smaller sizes. Interestingly, it was shown that the organic size distributions derived using the Q-AMS (using only a few m/z values) were comparable to the size distribution derived from the ToF-AMS (using all known organic m/z values). Such a result validates the use of these m/z values to derive size distributions of total organic aerosol species detected by the Q-AMS. The results indicated that the instruments typically agreed within their uncertainties.

2.2.2 Data quantification

A primary aim of the development of the Q-AMS was to provide quantitative species specific information on aerosol particles, particularly in the ambient environment. The techniques and developments regarding this aim have been discussed in Jayne et al. (2000), Jimenez et al. (2003) and Allan et al. (2003b,a). Central to this aim was the development of an AMS analysis suite by James Allan (described in Allan et al., 2003b) using the Igor Pro data analysis software (Wavemetrics, Inc., P.O. Box 2088, Lake Oswego, Oregon 97035, USA).

Mass concentrations derived from AMS data use the detected ion signals from the mass spectrometer. This is achieved using the following formula:

$$C = \frac{MW}{IE.Q.N_A} I \times 10^{12} \tag{2.1}$$

where C is the mass loading in $\mu g\,m^{-3}$ and MW is the relative molecular weight of the parent species in g mol^{-1}. Q is the volumetric flow rate entering the instrument in $cm^3 s^{-1}$ and NA is Avogadro's number, which is equal to 6.022×10^{23} mol^{-1}. IE is the ionisation efficiency of the parent species and I is the detected ion rate in Hertz (Hz). The factor 10^{12} is used to convert from g cm^{-3} to $\mu g\,m^{-3}$. Equation 2.1 is used to calculate the mass concentration at a particular m/z. Consequently, to calculate the mass concentration for a specific species, the summation of the ion signals for each mass fragment is required. Thus equation 2.1 becomes:

$$C_S = \left(\frac{MW_S}{IE_S.Q.N_A} \sum_{alli} I_{S,i} \right) \times 10^{12} \tag{2.2}$$

where the subscript S refers to a particular species and i refers to the mass fragments of species S.

The Ionisation Efficiency (IE) of a particle is a species specific dimensionless quantity. It is defined as the number of ions detected per molecule of the parent species (e.g. Canagaratna et al., 2007). Essentially, it is the probability of a sample particle being ionised, extracted through the mass spectrometer and subsequently being detected. Explicit categorisation of this quantity proves impossible because of the species specific nature of the IE. This is particularly the case for the vast array of organic molecules present in the atmosphere. Consequently, a reference framework is used to derive an appropriate IE, where the ion signals at m/z 30 and 46 are used. These m/z signals correspond to the strongest signal intensity for nitrate aerosol, which volatises efficiently upon contact with the vaporiser. This value is calculated regularly during AMS operation using a well documented experimental methodology (e.g. Jayne et al., 2000; Allan et al., 2003b; Canagaratna et al., 2007). Principally, a dry mono-disperse sample of ammonium nitrate requires generation. This is accomplished by generating an aqueous

ammonium nitrate solution, which is dried prior to size selection by a DMA system. The sample is then introduced to the AMS. The ion signals at m/z 30 and 46 are then counted in PToF mode based on single particle vaporisation events. Via normalising this value to an estimation of the number of ammonium nitrate molecules present in the calibration sample, the ionisation efficiency of nitrate may be calculated. The estimation of the number of ammonium nitrate molecules is accomplished as the size of the calibration particles has been pre-selected using the DMA system (usually 300 nm or 350 nm) whilst the bulk density (1.725 gcm^{-3}) and Jayne shape factor (0.8, Jayne et al., 2000) are known for ammonium nitrate. The ionisation efficiency of nitrate may then be used to deduce the ionisation efficiency of other chemical species based on the assumption that the ionisation cross section of the parent molecules is proportional to the number of molecules present (Jimenez et al., 2003). Furthermore, assuming that the ionisation cross section is proportional to the molecular weight of the species, the following equation may be used to deduce the ionisation efficiency of a particular chemical species:

$$\frac{MW_S}{IE_S} = RIE_S \frac{MW_{NO_3}}{IE_{NO_3}} \tag{2.3}$$

where subscript NO_3 refers to quantities pertaining to nitrate. RIE_S is a species specific constant known as the Relative Ionisation Efficiency (Alfarra et al., 2004). This value is calculated for different chemical species via laboratory experiments or during the routine ionisation efficiency calibration described above. The importance of equation 2.3 is that a generalised method for the calculation of mass loadings may be derived via substitution of equation 2.3 into equation 2.2:

$$C_S = \left(\frac{1}{RIE_S} \frac{MW_{NO_3}}{IE_{NO_3}.Q.N_A} \sum_{alli} I_{S,i} \right) \times 10^{12} \tag{2.4}$$

A major development regarding the analysis of AMS data was the introduction of the concept of 'fragmentation tables' by Allan et al. (2004b). This procedure allows extraction of species specific mass spectra by breaking up the ensemble mass spectra according to the chemical species. This technique is possible as a result of the reproducible dependencies between the relative sizes of the mass spectrum fragments. Such relationships are definable in laboratory conditions resulting in the generation of standard AMS fragmentation tables which can be used with the AMS analysis toolkit software (Allan et al., 2003b). Consequently, this technique has established a more systematic approach for the analysis of ambient data, which is consistent across different AMS users (Allan et al., 2003b). A major enhancement delivered by this approach has been the possibility to probe chemical types such as polycyclic aromatic hydrocarbons, oxygenated and non-oxygenated hydrocarbons (Allan et al., 2004b; Zhang et al., 2005a). Chemical markers from identifiable sources such as combustion have also been identified (e.g. Schneider et al., 2006; Alfarra et al., 2007). These tables are amendable

Table 2.1: Main inorganic and organic ion fragments used to distinguish different aerosol species in AMS spectra. The bold text refers to the most useful fragments when identifying species. The table is adapted from Canagaratna et al. (2007).

Group	Molecule	Ion Fragments	Mass Fragments
Water	H_2O	$\mathbf{H_2O^+}$, HO^+, O^+	**18**, 17, 16
Ammonium	NH_3	${NH_3}^+$, $\mathbf{NH_2}^+$, NH^+	17, **16**, 15
Nitrate	NO_3	${HNO_3}^+$, $\mathbf{NO_2}^+$, $\mathbf{NO}^+$	63, **46**, **30**
Sulphate	H_2SO_4	${H_2SO_4}^+$, ${HSO_3}^+$, ${SO_3}^+$, $\mathbf{SO_2}^+$, $\mathbf{SO}^+$	98, 81, 80, **64**, **48**
Organic (Oxygenated)	$C_nH_mO_y$	H_2O^+, CO^+, $\mathbf{CO_2^+}$, $\mathbf{H_3C_2O}^+$, HCO_2^+, C_nH_m	18, 28, **44**, **43**, 45, ...
Organic (Hydrocarbon)	C_nH_m	${C_nH_m}^+$	27, 29, **41**, **43**, **55**, **57**, 69, 71, ...

and are continually updated based on new laboratory studies emanating from the AMS community (Allan et al., 2004b). A summary from Canagaratna et al. (2007) of the key mass fragments used in the identification of aerosol species is shown in Table 2.1.

The general degradation of the performance of the mass spectrometer with time requires correction in order to perform quantitative measurements (Allan et al., 2003b). This degradation in performance results in the reduction of the signal magnitude detected during ion events. Such degradation will be uniform for all parent species present in the aerosol sample. A correction factor is applied based upon the relative strength of the ion signal at m/z 28 and 32, the mass spectrum peaks for nitrogen and oxygen respectively. These gas phase constituents, referred to as the 'air beam', are assumed to be constant in the ambient environment. Consequently, any reduction in signal strength with time at these two signals is a consequence of instrumental performance. Furthermore, the volumetric flow rate into the instrument is also included in the correction, as this can vary with time; especially when the AMS is located on board an aircraft. Consequently, a time resolved correction factor is applied across all recorded signals.

A further complicating factor regarding quantitative measurement of aerosol mass loadings detected by the AMS is the Collection Efficiency (CE) of the instrument. This quantity is the detected fractional mass compared to the mass which impacts upon the volatising heater (Huffman et al., 2005). It has been shown to be dependent upon the species of the aerosol sample, its mixing state and also the ambient environmental conditions, specifically the relative humidity. Internally mixed aerosol products will be subject to the same CE. Thus in such circumstances, the same CE would be prescribed to aerosol species such as sulphate, nitrate, ammonium and organics (Alfarra et al., 2004). For the opposite case of an external mixture, a species and size specific CE is required (Weimer et al., 2006). Currently, losses due to the CE of the AMS are

prescribed to particle bounce off the vaporiser (Quinn et al., 2006). Laboratory studies have indicated that the phase of a particle is the major controlling factor, which determines the particle bounce off the vaporiser (Matthew et al., 2008). Particles composed primarily of ammonium nitrate or acidic sulphates, existing in a liquid state, were shown to be sampled with a CE close to 100%. Conversely, dry and solid ammonium sulphate particles were sampled with a CE of 24$\pm$3%. Crosier et al. (2007a) developed a linear CE correction based on observed changes in collection efficiency due to changes in ambient nitrate content. The dependence of a particle's CE upon the ambient relative humidity has also been shown (Allan et al., 2004a). This study showed that the mass concentration of sulphate approximately doubled when the inlet temperature approached the dew point temperature i.e. at high relative humidity. Often the CE is either deduced via comparison with collocated instruments (Canagaratna et al., 2007, and references therein) or using the parameterised treatments presented by Crosier et al. (2007a) or Matthew et al. (2008).

2.3 Factor analysis of ambient organic aerosol

Categorisation of ambient aerosol into distinct subsets is a crucial tool for determining their impact, developing efficient control strategies and representation in numerical models (e.g. Lanz et al., 2007; Ulbrich et al., 2009). The AMS aims to resolve the whole organic aerosol component, thus it is a prime candidate for application of deconvolution techniques in order to extract information on the sources of organic aerosol (Zhang et al., 2005a; Ulbrich et al., 2009). Several methods have been applied with this goal in mind. Zhang et al. (2005a) employed a custom Principal Component Analysis (PCA), which successfully distinguished between a Hydrocarbon-like Organic Aerosol (HOA) and an Oxygenated Organic Aerosol (OOA). These components were interpreted as Primary Organic Aerosol (POA) and Secondary Organic Aerosol (SOA) respectively. Subsequently, Zhang et al. (2007) developed a Multiple Component Analysis (MCA) technique which was capable of resolving more than two factors from a vast number of ambient field campaigns in the Northern Hemisphere. Recent efforts have focused upon utilisation of Positive Matrix Factorisation (PMF, Paatero, 1997; Paatero and Tapper, 1994). Several recent publications have detailed its application to AMS data (e.g. Lanz et al., 2007; Ulbrich et al., 2009). A key feature of PMF is that it requires no a priori information in order to derive a solution. Another recent numerical method that has been applied to AMS data is the so-called Multilinear Engine (ME-2, Lanz et al., 2008). This model includes additional flexibility in that a-priori source profiles can be included in order to derive a factor solution. Such a method has been shown to be particularly useful in urban environments, where POA sources are known to be significant (Lanz et al., 2008).

The following section will include additional information regarding the PMF tech-

nique as this is the method employed later in this study. While the other techniques certainly have their merits when combined with AMS data, PMF was deemed the most appropriate means of analysing the airborne data in this study as it provides a more subjective means of exploring the organic aerosol component. This is a result of its constraint of requiring no a priori information regarding organic aerosol composition.

2.3.1 Positive Matrix Factorisation (PMF)

PMF employs a receptor-only factorisation model, which is based on mass conservation. PMF requires no a priori information regarding a factor profile or time trends in order to derive a solution. The model assumes that a dataset matrix is comprised of a linear combination of factors with constant profiles, which have varying contributions across the dataset. The model employs the constraint of positive values upon the profiles and contributions. This results in the derived solution being physically meaningful in the case of AMS data i.e. positive mass components and positive m/z signals.

The PMF model attempts to solve for the number of constant source profiles with a time varying concentration component assuming the following form:

$$X_{ij} = G_{ip}F_{pj} + E_{ij} \tag{2.5}$$

where i and j refer to row and column indices in the matrix respectively and p is the number of factors in the solution. For AMS data, the matrix $\mathbf{X}$ is a $m \times n$ matrix, where m corresponds to the ensemble mass spectra values and n refers to the time series of the data. $\mathbf{G}$ is a $m \times p$ matrix, where p is the factor time series with m representing a measurement point in time. $\mathbf{F}$ is a $p \times n$ matrix, where p corresponds to the average mass spectra model source profiles and n represents an individual point in the profile. $\mathbf{E}$ is a $m \times n$ matrix, which signifies the residual data which the PMF model has not apportioned at each data point i.e. **E=X-GF**. The aim of PMF is to minimise this quantity, thereby explaining a greater fraction of the measured mass.

In order to derive a solution, PMF utilises a least-squares algorithm to iteratively fit values of $\mathbf{G}$ and $\mathbf{F}$ to the data. This is achieved by minimisation of a quality of fit parameter, Q, which is defined by:

$$Q = \sum_{i=1}^{m}\sum_{j=1}^{n}(E_{ij}/\sigma_{ij})^2 \tag{2.6}$$

where σ is the $m \times n$ matrix of estimated errors, in the form of standard deviations, of the points in matrix $\mathbf{X}$. Utilising the data content coupled with the measurement error results in the most optimum use of the information content of the dataset (Paatero and Tapper, 1994).

The most challenging aspect of the analysis is the selection of the appropriate num-

ber of factors. This is a highly subjective aspect of the technique. Previous studies using AMS data (Lanz et al., 2007; Ulbrich et al., 2009; Allan et al., 2010) have employed both mathematical measures internal to the PMF solution and external parameters in order to choose the appropriate number of factors. Internal PMF diagnostics and similarity to reference mass spectra are insufficient to identify factors (Ulbrich et al., 2009). Complementary measurements of properties external to the organic AMS data are required in order to determine the relevant number of factors. These include measurements of inorganic chemical components measured by the AMS, other aerosol components or properties (e.g. BC) and trace gas species.

A potentially complicating issue when selecting an appropriate number of factors is the potential for linear transformations or "rotations" of the solution. Such transformations result in PMF solutions being non-unique, as the factor time series and mass spectra may be combined differently but yield an identical fit to the data. This is a significant complication as an infinite number of "rotations" may exist while still meeting the constraint of non-negativity (Ulbrich et al., 2009). The potential "rotations" for a given number of factors is usually explored by varying a parameter known as FPEAK, which recombines the time series and mass spectra for a given solution. Such rotations often produce a higher value of the Q parameter, indicating a poorer quality of fit. However, such changes can often be quite small (e.g. $<10\%$). Regardless of these difficulties and those mentioned previously, no single metric can determine the "true" factor solution. Consequently, the most justifiable solution is often chosen via a combination of PMF internal diagnostics, such as Q, comparison with reference mass spectra and time series of related tracer species and/or properties.

Chapter 3

Literature review

Constraint of uncertainties regarding aerosol properties is required on a range of spatial scales in differing environments in order to represent anthropogenic climate change and regional air quality. Furthermore, deposition of aerosols can also cause regional eutrophication and acidification. In-situ measurements provide a means of determining the processes governing aerosol formation and their subsequent impacts. Such studies also provide detailed information, which can be used to constrain model and remote sensing methods pertaining to the aerosol direct radiative effect. The following section will present an overview of aerosol chemical composition in polluted regions based upon measurement and modelling studies. More specific details will be discussed regarding regional measurements of aerosol chemical composition and their impact upon the climate system. Such measurement efforts will mainly concentrate upon online, highly time resolved measurement techniques, as these are more comparable with the methods employed in this thesis. Many of these studies employed the Aerodyne Aerosol Mass Spectrometer (AMS), which has been shown in the previous chapter to quantitatively measure the chemical composition of accumulation mode particulate matter. A key feature of the AMS is the ability to measure the total concentration of the organic aerosol component present in atmospheric aerosol, which will be a particular focus of the following discussion.

The following section is split between a general overview of the global aerosol distribution and a review of regional studies from polluted environments in the Northern Hemisphere. Key aspects of these studies will then be discussed, which will form the broad themes of the thesis.

3.1 Overview of global aerosol spatial distribution

The global emission, production and overall mass burden for several aerosol components is summarised in Fig. 3.1 based on estimates from Andreae and Rosenfeld (2008,

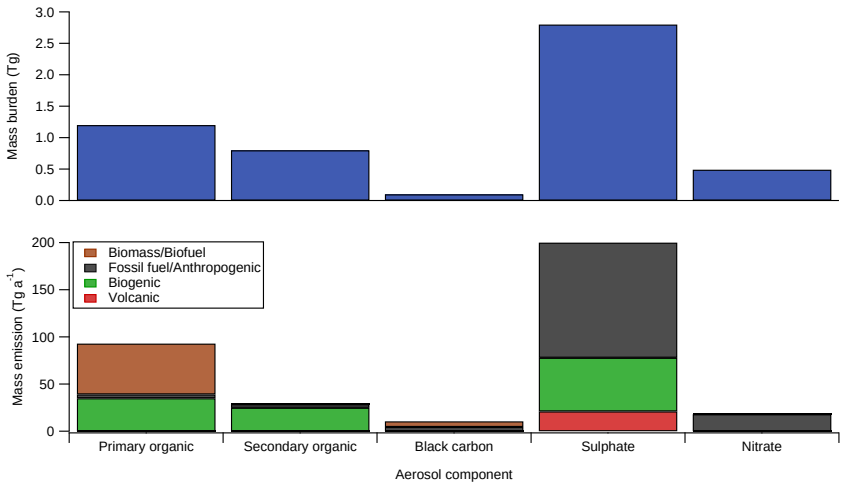

Figure 3.1: Summary of aerosol emission/production and burdens estimated for the year 2000 from Andreae and Rosenfeld (2008, and references therein). The mass emission values (in Tg per annum) represent the "best guess" from Andreae and Rosenfeld (2008) for total particulate matter.

and references therein). The components shown are the major aerosol species that include a significant anthropogenic fraction. Averaged globally, sulphate is the dominant chemical component, followed by organic aerosol. Global mass burdens for sulphate are estimated to be 2.8 Tg, approximately half of which is related to anthropogenic activities. Nitrate concentrations total 0.49 Tg, which represents approximately 35% of the anthropogenic sulphate concentration. Primary Organic Aerosol (POA) concentrations are estimated to be 1.2 Tg, with biomass burning and biogenic emissions being the major sources. The Black Carbon (BC) mass burden is estimated to be 0.1 Tg, with biomass and fossil fuel emissions contributing approximately equal fractions. Secondary Organic Aerosol (SOA) contributes 0.8 Tg and is thought to be dominated by biogenic emissions (approximately 90%). Fossil fuel contributions to POA and SOA range from 3.0-9.0 $\mathrm{Tg\,a^{-1}}$ and 0.05-4.0 $\mathrm{Tg\,a^{-1}}$ respectively.

Global model simulations of the inorganic component of atmospheric aerosols suggest that sulphate, ammonium and nitrate differ in terms of their spatial distribution (e.g. Adams et al., 1999; Metzger et al., 2002; Lauer et al., 2005; Myhre et al., 2006). Sulphate and ammonium are typically evenly distributed when focusing upon the Northern Hemisphere, due to their strong coupling in the form of ammonium sulphate. Nitrate is typically more heterogeneous, with strong gradients exhibited on the regional scale. Consequently, on the global scale, sulphate concentrations exceed those of nitrate. However, in locations associated with significant pollution at the regional scale, nitrate concentrations can be comparable to or greater than sulphate concentrations. Examples of such locations include North America, Western Europe and South-

East Asia. As a result of its semi-volatile nature, ammonium nitrate displays a significant seasonal and daily evolution (Metzger et al., 2002), with peak concentrations occurring when temperatures are decreased i.e. during winter and at night. Sulphate displays a significantly less variable seasonal cycle, although concentrations do tend to peak during summer when photochemical conversion of sulphur dioxide is greatest (Metzger et al., 2002). Consequently, the contribution of nitrate to the aerosol burden relative to sulphate displays a strong temporal and regional variation.

Organic Matter (OM) displays a relatively similar spatial distribution and comparable concentrations to sulphate in the Northern Hemisphere, although significant concentrations exist in the Southern Hemisphere in the major biomass burning regions (e.g. Tsigaridis and Kanakidou, 2003; Lauer et al., 2005; Textor et al., 2006; Hoyle et al., 2007). Two major features highlighted in such global modelling studies are that: (i) SOA is generally dominated by the condensation to the particle phase of biogenic gas phase precursors and (ii) POA is generally greater or equal in terms of absolute concentration than SOA.

Assessment of the validity of point (i) is particularly difficult, as current measurement techniques struggle to unambiguously discern biogenic SOA from anthropogenic SOA. Several previous studies in Europe have indicated that SOA is predominantly derived from biogenic sources, for instance in Zurich (Szidat et al., 2006), rural/remote areas (Gelencsér et al., 2007) and Göteborg (Szidat et al., 2009). A similar picture is presented for the United States by Bench et al. (2007), who demonstrated that modern carbon dominated in rural areas, which suggests a biogenic source. However, measurements in urban plumes and closer to major anthropogenic sources have indicated that anthropogenic Volatile Organic Compounds (VOCs) are the main source of OM (e.g. de Gouw et al., 2005, 2008; Bahreini et al., 2009). Furthermore, the presence of both significant anthropogenic and biogenic sources in close proximity in many areas could mean that SOA can result from a mixture of both. Studies in the South-Eastern United States (Weber et al., 2007; Goldstein et al., 2009) have shown that enhanced biogenic SOA is formed in the presence of anthropogenic pollution. Consequently, discerning a complete representation of the sources of atmospheric SOA is highly challenging.

Point (ii) contrasts markedly with recent measurements which suggest that secondary species are ubiquitous and dominant when considering the OM component in the Northern Hemisphere mid-latitudes, based on source apportionment of AMS data (Zhang et al., 2007). As previously established, such regions are dominated by anthropogenic influences. Zhang et al. (2007) demonstrated that in rural/remote areas, the oxidised component of OM was dominant and secondary in nature. The fractional contribution of POA to the OM burden was found to be negligible in such areas. In urban areas and areas immediately influenced by urban outflow, the contribution of the primary component was enhanced. However, the secondary component was still the dominant contributor in such areas. Furthermore, the concentration of Oxygenated Or-

ganic Aerosol (OOA) was shown to decrease little when comparing urban to downwind locations (Zhang et al., 2007). This was prescribed to the existence of an extended SOA source downwind of the urban conurbations.

3.2 Measurements of aerosol chemical composition

Intensive field studies providing measurements of aerosol parameters are of paramount importance. In-situ measurements provide essential information on aerosol processes, ranging from microphysical effects to bulk column or layer parameters. Such measurements may take place on a range of temporal and spatial scales. In-situ measurements take place on a range of platforms including surface measurements, from ground sites and ships, and airborne measurements, from aircraft and balloons. Intensive field studies often utilise combinations of such in-situ measurements, coupled with remote sensing measurement techniques.

Several overview articles concentrating on relating and comparing results from the vast number of in-situ studies have been presented. Some of these will be discussed in the following section.

Ship-based measurements on the NOAA R/V Ronald H. Brown from several projects (the first and second Aerosol Characterisation Experiments (ACE 1 and ACE 2), an Atlantic cruise (Aerosols99), the Indian Ocean Experiment (INDOEX), the Asian Aerosol Characterisation Experiment (ACE-Asia), the Tropospheric Aerosol Radiative Forcing Observational Experiment (TARFOX) and the New England Air Quality Study (NEAQS)) provided an excellent opportunity to compare results across a range of environments as common sampling techniques were employed for all of the studies (Quinn and Bates, 2005). The sources included sea salt-dominated marine environments, anthropogenic pollution, biomass burning, biogenic, volcanic and desert dust aerosols. Chemical composition was assessed based upon filter samples. Sulphate was found to make up 16-46% of the sub-micron aerosol mass and OM contributed between 1-51%. Consequently, there is substantial variability in the chemical composition of the sub-micron aerosol mass (Quinn and Bates, 2005). Sea salt was ubiquitous across both the sub-micron and super-micron size ranges. Nitrate was found predominantly in the super-micron size range. This was attributed to interaction of gas phase oxidised nitrogen species with sea salt aerosol. The single scattering albedo ranged from 0.89 to 0.99 for continental plumes, with the lowest values coincident with biomass burning plumes from Africa and plumes from the Indian subcontinent. A major identified deficiency was that dust, OM and elemental carbon were poorly characterised. The application of advanced instrumental techniques in order to study these chemical components was identified as a recommendation for future measurements (Quinn and Bates, 2005).

Bates et al. (2006) presented a comprehensive synopsis of the aerosol direct ra-

diative effect based on in-situ measurements, which took place downwind of major urban/population centres. The regions studied were the North-West Atlantic, North-West Pacific and North Indian Oceans. The in-situ measurements were also used to evaluate two chemical transport models. The measurements included mixing state, mass scattering efficiency, single scattering albedo and angular scattering properties. The optical properties were also determined in relation to their dependence upon relative humidity. Direct climate forcing attributed to aerosols was -3.3$\pm$0.47 Wm^{-2} (Northern Indian Ocean), -14.0$\pm$2.6 Wm^{-2} (North-West Pacific) and -6.4$\pm$2.1 Wm^{-2} (North-West Atlantic) with respect to the top of the atmosphere. However, the magnitude of the forcings are overestimates as they do not include representation of clouds in the model domain (Bates et al., 2006).

The dependence of light scattering by aerosols as a function of relative humidity is a key property required to estimate the aerosol direct radiative effect (Quinn et al., 2005; Bates et al., 2006). This relationship is known to be modulated by the chemical composition and size distribution of the aerosol (Bates et al., 2006). Quinn et al. (2005) developed empirical parameterisations based on the ratio of particulate OM to sulphate, based on measurements from ACE-Asia, ICARTT (International Consortium for Atmospheric Research on Transport and Transformation) and INDOEX. The composition measurements were made either from filter samples or an AMS. For each region, increased OM content led to reduced hygroscopicity. Linear fits were derived for each dataset and were found to be consistent within their overall uncertainties. The age of the aerosol was found to be the major determining factor controlling the hygroscopicity, based upon the degree of oxidation of the OM and the acidity of the inorganic component (Quinn et al., 2005). Increased acidity and enhanced OM oxidation coupled with a decreased OM component enhanced the water uptake of the aerosol.

Field studies focused upon the distribution and impacts of anthropogenic aerosols often focus upon the major source regions of North America, Asia and Europe. The following section will present details of previous studies, which have characterised aerosol properties in these regions. Several of the studies have also linked such properties to their resultant impacts.

3.2.1 Studies in North America

Several studies have concentrated upon the spatial distribution of aerosol across North America. Heald et al. (2008) compiled measurements of both gas and particulate Organic Carbon (OC) compounds across North America. Eleven datasets were examined in total, with Total Observed Organic Carbon (TOOC), which is the summation of both gas and particle phase OC, being derived for each study. For eight of the eleven studies, an AMS instrument provided the organic aerosol concentration measurement. Whilst a clear declining trend in absolute concentrations of TOOC was observed with

distance from sources, the trend in the relative TOOC contribution to the particle phase was much less distinct. This was prescribed to the complex balance between aerosol formation and loss. The observed OC aerosol was dominated by SOA from both anthropogenic and biogenic oxidation. Furthermore, particulate OM concentrations often exceeded that of sulphate, making up between 25% and 54% of the total mean aerosol mass. Carbon monoxide was found to be well correlated with both gas-phase and particle-phase OC across all of the studies. The oxygenated component of the particulate OM was found to be well correlated with sulphate. This was most likely attributed to common formation pathways/processes rather than common emission sources.

The first NEAQS field campaign took place across New England and the Middle Atlantic States during the summer of 2002 (Bates et al., 2005; Kleinman et al., 2007). Kleinman et al. (2007) reported results from the operation of an AMS on 17 flights across the region. The study noted that the substantial spatially inhomogeneous distribution of emission sources would provide a particularly demanding application for the AMS. Bates et al. (2005) reported concurrent measurements from the NOAA R/V Ronald H. Brown conducted in the Gulf of Maine. The aircraft AMS results indicated high average aerosol concentrations (11.1 $\mu g\,m^{-3}$) during the study. The OM fraction of this average was found to be 6.5 $\mu g\,m^{-3}$. This fraction was found to vary from more than 70% when aerosol concentrations were low and 40% when high concentration sulphate plumes were detected. The concurrent sampling in the marine boundary layer reported by Bates et al. (2005) indicated high levels of OM consistent with these measurements. The aircraft data indicated that such high concentrations were present over a large geographical area. Comparisons between the OM concentration and trace gas species indicated that OM in the region was primarily a result of secondary formation processes and atmospheric processing. The relationship between light scattering and non-refractory mass detected by the AMS from the ship-based measurements was investigated. Based on Mie calculations, OM was found to account for 60$\pm$6% and 57$\pm$11% of the light scattering (measured at a relative humidity of 55%) during two pollution events (Bates et al., 2005). However, these measurements were performed at relative humidities much lower than the measured ambient relative humidity, thus this does not reflect the water uptake of the aerosol. Bates et al. (2005) speculated that the reduction in sulphate aerosol concentrations across the United States (Malm et al., 2002) could eventually lead to the dominance of OM in many regions of the USA. The study concluded that further elucidation of its impact on both radiative properties and health is required.

The second NEAQS field campaign took place across the north-east coast of North America during the summer of 2004 (Wang et al., 2007). Wang et al. (2007) presented results detailing the dependence of aerosol optical properties upon relative humidity, which were measured on the NOAA R/V Ronald H. Brown during the study. The optical properties studied were the hemispheric backscatter, the single scattering albedo

and the total light scattering coefficient. The hygroscopicity of the aerosol particles was found to be dependent upon the aerosol chemical composition. Particles containing a greater proportion of particulate OM were found to exhibit lower hygroscopic response. Furthermore, less acidic particles were shown to increase the ability of the aerosol to exhibit hysteresis. A sensitivity study of the influence of relative humidity upon the aerosol optical properties and its resultant top of the atmosphere aerosol radiative forcing was carried out. Cooling at the top of the atmosphere was found to increase by 57% as a result of changing the relative humidity from 26% to 82%.

The 2004 ICARTT study included extensive measurements from both ship and airborne platforms, which probed the sources of particulate matter in the North Eastern USA (Quinn et al., 2006; Williams et al., 2007; Brock et al., 2008; de Gouw et al., 2008). The source regions ranged from local emissions from urbanised areas, emissions from the wider-scale local region and more long-range emissions from industrial and North American forest fires. Particulate OM was shown to be predominantly secondary, anthropogenic in origin and photochemically produced within a day subsequent to the emission of VOCs (de Gouw et al., 2008). The composition of industrial or urban plumes was primarily composed of sulphate, ammonium and OM (Brock et al., 2008). The relative fraction of sulphate or OM was modulated by the source history of the plume. For plumes originating from regions dominated more by industrial and power generation facilities, the sub-micron particle mass was larger than those from more urban sources and composed primarily of sulphate and associated ammonium. Furthermore, plumes associated with longer transit histories (3-4 days) were found to be dominated by sulphate due to enhanced oxidation of SO_2 associated with the plumes. This was in agreement with the ship-based measurements presented by Quinn et al. (2006). This contrasts with the relatively short ($<$1 day) time scale for oxidation of gas-phase VOCs to form SOA (Brock et al., 2008). Consequently, in the North-Eastern USA, the potential inorganic particulate mass derived from SO_2 was determined to be greater than the potential OM associated with anthropogenic emissions of CO (Brock et al., 2008).

Williams et al. (2007) presented a novel deployment of a Thermal desorption Aerosol GC/MS-FID (TAG, Williams et al., 2006) alongside an AMS at Cheboque Point, Nova Scotia during ICARTT. This provided high time resolution (1 hour) measurements of organic marker compounds alongside the total OM measurements from the AMS. The organic markers were used to discern several differing aerosol source types, ranging from anthropogenic sources from the United States to both longer range and local biogenic sources from Maine and Canada. The AMS data was then separated into distinct time periods during these source events, revealing that average OM concentrations ranged from 33% of the total aerosol mass during the anthropogenic United States outflow events and 81% during the longer-range biogenic events transported from Maine and Canada. Aside from local sources associated with primary aerosol sources, the OM

was shown to be largely secondary in nature. Such measurements demonstrate both the importance of air mass history upon the aerosol chemical composition and the major role of OM in both anthropogenically perturbed and biogenically perturbed air masses.

Quinn et al. (2006) used the ship-based measurements during ICARTT to determine how sources and processing of ambient aerosol affected its chemical and optical properties. The acidity of the aerosol population was determined based upon calculated equivalence ratios based on ammonium, sulphate and nitrate concentrations determined from AMS measurements. Additionally, the oxygen content of the OM was determined based upon the contribution of signal intensity at m/z 44 to the total OM concentration. The signal at m/z 44 corresponds to the CO_2^+ ion, which arises from decarboxylation on the vaporiser surface of the AMS, and is used as a proxy for the level of oxidation of the OM. Aerosol from local sources was found to be neutralised and composed predominantly of OM (91%), which was relatively unoxidised. Aerosol from long-range sources was acidic and comprised of much less OM (30%) but with a much higher degree of oxidation. These factors were related to the relative humidity dependence of light extinction, a crucial climate property. Aerosol closer to source was characterised by lower hygroscopicity in contrast to the more aged and acidic aerosol. However, sampled forest fire aerosol had a lower hygroscopicity despite its age due to the high mass fraction of OM. This illustrates that OM can diminish the hygroscopic nature of the aerosol population.

The Intercontinental Chemical Transport Experiment-North America (INTEX-NA) experiment was a major NASA science campaign to understand the transport and transformation of gases and aerosols on large spatial scales and their resultant impact (Shinozuka et al., 2007). The experiment took place during the summer of 2004 across North America. Measurements onboard the NASA DC-8 research aircraft were used to quantify the aerosol optical properties (Shinozuka et al., 2007). Vertical profiles of the aerosol optical properties, including measurements of their relative humidity dependence were conducted on the DC-8. These were used to calculate the aerosol optical depth for each profile. The majority of the aerosol optical depth (80%) was concentrated in the bottom 3 km of the atmosphere for 53% of the profiles. This rose to 74% when considering the bottom 5 km. High Aerosol Optical Depth (AOD$>$0.4) was associated with high aerosol loading from the surface layer up to 2.5 km and high ambient relative humidity. The sampled aerosol in the boundary layer primarily originated from urban sources. The dry scattering coefficient per dry PM2.5 mass was 3.6 $\pm$ 1.3 m^2g^{-1}. The ambient scattering coefficient per dry PM2.5 mass was calculated as 5.0 $\pm$ 2.2 m^2g^{-1}. The relationship between AOD and aerosol dry mass was postulated as a means of estimating aerosol mass over regions observed by satellites, which commonly derive the AOD field.

The Megacity Initiative: Local and Global Research Observations (MILAGRO) included measurements of aerosol chemical composition by an AMS on two airborne

platforms (DeCarlo et al., 2008; Kleinman et al., 2008) and several ground-based deployments in and around Mexico City (e.g. Aiken et al., 2009; Baumgardner et al., 2009; de Gouw et al., 2009). MILAGRO was conducted during March 2006 in Mexico City and the surrounding region. Aiken et al. (2009) presented aerosol chemical composition measurements from an AMS from an urban supersite in the heart of Mexico City. OM was found to comprise approximately 50% of the sub-micron particulate mass, with SOA being the dominant OM component (close to 50%). Biomass burning aerosol was also periodically a major component of the sub-micron OM burden. The results highlighted the strong contribution of secondary species even within an area heavily associated with major primary emissions from automobile sources and other primary urban emission sources. de Gouw et al. (2009) reported chemical composition measurements from a sub-urban site near Mexico City. They included a budget analysis of TOOC which indicated that SOA formation displayed a strong diurnal cycle, with peak concentrations/formation in the afternoon, consistent with photochemical processing. Comparisons with US studies indicated that secondary formation of OM was relatively similar to those observed in Mexico City.

Baumgardner et al. (2009) presented measurements from the mountain site of Altzomoni (4010m altitude) located 60 km south-east of Mexico City. Thus the site represented more regional measurements of Mexico City and also the surrounding area. Air masses arriving at the mountain site from the Mexico City area contained a greater proportion of OM compared to aircraft measurements over the city itself. An interesting observation was that relatively similar gas-phase and particulate concentrations were observed for air masses originating from areas not directly associated with Mexico City. This was attributed to either recirculating of Mexico City air masses on the regional scale or smaller scale dynamical features associated with the mountain top location.

DeCarlo et al. (2008) reported the deployment of an AMS onboard the NSF/NCAR C-130 during MILAGRO, while Subramanian et al. (2010) reported the deployment of a Single Particle Soot Photometer (SP2) on the same platform. OM was found to dominate the sub-micron non-refractory particulate mass and was found to primarily originate from pollution and biomass burning sources. The pollution OM component was mainly comprised of SOA. SOA formation from urban sources was found to rapidly overwhelm POA emissions. Furthermore, OM was found to increase with photochemical age. Inorganic sulphate was shown to be relatively regional in its extent, with volcanoes and petrochemical/power plants being the primary sources. Nitrate was found to be a significant component within the urban area and immediate outflow region. Nitrate concentrations were highly correlated with CO, indicating an urban source. Further from the city, its concentration and importance was found to decrease, which was prescribed to evaporation. Significant BC concentrations were observed over the city itself, with concentrations exceeding 2 $\mu g\,m^{-3}$, with older/diluted air masses con-

taining reduced concentrations. More BC containing particles were shown to have a thicker coating of secondary aerosol species downwind of the city, whereas over the city, fresher emissions displayed only thin coatings. This is consistent with internal mixing of the BC containing particles in more-aged air masses downwind of the major emission source of Mexico City.

Kleinman et al. (2008) reported measurements from an AMS on the DOE G-1 aircraft during MILAGRO. The composition results were consistent with those presented by DeCarlo et al. (2008). The ratio of OM to CO was compared to values derived from measurements in the Eastern US. The comparison found that for OM that had undergone approximately 1 day of aging, similar amounts of OM were produced per unit of CO. Consequently, no "megacity" effect was determined, whereby conversion of OM precursors in a region characterised by very large emission rates results in greater yields of OM.

3.2.2 Studies in Asia

INDOEX sought to assess the impact of anthropogenic aerosols on a range of spatial scales, from individual particles through to the regional climate forcing (Ramanathan et al., 2001). The most prominent result was the sheer spatial extent of the anthropogenic influence on a regional scale across the South Asian region and the North Indian Ocean (Lelieveld et al., 2001). Averaged over the North Indian Ocean region during the course of the experiment, the surface forcing was calculated to be strongly negative, with a magnitude of 20 ± 4 Wm^{-2}. Strong heating in the lower troposphere was also diagnosed.

Takami et al. (2005) presented measurements of aerosol chemical composition by an AMS from Fukue island, Japan in the spring of 2003. The site is predominantly representative of regional Asian aerosol as no large industrial areas are present upon the island. OM was shown to be largely secondary in nature and mass concentrations generally exceeded sulphate concentrations. The aerosol chemical concentration was strongly determined by the air mass, with high OM mass fractions associated with Japanese and Korean outflow, whilst sulphate was enhanced during periods associated with outflow from mainland China. Enhanced fine-mode nitrate concentrations were observed in the Chinese outflow periods also. Average total mass concentrations measured by the AMS exceeded 10 $\mu\mathrm{g}\,\mathrm{m}^{-3}$, indicating the level to which major upwind pollution sources can perturb relatively clean, regional locations. Shiraiwa et al. (2008) presented measurements from a follow up study on Fukue island in the spring of 2007, which combined SP2 and AMS measurements in order to investigate the mixing state of BC in Asian outflow. The mixing state and impact of BC was found to vary with meteorological conditions due to differing air mass trajectories. An important observation was that BC containing particles had a non-uniform distribution of coating thickness

i.e. particles in the same air mass ranged from having thin coatings through to thicker coatings associated with sulphate and organic coatings. This is an important observation as numerical models often treat BC as either exclusively externally or internally mixed. Thick coatings upon BC containing particles were shown to enhance aerosol absorption by 50-60% based upon Mie theory calculations, which led to a decrease in the single scattering albedo.

The International Global Atmospheric Chemistry Program (IGAC) conducted the fourth Aerosol Characterisation Experiment (ACE) in South-East Asia. ACE-Asia comprised two focused components (Huebert et al., 2003):

1. An intensive field campaign, which took place from March to May 2001.

2. A longer-term network of ground stations to probe the spatial and temporal, both seasonal and interannual, variability from 2000 to 2003.

These components included quantification of the aerosol chemical, physical and optical properties with the end goal of elucidating their contribution to the radiative impact of aerosols across the region (Huebert et al., 2003). A wide range of aerosol models were used in both the planning stages for observations from mobile platforms and post-experiment, in order to constrain and improve the model representation of aerosol properties (Huebert et al., 2003). The following discussion will present some key results relating the in-situ derived chemical composition to the resultant impact of the aerosol population.

Topping et al. (2004) presented aerosol chemical composition results during ACE-Asia from the island of Jeju, Korea during April 2004. Size-resolved aerosol chemical composition measurements from an AMS indicated little variation over the period and little contribution from sub-100nm particles, indicating that the site was representative of more-aged air masses. Similarly to the studies by Takami et al. (2005) and Shiraiwa et al. (2008), OM and sulphate were found to dominate the accumulation mode aerosol. The relative dominance of these components was strongly dependent upon air mass history, with OM concentrations increasing significantly when the air mass originated from Korea. Furthermore, OM measured at the site was shown to be largely secondary in nature and water-soluble.

Aerosol chemical composition was measured on the Center for Interdisciplinary Remotely Piloted Aircraft Studies (CIRPAS) Twin Otter and C-130 aircraft during ACE-Asia (Bahreini et al., 2003; Heald et al., 2005). The Twin Otter study reported the first deployment of an AMS on an airborne platform (Bahreini et al., 2003). The measurements indicated the impact of different meteorological regimes upon the aerosol composition in the region. Pollution layers originating from Korea were primarily composed of OM. Chinese pollution layers advecting over the region were found to contain a higher sulphate fraction. Background aerosol concentrations during the study were found to be composed of sulphate and ammonium. Such measurements demonstrate

the spatial variability of aerosol composition and its modification by the large scale synoptic situation.

Heald et al. (2005) detailed two independent methods of measuring OC from both aircraft; thermal optical analysis and Fourier transform infrared transmission spectroscopy. The measurements indicated unexpectedly large concentrations in the free troposphere between 2-6.5 km with little vertical variation, with average concentrations of 4 μg sm^{-3}. The measurements were 10-100 times higher than those computed with a global chemical transport model (Heald et al., 2005). The detected OC was prescribed to oxidation in the free troposphere of long-lived VOCs. The results have major implications for long-range pollution transport due to aerosol in the free troposphere being inefficiently removed from the atmosphere and subsequent radiative forcing of climate (Heald et al., 2005).

Numerous studies during ACE-Asia detailed the optical properties of the aerosol in the region and their subsequent radiative perturbation (Carrico et al., 2003; Markowicz et al., 2003; Quinn et al., 2004; Doherty et al., 2005). ACE-Asia was characterised by a diverse range of sources including pollution, dust, sea salt and volcanic aerosol. Mass scattering efficiencies for sulphate, sub-micron OM, sea salt and dust were derived and were found to be comparable to values from previous studies (Quinn et al., 2004). This indicates that values are relatively constant across different source regions. The prevalence of dust in the region dramatically altered the chemical composition, size distribution and optical properties of the aerosol (Quinn et al., 2004). Dust was the dominant component in terms of the super-micron and sub-1 μm light scattering (Quinn et al., 2004). Regimes dominated by dust were found to be the least hygroscopic, whilst volcanic aerosol was found to exhibit the greatest hygroscopicity (Carrico et al., 2003). Intermediate hygroscopicity was determined for pollution and marine dominated aerosol, with marine aerosol exhibiting greater hygroscopicity than pollution aerosol. The influence of relative humidity on aerosol radiative forcing was probed based on radiometric observations and sensitivity studies using modelled radiative transfer calculations (Markowicz et al., 2003). The mean surface aerosol forcing efficiency over the Sea of Japan was calculated as -60 Wm^{-2} with strong enhancements under high relative humidity conditions (Markowicz et al., 2003).

3.2.3 Studies in Europe

Putaud et al. (2004) presented an overview of aerosol chemical characteristics from a range of ground-based locations between 1991 and 2001. The 24 included sites ranged from kerbside, urban, rural and background locations which were mainly located in North-Western Europe, with some sites in the Mediterranean but none in Eastern Europe. OM was found to be the dominant component at the majority of sites aside from some natural and/or background locations where the sulphate contribution was greater.

A major finding was that in major pollution episodes, nitrate was found to be the dominant chemical component, exceeding that of OM and sulphate. High particulate loadings were often associated with colder periods, where pollution dispersion was reduced and condensation of semi-volatile species to the particle phase was favoured. Abdalmogith and Harrison (2005) found a similar relationship between nitrate and high particulate loading episodes when examining two sites in the UK. Consequently, control of NO_x emissions was established as a significant feature required in pollution control strategies, particularly in North-Western Europe where NO_x and ammonia emissions reach their maximum (Reis et al., 2009).

Schaap et al. (2002) constructed a European aerosol nitrate concentration field based upon filter measurements from 1994-1997. Nitrate was found to be a major contributor to the aerosol burden in Europe, with concentrations exceeding 5 $\mu g\,m^{-3}$ in many areas ranging from Southern England and over continental Europe as far east as Poland. Nitrate was predominantly found in the fine aerosol fraction (below 2.5 μm). During winter in the area to the north of the Alps, nitrate was 60% or more than the concentration of sulphate. Comparable nitrate concentrations to Western Europe were found in the Po-Valley, a highly polluted region in Northern Italy. This work was followed up in Schaap et al. (2004), where a chemical transport model was used to simulate the European inorganic aerosol field. Nitrate was found to be a significant component of European aerosols and displayed a pronounced seasonal cycle. Sulphate displayed a far less pronounced seasonal variation. During winter, autumn and especially spring, enhanced nitrate concentrations were shown to exist over much of Northern Europe. During summer, enhanced nitrate concentrations were mainly located in regions with significant ammonia emissions, such as the Netherlands. The contribution of nitrate to the AOD was approximately equal to that of sulphate in winter and spring over Europe.

The Aerosol Direct Radiative Impact Experiment (ADRIEX) took place over the Adriatic and Black Seas during August and September 2004 (Highwood et al., 2007). The aim of the study was to characterise anthropogenic aerosol in the region and establish its radiative impacts (Highwood et al., 2007). Crosier et al. (2007a) presented chemical composition measurements using a Q-AMS, while Osborne et al. (2007) presented measurements of the associated aerosol optical properties. The study found that ammonium nitrate concentrations were large in the Po Valley and in the outflow from this region, particularly over the Northern Adriatic. Furthermore, it was found that it made a significant contribution to the radiative budget in the region. Particularly important was the effect of the hygroscopic nature of the aerosol when associated with moist air masses. The scattering intensity increased considerably when water vapour was able to condense upon the ammonium nitrate aerosol in such air masses. In the region, another regime was distinguished, which was composed primarily of OM and ammonium sulphate aerosol. The dominance of either regime was dependent upon the

emission history of the air mass. OM in the region was found to be secondary and originating from anthropogenic sources. The pollution in the region was mainly constrained to the accumulation mode and resulted in AOD measurements often exceeding 0.2 (Osborne et al., 2007), demonstrating the level to which such aerosol chemical components can perturb the radiative balance in the region. The study underlined the importance of ammonium nitrate aerosol on regional scales in Europe. The large reductions in SO_2 emissions in Northern and Western Europe when compared to emissions of NO_x has resulted in nitrate aerosols becoming more important in these areas (Crosier et al., 2007a).

Robles González et al. (2003) demonstrated that strong regional gradients in AOD were prevalent over Europe, based upon satellite data. These were strongly coupled to the anthropogenic emissions of SO_2 and NO_x in major industrial and urban areas. A regional chemical transport model was combined with the satellite data to investigate the contribution of specific aerosol species to the AOD over Europe. Sulphate was estimated to contribute from 15-70% depending upon the proximity to the major source regions. Nitrate was a major factor across Europe, with between 5-25% of the AOD being attributed to nitrate. This contribution was particularly large in North-Western Europe in the Netherlands region and the immediate vicinity in the North Sea.

Koelemeijer et al. (2006) presented a study linking the measurements of particulate matter across Europe with MOderate Resolution Imaging Spectrometer (MODIS) AOD retrievals. The MODIS measurements showed that the major aerosol source regions in Europe were concentrated in the Belgium/Netherlands/Ruhr area, Northern Italy (particularly the Po Valley) and Southern Poland. This was consistent with the particulate matter measurements, particularly for the Belgium/Netherlands/Ruhr area where spatial coverage was better than the other major regions identified. This is consistent with the previously identified prevalence of ammonium nitrate when considering the sub-micron aerosol chemical composition.

3.3 Key themes relevant to this study

The previous sections have outlined several areas regarding the properties and processes that govern atmospheric aerosol. Two key themes have emerged, which are:

1. The evolution of SOA in the atmosphere.
2. The contribution of ammonium nitrate to the European aerosol burden and how it modulates the resultant AOD field.

These themes will be discussed in the following sections and key questions to be addressed by this study will be presented.

3.3.1 Evolution of secondary organic aerosol

Clearly, OM is a major component of the global aerosol burden, with concentrations often comparable to, or exceeding those of, sulphate. Sizeable contributions and concentrations have been observed across the Northern Hemisphere in polluted environments. However, major deficiencies in our understanding of the life cycle of OM exist. The differing estimates of the contribution of biogenic and anthropogenic precursors point to one such deficiency. The large discrepancies between measurements and models when assigning OM to be either primary or secondary is a further concern. The subsequent evolution of OM downwind of its source regions presents a major challenge to ambient measurements, laboratory or chamber measurements and aerosol models. These factors present sizeable questions relating to our ability to understand and predict the evolution and impact of OM on global and regional climate change, air quality and environmental degradation.

The high proportion of OM contributing to the sub-micron particulate burden and apparent dominance by secondary species has been shown to contrast with traditional atmospheric chemistry models (Volkamer et al., 2006, and references therein), which generally assign much of the OM to the primary fraction. Furthermore, such discrepancies increase as a function of photochemical age. Such studies have profound implications for global models, which suggest that the contribution of SOA to the aerosol burden is limited (e.g. Kanakidou et al., 2005). This directly contrasts with the now large body of observational evidence.

One avenue of research regarding the mismatch between measurements and modelling of OM, which has gained significant interest recently, is the volatility distribution of OM. Traditional modelling approaches have prescribed POA to be non-volatile and inert (Donahue et al., 2009). Furthermore, traditional models have used chamber measurements of SOA, relative to known precursors to derive yield estimates. Such traditional approaches may not be representative of the ambient atmosphere, in terms of their initial concentrations, precursor mixtures and eventual SOA composition and evolution (e.g. de Gouw et al., 2005; Heald et al., 2005; Volkamer et al., 2006; Kroll and Seinfeld, 2008). Coupling of a thermodenuder system with an AMS has shown that the SOA component can be separated in terms of its volatility, with more aged SOA being less volatile than fresher SOA (Huffman et al., 2009). Additionally, the POA component was shown to be semi-volatile. Ng et al. (2010) demonstrated conclusively that laboratory derived SOA from chamber studies does not match the observed ambient composition from a worldwide dataset of AMS measurements; chamber SOA is typically far less oxygenated than ambient SOA. Heald et al. (2010) showed that the evolution of OM composition in the atmosphere is a continuum, resulting in a more oxidised aerosol due to chemical processing.

Recent frameworks have attempted to reconcile such discrepancies by consider-

ing the entire OM component as semi-volatile (Donahue et al., 2006; Robinson et al., 2007; Donahue et al., 2009). Consequently, primary emissions of OM are able to partially evaporate upon atmospheric dilution, potentially creating a significant source of low-volatility gas phase material. Such material may then undergo photochemical reactions, namely oxidation, to form SOA. OM components in the Earth's atmosphere are thus treated in terms of their volatility distribution, known as the volatility basis set (Donahue et al., 2006). Such an approach allows atmospheric aging processes to occur in both the gas and particle regimes via repartitioning and oxidation of OM components. This framework has been shown to represent the evolution of OM in laboratory experiments (e.g. Donahue et al., 2006; Sage et al., 2008; Grieshop et al., 2009) and a more accurate spatial distribution of modelled OM (e.g. Robinson et al., 2007; Dzepina et al., 2009). Recently, this paradigm has been implemented to explain OM volatility and composition variations both downwind of a megacity source (Mexico City) and across a global ground-based dataset of sites in the Northern Hemisphere (Jimenez et al., 2009).

The present study is well placed to consider the distribution and evolution of OM on the regional scale in locations predominantly downwind of their major sources. Currently the spatial and temporal scales governing the transformation of OM in the ambient atmosphere are poorly constrained. This study will examine the controlling features upon its spatial distribution in Northern Europe and its evolution across a range of spatial scales. This will encompass freshly formed plumes through to background aerosol, which has undergone significant chemical and atmospheric processing. Such transformations are vital for assessment of the impacts of OM as they ultimately control the concentration and properties of the OM burden.

This study will focus upon these key questions related to organic aerosol across Northern Europe:

1. Is organic aerosol ubiquitous across Northern Europe and what modulates its concentration fields?

2. To what extent is the regional organic aerosol component secondary in nature?

3. How does the organic aerosol component evolve on the regional scale?

3.3.2 Ammonium nitrate in North-Western Europe

Studies in the North America and Eastern Asia have highlighted the predominance of sulphate and OM in the sub-micron aerosol mass. Little input from ammonium nitrate aerosol to the accumulation mode mass has been shown in such studies, except in the vicinity of Mexico City (e.g. DeCarlo et al., 2008; Kleinman et al., 2008). A major observation of the European-based studies is the significance of ammonium nitrate, particularly under polluted conditions in North-Western Europe (e.g. Schaap

et al., 2002; Putaud et al., 2004; Abdalmogith and Harrison, 2005; Koelemeijer et al., 2006) and in the Po Valley region (Schaap et al., 2002; Crosier et al., 2007a). Such observations are a consequence of the changing emission footprints in these different regions of SO_2, NO_x and NH_3. Several modelling studies (e.g. Bauer et al., 2007; Pinder et al., 2007; Makar et al., 2009) have noted that changes in ammonia emissions result in substantial changes in ammonium nitrate concentrations. Substantial emission reductions have occurred in Europe, particularly over the past 20 years, with relative reductions in SO_2 emissions decreasing by 66% from 1990-2005 (Monks et al., 2009). Reductions in NO_x (32%) and NH_3 (23%) have been much less pronounced over this period, due to differences in source distributions, abatement measures and reduction efficiency (Monks et al., 2009). The emission reductions in the United States were less pronounced than in Europe, while in Eastern Asia, emissions increased (Monks et al., 2009). Reductions in SO_2 emissions were particularly pronounced in Western Europe, which reduced emissions by 60-80% (Monks et al., 2009). Such relative changes in aerosol precursor emissions have a direct impact upon the aerosol chemical composition in Europe, as the reductions in SO_2 emissions and associated particulate sulphate result in a greater availability of NH_3 to form ammonium nitrate in the particle phase. Furthermore, the noted emission changes in Europe are liable to occur in other polluted regions both at present and in the future. This is indicated by the contribution of ammonium nitrate to pollution episodes in California, which has long been known (e.g White and Roberts, 1977).

The present study will explore the contribution of ammonium nitrate to the aerosol burden and its resultant climate impact in Western Europe. Ammonium nitrate is particularly relevant to studies of the aerosol direct effect as a result of its large light scattering potential and affinity for water uptake. Furthermore, its formation pathways are a prime example of how the vertical distribution may impact upon the aerosol radiative affect. Ammonium nitrate formation is dependent on the vertical mixing state of the atmosphere (Neuman et al., 2003; Morino et al., 2006). It often forms at the top of the boundary layer as a consequence of partitioning of gaseous NH_3 and HNO_3 to the particle phase. This partitioning process is biased towards the particle phase at lower temperatures. As a result, the formation of the particulate mass occurs in an area of greater relative humidity; thus the aerosol formed will be larger in size due to additional water uptake. Consequently, the resultant aerosol is likely to significantly perturb the radiative balance in such circumstances. Representation of the vertical distribution of aerosols is a significant deficiency in current numerical models (e.g. Easter et al., 2004; Textor et al., 2006; Isaksen et al., 2009), thus such a phenomenon is of particular relevance. Ammonium nitrate is often not included in global and regional aerosol models (e.g. Myhre et al., 2006), as a result of the complexity of representing semi-volatile components and its interaction with both coarse and fine mode aerosol. Such an omission could have major implications for regional weather and climate in

Western Europe, where ammonium nitrate has been shown to be an important constituent of the aerosol burden. Consequently, this study will attempt to characterise the controlling features related to the spatial distribution of ammonium nitrate in Western Europe and its resultant optical and radiative impacts.

This study will focus upon these key questions related to ammonium nitrate across Europe:

1. How much does ammonium nitrate contribute to the European aerosol burden and what modulates this contribution?

2. How important are its semi-volatile properties in terms of its vertical distribution?

3. What is the impact of ammonium nitrate upon the European AOD field and resultant direct radiative effect?

Chapter 4

Papers

4.1 Overview of ADIENT and EUCAARI-LONGREX experiments

The present study mainly draws upon data associated with two major scientific research programmes; the European Integrated Project on Aerosol Cloud Climate and Air Quality Interactions (EUCAARI, Kulmala et al., 2009) and the UK Aerosol Properties, PRocesses And InfluenceS on the Earth's climate (APPRAISE).

EUCAARI is an EU Framework 6 Integrated Project focussing on aerosol particles and their effect on regional air quality and climate. EUCAARI brings together the leading European research groups, state-of-the-art infrastructure and key players from third countries to investigate the role of aerosol on climate and air quality. The stated objectives for the EUCAARI project are as follows:

1. Reduction of the current uncertainty of the impact of aerosol particles on climate by 50% and quantification of the relationship between anthropogenic aerosol particles and regional air quality, and

2. Quantification of the side effects of European air quality directives on global and regional climate, and provide tools for future quantifications for different stakeholders.

One aspect of EUCAARI was a major airborne intensive operation period which took place during May 2008. This period involved utilisation of multiple airborne platforms and long-term sampling at a variety of ground-based locations across Northern Europe. Two parallel airborne studies were conducted during this period and were known as the EUCAARI-LONG Range EXperiment (EUCAARI-LONGREX, henceforth referred to as LONGREX) and the Intensive Observation Period at Cabauw Tower (IMPACT). The BAe-146 took part in the LONGREX campaign in conjunction with

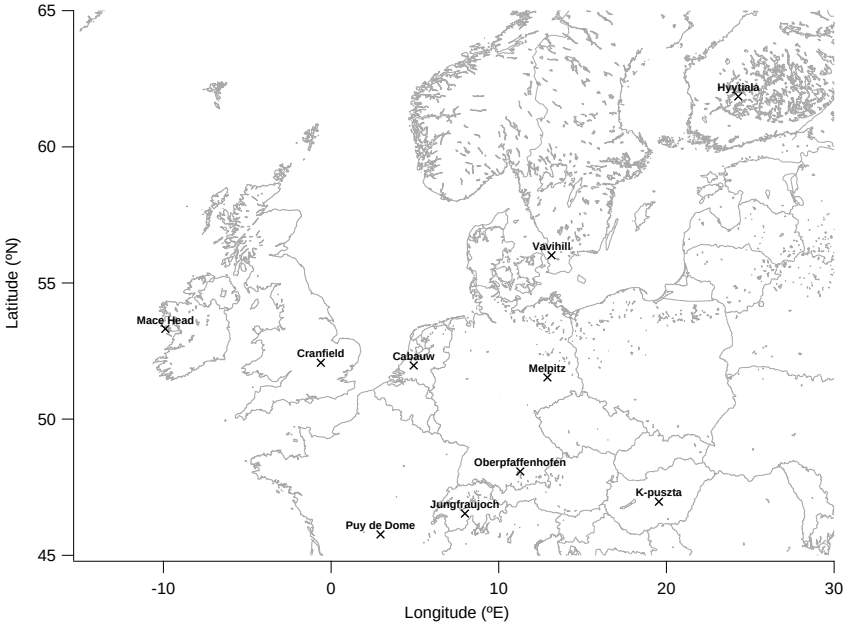

Figure 4.1: Location of relevant ground-based sites associated with ADIENT and LONGREX. Cranfield and Oberpfaffenhofen represesent the principal bases of operation for ADIENT and LONGREX respectively. The other ground-based locations represent the locations of major instrument deployments during the LONGREX flying period associated with the EUCAARI programme.

the Deutsches Zentrum für Luft-und Raumfahrt (DLR) Falcon 20-E5 (e.g. Wandinger et al., 2002). The aim of the project was to measure the distribution of aerosol over Europe via utilisation of airborne in-situ and remote sensing measurements. The general strategy for each flight was for the Falcon to fly at high altitude ahead of the BAe-146 using remote sensing LIDAR to derive on-line profiles of the tropospheric column. Such information could then be used by the BAe-146 to target areas suitable for in-situ sampling, generally at low-level. The IMPACT experiment centred around a ground-based measurement tower at Cabauw, in the Western Netherlands. Airborne measurements during IMPACT were provided by the French ATR-42 and an Airborne Cloud Turbulence Observation System (ACTOS), which was suspended from a helicopter which operated during the campaign. IMPACT focussed upon cloud-aerosol interactions in the vertical column above Cabauw, with additional operations in the North Sea off the Dutch coast. Cabauw formed one part of a network of ground sites across Europe which included an extensive suite of aerosol and other atmospheric measurements. The locations of these are shown in Figure 4.1. The Falcon and BAe-146 performed several overpasses and vertical profiles over Melpitz, Cabauw and Mace Head during the course of the campaign.

APPRAISE is similarly interested in the impact of aerosol particles on climate as the central aspect is upon understanding atmospheric aerosols in order to improve models of likely climate changes, with particular emphasis on regional scales. One aspect of APPRAISE was the Appraising the Direct Impacts of Aerosol on Climate (ADIENT) project, which aimed to provide information and understanding of the properties and processes that determine aerosol radiative properties and impacts. This encompassed a range of spatial scales, from individual plumes up to the regional scale of continental Europe. The key objectives of ADIENT were as follows:

1. Improved quantification of the key parameters controlling the evolution of the single scattering albedo and radiative effect of key aerosol types.

2. Assess the relative contribution of primary and secondary aerosol to the global aerosol burden and their subsequent effects on the radiative budget.

3. Assess the regional variability of aerosol and their effects.

4. The provision of an initial framework for assessments of the climatic impacts of air quality regulation of particulate material.

The LONGREX campaign formed the broader regional scope of ADIENT, consequently they are heavily linked in terms of their aims and scope. The following papers will present results and discussions related to the broad aims of these projects. Specifically, this will include the properties, processes and climate impacts of atmospheric aerosol across Europe.

4.2 Paper I: Vertical distribution of sub-micron aerosol chemical composition

Vertical distribution of sub-micron aerosol chemical composition from North-Western Europe and the North-East Atlantic

W.T. Morgan, J.D. Allan, K.N. Bower, G. Capes, J. Crosier, P.I. Williams and H. Coe

Atmospheric Chemistry & Physics, 9, 5389-5401, 2009

Publication date: 3 August 2009

Supplementary material available in Section 6.1.

Overview: This paper is a compilation of aerosol chemical composition measurements from the Q-AMS made on-board the BAe-146 in the UK region. Vertical profiles of aerosol chemical components are analysed, supplemented by measurements of aerosol microphysical properties and trace gas species. A cluster analysis of meteorological back-trajectories is used in order to distinguish the influence of air mass history upon the aerosol properties. Major differences in the aerosol chemical composition were distinguished between air masses originating from continental Europe when contrasted with air masses that had traversed the Atlantic Ocean. Continental air masses contained significantly more pollution, which was predominantly driven by an increased fractional and absolute contribution from ammonium nitrate. A key observation was the association of ammonium nitrate with regional pollution episodes in North-Western Europe. I led the data analysis and manuscript preparation.

Contributions from co-authors: Bower and Williams developed the Q-AMS for use on-board the BAe-146. Allan, Bower, Capes, Crosier and Williams participated in the fieldwork. Bower and Coe were involved in flight planning for some of the flights. Coe assisted in the data analysis and manuscript preparation.

Atmos. Chem. Phys., 9, 5389–5401, 2009
www.atmos-chem-phys.net/9/5389/2009/

Atmospheric Chemistry and Physics

Vertical distribution of sub-micron aerosol chemical composition from North-Western Europe and the North-East Atlantic

W. T. Morgan[1], **J. D. Allan**[1,2], **K. N. Bower**[1], **G. Capes**[1], **J. Crosier**[1,2], **P. I. Williams**[1,2], **and H. Coe**[1]

[1]Centre for Atmospheric Science, University of Manchester, Manchester, UK
[2]National Centre for Atmospheric Science, University of Manchester, Manchester, UK

Received: 6 March 2009 – Published in Atmos. Chem. Phys. Discuss.: 6 April 2009
Revised: 10 July 2009 – Accepted: 27 July 2009 – Published: 3 August 2009

Abstract. A synthesis of UK based airborne in-situ measurements of aerosol properties representing air masses from North-West Europe and the North-East Atlantic is presented. The major focus of the study is the vertical distribution of sub-micron aerosol chemical composition. Vertical profiles are derived from a Quadrupole Aerosol Mass Spectrometer (Q-AMS). Background sub-micron aerosol vertical profiles are identified and are primarily composed of organic matter and sulphate aerosol. Such background conditions occurred predominantly during periods associated with long-range air mass transport across the Atlantic. These instances may serve as useful model input of aerosol to Western Europe. Increased mass concentration episodes are coincident with European outflow and periods of stagnant/recirculating air masses. Such periods are characterised by significantly enhanced concentrations of nitrate aerosol relative to those of organic matter and sulphate. Periods of enhanced ground level $PM_{2.5}$ loadings are coincident with instances of high nitrate mass fractions measured on-board the aircraft, indicating that nitrate is a significant contributor to regional pollution episodes. The vertical structure of the sulphate and organic aerosol profiles were shown to be primarily driven by large-scale dynamical processes. The vertical distribution of nitrate is likely determined by both dynamic and thermodynamic processes, with chemical partitioning of gas phase precursors to the particle phase occurring at lower temperatures at the top of the boundary layer. Such effects have profound implications for the aerosol's lifetime and subsequent impacts, highlighting the requirement for accurate representation of the aerosol vertical distribution.

Correspondence to: W. T. Morgan
(william.morgan@postgrad.manchester.ac.uk)

1 Introduction

Uncertainty surrounding the impact of atmospheric aerosol is a major barrier to accurate prediction of future anthropogenically induced climate change (Forster et al., 2007). Human activity has increased the atmospheric aerosol concentration, which is known to significantly alter the Earth's radiative equilibrium on regional to global scales (e.g. Haywood and Boucher, 2000). The direct and indirect aerosol radiative forcing strongly depends upon aerosol properties as a function of height (e.g. Forster et al., 2007). The chemical composition of the aerosol is one such property. Global aerosol models require direct representation of aerosol chemical composition (e.g. Textor et al., 2006). The AeroCom exercise (Kinne et al., 2006; Schulz et al., 2006; Textor et al., 2006) established significant differences between participating models in terms of vertical aerosol dispersion (Textor et al., 2006). This variance contributes significantly to uncertainties in estimates of aerosol lifetimes in the atmosphere, which in turn impacts their climate effect. Ground based measurements of aerosol composition are numerous, facilitating model comparisons at the surface. However, in-situ vertical profiles of aerosol chemical speciation are sparse. Consequently, there is a need for high-quality measurement data of aerosol properties as a function of altitude.

Traditional methods for aerosol composition measurements, such as filter based techniques, are incapable of providing highly time resolved vertical profiles. Novel online techniques are required to accurately measure the vertical distribution of aerosol composition. Examples of such instruments are the Particle-Into-Liquid Sampler (PILS, Weber et al., 2001) and the Aerodyne Aerosol Mass Spectrometer (AMS, Jayne et al., 2000; Canagaratna et al., 2007). Both have demonstrated the capability to quantitatively measure aerosol composition from airborne platforms (Bahreini et al., 2003; Lee et al., 2003; Orsini et al., 2003; Crosier et al., 2007a).

Published by Copernicus Publications on behalf of the European Geosciences Union.

Dynamical processes control the advection of aerosol and their precursors to the sampling region. This has been shown to modify the concentration and relative distribution of chemical species of sub-micron aerosol in the planetary boundary layer (e.g. Bahreini et al., 2003; Schneider et al., 2006; Crosier et al., 2007a). A complicating factor regarding the aerosol vertical distribution is the role of chemical, rather than large-scale dynamical effects. Ammonium nitrate formation close to the top of the boundary layer is an example of this (Neuman et al., 2003; Morino et al., 2006). This phenomenon is driven by partitioning between the gas and particle regimes, which is strongly dependent upon temperature and relative humidity (Stelson and Seinfeld, 1982; Mozurkewich, 1993). The partitioning is biased towards the particle phase at lower temperatures and high relative humidity.

Characterisation of aerosol processes and properties on regional scales is paramount in order to assess regional air quality and to predict future changes in atmospheric variables, such as temperature and precipitation. Atmospheric processes over the UK provide a useful test case, as aerosol properties are expected to be significantly modulated by the dominant meteorological synoptic situation. As a result, the UK is representative of a much wider region encompassing North-Western Europe and the North-East Atlantic. Abdalmogith and Harrison (2005) found significant variations in sulphate and nitrate at two ground based locations in the UK due to differing air mass histories. Higher concentrations were associated with south-easterly and easterly back trajectories originating from continental Europe. Coe et al. (2006) showed that, during marine conditions, background input of sulphate and organic aerosol into Western Europe were between 0.5 and 1.0 $\mu g\,sm^{-3}$. Thus variability in mass concentrations and the relative fraction of chemical species is well established.

This paper presents measurements of aerosol properties in the UK region from the UK Facility for Airborne Atmospheric Measurements (FAAM) BAe-146 research aircraft. The vertical distribution of aerosol chemical composition is the major focus of the study. The influence of air mass history upon the aerosol mass concentration and relative chemical components will be investigated based upon a back trajectory cluster analysis. High pollution episodes identified via the UK ground based measurement network will be examined using the aircraft data coupled with the back trajectory analysis.

2 Methodology

2.1 Sampling platform and instrumentation

The FAAM BAe-146 research aircraft has a typical range of over 3000 km and a height ceiling of over 10.5 km. The aircraft's science speed is approximately 100 $m\,s^{-1}$. Profile ascents and descents are made at approximately 150 m per minute below 1 km and at 300 m per minute above 1 km. The aircraft houses a suite of instruments capable of resolving aerosol properties. Only instruments used in this analysis are discussed further. Number size distributions are measured via a wing-mounted Particle Measurement Systems (PMS) Passive Cavity Aerosol Spectrometer Probe 100X (PCASP, Liu et al., 1992; Strapp et al., 1992). The instrument optically counts particles between 0.1–3 µm diameter across 15 channels. Particle number concentrations greater than 3 nm were measured by a TSI Inc. Ultrafine Condensation Particle Counter (CPC, Model 3025A). Furthermore, the facility provides aircraft position information and measurements of standard atmospheric variables, such as temperature and relative humidity.

Measurements made by the Aerodyne Quadrupole Aerosol Mass Spectrometer (Q-AMS) will be the major focus of this study. The Q-AMS has demonstrated the capability to quantitatively measure the size-resolved chemical composition of non-refractory particulate matter of widely varying volatility (Jayne et al., 2000; Allan et al., 2003; Jimenez et al., 2003). Furthermore, it is capable of providing such quantitative measurements with high time resolution in a range of environments from different platforms, such as aircraft. Standard operating practises are followed for ambient sampling (Jimenez et al., 2003), data quantification (Allan et al., 2003) and mass spectrum deconvolution (Allan et al., 2004). Recent laboratory evidence (Matthew et al., 2008) indicates that the AMS collection efficiency is significantly modulated by particle phase. Here a collection efficiency correction is applied following the principle developed by Crosier et al. (2007a), which takes into account the nitrate content of the sampled aerosol.

Crosier et al. (2007a) detailed the operating practises and sampling strategy for the Q-AMS on-board the BAe-146, which is summarised here. The Q-AMS was connected to a Rosemount inlet (Foltescu et al., 1995) via approximately 0.7 m of stainless steel tubing with a total residence time of approximately 4 s for the entire inlet system. Samples were introduced at ambient pressure and sub-micron particle losses are considered negligible for the operating altitudes considered by this study (Zhang et al., 2002; Osborne et al., 2007). Furthermore, wing tip to wing tip comparisons between different AMS instruments using different inlets have shown less than 15% difference (Crosier, 2007). The aerosol sample introduced to the Q-AMS is considered dry. This is due to the coupled effect of the aircraft cabin temperature (approximately 298.15 K) exceeding ambient temperatures and additional ram heating due to the decelerating sample airflow. The ram heating is approximated to be 5 K, with an additional heating of approximately 10–70 K for the operating altitudes of the aircraft considered by this study. As the flow is controlled by a critical orifice, increases in altitude cause decreases in the standard flow rate into the instrument. This results in an increase in the species specific detection limits

of the Q-AMS. Mass concentration values are reported as micrograms per standard cubic metre ($\mu g\,sm^{-3}$) i.e. at a temperature of 273.15 K and pressure of 1013.25 hPa. Q-AMS data points are reported as 30 s time intervals.

The Q-AMS comprises three fundamental sections: the particle beam generation region; the aerodynamic sizing region and the particle composition region. The particle beam generation comprises a 130 µm critical orifice, which controls the flow rate into the instrument. An aerodynamic lens system (Liu et al., 1995a,b) is used to collimate the sampled air into a narrow particle beam with 100% transmission for 40–700 nm vacuum aerodynamic diameter (DeCarlo et al., 2004) particles. DeCarlo et al. (2004) showed that the vacuum aerodynamic diameter is related to the mobility diameter by the particle density when assuming spherical particles. For example, the AMS size range for a dry spherical particle with a density of $1.6\,g\,cm^{-3}$ would equate to a mobility range of approximatley 25–440 nm. At reduced ambient pressure, the lens pressure is reduced as a constant pressure inlet system was not used. Thus, at reduced pressure, the transmission efficiency through the lens is shifted towards smaller particle sizes. Consequently, at the highest operating altitudes, this may degrade the transmission efficiency of the lens. Concentrations at such levels may thus represent lower limits of the submicron concentrations. Upon exiting the lens system, the gas undergoes a supersonic expansion and the particle's velocity increases as a function of its vacuum aerodynamic diameter. The expansion into the vacuum chamber is dependent upon the upstream lens pressure, which is taken into account when calibrating the instrument. The particle's size may thus be inferred via measurement of its flight time through the length of the vacuum chamber. Particles then impact upon a resistively heated surface at a temperature of approximately 550°C where they undergo flash vaporisation. The resultant gas is then ionized via 70 eV electrons emitted by a Tungsten filament. A quadrupole mass spectrometer then classifies the sample ions according to a specific mass-to-charge (m/z) ratio. An electron multiplier detects the resultant ion signal. The aerosol beam is blocked periodically to obtain a mass spectrum of the background in the vacuum chamber. This is subtracted from the mass spectrum of the aerosol laden air to remove the background component. The Q-AMS employed a Jump Mass Spectrum (JMS, Crosier et al., 2007b) mode of operation to measure discrete mass fragments, which enhances the detection limit and time resolution of the measurements. A zero particle filter can be used to determine the detection limit of the instrument intermittently from the standard deviation of the signal fluctuating about zero. This fluctuation about zero is a consequence of low signal-to-noise, which can result in negative mass concentrations when sampling concentrations are close to the detection limit. Negative concentrations are not removed so as not to bias the statistical vertical profiles.

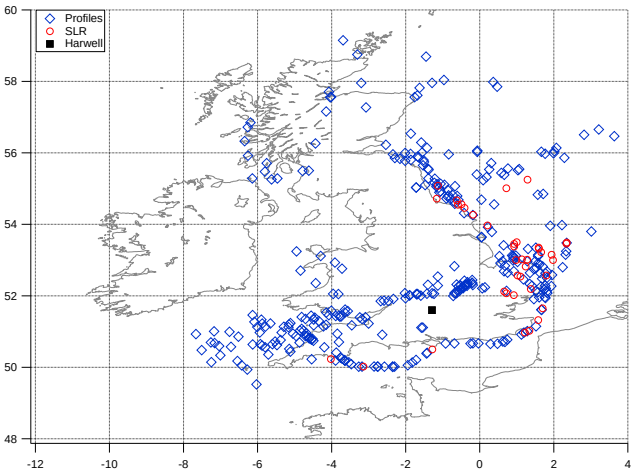

Fig. 1. Location of vertical profiles and constant altitude straight and level runs (SLRs). The latitude/longitude grid marks out the sectors referred to in Sect. 2.2. The location of the ground based monitoring station at Harwell is also shown.

2.2 Location of measurements

The present analysis uses data from 41 flights based in the UK region. The period covered is from 5 April 2005 to 27 September 2006. The full dataset for both the Q-AMS data and flight parameters is available from the British Atmospheric Data Centre (BADC, http://badc.nerc.ac.uk). The flights are drawn from several projects associated with aerosol and cloud studies. A total of 339 profiles were identified from these flights. Low-level (defined as those below 2.5 km) Straight Level Runs (SLRs) were also identified. Size distributions from the PCASP were available on 82 SLRs. The location of these profiles and SLRs are summarised in Fig. 1. Predominantly, the measurements presented are located over marine areas due to air traffic restrictions placed upon the aircraft. Profiles and SLRs were grouped into "sectors" encompassing a 2° by 2° latitude/longitude grid based on their median longitude and latitude point. The sectors were assigned on a grid from 48–60° N and between 8° W and 4° E.

2.3 Back trajectory cluster analysis

Three-dimensional air mass back trajectories were derived from European Centre for Medium-Range Weather Forecasts (ECMWF) wind fields. The start points of the trajectories of each profile were defined from the latitude and longitude coordinates of the centre of the sector associated with that profile. The initialisation start time was chosen as 12:00 UTC as this time corresponded most closely to the airborne operations in all cases. Trajectories were established for the previous three days at 6 hourly intervals. Three vertical levels were chosen; 950 hPa, 750 hPa and 500 hPa. A total of 159

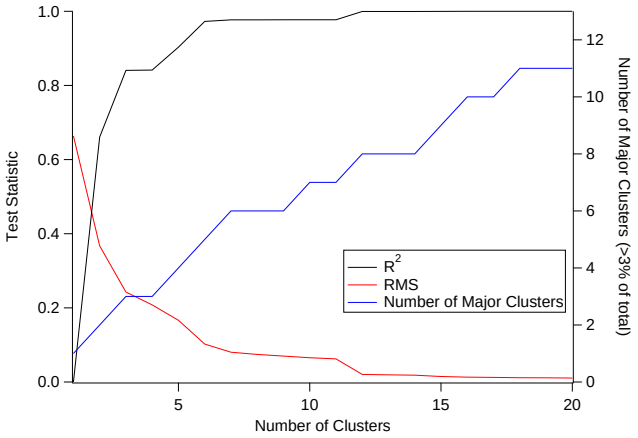

Fig. 2. Variation in R^2 and RMS as a function of the number of clusters. The number of major cluster is also shown which is defined as clusters containing more than 3% of the total back trajectories.

back trajectories were generated. The latitude and longitude coordinates were converted to km north and km east respectively (assuming a spherical Earth), whilst the pressure was retained as hPa.

Back trajectories were processed using a custom made cluster analysis routine, based on the method described in Cape et al. (2000). An average linkage method was used to compute the squared distance between each trajectory at individual time steps using Eq. (1):

$$d(x_i, x_j) = \sum_k \left\{ (x_{ki} - x_{kj})^2 + (y_{ki} - y_{kj})^2 + (p_{ki} - p_{kj})^2 \right\} \quad (1)$$

where x_{ki}, y_{ki}, p_{ki} are coordinates of trajectory x_i at each time point k. The average distance between two trajectories, x_i and x_j, are calculated. At the start of the analysis, each trajectory is assigned to its own cluster. All possible pairs are evaluated with the two clusters with the smallest average distance between their members joining. An iterative process is employed until all trajectories reside in one cluster. The "optimum" number of clusters may then be selected. The procedure seeks to minimize within cluster variance and maximize between cluster variance (Cape et al., 2000). This method has been shown to be the most appropriate means of classifying meteorological data (Kalkstein et al., 1987).

The number of clusters to retain for analysis is subjective (Kalkstein et al., 1987). Several indicators may be used in order to select an appropriate number of clusters, N. One such indicator is the coefficient of determination, R^2, which is defined as the proportion of the variance explained by the current number of clusters at each iteration step:

$$R^2 = 1 - \sum_N \frac{\text{(within cluster variance)}}{\text{(variance of all trajectories)}} \quad (2)$$

where the first sharp decrease can be used as a subjective indicator of the number of clusters to retain (Kalkstein et al., 1987). The Root Mean Square (RMS) distance between clusters may also be used, where an increase signifies that two dissimilar clusters have been joined (Cape et al., 2000). Similarly to Cape et al. (2000), an indication of the number of major clusters is defined based on the number of clusters containing more than 3% of the total number of trajectories. Figure 2 displays the change in these measures as a function of the number of clusters for the trajectories initialized at 750 hPa. A comparison between R^2 and RMS indicates that the initial number of clusters to retain is 12 based on a "step" in both statistics. The number of clusters was reduced to 5 after examination of the trajectories and average 850 hPa geopotential height fields for each of the 12 clusters. The clustering routine was also run for the 950 hPa and 500 hPa pressure levels to ensure vertical consistency, which resulted in a similar solution. Comparison of the retrieved solution when the pressure term was excluded also resulted in a similar solution. Thus the transport is dominated by changes in the horizontal components. Furthermore, the 750 hPa solution was found to be similar when the analysis was performed on five day back trajectories. Consequently, the subsequent discussion and analysis will be based upon the three day back trajectories initialized at 750 hPa.

Table 1. Summary of cluster solution including details of the number of profiles, SLRs and back trajectories associated with each cluster.

Cluster	Condition	Profiles	SLRs	Back trajectories
1	Atlantic origin	181	51	84
2	Easterly	44	19	19
3	Southerly	18	7	6
4	Northerly	29	N/A	18
5	Stagnant air masses	67	5	32

The five cluster solution derived from the back trajectory analysis is summarised in Table 1 and Fig. 3. To facilitate interpretation of the cluster solutions, average geopotential height fields were generated from ECMWF operational analysis data. These are included along with the full back trajectory solutions for each cluster in the supplementary material section (http://www.atmos-chem-phys.net/9/5389/2009/acp-9-5389-2009-supplement.pdf). Cluster 1 encompasses three initial clusters, which were dominated by westerly, south-westerly and north-westerly trajectories. Thus this cluster was prescribed as the Atlantic cluster. The associated synoptic conditions are representative of westerly flow into the UK region and northern Europe, consistent with the clusters mean back trajectory. Cluster 2 comprised two clusters made of easterly back trajectories from northern to central Europe. The geopotential height field shows a relatively weak anticyclonic pressure system over the UK with outflow

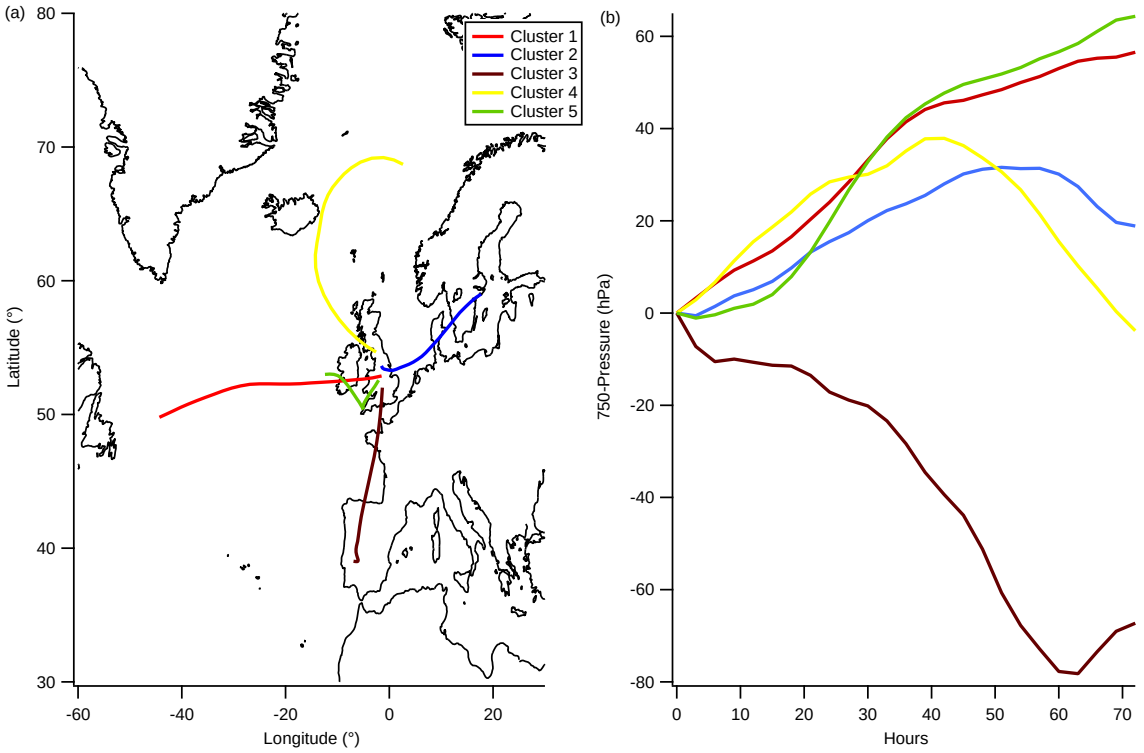

Fig. 3. (a) Mean back trajectories for the five cluster solution at six-hourly time steps. **(b)** Mean back trajectories for the five cluster solution displaying the vertical deviation for an air mass with six-hourly time steps. Positive values indicate that an air mass has descended at a time step.

from northern Europe. Cluster 3 comprised air masses originating from Spain and France. The synoptic situation is characterised by high pressure over southern/central Europe and over the central Atlantic. A low pressure system is situated off the west coast of Ireland in the North Atlantic. This results in broadly southerly flow consistent with the back trajectories. Cluster 4 comprised largely north-westerly back trajectories with a cyclonic rotational component distinct from the previous north-westerly trajectories, which were assigned to cluster 1. The geopotential height field is consistent with the interpretation from the back trajectories. Cluster 5 comprises back trajectories centred on the UK representing a relatively stagnant air mass. This is in agreement with the geopotential height field that displays a ridge of high pressure situated over the UK. Cluster 3 is distinct from the other clusters in terms of its vertical displacement as it is the only cluster which ascends during its transit to the UK region.

3 UK aerosol chemical composition profiles

3.1 Full dataset characterisation

Summary statistics and individual data points of aerosol chemical composition measured by the Q-AMS for the full profile dataset are presented in Figs. 4 and 5. The black raw data points are those which fall above the 2σ profile for each individual species, where 2σ is defined as two times the standard deviation for a 30 s average data point. These are calculated for 500 m altitude bins when the detected signal by the Q-AMS is close to zero. In particular, resolving low mass concentrations for organics and ammonium is difficult due to the signal-to-noise constraints of the Q-AMS. The variability and indication of the number of points within an altitude bin is represented by calculating the variability about the mean value in each bin. This is defined as the Mean Absolute Deviation (MAD) divided by the square root of the number of points, n, in an altitude bin. MAD is defined as:

$$\mathrm{MAD} = \frac{1}{n}\sum_{i=1}^{n} |\epsilon_i| \tag{3}$$

where ϵ_i is the absolute difference between the mean bin value and the raw data value. The profiles are categorised by a relatively small Inter Quartile Range (IQR, defined as the difference between the 75th and 25th percentile) with sulphate and organics having an IQR between 0–2 $\mu g\,sm^{-3}$ below 3000 m. This is interpreted as background mass concentration levels. The higher concentrations above the 75th percentile are likely associated with pollution plumes. Nitrate

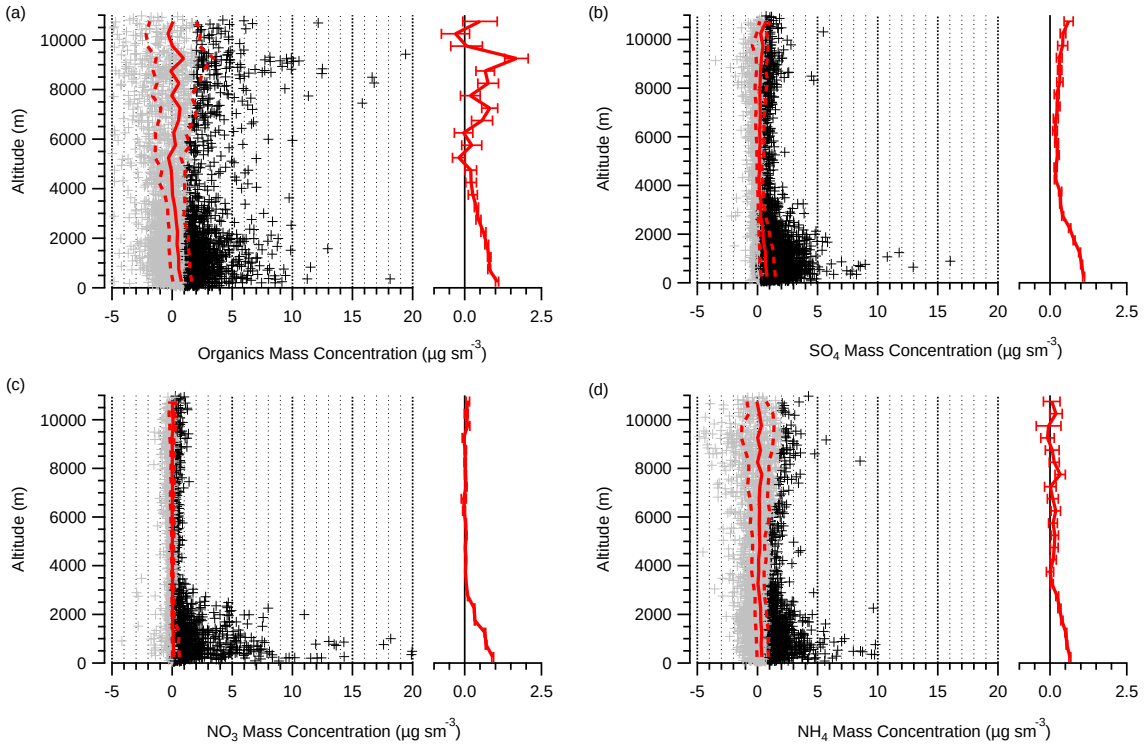

Fig. 4. Vertical profiles of aerosol chemical composition from the AMS for the UK for each chemical species. Black crosses are individual data points above the 2σ profile for each species whilst grey crosses correspond to those below. Red lines are the 25th, 50th and 75th percentiles for 500 m altitude bins. On the right hand side panel for each species the red line shows the mean for each altitude bin with the horizontal bar indicating the variability about the mean value, defined in Sect. 3.1. Tabulated statistics are available in the supporting material (http://www.atmos-chem-phys.net/9/5389/2009/acp-9-5389-2009-supplement.pdf).

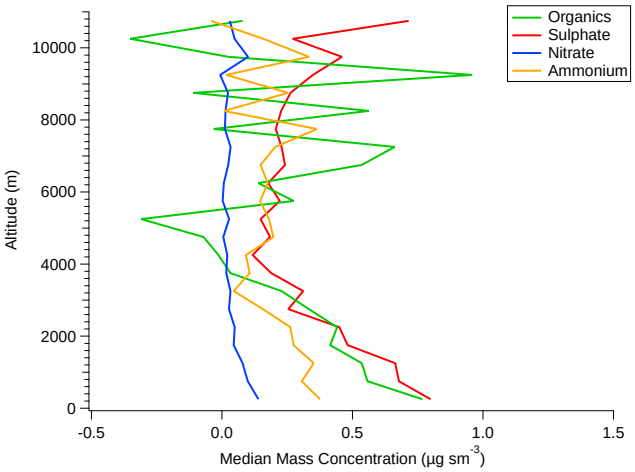

Fig. 5. Sulphate, organics, nitrate and ammonium median mass concentration profiles for the full dataset.

mass concentrations are generally much lower than organics and sulphate with the peak concentration for the 75th percentile being less than 1.0 µg sm^{-3}. However, when nitrate is enhanced, it is a major constituent of the sub-micron mass detected by the AMS. Ammonium is broadly similar to the sulphate and nitrate profiles due to its association with those species in the form of ammonium sulphate and ammonium nitrate, respectively.

Above 4000 m, data coverage is much more limited and the mass of aerosol is significantly decreased. Sulphate and nitrate mass concentrations are low with little variability, although there is some evidence for enhanced sulphate concentration above 8000 m. In contrast, organic mass is characterised by low or negative mass concentrations, punctuated by significantly enhanced concentrations above the 2σ profile. The 25th percentile for both the organics and ammonium are negative above 4000 m. The organic mass median profile is relatively low (less than 1.0 µg sm^{-3}), whilst the 75th percentile profile above approximately 7000 m is higher than the corresponding profile in the boundary layer. The variability about the mean in each bin is significantly enhanced compared with those below 4000 m. This suggests large variability coupled with potentially low statistical significance above this level. Above approximately 5000 m, the variability and lower number of data points results in the variability about the mean being more than two times greater than

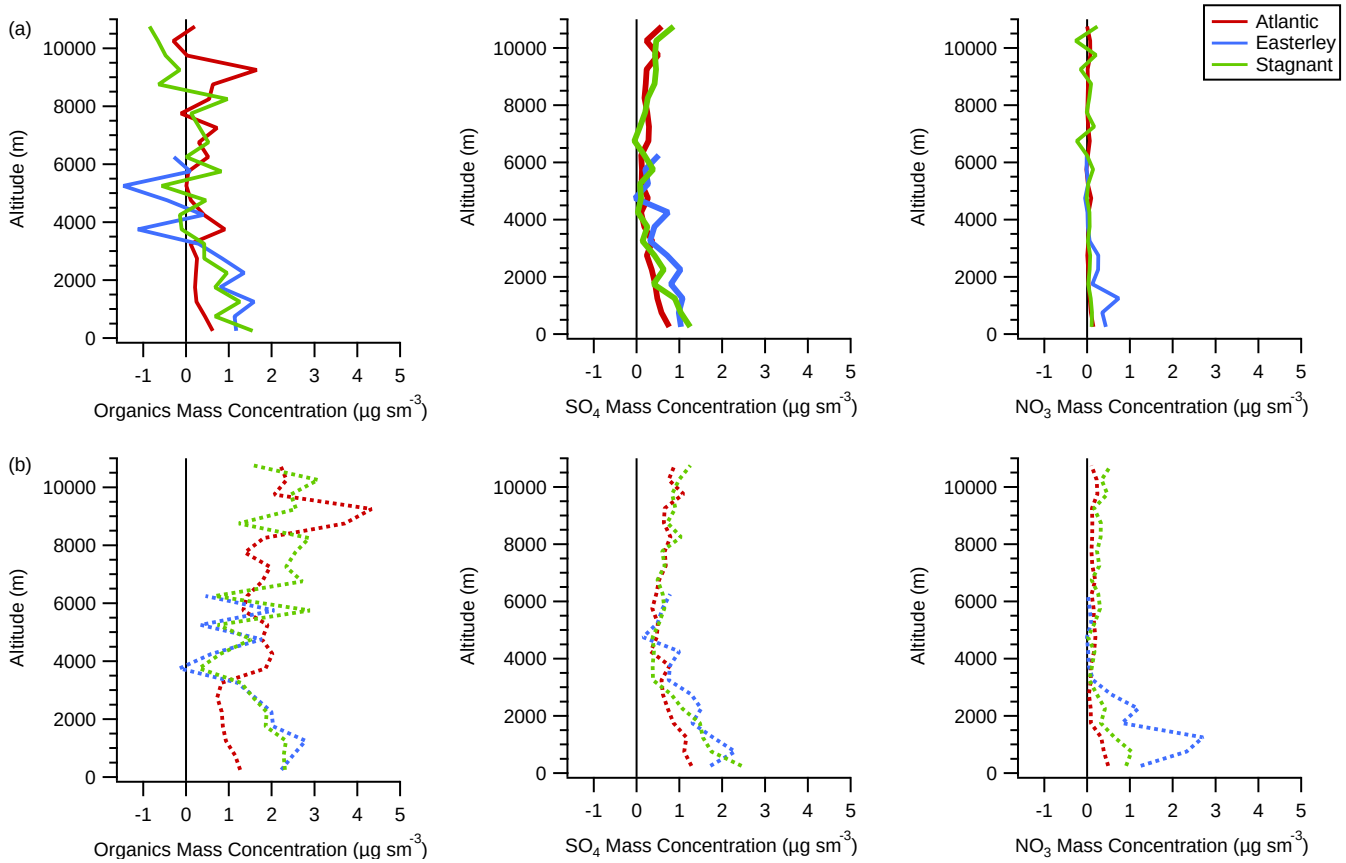

Fig. 6. (a) shows the median mass concentration profiles for the clusters for organics, sulphate and nitrate and **(b)** displays the corresponding 75th percentile mass concentration profiles. The legend indicates the respective cluster. Tabulated statistics are available in the supporting material (http://www.atmos-chem-phys.net/9/5389/2009/acp-9-5389-2009-supplement.pdf).

values in the boundary layer. The variability in the values for nitrate and sulphate are much lower due to improved SNR for these species at higher altitudes compared with organic mass. Bahreini et al. (2003) noted that the Q-AMS required greater than one minute in order to yield statistically reasonable mass concentrations using mass spectrum mode, although this is improved when using selected ion monitoring (DeCarlo et al., 2006) such as JMS mode. Consequently, the concentrations sampled above the estimated detection limit are statistically representative. However, in the case of the organic mass outside of the boundary layer, the uncertainty increases substantially.

3.2 Aerosol properties as a function of air mass history

The clusters identified in Sect. 2.3 present an opportunity to compare aerosol properties in differing air masses. The Atlantic cluster represents a largely clean air mass entering the UK region. The cluster is representative of the input of aerosol to Western Europe during such conditions. When sampling in coastal areas downwind of the UK, such an air mass will also be associated with pollution originating from the UK itself. Profiles upwind of the UK in Atlantic conditions are likely a combination of long-range transport and potential marine sources. The easterly cluster is characteristic of pollution transport from northern/central Europe. Some additional input from the UK region may also occur depending upon the location of the sampling. The stagnant air mass cluster will be examined also. The southerly and northerly clusters are under-sampled relative to the other clusters. Thus these are omitted from the subsequent analysis which will focus on the three dominant transport patterns.

Figure 6 indicates that aerosol concentrations are enhanced for the easterly cluster compared with the Atlantic cluster. This is particularly evident in the case of nitrate, which is very low for the Atlantic cluster, whereas for the easterly condition it is a substantial component of the submicron mass. This is consistent with European pollution outflow leading to an enhancement in the mass concentration of nitrate. Sulphate and organic concentrations are also enhanced due to the large availability of sources in continental Europe. Concentrations for the stagnant condition are

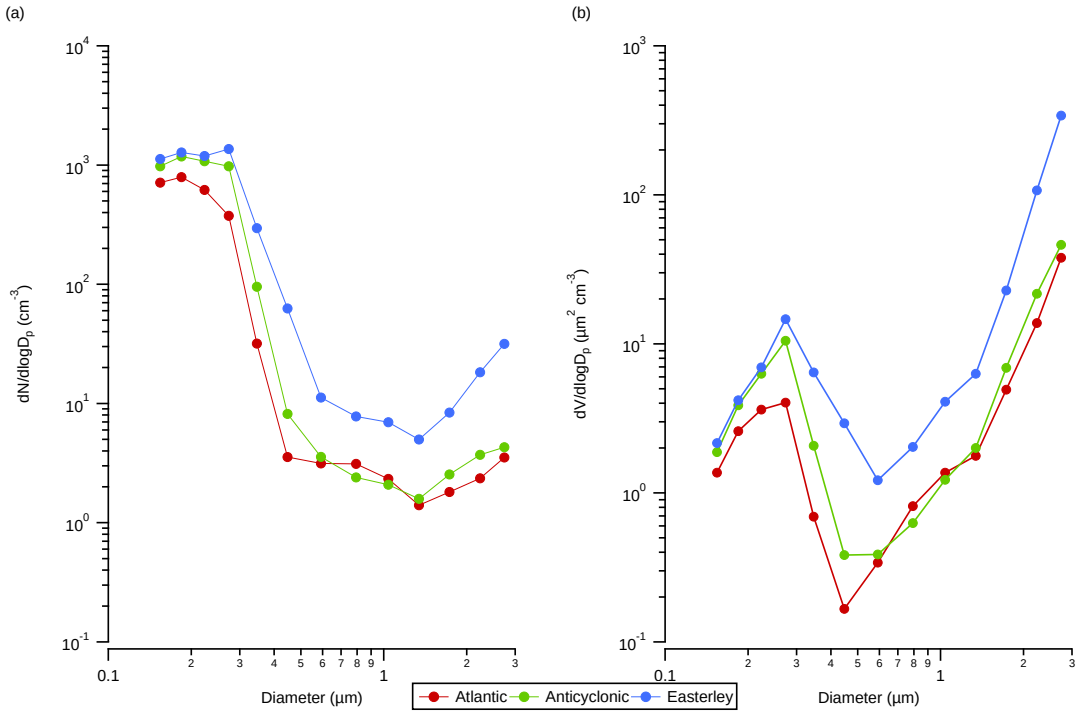

Fig. 7. Average PCASP size distributions for **(a)** number and **(b)** volume. The legend indicates the respective clusters the distributions are averaged over.

increased relative to the Atlantic case. This is consistent with the general build-up of pollution during a stagnant air mass episode.

Generally, the organics and sulphate profiles do not exhibit strong gradients within the boundary layer itself. Nitrate displays strong coupling with NO_x close to the surface (not shown), decreasing to close to zero between 1000–1500 m. Such features are primarily a result of the advection of pollution plumes driven by the larger scale dynamical situation. Above 1500 m, a secondary maximum occurs. Potentially, this is a result of partitioning between the gas and particulate phase at lower temperatures and enhanced relative humidity. This is suggestive of nitrate formation being primarily driven by the thermodynamics in this atmospheric layer.

Number-size distributions and estimated volume size distributions from the PCASP are shown in Fig. 7. These are extracted from the SLRs identified in Fig. 1 and the relevant number of SLRs for each cluster is shown in Table 1. The first two channels from the PCASP are omitted as these have been known to experience elevated levels of intermittent electronic noise. Consequently, the distributions shown are from 0.15 μm to 3 μm. The shape of the distributions is broadly similar. The number-size distributions all peak between 0.15 μm and 0.3 μm. The volume distributions for the Atlantic, easterly and stagnant air masses peak at approximately 0.3 μm. However, the distributions display significant differences between their concentrations, particularly above 0.3 μm. Due to the relatively small number of SLRs for the stagnant cluster, direct comparisons will be drawn between the easterly and Atlantic only. Based on the volume distributions, the majority of the mass sampled by the Q-AMS will be for particles smaller than 600 nm. The volume distributions indicate the presence of significant super-micron aerosol. This is likely composed of primary particles and is not discussed further in this paper.

The easterly number-size and volume distributions are enhanced compared to the Atlantic distribution. This is particularly pronounced above 0.3 μm. This is consistent with the higher mass concentrations observed in the profile data for the easterly condition. Newly formed secondary species condense upon available surfaces, further increasing the volume of material at larger sizes. Consequently, the distinctions between the distributions for the easterly and Atlantic clusters are consistent with the Q-AMS profile data. The size distributions from this analysis are consistent with those obtained by Osborne and Haywood (2005) during the ACE-2 experiment within the instrument's uncertainty. Osborne and Haywood (2005) also noted an enhancement in the accumulation mode as a result of aerosol aging.

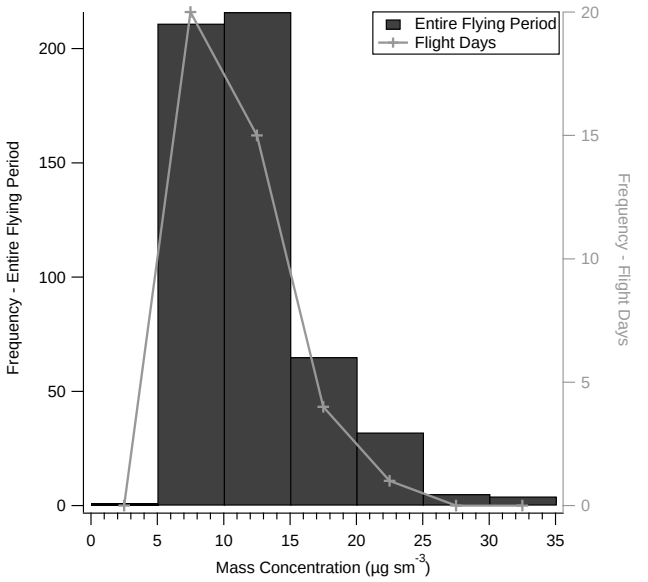

Fig. 8. Histogram of daily mean $PM_{2.5}$ mass concentrations at Harwell for the entire flying period (5 April 2005 to 27 September 2006) covered by this study and the individual flight days.

3.3 Pollution episodes and comparison with the surface-based network

In order to study the characteristics of high pollution episodes, several flights have been selected based on elevated measurements of $PM_{2.5}$ mass concentrations from the UK surface-based measurement network. The aircraft data is compared with a rural monitoring station in Harwell, Oxfordshire (51°36′0″ N, 1°17′24″ W) in the South East of the UK. The site is marked in Fig. 1. This station was selected due to its location away from major population centres, roads or industrial sources. Measurements made at the site are therefore largely representative of regional aerosol concentrations. Thus it provides an indication of the general pollution situation, which is independent of the measurements made on the aircraft. The data is provided by the UK Air Quality Archive website (http://www.airquality.co.uk/archive/index.php) for the period covered by the analysis, which runs from 5 April 2005 to 27 September 2006. Daily mean values at Harwell were available for 40 out of 41 flights and were ranked according to total mean loading. The data is summarised by a frequency distribution shown in Fig. 8. The distribution for the entire flying period and the distribution for the flying days are investigated using a two-sample T-test on unpaired means in order to discern whether the distributions are statistically different. The null hypothesis is that the population means are equal at the 0.05 (5%) significance level. The T-statistic for the distributions is 1.930, with a p-value of 0.101. Consequently, the null hypothesis may not be rejected at the 5% level and the flights are considered to be representative of the entire analysis period. For the majority of the analysis period (80% of the time), daily mean loadings were between 5–15 µg sm^{-3}. High pollution episodes are accordingly defined as those when the daily mean exceeds 15 µg sm^{-3}. Such episodes occur on 106 days out of the 534 days during the considered analysis period. Flight days where this value was exceeded are extracted for further analysis and are summarized in Table 2. Five flights in total are extracted. The average synoptic situation, derived from ECMWF geopotential height fields (not shown), for these flights consists of high pressure situated across much of the UK region. This is consistent with a relatively stagnant or recirculating air mass advecting European pollution outflow to the UK.

Table 2. Details of flights which occurred when daily mean $PM_{2.5}$ measurements at Harwell, UK exceeded 15 µg sm^{-3}.

Date	Flight number	$PM_{2.5}$ mass concentration (µg sm^{-3})
21 Apr 2005	B091	16
13 Jul 2005	B110	16
17 Aug 2005	B122	17
22 Sep 2005	B133	16
12 May 2006	B198	21

Figure 9 displays the median and 75th percentile mass concentrations of chemical composition as a function of height for the high pollution episode data. Nitrate mass fraction for the pollution episode data and the full dataset are also shown. The data is consistent with the ground based data from Harwell with increased mass concentrations detected from the aircraft during the high pollution cases compared to the full dataset. This is consistent with the air mass history analysis in Sect. 3.2, with enhanced mass concentrations due to the large availability of sources in continental Europe. For the full dataset, sulphate and organics are the dominant components, with concentrations of less than 1.6 µg sm^{-3} each close to the surface. Nitrate accounts for a small fraction of the sub-micron mass. For the high pollution cases, all components are enhanced relative to the full dataset. In particular, nitrate is significantly enhanced for both the median and 75th percentile mass loading. For the 75th percentile high pollution cases, nitrate is the dominant chemical constituent between 0–1000 m, with nitrate mass concentrations exceeding 5 µg sm^{-3}. Thus, the nitrate mass concentration is enhanced by a factor of 10 for the high pollution cases relative to the full dataset. Below 3000 m, nitrate is the dominant inorganic constituent. These characteristics are consistent with Sect. 3.1, with the high mass concentrations being quite distinct from the general background trend. Such high pollution episodes are coincident with considerable enhancements in the nitrate mass concentration and occurred

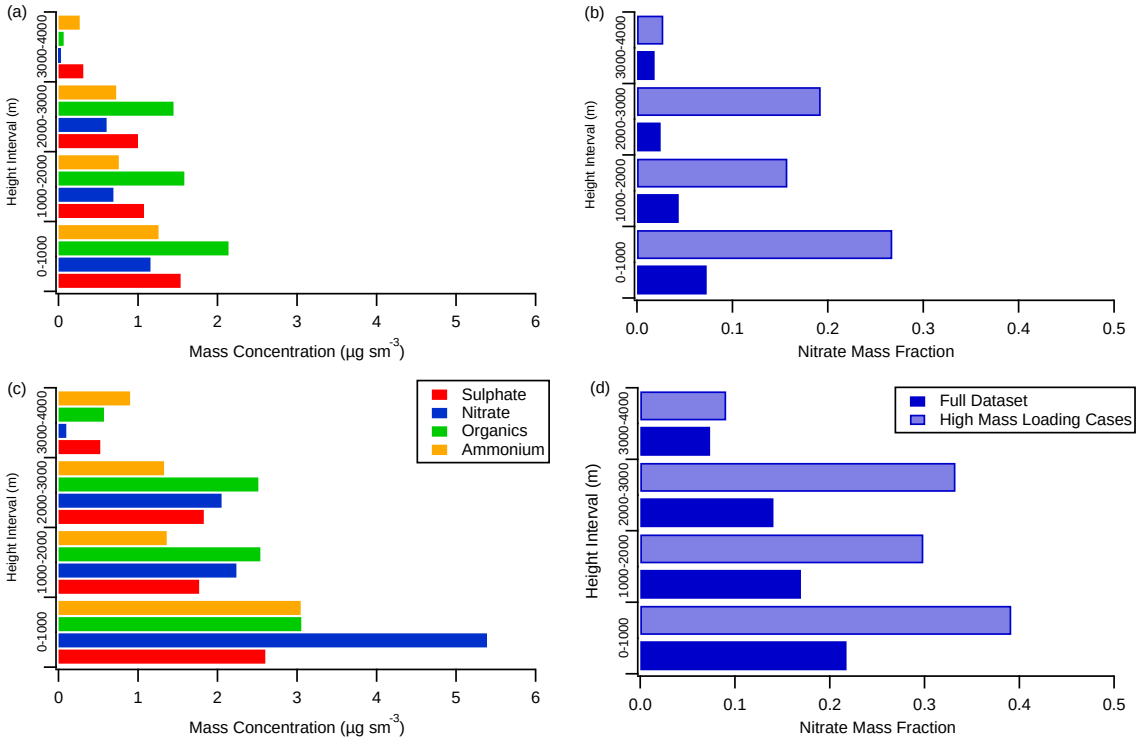

Fig. 9. Distribution of Q-AMS mass as a function of height for high mass loading cases where **(a)** represents the median mass concentration for each height interval and **(c)** represents the 75th percentile mass concentration for each height interval. **(b)** and **(d)** contrast the nitrate mass fraction for the high mass loading cases and the full dataset for the median and 75th percentile, respectively.

on average 20% of the time during the flying period (5 April 2005 to 27 September 2006) considered by this analysis.

4 Conclusions

The vertical distribution of aerosol chemical composition has been characterised for the UK region. A back trajectory cluster analysis formed the basis for categorizing the source history of the aerosol properties. A key general feature of the profiles is the trend showing a relatively consistent background primarily composed of organic matter and ammonium sulphate. The organic matter concentrations are similar to the sulphate concentrations. The background conditions are likely driven by long-range transport plus a potential influence of local marine sources, which may be biogenic (e.g. O'Dowd et al., 2002) or anthropogenic (e.g. Petzold et al., 2008) in origin. The background mass concentrations are similar to those measured by Coe et al. (2006) on the west coast of Ireland during westerly conditions. Enhanced organic matter concentrations are infrequently observed in the mid-troposphere, likely a result of long-range transport. Sulphate also showed a subtle increase above 8000 m, potentially as a result of long-range transport. Vertical mixing of sulphate-enriched stratospheric air to the troposphere could potentially contribute in this layer, although the coincident ozone profiles do not show an increasing trend with altitude in this region, which would be expected if troposphere-stratosphere exchange was prevalent. The background profiles for the Atlantic cluster are representative of the input of aerosol to Western Europe. The Atlantic cluster represented the predominant condition (53% of all back trajectories) of the cluster solution. Such profiles should serve as a useful constraint for modelling studies. Summary statistics for the vertical profiles are presented in the supplementary material section (http://www.atmos-chem-phys.net/9/5389/2009/acp-9-5389-2009-supplement.pdf) for the full dataset and the cluster solutions. The background trend is punctuated by higher concentrations associated with pollution plumes. Such plumes are shown to be more intense and more frequent during periods of European outflow and periods of stagnant/recirculating air masses. Analysis of the UK surface-based measurement network corroborates this conclusion, with pollution episodes occurring on average 20% of the time during the flying period. Furthermore, Abdalmogith and Harrison (2005) showed enhanced mass concentrations during periods of European outflow compared to inflow from the Atlantic. Consequently, differing meteorological regimes have a substantial impact upon the concentration, composition and microphysical properties of the aerosol input to the

UK region. Such conditions increase the prospect of maximum mass concentration targets being exceeded and amplified perturbations of the radiative equilibrium in the UK region. This has major implications for source apportionment and impact studies.

A major facet of the enhanced mass concentrations observed was the increase in the fractional contribution of nitrate to the particulate mass. This is consistent with previous composition profiles derived from AMS measurements in Europe (Crosier et al., 2007a; Schneider et al., 2006).This was particularly evident when assigning high pollution episodes based upon the surface-based data and the general features of the European outflow cluster. Furthermore, nitrate was shown to exhibit more variability as a function of height within the boundary layer compared to organic matter and sulphate. Nitrate exhibited two maxima within the boundary layer; one close to the surface and a second close to the top of the boundary layer. Formation occurring higher in the boundary layer is likely due to thermodynamics driving the chemical partitioning of the gas phase precursors to the particle phase. Such effects have previously been observed on the west coast of the USA (Neuman et al., 2003) and demonstrated using 1-D thermodynamic modelling above Tokyo, Japan (Morino et al., 2006). On the regional scale, organic matter is predominantly composed of Secondary Organic Aerosol (SOA) under polluted conditions in the Northern Hemisphere (Zhang et al., 2007), which potentially contains a significant semi-volatile fraction (Donahue et al., 2006). Whether the organic matter displays similar semi-volatile behaviour to the nitrate is unclear from this dataset. The dataset does indicate that ammonium nitrate can be a substantial component of the regional aerosol burden. Its complex vertical distribution highlights the requirement for accurate representation of aerosol formation and processes away from the surface.

These findings have significant implications for treatment of the radiative and ecological effects of anthropogenic aerosol. Firstly, the addition of relatively more inorganic material to a mixed inorganic-organic system will enhance the hygroscopic nature of the aerosol. Consequently, the addition of particulate mass coupled with enhanced hygroscopicity will greatly enhance the Aerosol Optical Depth (AOD) of the atmospheric burden. Such impacts will be exacerbated in areas exhibiting high relative humidity, such as the top of the boundary layer. The deliquescence relative humidity of ammonium nitrate is 62% (Tang, 1996) with a growth factor of 1.59 at a relative humidity of 85% (Topping et al., 2005), thus the wet size of the aerosol is enhanced. Such effects combine to greatly increase the scattering potential of the aerosol, increasing the magnitude of the aerosol direct effect. Secondly, clouds forming at the top of the boundary layer entrain air from beneath them into the cloud. Enhanced ammonium nitrate concentrations in such air will lead to a modification of the microphysical properties of the cloud. Such modifications are known to modify the amount, lifetime and radiative impact of clouds, the so-called indirect effect of aerosols (e.g. McFiggans et al., 2006). As well as such climate related impacts, nitrate partitioning significantly perturbs the nitrogen cycle of the atmosphere. Particulate nitrate has a dry deposition velocity which is ten times slower than that of nitric acid (Seinfeld and Pandis, 1998). Consequently, transport and ultimately deposition can be substantially altered by this partitioning phenomenon. Further elucidation of the impact of ammonium nitrate is required across Europe, particularly in terms of its direct and indirect radiative effects.

Acknowledgements. We would like to acknowledge the efforts of FAAM, DirectFlight, Avalon and the Met Office and everyone associated with the various projects from which data was used for this study. W. T. Morgan was supported by a Natural Environment Research Council (NERC) studentship NER/S/A/2006/14040 and a CASE sponsorship from Aerodyne Research Inc. The NERC National Centre for Atmospheric Science (NCAS) Facility for Ground based Atmospheric Measurements (FGAM) supported the maintenance of the Q-AMS. NCAS also supported the development of the data interpretation methods employed here through its Composition Directorate. Several NERC funded projects were used in this study including AMPEP (NER/T/S/2002/00493), CIRRUS (NER/T/S/2002/00135), CLOPAP (NER/T/S/2002/00147) and ICEPIC (NER/A/S/2002/01021). Thanks to the British Atmospheric Data Centre (BADC) for the calculation of trajectories and access to ECMWF data. The UK Air Quality Archive website is prepared and hosted by AEA Energy & Environment, on behalf of the UK Department for Environment, Food & Rural Affairs and the Devolved Administrations. We also thank G. McFiggans and G. R. McMeeking for useful critical comments.

Edited by: A. Pszenny

References

Abdalmogith, S. S. and Harrison, R. M.: The use of trajectory cluster analysis to examine the long-range transport of secondary inorganic aerosol in the UK, Atmos. Environ., 39, 6686–6695, 2005.

Allan, J., Jimenez, J., Williams, P., Alfarra, M., Bower, K., Jayne, J., Coe, H., and Worsnop, D.: Quantitative sampling using an Aerodyne aerosol mass spectrometer: 1. Techniques of data interpretation and error analysis, J. Geophys. Res.-Atmos., 108, 4090, doi:10.1029/2003JD001607, 2003.

Allan, J. D., Delia, A. E., Coe, H., Bower, K. N., Alfarra, M. R., Jimenez, J. L., Middlebrook, A. M., Drewnick, F., Onasch, T. B., Canagaratna, M. R., Jayne, J. T., and Worsnop, D. R.: A generalised method for the extraction of chemically resolved mass spectra from aerodyne aerosol mass spectrometer data, J. Aerosol Sci., 35, 909–922, 2004.

Bahreini, R., Jimenez, J., Wang, J., Flagan, R., Seinfeld, J., Jayne, J., and Worsnop, D.: Aircraft-based aerosol size and composition measurements during ACE-Asia using an Aerodyne aerosol mass spectrometer, J. Geophys. Res.-Atmos., 108(D23), 8645, doi:10.1029/2002JD003226, 2003.

Canagaratna, M. R., Jayne, J. T., Jimenez, J. L., Allan, J. D., Alfarra, M. R., Zhang, Q., Onasch, T. B., Drewnick, F., Coe, H.,

Middlebrook, A., Delia, A., Williams, L. R., Trimborn, A. M., Northway, M. J., DeCarlo, P. F., Kolb, C. E., Davidovits, P., and Worsnop, D. R.: Chemical and microphysical characterization of ambient aerosols with the aerodyne aerosol mass spectrometer, Mass Spectr. Rev., 26, 185–222, 2007.

Cape, J. N., Methven, J., and Hudson, L. E.: The use of trajectory cluster analysis to interpret trace gas measurements at Mace Head, Ireland, Atmos. Environ., 34, 3651–3663, 2000.

Coe, H., Allan, J. D., Alfarra, M. R., Bower, K. N., Flynn, M. J., McFiggans, G. B., Topping, D. O., Williams, P. I., O'Dowd, C. D., Dall'Osto, M., Beddows, D. C. S., and Harrison, R. M.: Chemical and physical characteristics of aerosol particles at a remote coastal location, Mace Head, Ireland, during NAMBLEX, Atmos. Chem. Phys., 6, 3289–3301, 2006, http://www.atmos-chem-phys.net/6/3289/2006/.

Crosier, J.: Airborne Measurements of Aerosol Composition using an Aerosol Mass Spectrometer: Insights into the lifecycle of anthropogenic emissions, Phd thesis, University of Manchester, 2007.

Crosier, J., Allan, J. D., Coe, H., Bower, K. N., Formenti, P., and Williams, P. I.: Chemical composition of summertime aerosol in the Po Valley (Italy), northern Adriatic and Black Sea, Quarterly Journal of the Royal Meteorological Society, 133, 61–75, suppl. 1, 2007a.

Crosier, J., Jimenez, J., Allan, J., Bower, K., Williams, P., Alfarra, M., Canagaratna, M., Jayne, J., Worsnop, D., and Coe, H.: Technical Note: Description and Use of the New Jump Mass Spectrum Mode of Operation for the Aerodyne Quadrupole Aerosol Mass Spectrometers (Q-AMS), Aerosol Sci. Technol., 41, 865–872, 2007b.

DeCarlo, P. F., Slowik, J. G., Worsnop, D. R., Davidovits, P., and Jimenez, J. L.: Particle morphology and density characterization by combined mobility and aerodynamic diameter measurements. Part 1: Theory, Aerosol Sci. Technol., 38, 1185–1205, 2004.

DeCarlo, P. F., Kimmel, J. R., Trimborn, A., Northway, M. J., Jayne, J. T., Aiken, A. C., Gonin, M., Fuhrer, K., Horvath, T., Docherty, K. S., Worsnop, D. R., and Jimenez, J. L.: Field-deployable, high-resolution, time-of-flight aerosol mass spectrometer, Analyt. Chem., 78, 8281–8289, 2006.

Donahue, N. M., Robinson, A. L., Stanier, C. O., and Pandis, S. N.: Coupled partitioning, dilution, and chemical aging of semivolatile organics, Environ. Sci. Technol., 40, 2635–2643, 2006.

Foltescu, V. L., Selin, E., and Below, M.: Corrections for Particle Losses and Sizing Errors During Aircraft Aerosol Sampling Using a Rosemount Inlet and the Pms Las-X, Atmos. Environ., 29, 449–453, 1995.

Forster, P., Ramaswamy, V., Artaxo, P., Berntsen, T., Betts, R., W. Fahey, D., Haywood, J., Lean, J., Lowe, D., Myhre, G., Nganga, J., Prinn, R., Raga, G., Schulz, M., and Van Dorland, R.: Changes in Atmospheric Constituents and in Radiative Forcing, Climate Change 2007: The Physical Science Basis. Contribution of Working Group I to the Fourth Assessment Report of the Intergovernmental Panel on Climate Change, Cambridge University Press, Cambridge, United Kingdom and New York, NY, USA, 2007.

Haywood, J. and Boucher, O.: Estimates of the direct and indirect radiative forcing due to tropospheric aerosols: A review, Rev. Geophys., 38, 513–543, 2000.

Jayne, J. T., Leard, D. C., Zhang, X. F., Davidovits, P., Smith, K. A., Kolb, C. E., and Worsnop, D. R.: Development of an aerosol mass spectrometer for size and composition analysis of submicron particles, Aerosol Sci. Technol., 33, 49–70, 2000.

Jimenez, J. L., Jayne, J. T., Shi, Q., Kolb, C. E., Worsnop, D. R., Yourshaw, I., Seinfeld, J. H., Flagan, R. C., Zhang, X. F., Smith, K. A., Morris, J. W., and Davidovits, P.: Ambient aerosol sampling using the Aerodyne Aerosol Mass Spectrometer, J. Geophys. Res.-Atmos., 108(D7), 8425, doi:10.1029/2001JD001213, 2003.

Kalkstein, L. S., Tan, G. R., and Skindlov, J. A.: An Evaluation of 3 Clustering Procedures for Use in Synoptic Climatological Classification, J. Clim. Appl. Meteorol., 26, 717–730, 1987.

Kinne, S., Schulz, M., Textor, C., Guibert, S., Balkanski, Y., Bauer, S. E., Berntsen, T., Berglen, T. F., Boucher, O., Chin, M., Collins, W., Dentener, F., Diehl, T., Easter, R., Feichter, J., Fillmore, D., Ghan, S., Ginoux, P., Gong, S., Grini, A., Hendricks, J., Herzog, M., Horowitz, L., Isaksen, I., Iversen, T., Kirkevåg, A., Kloster, S., Koch, D., Kristjansson, J. E., Krol, M., Lauer, A., Lamarque, J. F., Lesins, G., Liu, X., Lohmann, U., Montanaro, V., Myhre, G., Penner, J., Pitari, G., Reddy, S., Seland, O., Stier, P., Takemura, T., and Tie, X.: An AeroCom initial assessment – optical properties in aerosol component modules of global models, Atmos. Chem. Phys., 6, 1815–1834, 2006, http://www.atmos-chem-phys.net/6/1815/2006/.

Lee, Y. N., Weber, R., Ma, Y., Orsini, D., Maxwell-Meier, K., Blake, D., Meinardi, S., Sachse, G., Harward, C., Chen, T. Y., Thornton, D., Tu, F. H., and Bandy, A.: Airborne measurement of inorganic ionic components of fine aerosol particles using the particle-into-liquid sampler coupled to ion chromatography technique during ACE-Asia and TRACE-P, J. Geophys. Res.-Atmos., 108, 8646, doi:10.1029/2002JD003265, 2003.

Liu, P., Ziemann, P. J., Kittelson, D. B., and McMurry, P. H.: Generating Particle Beams of Controlled Dimensions and Divergence .1. Theory of Particle Motion in Aerodynamic Lenses and Nozzle Expansions, Aerosol Sci. Technol., 22, 293–313, 1995a.

Liu, P., Ziemann, P. J., Kittelson, D. B., and McMurry, P. H.: Generating Particle Beams of Controlled Dimensions and Divergence .2. Experimental Evaluation of Particle Motion in Aerodynamic Lenses and Nozzle Expansions, Aerosol Sci. Technol., 22, 314–324, 1995b.

Liu, P. S. K., Leaitch, W. R., Strapp, J. W., and Wasey, M. A.: Response of Particle Measuring Systems Airborne ASASP and PCASP to Nacl and Latex-Particles, Aerosol Sci. Technol., 16, 83–95, 1992.

Matthew, B. M., Middlebrook, A. M., and Onasch, T. B.: Collection efficiencies in an Aerodyne Aerosol Mass Spectrometer as a function of particle phase for laboratory generated aerosols, Aerosol Sci. Technol., 42, 884–898, 2008.

McFiggans, G., Artaxo, P., Baltensperger, U., Coe, H., Facchini, M. C., Feingold, G., Fuzzi, S., Gysel, M., Laaksonen, A., Lohmann, U., Mentel, T. F., Murphy, D. M., O'Dowd, C. D., Snider, J. R., and Weingartner, E.: The effect of physical and chemical aerosol properties on warm cloud droplet activation, Atmos. Chem. Phys., 6, 2593–2649, 2006, http://www.atmos-chem-phys.net/6/2593/2006/.

Morino, Y., Kondo, Y., Takegawa, N., Miyazaki, Y., Kita, K., Komazaki, Y., Fukuda, M., Miyakawa, T., Moteki, N., and Worsnop, D. R.: Partitioning of HNO3 and particulate nitrate

over Tokyo: Effect of vertical mixing, J. Geophys. Res.-Atmos., 111, d15215, doi:10.1029/2005JD006887, 2006.

Mozurkewich, M.: The Dissociation-Constant of Ammonium-Nitrate and Its Dependence on Temperature, Relative-Humidity and Particle-Size, Atmospheric Environment Part a-General Topics, 27, 261–270, 1993.

Neuman, J. A., Nowak, J. B., Brock, C. A., Trainer, M., Fehsenfeld, F. C., Holloway, J. S., Hubler, G., Hudson, P. K., Murphy, D. M., Nicks, D. K., Orsini, D., Parrish, D. D., Ryerson, T. B., Sueper, D. T., Sullivan, A., and Weber, R.: Variability in ammonium nitrate formation and nitric acid depletion with altitude and location over California, J. Geophys. Res.-Atmos., 108, 4557, doi:10.1029/2003JD003616, 2003.

O'Dowd, C., Jimenez, J., Bahreini, R., Flagan, R., Seinfeld, J., Hameri, K., Pirjola, L., Kulmala, M., Jennings, S., and Hoffmann, T.: Marine aerosol formation from biogenic iodine emissions, Nature, 417, 632–636, 2002.

Orsini, D. A., Ma, Y. L., Sullivan, A., Sierau, B., Baumann, K., and Weber, R. J.: Refinements to the particle-into-liquid sampler (PILS) for ground and airborne measurements of water soluble aerosol composition, Atmos. Environ., 37, 1243–1259, 2003.

Osborne, S. R. and Haywood, J. M.: Aircraft observations of the microphysical and optical properties of major aerosol species, Atmos. Res., 73, 173–201, 2005.

Osborne, S. R., Haywood, J. M., and Bellouin, N.: In situ and remote-sensing measurements of the mean microphysical and optical properties of industrial pollution aerosol during ADRIEX, Q. J. Roy. Meteorol. Soc., 133, 17–32, 2007.

Petzold, A., Hasselbach, J., Lauer, P., Baumann, R., Franke, K., Gurk, C., Schlager, H., and Weingartner, E.: Experimental studies on particle emissions from cruising ship, their characteristic properties, transformation and atmospheric lifetime in the marine boundary layer, Atmos. Chem. Phys., 8, 2387–2403, 2008, http://www.atmos-chem-phys.net/8/2387/2008/.

Schneider, J., Hings, S. S., Hock, B. N., Weimer, S., Borrmann, S., Fiebig, M., Petzold, A., Busen, R., and Karcher, B.: Aircraft-based operation of an aerosol mass spectrometer: Measurements of tropospheric aerosol composition, J. Aerosol Sci., 37, 839–857, 2006.

Schulz, M., Textor, C., Kinne, S., Balkanski, Y., Bauer, S., Berntsen, T., Berglen, T., Boucher, O., Dentener, F., Guibert, S., Isaksen, I. S. A., Iversen, T., Koch, D., Kirkevåg, A., Liu, X., Montanaro, V., Myhre, G., Penner, J. E., Pitari, G., Reddy, S., Seland, Ø., Stier, P., and Takemura, T.: Radiative forcing by aerosols as derived from the AeroCom present-day and pre-industrial simulations, Atmos. Chem. Phys., 6, 5225–5246, 2006, http://www.atmos-chem-phys.net/6/5225/2006/.

Seinfeld, J. H. and Pandis, S.: Atmospheric chemistry and physics: from air pollution to climate change, John Wiley & Sons, New York, 1998.

Stelson, A. W. and Seinfeld, J. H.: Relative-Humidity and Temperature-Dependence of the Ammonium-Nitrate Dissociation-Constant, Atmos. Environ., 16, 983–992, 1982.

Strapp, J. W., Leaitch, W. R., and Liu, P. S. K.: Hydrated and Dried Aerosol-Size-Distribution Measurements from the Particle Measuring Systems FSSP-300 Probe and the Deiced PCASP-100x Probe, J. Atmos. Oceanic Technol., 9, 548–555, 1992.

Tang, I. N.: Chemical and size effects of hygroscopic aerosols on light scattering coefficients, J. Geophys. Res.-Atmos., 101, 19245–19250, 1996.

Textor, C., Schulz, M., Guibert, S., Kinne, S., Balkanski, Y., Bauer, S., Berntsen, T., Berglen, T., Boucher, O., Chin, M., Dentener, F., Diehl, T., Easter, R., Feichter, H., Fillmore, D., Ghan, S., Ginoux, P., Gong, S., Grini, A., Hendricks, J., Horowitz, L., Huang, P., Isaksen, I., Iversen, I., Kloster, S., Koch, D., Kirkevåg, A., Kristjansson, J. E., Krol, M., Lauer, A., Lamarque, J. F., Liu, X., Montanaro, V., Myhre, G., Penner, J., Pitari, G., Reddy, S., Seland, Ø., Stier, P., Takemura, T., and Tie, X.: Analysis and quantification of the diversities of aerosol life cycles within AeroCom, Atmos. Chem. Phys., 6, 1777–1813, 2006, http://www.atmos-chem-phys.net/6/1777/2006/.

Topping, D. O., McFiggans, G. B., and Coe, H.: A curved multi-component aerosol hygroscopicity model framework: Part 1 – Inorganic compounds, Atmos. Chem. Phys., 5, 1205–1222, 2005, http://www.atmos-chem-phys.net/5/1205/2005/.

Weber, R. J., Orsini, D., Daun, Y., Lee, Y. N., Klotz, P. J., and Brechtel, F.: A particle-into-liquid collector for rapid measurement of aerosol bulk chemical composition, Aerosol Sci. Technol., 35, 718–727, 2001.

Zhang, Q., Jimenez, J. L., Canagaratna, M. R., Allan, J. D., Coe, H., Ulbrich, I., Alfarra, M. R., Takami, A., Middlebrook, A. M., Sun, Y. L., Dzepina, K., Dunlea, E., Docherty, K., DeCarlo, P. F., Salcedo, D., Onasch, T., Jayne, J. T., Miyoshi, T., Shimono, A., Hatakeyama, S., Takegawa, N., Kondo, Y., Schneider, J., Drewnick, F., Borrmann, S., Weimer, S., Demerjian, K., Williams, P., Bower, K., Bahreini, R., Cottrell, L., Griffin, R. J., Rautiainen, J., Sun, J. Y., Zhang, Y. M., and Worsnop, D. R.: Ubiquity and dominance of oxygenated species in organic aerosols in anthropogenically-influenced Northern Hemisphere midlatitudes, Geophys. Res. Lett., 34, l13801, doi:10.1029/2007GL029979, 2007.

Zhang, X. F., Smith, K. A., Worsnop, D. R., Jimenez, J., Jayne, J. T., and Kolb, C. E.: A numerical characterization of particle beam collimation by an aerodynamic lens-nozzle system: Part I. An individual lens or nozzle, Aerosol Sci. Technol., 36, 617–631, 2002.

4.3 Paper II: Spatial distribution of aerosol chemical composition across Europe

Airborne measurements of the spatial distribution of aerosol chemical composition across Europe and evolution of the organic fraction

W.T. Morgan, J.D. Allan, K.N. Bower, E.J. Highwood, D. Liu, G.R. McMeeking, M.J. Northway, P.I. Williams, R. Krejci and H. Coe

Atmospheric Chemistry & Physics, 10 (8), 4065-4083, 2010

Publication date: 29 April 2010

Supplementary material available in Section 6.2.

Overview: This paper presents aerosol chemical composition measurements from the cToF-AMS made on-board the BAe-146 across Europe. The spatial distribution and evolution of aerosol chemical composition is analysed, supplemented by measurements of aerosol microphysical properties and trace gas species. The ubiquity of organic aerosol across Northern Europe was established, while the dominance of ammonium nitrate during polluted episodes in North-Western Europe was shown. A factor analysis identified two separate Oxygenated Organic Aerosol (OOA) components; one representing an aged-OOA, termed Low Volatility-OOA and another representing fresher-OOA, termed Semi Volatile-OOA on the basis of their mass spectral similarity to previous studies. Significant chemical processing of the OA was observed downwind of major sources in North-Western Europe, with the LV-OOA component becoming increasingly dominant as the distance from source and photochemical processing increased. Ammonium nitrate and organic aerosol were shown to be major constituents of the sub-micron aerosol burden in polluted air masses advected far downwind of continental Europe. I led the AMS data collection, the data analysis and manuscript preparation.

Contributions from co-authors: Bower and Williams developed the cToF-AMS for use on-board the BAe-146. Allan, Liu, McMeeking and Williams participated in the fieldwork. Bower, Highwood, Northway, Krejci and Coe were involved in flight planning for the flights. Allan, Liu, McMeeking, Northway, Krejci and Coe assisted in the data analysis. Allan, McMeeking, Krejci and Coe assisted in manuscript preparation.

Atmos. Chem. Phys., 10, 4065–4083, 2010
www.atmos-chem-phys.net/10/4065/2010/
doi:10.5194/acp-10-4065-2010

Atmospheric Chemistry and Physics

Airborne measurements of the spatial distribution of aerosol chemical composition across Europe and evolution of the organic fraction

W. T. Morgan[1], **J. D. Allan**[1,2], **K. N. Bower**[1], **E. J. Highwood**[3], **D. Liu**[1], **G. R. McMeeking**[1], **M. J. Northway**[3], **P. I. Williams**[1,2], **R. Krejci**[4], **and H. Coe**[1]

[1]Centre for Atmospheric Science, University of Manchester, Manchester, UK
[2]National Centre for Atmospheric Science, University of Manchester, Manchester, UK
[3]Department of Meteorology, University of Reading, Reading, UK
[4]Department of Applied Environmental Science, Atmospheric Science Unit, Stockholm University, Stockholm, Sweden

Received: 27 November 2009 – Published in Atmos. Chem. Phys. Discuss.: 16 December 2009
Revised: 1 April 2010 – Accepted: 27 April 2010 – Published: 29 April 2010

Abstract. The spatial distribution of aerosol chemical composition and the evolution of the Organic Aerosol (OA) fraction is investigated based upon airborne measurements of aerosol chemical composition in the planetary boundary layer across Europe. Sub-micron aerosol chemical composition was measured using a compact Time-of-Flight Aerosol Mass Spectrometer (cToF-AMS). A range of sampling conditions were evaluated, including relatively clean background conditions, polluted conditions in North-Western Europe and the near-field to far-field outflow from such conditions. Ammonium nitrate and OA were found to be the dominant chemical components of the sub-micron aerosol burden, with mass fractions ranging from 20–50% each. Ammonium nitrate was found to dominate in North-Western Europe during episodes of high pollution, reflecting the enhanced NO_x and ammonia sources in this region. OA was ubiquitous across Europe and concentrations generally exceeded sulphate by 30–160%. A factor analysis of the OA burden was performed in order to probe the evolution across this large range of spatial and temporal scales. Two separate Oxygenated Organic Aerosol (OOA) components were identified; one representing an aged-OOA, termed Low Volatility-OOA and another representing fresher-OOA, termed Semi Volatile-OOA on the basis of their mass spectral similarity to previous studies. The factors derived from different flights were not chemically the same but rather reflect the range of OA composition sampled during a particular flight. Significant chemical processing of the OA was observed downwind of major sources in North-Western Europe, with the LV-OOA component becoming increasingly dominant as the distance from source and photochemical processing increased. The measurements suggest that the aging of OA can be viewed as a continuum, with a progression from a less oxidised, semi-volatile component to a highly oxidised, less-volatile component. Substantial amounts of pollution were observed far downwind of continental Europe, with OA and ammonium nitrate being the major constituents of the sub-micron aerosol burden. Such anthropogenically perturbed air masses can significantly perturb regional climate far downwind of major source regions.

Correspondence to: W. T. Morgan
(william.morgan@postgrad.manchester.ac.uk)

1 Introduction

The chemical composition of the atmospheric aerosol burden has significant implications for its climate impacts (e.g. Forster et al., 2007). Specifically, it plays a major role in determining the scattering or absorbing nature of the aerosol and has an important control upon its affinity for water uptake. Furthermore, the chemical composition of the particle phase is an important component of global and regional biogeochemical cycles (Andreae and Crutzen, 1997). These include the cycling of carbon, sulphur, nitrogen, oxygen and water. The spatial heterogeneity of the aerosol burden has significant implications for its subsequent impact. On regional scales, the direct effect of aerosols is capable of

Published by Copernicus Publications on behalf of the European Geosciences Union.

substantially reducing the impact of greenhouse gas radiative forcing, due to their competing cooling and warming effects respectively (Charlson et al., 1992). This is particularly evident over industrialized and heavily populated regions of the Northern Hemisphere such as North America, Europe and South-East Asia. Additionally, aerosols can alter the microphysical properties of clouds (e.g. Haywood and Boucher, 2000), leading to changes in the radiation balance of the climate system and also regional meteorology (Denman et al., 2007).

Several recent intensive field studies have sought to elucidate aerosol chemical composition and the processes which change it, with a focus upon their regional impacts. These include studies in Asia such as the Indian Ocean Experiment (INDOEX, Ramanathan et al., 2001) and North America such as the New England Air Quality Study (NEAQS, Bates et al., 2005; Kleinman et al., 2007; Wang et al., 2007), the International Consortium for Atmospheric Research on Transport and Transformation (ICARTT, Quinn et al., 2006; Williams et al., 2007; Brock et al., 2008; de Gouw et al., 2008) and the Megacity Initiative: Local and Global Research Observations (MILAGRO, DeCarlo et al., 2006; Kleinman et al., 2008; Baumgardner et al., 2009; Fast et al., 2009). Recent airborne studies in Europe have focused upon polluted environments in the Adriatic and Black Seas (Crosier et al., 2007) and the UK region (Morgan et al., 2009). A major conclusion of these European studies was the significant contribution of ammonium nitrate to the submicron particulate burden, particularly during highly polluted conditions. Zhang et al. (2007) presented a summary of numerous field studies in the Northern Hemisphere from the Aerodyne Aerosol Mass Spectrometer (AMS, Jayne et al., 2000; Canagaratna et al., 2007). A major theme of such analyses was the high proportion of Organic Matter (OM) contributing to the sub-micron particulate burden. The study by Zhang et al. (2007) indicated that the OM component was dominated by oxygenated species relative to Primary Organic Aerosol (POA) and that the mass fraction of the more oxidised component compared to the total organic mass increases away from urban environments. Comparison of such ambient measurements of Secondary Organic Aerosol (SOA) with atmospheric chemistry models reveals significant discrepancies between them (Volkamer et al., 2006, and references therein). Furthermore, such discrepancies increase as a function of photochemical age.

Coupling of a thermodenuder system with an AMS indicated that the SOA component could be separated in terms of their volatility, with more aged-SOA being less volatile than fresher-SOA (Huffman et al., 2009). Furthermore, the POA component was shown to be semi-volatile. Such results are consistent with recent frameworks which have treated the entire OM component as semi-volatile (Donahue et al., 2006; Robinson et al., 2007). This is in contrast to traditional modelling approaches that prescribe the POA to be non-volatile and inert (Donahue et al., 2009). Recently, such a framework has been implemented to explain OM volatility and composition variations both downwind of a megacity source and across a global ground-based dataset (Jimenez et al., 2009).

The present study seeks to elucidate the spatial distribution and chemical evolution of the sub-micron particulate mass across a broad range of scales, with particular emphasis upon the OM component and its contrasting behaviour compared to inorganic species. We do so using measurements drawn from two related aircraft campaigns across Northern Europe, a region that plays an important role in the global aerosol budget.

The major part of the analysis consists of measurements made during May 2008 as part of the European Integrated Project on Aerosol Cloud Climate and Air Quality Interactions (EUCAARI, Kulmala et al., 2009) airborne intensive study, known as the EUCAARI-LONG Range EXperiment (EUCAARI-LONGREX, henceforth referred to as LONGREX). These measurements are complemented by flight operations based out of the UK, which took place during April and September 2008 as part of the Appraising the Direct Impacts of Aerosol on Climate (ADIENT) project. A key aim of these projects is an evaluation of the relative contribution of particular chemical components to the aerosol burden. This includes characterisation of the multiple components which make up the OM burden, along with their subsequent evolution in the atmosphere. The present dataset is well placed to investigate processes governing the formation and transformation of atmospheric aerosol due to the broad range of spatial scales investigated.

2 Method

The UK Facility for Airborne Atmospheric Measurements (FAAM) BAe-146 research aircraft took part in the LONGREX campaign in conjunction with the Deutsches Zentrum für Luft-und Raumfahrt (DLR) Falcon 20-E5. The LONGREX campaign was closely coordinated with the Intensive Observation Period at Cabauw Tower (IMPACT), the second major part of the EUCAARI airborne intensive operational period, although the analysis presented here is based solely on data obtained during LONGREX. Principally, the BAe-146 operated within the planetary boundary layer, while the Falcon operated at high-altitude in the free troposphere. The Falcon operated a LIDAR system which included a High Spectral Resolution LIDAR mode (HSRL, Esselborn et al., 2008) delivering aerosol backscatter and extinction coefficients. Real time LIDAR data were utilised during flight operations to identify the location of pollution plumes, which were subsequently sampled in-situ by the BAe-146. Flight operations were conducted across Northern Europe from the 6–22 May. A period of stable anticyclonic conditions characterised the first eight days of the project from the 6–14 May. Two more flights were conducted during LONGREX over the 21–22 May period,

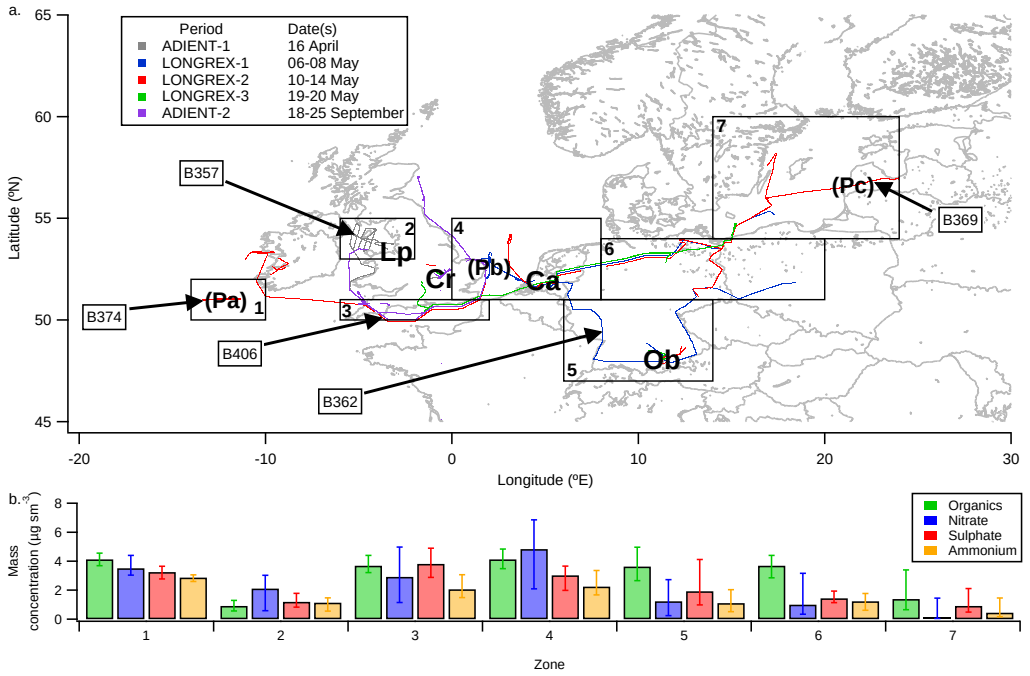

Fig. 1. **(a)** Flight tracks of the BAe-146 considered by this analysis for segments below 3000 m. The periods identified in the figure are described in the main text and Table 1. Overlapping flight tracks are offset slightly in order to clearly discern them. The flight numbers and arrows refer to the example flights discussed in the main text. Locations relevant to this study are marked, including Liverpool (Lp), Cranfield (Cr), Cabauw (Ca) and Oberpfaffenhofen (Ob). The locations of the vertical profiles displayed in Fig. 3 are indicated by the Pa (Profile-a), Pb (Profile-b) and Pc (Profile-c) markers. **(b)** Summary of the AMS median mass concentrations for each zone identified in **(a)**. The vertical bars represent the 25th and 75th percentiles.The percentile concentrations are included in the Supplementary materials in Table S3 (http://www.atmos-chem-phys.net/10/4065/2010/acp-10-4065-2010-supplement.pdf).

which was characterised by predominantly easterley conditions. Flights from LONGREX are considered along with the ADIENT flights from April and September 2008. The ADIENT flights were conducted in differing meteorological conditions, with the April flight conducted in south-easterley conditions, while the September flights took place during easterley conditions with similar transport patterns to the LONGREX period. The flight tracks are shown on Fig. 1 and are coloured according to the different flying periods and conditions. The meteorological conditions for the different periods are relatively consistent in terms of their transport patterns, with air masses advecting pollution from continental Europe downwind to either the UK region or the Eastern Atlantic Ocean (see Supplementary Materials Sect. 2, Figs. S1 and S2; http://www.atmos-chem-phys.net/10/4065/2010/acp-10-4065-2010-supplement.pdf). Some flights concentrated on instrument testing/calibration and are not included in the analysis. During some flights instrument performance was not optimal; data from these 3 flights have not been included. The flights included in this analysis are summarised in Table 1.

2.1 Instrumentation

The FAAM BAe-146 research aircraft houses a suite of instruments capable of resolving the chemical composition, microphysical, optical and hygroscopic properties of the in-situ aerosol population. Inboard aerosol instrumentation samples ambient air via stainless steel tubing from Rosemount inlets (Foltescu et al., 1995). Sub-micron particle losses have been shown to be negligible (Osborne et al., 2007). Number size distributions were measured using a wing-mounted Particle Measurement Systems (PMS) Passive Cavity Aerosol Spectrometer Probe 100X (PCASP, Liu et al., 1992; Strapp et al., 1992). The PCASP instrument optically counts and sizes particles between 0.1–3 μm diameter across 15 channels. Particle size is determined via experimental calibrations using Di-Ethyl-Hexyl-Sebacate (DEHS), which is converted to a Polystyrene Latex Sphere (PSL) equivalent size. Black Carbon (BC) mass and the number of particles containing a BC core were characterised as a function of particle size using a Droplet Measurement Technologies (DMT) Single Particle Soot Photometer (SP2, Stephens et al., 2003; Baumgardner et al., 2004). The SP2 was modified to include a two-element avalanche photodiode to improve determination of the optical size of absorbing

Table 1. Flight summary for ADIENT (B357, B401-B406) and LONGREX (B362-B380) operations included in this study. All flights were conducted during 2008. The predominant meteorological conditions present are summarised, where SE refers to south-easterley, E refers to easterley and HP refers to the high pressure system during the initial LONGREX flights described in the main text. Also included is an indication of which period each flight took place during, which are abbreviated as A1 (ADIENT-1) and A2 (ADIENT-2). The LONGREX flights refer to the 3 periods in the main text, which are referred to as LONGREX-1 (L1), LONGREX-2 (L2) and LONGREX-3 (L3).

Flight	Date	Meteorology	Period	Operating Region
B357	16 April	SE	A1	North-West UK coast
B362	6 May	HP	L1	North-Western Europe & North Sea
B365	8 May	HP	L1	Eastern Europe & Baltic Sea
B366	8 May	HP	L1	North-Western Europe
B369	10 May	HP	L2	Baltic Sea
B370	12 May	HP	L2	North-Western Europe & North Sea
B371	12 May	HP	L2	North-Western Europe & North Sea
B373	13 May	HP	L2	Southern UK coast
B374	14 May	HP	L2	Eastern Atlantic
B379	21 May	E	L3	North-Western Europe
B380	22 May	E	L3	North-Western Europe and Southern UK coast
B401	18 September	E	A2	Southern UK coast
B402	19 September	E	A2	Eastern UK coast
B406	25 September	E	A2	Southern and Western UK coasts

particles (Gao et al., 2007). Additionally, gas phase concentrations of CO (Carbon Monoxide), O_3 (Ozone) and NO_x (defined as the sum of NO (Nitric Oxide) and NO_2 (Nitrogen Dioxide)) were measured. The facility also provides aircraft position information and measurements of standard atmospheric variables, such as temperature and relative humidity.

Measurements made by an Aerodyne compact Time-of-Flight Aerosol Mass Spectrometer (cToF-AMS, Drewnick et al., 2005; Canagaratna et al., 2007) form the major part of this study. The instrument provides the capability to quantitatively measure the size-resolved chemical composition of non-refractory particulate matter, including OM, sulphate, nitrate, ammonium and chloride. A major advantage of the cToF-AMS is the ability to provide high time resolution measurements with enhanced precision and sensitivity. Thus it is ideal for airborne deployments. Previous studies (Crosier et al., 2007; Capes et al., 2008; Morgan et al., 2009) have detailed the AMS sampling strategy onboard the BAe-146. The sampling losses for the cToF-AMS inlet system were estimated experimentally to be approximately 10% by number across the size range of the AMS. This was accomplished by comparing a Condensation Particle Counter (CPC) upstream of the inlet system with one situated immediately prior to the sampling orifice of the AMS while sampling monodisperse aerosol. Details specific to the cToF-AMS data analysis will be discussed in the following subsection.

2.2 AMS data quantification

The AMS data analysis was performed using the standard SQUIRREL (SeQUential Igor data RetRiEvaL) ToF-AMS software package. Mass spectrum deconvolution is accomplished using the fragmentation table approach described by Allan et al. (2004). Error estimates are generated according to the model documented by Allan et al. (2003). Mass concentrations derived from the AMS are reported as micrograms per standard cubic metre ($\mu g\,sm^{-3}$) i.e. at a temperature of 273.15 K and pressure of 1013.25 hPa. Power was unavailable to the AMS between flights due to operational constraints. Through the use of plug valves to isolate the AMS chamber, a vacuum of typically less than 0.5 Torr is maintained while the turbo-pumps are powered down. Ionisation efficiency (IE) calibrations were performed regularly before and after each flight during the flying periods. Values determined from both pre-flight and post-flight calibrations (i.e. taking place on the same day) exhibited little variability. Post-flight values were used as these were considered to be more reliable compared with pre-flight values due to the reduced instrument background post-flight. A faulty ground power unit during LONGREX caused a loss of power to the aircraft prior to flight B365 while the AMS was pumping down. This led to slightly enhanced background concentrations in the AMS vacuum chamber due to a filament failure associated with the power loss during flights B365–B369.

Recent laboratory evidence (Matthew et al., 2008) suggests that the AMS Collection Efficiency (CE, Huffman et al., 2005) is significantly modulated by particle phase. Previous AMS data collected in Europe on the BAe-146

has used a CE correction following the principle developed by Crosier et al. (2007). This was developed using a simple empirical treatment of the CE as a linear function of the nitrate content of the aerosol based upon comparison of AMS sulphate with filter measurements. Matthew et al. (2008) conducted a detailed laboratory study of the AMS CE across a range of compositions. Their study included a comparison of their laboratory derived correction with the Crosier et al. (2007) parameterisation. This indicated that the simpler linear treatment overestimated the CE at intermediate ammonium nitrate mass fractions. A comparison between the two techniques as part of this work revealed that the two approaches showed a maximum discrepancy at intermediate ammonium nitrate mass fractions that did not typically exceed 25% and was considerably less at high and low mass fractions. Consequently, we use the correction developed by Matthew et al. (2008) to estimate the CE of the AMS in this study. The AMS total mass concentrations were converted to total volume concentrations using the densities reported by Cross et al. (2007), which correspond to 1.27 g cm^{-3} for organics and 1.77 g cm^{-3} for inorganics. Comparison of the estimated AMS total volume with the PCASP indicates that campaign average agreement was within 30% (see Supplementary Materials Sect. 3, Fig. S4; http://www.atmos-chem-phys.net/10/4065/2010/acp-10-4065-2010-supplement.pdf). This is within the 30–50% uncertainty previously reported for PCASP volume concentration estimates (e.g. Moore et al., 2004; Hallar et al., 2006). All flights fall within the 50% agreement range except for B357. The uncertainties in the estimate are large due to the high sensitivity of the volume calculations to diameter (proportional to diameter^3) and the uncertainties in density required to convert the AMS mass to volume.

3 Spatial distribution of aerosol chemical composition across Europe

The differing spatial scales and meteorological contexts considered by this analysis provide a thorough examination of the aerosol chemical composition in Europe during anticyclonic conditions. The distribution of the chemical components measured by the AMS will be discussed here in order to set the context for the subsequent analysis and discussion. Both the broader scale and flight period/condition specific details will be summarised. The flight periods were split according to the period in which they were conducted and their general meteorological conditions. Their designations are summarised in Table 1 and Fig. 1.

The spatial distribution of the total OM for Straight and Level Runs (SLRs) below 3000 m is shown for the entire dataset in Fig. 2. The boundary layer height was predominantly below 2000 m but during some conditions, an elevated planetary boundary layer was observed so 3000 m was used as a threshold altitude. The distribution indicates that OM is

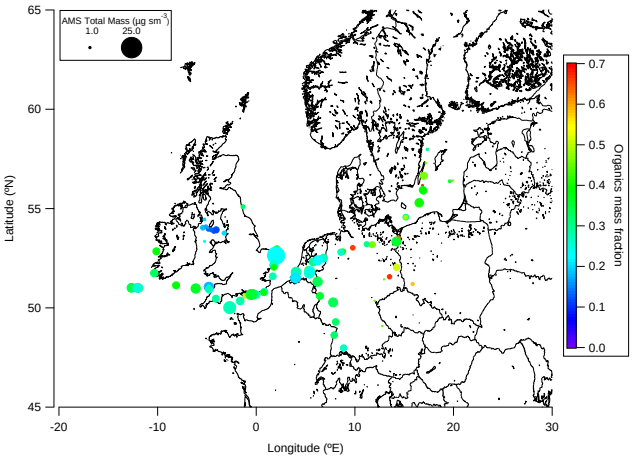

Fig. 2. AMS total mass concentrations (symbol size) and organic mass fraction (symbol colour) for low-level Straight and Level Runs (SLRs < 3000 m). Median values are reported for both symbol size and symbol colour.

a major contributor to the sub-micron aerosol burden, with typical mass fractions from 20–50%. Importantly, OM is a significant component during both background and highly polluted conditions. This is illustrated in Fig. 2, as the OM mass fraction almost always accounts for more than 20% of the total mass measured by the AMS.

The absolute and relative contributions of the chemical components measured by the AMS can be discerned from Fig. 1b. The flight data have been separated into different zones representing the main areas and emission fields sampled across Northern Europe and average composition data has been determined for each area. The OM concentration is typically 1.4–2.6 times greater than that of sulphate further east (zones 4–5) and is the dominant component mass in submicron aerosol in central and eastern Europe (zones 5 and 6), while in zones further west, the OM and sulphate mass concentrations are comparable. Sulphate contributes approximately 1.0–4.0 µg sm^{-3} to the regional aerosol burden, with typical mass fractions of 10–30%. The spatial distribution of nitrate indicates large gradients in the concentration and relative contribution of this component. In particular, the nitrate mass concentration is enhanced in North-Western Europe compared to locations further east. In terms of its relative contribution, nitrate accounts for approximately 20–50% of the sub-micron mass across a wide range of locations and conditions. Furthermore, increases in the nitrate concentration are associated with enhanced total mass loadings, indicating that nitrate is a significant contributor under highly polluted conditions. Examination of the sulphate, nitrate and ammonium concentrations indicate that the aerosol was neutralised, thus sulphate is present in the form of ammonium sulphate and nitrate is in the form of ammonium nitrate.

The ADIENT-1 period focuses on one flight (B357, zone 2), which was conducted in the large-scale outflow

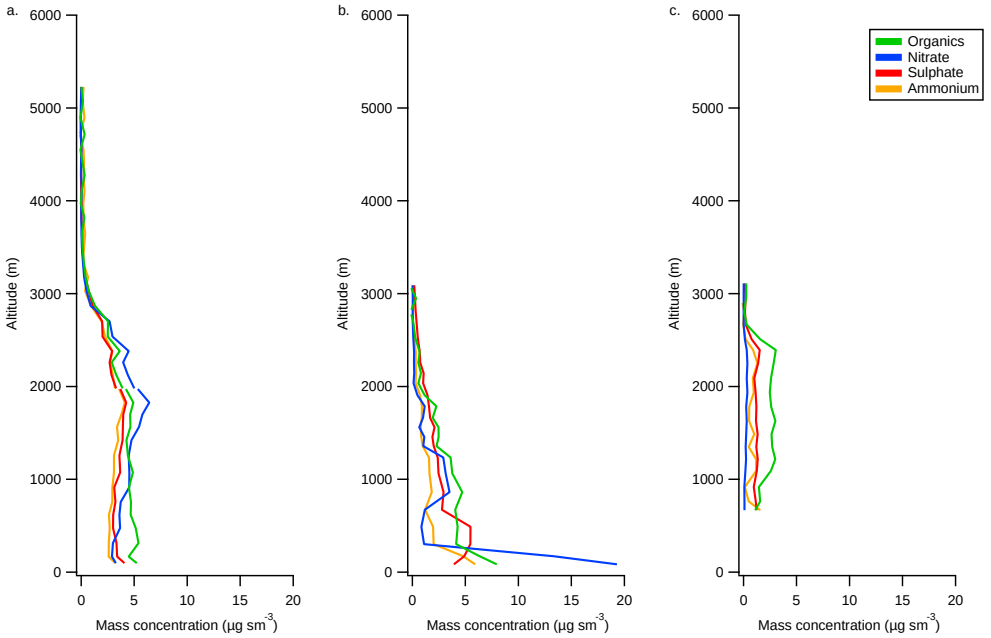

Fig. 3. Vertical profiles of aerosol chemcial composition from **(a)** B374 in the Eastern Atlantic (zone 1), **(b)** B362 in the North Sea off the UK east coast and **(c)** B369 over Latvia in North-Eastern Europe. The profile locations are marked on Fig. 1a.

from continental Europe and the southern UK along the UK's western edge. The flight included close to source sampling downwind of Manchester and Liverpool, in the north-west of England (identified on Fig. 1). During this flight, the secondary aerosol species' mass concentrations were reduced when compared to the other periods. This is potentially a consequence of reduced photochemistry as the flight took place earlier in the year than the LONGREX and ADIENT-2 flying.

Analysis of the high pressure phase of LONGREX indicated significant differences in gas-phase and particulate loadings, which could be categorised into two distinct meteorological periods. During the initial phase of LONGREX from the 6–8 May (referred to as LONGREX-1), the air mass trajectories displayed a more zonal flow from east-to-west. The second phase from the 10–14 May (henceforth referred to as LONGREX-2) is characterised by the then well established high pressure system centred over northern Germany and Denmark, yielding more rotational anticyclonic flow. The LONGREX-1 period was characterised by enhanced CO and NO_x levels compared to the second period. These strong signatures of urban pollution on the regional scale correlated with significant amounts of secondary material, with total mass concentrations reported by the AMS exceeding 25 µg sm^{-3}. Such instances were dominated by ammonium nitrate and OM. Such conditions were also prevalent during the LONGREX-3 and ADIENT-2 flying periods. These aforementioned periods concentrated upon sampling close to major anthropogenic sources and the immediate near-field downwind evolution of such sources.

The major distinction between LONGREX-2 and the operations conducted in each of the other identified periods was the large spatial scale sampled, where the measurements extended from the Baltic Sea region in Northern Europe, to the Eastern Atlantic Ocean, off the southern Irish coast. The operations represented approximately 3000 km and approximately 4–5 days of air mass transit based on air mass back trajectories. These were derived from European Centre for Medium-Range Weather Forecasts (ECMWF) wind fields, initialised from the SLRs in the east-Atlantic (51 N, 12 W). During the LONGREX-2 period, when NO_x and background CO levels were reduced, the mass concentration of ammonium nitrate was diminished in North-Western Europe. In terms of the median AMS aerosol concentrations, LONGREX-2 was similar to LONGREX-1 in terms of sulphate and OM, while nitrate was reduced. The main difference between the periods was the absence of the more intense ammonium nitrate concentrations, which contributed to the significant pollution episodes encountered during LONGREX-1. The operations in the Eastern Atlantic probed total sub-micron mass loadings from the AMS exceeding 15 µg sm^{-3} with OM and ammonium nitrate being the dominant chemical components. The Falcon's HSRL measured aerosol optical depth values from 0.3–0.5 in these conditions far downwind of the major source regions in Western Europe.

Vertical profiles of aerosol chemical composition are shown in Fig. 3 from the LONGREX-1 and LONGREX-2 periods. The location of each profile are shown in Fig. 1. The profiles represent the broad range of conditions sampled,

with the cleaner conditions in the Baltic region (panel C, zone 7), the immediate outflow from North-Western Europe into the North Sea (panel B, zone 4) and the outflow from continental Europe far downwind in the Eastern Atlantic (panel A, zone 1). The profiles show that the boundary layer typically extended to between 2000–3000 m, the actual height of which as determined by the location of the measurements in relation to the centre of the high pressure system. Also evident in panel B is the strong increase in concentrations close to the sea surface, which was coincident with a shallow moist layer where concentrations of both ammonium nitrate and OM increased significantly. Also discernible is the increase in sulphate at lower levels (below 1000 m) which is likely attributable to shipping activities. This was also observed in zone 3, which covers the English Channel region, where sulphate concentrations increased and the largest sulphate mass fractions were observed. Further details and observations regarding the vertical distribution of aerosol chemical composition are discussed in Morgan et al. (2010) in the EUCAARI special issue.

The following analysis and discussion will focus upon the evolution of the ubiquitous OM component across the full range of spatial scales investigated. This is accomplished using a factor analysis technique which will be presented and discussed in the following section. The results of this analysis will then be used to probe the evolution of the OM component and contrast it with the observed gradients in the ammonium nitrate and ammonium sulphate fields across Europe.

4 Factor analysis of organic aerosol: technique and discussion

Several recent studies have employed various factor analysis techniques in order to deconvolve the organic mass spectra derived from ambient AMS measurements (e.g. Zhang et al., 2005a,b; Lanz et al., 2007, 2008; Ulbrich et al., 2009). With the exception of biomass burning, wood combustion or urban environments with a prevalent cooking signature, such studies have attributed the OM component to be a combination of Hydrocarbon-like Organic Aerosol (HOA) and Oxygenated Organic Aerosol (OOA). These two factors commonly explain more than 90% of the variance in the ambient organic mass spectra (McFiggans et al., 2005; Zhang et al., 2005a; Rudich et al., 2007). Furthermore, such factors remain relatively constant across differing environments. Several studies (e.g. Lanz et al., 2007; Zhang et al., 2007; Ulbrich et al., 2009) have identified multiple OOA factors, which have been classified according to their level of oxidation.

Jimenez et al. (2009) characterised the evolution and volatility of these multiple OOA components using the terms Low-Volatility OOA (LV-OOA) and Semi-Volatile OOA (SV-OOA). These terms represent the OOA-1 and OOA-2 components identified in previous studies (e.g. Lanz et al., 2007; Ulbrich et al., 2009), though Jimenez et al. (2009) demonstrated that these factors were systematically correlated with lower and higher volatile fractions of the OM. LV-OOA is distinguished by the predominance of signal at *m/z* 44 (corresponding to the CO_2^+ ion arising from decarboxylation on the vaporiser surface). SV-OOA components typically exhibit enhanced signal at *m/z* 43 ($C_2OH_3^+$ and $C_3H_7^+$) and reduced signal at *m/z* 44, when compared to LV-OOA mass spectra. Examination of high-resolution AMS data has demonstrated the dominance of the $C_2OH_3^+$ ion at *m/z* 43 in ambient spectra when the contribution of OOA is high (Mohr et al., 2009). Thus this SV-OOA component represents a less oxidised OM fraction. Jimenez et al. (2009) argue that the atmospheric OOA evolves through a dynamic aging process of continual repartitioning between the particle and gas phases, which leads to a more oxidised, less volatile and more hygroscopic aerosol. Thus the initial OOA, which resembles SV-OOA, undergoes transformation processes that ultimately result in an OOA that exhibits LV-OOA like characteristics. Following this framework, the present analysis strives to simplify the OM burden into a limited number of key factors in order to probe their relative magnitudes, relations and evolution across Europe for the first time.

4.1 Positive Matrix Factorisation (PMF)

Positive Matrix Factorisation (PMF, Paatero and Tapper, 1994; Paatero, 1997) was utilised in order to accomplish some simplification of the OM burden. Several recent studies have detailed its application to AMS data (Lanz et al., 2007; Docherty et al., 2008; Ulbrich et al., 2009; Aiken et al., 2009). PMF employs a receptor-only factorisation model, which is based on mass conservation. The model assumes that a dataset matrix is comprised of a linear combination of factors with constant profiles, which have varying contributions across the dataset. The model employs the constraint of positive values upon the profiles and contributions. This work will follow the procedures identified by Ulbrich et al. (2009) in order to apply the PMF technique to AMS data. Version 4.2 of the PMF2 algorithm (provided by the University of Helsinki) is employed in robust mode to perform the factorisation.

The sampling and data collection strategy detailed in Sect. 2.2 resulted in the requirement that PMF be applied to each flight separately. Application of PMF to the whole dataset in one single matrix was found to be problematic due to the subtle changes in instrument performance across the 6 month flying period considered by this study coupled with the broad range of scales examined. Such changes impact the retrieved factors as instrument performance changes dominate the variability in the dataset, rather than the atmospheric processes and sources of interest here. Vertical profiles of temperature and AMS chemical composition indicated that the boundary layer top was typically between 2000–3000 m. Only data from below 3000 m was included in the analysis as we wish to consider boundary layer processes only and the

pollution transport was restricted to the boundary layer. Also, we do not wish to include data from above the boundary layer as purely free tropospheric factors would be virtually impossible to discern due to signal-to-noise constraints.

The analysis was limited to *m/z* channels less than 200 due to low signals at higher masses and thus minor contributions to the OM. Four flights during LONGREX suffered from enhanced background concentrations and the analysis was performed on *m/z* channels smaller than 100 in these cases due to enhanced residuals at larger *m/z* values. Intense organic mass concentrations, which were predominantly present for single data points, led to short pulses in the value of the scaled residual. These events were often associated with local sources close to airfields upon landing or takeoff. Such instances are not well constrained by a single factor although their occurrence is relatively infrequent and are not representative of the regional scale composition of interest to this study. Consequently, such points are omitted from the analysis.

The ability to rigourously compare the factor solutions from both individual and different flights was the primary objective of the analysis. Thus, the identification of the most appropriate factor solution is determined based upon consistency and objectivity across the range of conditions encountered by the dataset. A detailed discussion of the methodology used in the PMF analysis and examples of the solutions for individual flights and a summary of the retrieved solutions for all of the flights considered are included in the Supplementary Materials Sect. 5 (http://www.atmos-chem-phys.net/10/4065/2010/acp-10-4065-2010-supplement.pdf).

4.2 Results of the factor analysis

For the purposes of the subsequent discussions, the retrieved factor components are classified according to their level of oxidation, which is signified by their relative organic intensity at *m/z* 44. Thus, factors with the greatest *m/z* 44 signal are designated OOA-1 with subsequent factors designated as OOA-2, OOA-3 etc. This is conceptually similar to the nomenclature introduced by Lanz et al. (2007) and is used to initially compare the retrieved factors with reference mass spectra and external tracers. These will then be discussed in terms of their resemblance to LV-OOA, SV-OOA and HOA factors derived by Jimenez et al. (2009).

For all of the flights considered, two factor solutions were found to be the most appropriate; one that is highly oxidised (OOA-1) and a second that is less oxidised (OOA-2), which often represented a combination of HOA with fresher OOA components. The factors were chosen based upon comparison with reference mass spectra, external tracers and their numerical stability. Case study examples of a range of flights in differing conditions are presented in the Supplementary Materials (Sect. 5) (http://www.atmos-chem-phys.net/10/4065/2010/acp-10-4065-2010-supplement.pdf). When more than two factors were chosen, the solutions were found to be numerically unstable based upon a bootstrapping analysis (Ulbrich et al., 2009, and references therein), where random resampling of the data matrix is performed in the time dimension.

The retrieved factors for the 2-factor solutions were compared with reference mass spectra in Fig. 4a. OOA-1 type mass spectra were highly correlated ($r>0.9$) with fulvic acid across the dataset and variability in the retrieved mass spectrum was low. Furthermore, the OOA-1 profiles had low correlation with the reference HOA mass spectrum from Pittsburgh ($r<0.45$ for all cases). The OOA-2 component typically exhibits enhanced signal at *m/z* 43 relative to signal at *m/z* 44, when compared to the OOA-1 mass spectra. The OOA-2 components had lower correlations with fulvic acid. The OOA-2 also exhibited greater correlation with the reference HOA spectrum with coefficients ranging from 0.5–0.9. This is unsurprising given that we have not separated the HOA contribution from the fresher-OOA component. The correlations of OOA-2 with fulvic acid and reference HOA reflect the chemical variation in the OOA component as they are anti-correlated with each other. Thus, as the OOA-2 becomes more oxidised it resembles HOA less and approaches a more LV-OOA or fulvic acid-like mass spectrum.

Previous studies (e.g. Lanz et al., 2007; Ulbrich et al., 2009) have reported that the time series of nitrate and OOA-2 show a close coupling, thus exhibiting an enhanced correlation coefficient. Similarly, OOA-1 and sulphate have been shown to exhibit enhanced correlation coefficients. Figure 4a displays the correlation coefficients for OOA-1 and OOA-2 with sulphate and nitrate in order to compare with previous results. The results from this study somewhat corroborate previous findings regarding such associations but some flights indicate substantial differences. Nitrate and OOA-2 are frequently found to be well correlated ($r>0.7$) but the same is also true for nitrate and OOA-1. The high correlations between nitrate and OOA-2 principally occur closer to source regions due to their semi-volatile nature. The examples of high correlation of nitrate and OOA-1 are further away from source due to the ammonium nitrate concentration being sustained downwind, while the OOA-2 has been processed to OOA-1. The most stark example of this is B374, where nitrate and OOA-2 are anti-correlated while nitrate and OOA-1 are highly correlated. B374 took place far downwind of the major sources in continental Europe in the Eastern Atlantic Ocean, where the air mass had aged significantly and little precipitation had occurred upwind. Once formed, ammonium nitrate exists in a chemical equilibrium with ammonia and nitric acid, the losses of which are via dry and wet deposition only. This contrasts with OOA, which undergoes complex and continual processing involving repartitioning and oxidation. Thus the OM transforms from more volatile to less volatile condensable products as the air parcel ages downwind of source. Thus the OM is dominated by the more-oxidised form downwind of the major emission sources and is then well correlated with ammonium nitrate.

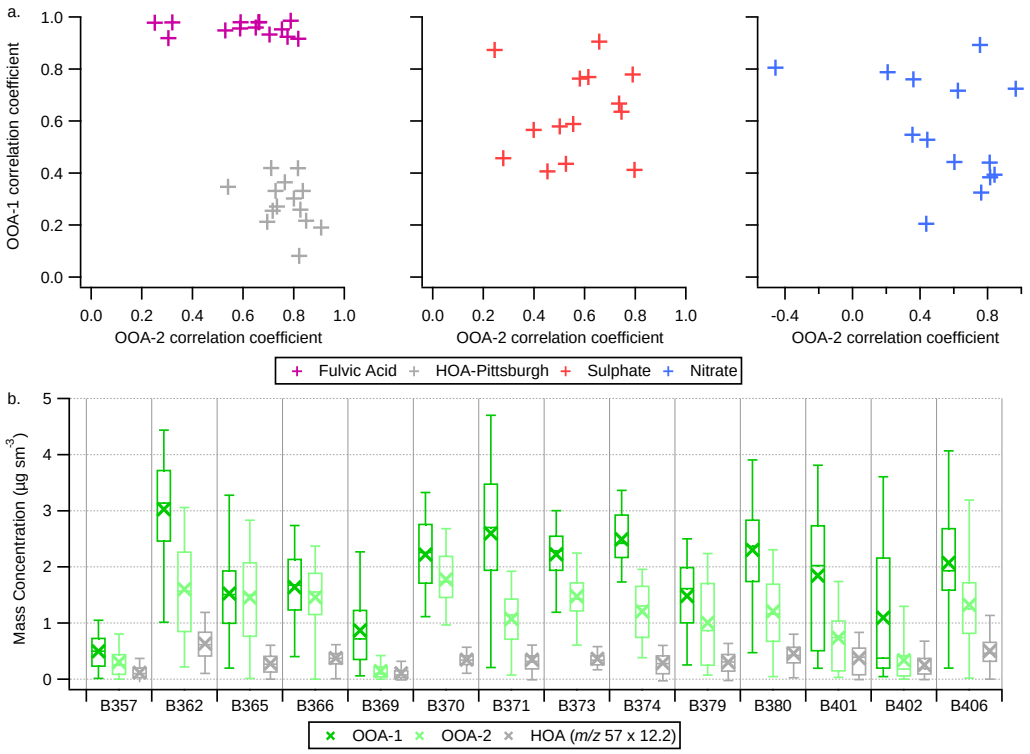

Fig. 4. (a) Summary of correlations for OOA-1 and OOA-2 with both reference mass spectra and external time series. Uncentered correlation coefficients are used for the mass spectra, while Pearson's R are used for the external time series. The fulvic acid mass spectrum is from Alfarra et al. (2004) and the HOA-Pittsburgh refers to to the deconvolved HOA solution from Zhang et al. (2005a). **(b)** Boxplot summary statistics of OOA-1, OOA-2 and estimated HOA mass concentrations for each flight considered in the analysis. Crosses represent the mean value, while horizontal lines represent the 25th, 50th and 75th percentiles. The whiskers represent the 5th and 95th percentiles.

Sulphate is often well correlated with OOA-2 and OOA-1, which is likely due to the regional nature of these measurements and the covariance between the different chemical species. Thus factor interpretations where multiple OOA components are identified need to consider the meteorological, photochemical and geographical context at individual sampling locations when making suppositions based upon comparison with other secondary particulate species.

Given that the OOA-2 component generally contains a HOA contribution, it is desirable to estimate the relative importance of the primary versus secondary components. Some previous studies have included first order estimates of OM components based upon absolute intensities at specific mass spectral markers by comparing such markers with factor component solutions (e.g. Zhang et al., 2005a; Aiken et al., 2009). Zhang et al. (2005a) reported that the HOA mass concentration can be approximated based upon a linear scaling of the signal intensity at *m/z* 57. Aiken et al. (2009) reported a similar relationship but with an additional correction for oxidised fragments associated with *m/z* 57 based upon the organic signal intensity at *m/z* 44. In order to derive an approximate estimate of the contribution of HOA to the OM burden in this dataset, these first order estimates are used.

While such estimations are not fully quantitative, they do at least represent an approximate reference point which provides a level of justification for the decision to limit the analysis to the 2-factor solution sets. Furthermore, the estimated HOA is typically less than the OOA-2 concentration reported from the factor analysis. An important observation is that the enhanced HOA mass fractions are predominantly driven by the reduced contribution from secondary species, rather than a major increase in the absolute HOA mass loading.

The Aiken et al. (2009) estimate was found to be inappropriate for this dataset as the *m/z* 57 contribution was often close to zero, while the organic intensity at *m/z* 44 was typically an order of magnitude greater. This led to negative HOA concentrations frequently being estimated using this approximation. The solutions for the entire dataset are summarised in Fig. 4b by comparing the absolute mass concentrations for the OOA-1, OOA-2 and estimated HOA. The HOA contribution is calculated using the estimation from Zhang et al. (2005a) and indicates that the median concentration is typically less than $0.5\,\mu g\,sm^{-3}$, with concentrations rarely exceeding $1\,\mu g\,sm^{-3}$. Such a result indicates that HOA typically contributes 5–20% to the regional OM burden, which is in line with previous studies (Zhang et al.,

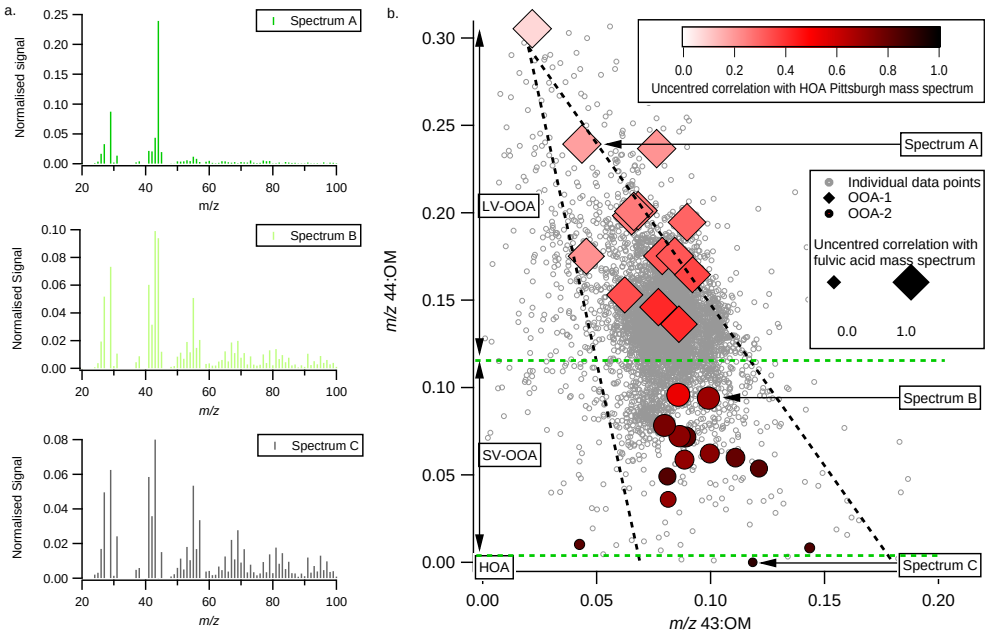

Fig. 5. **(a)** Examples of mass spectra derived from the PMF analysis. **(b)** Relationship between the fractional signal at *m/z* 44 normalised to the total organic loading and *m/z* 43 normalised to the total organic loading. Grey markers refer to individual data points from all of the flights. Diamond and circle markers denote the same measures from the high and low oxygenated factors (OOA-1 and OOA-2) identified from the PMF analysis, coloured and sized according to their correlation with Pittsburgh HOA and laboratory derived fulvic acid respectively. The mass spectra shown in (a) are identified on (b) by the arrow and text box. The thick dashed black lines refer to guidelines from Ng et al. (2009) discussed in the main text. The dashed green lines refer to guideline bounds for the different PMF clusters identified as LV-OOA, SV-OOA and HOA.

2007). Consequently, the dataset indicates that the OOA component dominates the OM burden across Europe on the regional scale, thus this will be the focus of the subsequent discussion.

4.3 Interpretation of the factor analysis

Typical example mass spectra from different flights from the 2 factor solutions are presented in Fig. 5a. Spectrum A is highly consistent with LV-OOA, with the spectrum being dominated by normalised organic signal intensity at *m/z* 44 and with a correlation coefficient of 0.99 with fulvic acid. This spectrum is taken from flight B366, as is spectrum B which is distinguished by the normalised *m/z* 43 and 44 peaks being almost equal. This is consistent with SV-OOA spectra (e.g. Ulbrich et al., 2009; Jimenez et al., 2009) and the relative concentration of this component versus the HOA estimated suggests it is dominated by OOA. Spectrum C is the B357 HOA-type factor which had a correlation coefficient of 0.91 with the reference HOA spectrum. This factor is likely dominated by HOA-like components rather than OOA. A key feature of these example spectra is the changing normalised signal intensities at *m/z* 43 and 44, with HOA being dominated by *m/z* 43, SV-OOA being closer to a 1:1 ratio and LV-OOA being dominated by *m/z* 44.

This is illustrated in Fig. 5b by the relationship between the organic signal intensity at *m/z* 43 and 44, which are both normalised to the total OM loading. Both individual data points from all of the flights and the normalised signal intensities from the resolved factor components for each flight are shown. This shows that as the *m/z* 43:OM ratio decreases, the *m/z* 44:OM ratio increases. This is suggestive of the OM burden aging as a continuum in terms of its oxygen content from freshly formed OOA, through to highly aged OOA which exhibits a high resemblance to fulvic acid-like mass spectra. The flight operations, given their transient nature, tend to probe this continuum which is a consequence of the constant evolution of the OM component on the regional scale. This is consistent with the difficulty in separating the OOA from the HOA in the factor analysis. The relative contribution of *m/z* 43 and 44 to the PMF factor components also vary from flight to flight. Clearly, while the generic terms OOA-1 and OOA-2 have been widely used to label different factors retrieved by PMF analysis, they are not chemically identical but vary from one dataset to another. Hence they also exhibit this continuum feature which can be seen in Fig. 5b. The mass spectra shown in Fig. 5a are identified on Fig. 5b in order to distinguish the general classification of the OM components. The factor components retrieved by this dataset indicate that the OOA-1 and OOA-2 are separated in terms

of their *m/z* 44:OM ratio, with OOA-2 being less than 0.10 and OOA-1 being greater than 0.14. This is reflected by the green dashed horizontal line on Fig. 5b between these two clusters. B357 is the only flight where the second factor is interpreted as being dominated by HOA rather than SV-OOA due to its high resemblance to reference spectra and good agreement with literature values for POA to primary emission tracers. The two factors (from B365 and B371) which also exhibit reduced signal at *m/z* 44 do not agree as well with such literature values. Furthermore, they are partially oxidised (*m/z* 44=0.01) and as shown in Fig. 4b, their absolute concentrations are significantly greater than the estimated HOA. Thus the second green dashed horizontal line is used to separate the B357 factor from the other OOA-2 components identified. The identified continuum is consistent with a PMF analysis of a worldwide AMS ground-based dataset by Ng et al. (2009). The black dotted lines in Fig. 5b show the general relationship between the *m/z* 44:OM ratio and the *m/z* 43:OM ratio from this worldwide dataset.

Based upon the framework presented by Jimenez et al. (2009), we classify the OOA-1 components as LV-OOA and the OOA-2 as SV-OOA except for the B357 OOA-2 factor, which is classified as HOA. Aiken et al. (2008) showed that the contribution of *m/z* 44 to the OM is an excellent proxy for the Oxygen-to-Carbon (O:C) ratio of OM. Such an observation is attributed to SOA formation and photochemical aging. Thus the observed continuum of organic evolution is reflected by progressive aging from a SV-OOA dominated burden to a LV-OOA dominated burden.

The separation of the factor profiles in terms of their normalised *m/z* 44 signal highlights that retrieved PMF profiles tend to be strongly determined by the extremes in the examined dataset as the actual data predominantly fall within a band of relatively oxidised OM between 0.10–0.20. The extremes on either side of this band are representative of very fresh and very aged OM respectively. The key question regarding this analysis technique is whether static PMF factor profiles are capable of reflecting changes in a continuum i.e. is it possible to simplify the observed evolution using such a limited number of factors? The variability in terms of the mass spectral fingerprints of the LV-OOA and SV-OOA components shown in Fig. 4b highlight this point. Such variations are likely a complex combination of both atmospheric/chemical processes and instrumental variability from flight to flight (and also within a single flight). Ng et al. (2009) show the same phenomenon in their multiple ground-based dataset. In order to test whether the mass fractions of LV-OOA and SV-OOA can replicate the evolution in the *m/z* 44:OM ratio, correlation coefficients for each flight are calculated. The LV-OOA organic mass fraction and *m/z* 44:OM have a correlation coefficient ranging from 0.55–0.98 across the dataset (see Supplementary Material Fig. S11; http://www.atmos-chem-phys.net/10/4065/2010/acp-10-4065-2010-supplement.pdf). This indicates that the dataset can reproduce the evolution in the OM by comparing the relative concentrations of the LV-OOA and SV-OOA components. Thus the retrieved factors reflect the continuity of processing by increased oxidation in the atmosphere, consistent with the processing paradigm proposed by Jimenez et al. (2009).

5 Evolution of the organic aerosol component

5.1 Transformation across Europe during a anticyclonic case study

The LONGREX-2 period presents an opportunity to probe the evolution of the chemical composition across the regional scale due to the consistent meteorological situation and reduced influence of wet deposition. Geopotential height fields and air mass back trajectories during the period are included in Supplementary Material Sect. 2, Fig. S3 (http://www.atmos-chem-phys.net/10/4065/2010/acp-10-4065-2010-supplement.pdf). The flight operations conducted during the period are summarised in Fig. 6a, where absolute mass concentrations between 250–2500 m are shown as a function of longitude. Points above 2500 m were generally outside of the boundary layer so are not included. Points lower than 250 m are omitted due to the formation of shallow layers over the sea surface decoupled from the atmosphere above. These were frequently encountered in marine regions sampled in this study. Such features, while interesting, are considered unrepresentative of the evolution of the chemical composition on the European scale. The aircraft flew on a roughly east-to-west transect across Northern Europe over the course of 4 days. At longitudes between 20 E and 25 E, concentrations were typically low ($\approx$1 µg sm^{-3} for sulphate and organics) and constituted background conditions relative to the other locations sampled. Concentrations of both organic and inorganic species increased substantially to the west, with concentrations in the range of 3–7 µg sm^{-3} at the 75–95th percentiles, reflecting the increased density of anthropogenic sources encountered. The longitudinal gradients reveal that the median and the Inter Quartile Range (IQR) of the OM concentration is relatively constant west of 15 E, with concentrations typically between 3–5 µg sm^{-3}. The larger IQR in the 15–20 E band is likely due to the transition from background conditions to polluted conditions. The OM concentrations contrast with the inorganic mass concentrations, which display somewhat differing trends and variability. The ammonium sulphate concentrations tend to build from east-to-west but with greater variability than the OM. This contrast is likely a consequence of the differing formation/processing time scales and source distributions for ammonium sulphate versus OM. The ammonium nitrate concentrations show enhanced variability throughout with no noticeable trend to the east of the meridian, although the median concentration increases to the west of this longitude. This is a reflection of the NO_x and ammonia source fields across

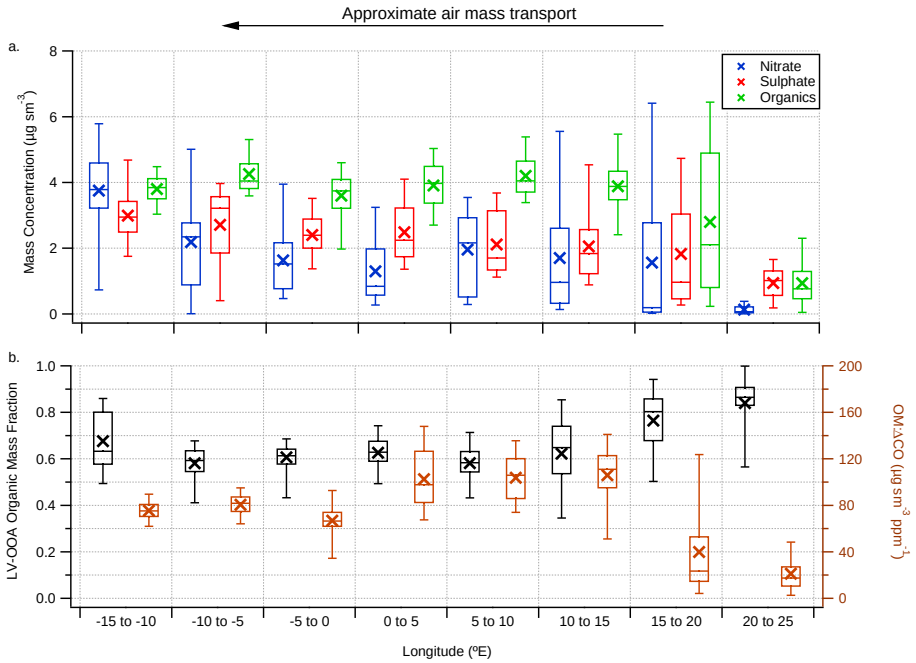

Fig. 6. Boxplot summary statistics of aerosol chemical composition as a function of longitude during LONGREX-2, where the air mass transport was approximately east-to-west. **(a)** Summarises the concentrations for nitrate, sulphate and organics. **(b)** Presents the LV-OOA organic mass fraction (left) and the OM:ΔCO ratio (right). Crosses represent the mean value, while horizontal lines represent the 25th, 50th and 75th percentiles. The whiskers represent the 5th and 95th percentiles. Values are for altitudes between 250–2500 m.

Europe, with peak emissions of these emissions occurring in North-Western Europe (e.g. Reis et al., 2009). This is especially true in terms of ammonia, which is more readily available in Western Europe compared to further east due to intensive agricultural activities. The contrast with OM reflects this source distribution. Additionally, their differing formation and processing time scales discussed in Sect. 4.3 likely play a role.

In terms of the chemical evolution of the OM, this period highlights the highly dynamic nature of the OM burden and is shown in Fig. 6b. In the background conditions to the east, the LV-OOA dominates, with a median mass fraction of close to 90%. Between 15 E and 20 E, where OM concentrations sharply increase, the LV-OOA mass fraction is highly variable due to the transition from background to more polluted conditions. The enhanced OM concentrations are driven by the SV-OOA component, as more freshly formed material is encountered as the aircraft travels westwards. This input of fresher material continues further to the west as the SV-OOA fraction increases (decreasing LV-OOA fraction), which is consistent with the urban source distribution in continental Europe. The LV-OOA fraction is then relatively constant as far west as 10 W. West of this, over the Eastern Atlantic Ocean, LV-OOA undergoes a marked increase with the median and 75th percentiles being 65% and 80% respectively. This increase in the LV-OOA reflects the lack of fresh pollution contributing to new SV-OOA formation and is coincident with an increase in the median concentration of ozone beyond the zero meridian line, from 60 ppb to 80 ppb, which is suggestive of photochemical processing within the high pressure system. Based upon the aforementioned back trajectories, this represents approximately one day of air mass transit. A key observation during the LONGREX-2 period is the relationship between the LV-OOA mass fraction and the OM:ΔCO ratio shown in Fig. 6b (where ΔCO correponds to CO minus the background value), with the enhancement in the OM:ΔCO ratio from a median value of approximately 20 $\mu g\,sm^{-3}\,ppm^{-1}$ to over 100 $\mu g\,sm^{-3}\,ppm^{-1}$ west of 15 E occurring upon the addition of SV-OOA mass which enhances the OM concentrations. These values then decrease west of the meridian to 60–100 $\mu g\,sm^{-3}\,ppm^{-1}$ as the LV-OOA mass fraction becomes more dominant and OM concentrations decrease slightly. De Gouw and Jimenez (2009) reported OM:ΔCO ratio's for urban emissions containing large amounts of SOA in the range of approximately 50–90 $\mu g\,sm^{-3}\,ppm^{-1}$ in North America and Tokyo. Thus the values reported here tend towards greater values or even exceed those reported previously. The measurements presented here are close to those reported for the highly polluted Po Valley region in Northern Italy described in Crosier et al. (2007).

The measurements are consistent with a rapidly formed OM close to source, which subsequently ages substantially downwind. This contrasts with the evolution of the inorganic

constituents in the form of ammonium nitrate and ammonium sulphate, which evolve on differing time scales during this period.

5.2 Transformation with respect to distance from source and photochemical processing

The broadly similar transport patterns prevalent throughout the dataset (i.e. sampling of European air masses at distances both upwind, over continental Europe itself and at varying scales downwind) provides the potential to link the evolution of the aerosol chemical composition across this large range of spatial scales. The flight operations can be characterised according to the CO:NO_x and O_3:NO_x ratios, which are qualitatively used as proxies for proximity to major sources and photochemical processing. The O_3:NO_x ratio is shown versus the CO:NO_x ratio in Fig. 7c, indicating good first order agreement between their respective evolutions. In urban areas, CO concentrations are typically 5–15 times NO_x concentrations (e.g. Parrish et al., 2009) due to enhanced NO_x emissions associated with primary combustion sources. Furthermore, on urban-to-near-urban scales, NO_x levels are enhanced relative to O_3 due to titration by NO. This yields an O_3:NO_x ratio less than 1, thus this range in O_3:NO_x and CO:NO_x is classified as near-urban. Subsequent dilution and photochemistry downwind of urban emissions will lead to an enhancement in the ratios, as NO_x is oxidised to form HNO_3 and PAN on a time scale of a few hours (e.g. Neuman et al., 2009). This evolution is characterised by ratio values between 1 and 100, where O_3 concentrations steadily increase (see Supplementary Material Sect. 4, Fig. S5; http://www.atmos-chem-phys.net/10/4065/2010/acp-10-4065-2010-supplement.pdf). This increase in O_3 and decrease in NO_x is characteristic of photochemical activity. Furthermore, across this range of O_3:NO_x, CO tends to steadily decrease, indicative of dilution downwind of its major sources. The 1–10 O_3:NO_x is chosen as the near-source range as the CO concentrations are similar to those at less than 1, while O_3 levels are steadily increasing from their minimum value close to urban sources. The 10–100 O_3:NO_x range is then split between near-outflow and far-outflow regimes, principally based upon its gradient across the LONGREX-2 period (not shown) where it increased above 50 at longitudes to the west of 10W. Values greater than 100 are characteristic of background conditions, with reduced O_3, CO and NO_x concentrations indicative of dilution.

The O_3:NO_x ratio is used to characterise the flights as both measurements were available on all flights, whereas CO was absent during ADIENT-2. The results of this grouping are shown in Fig. 7 by contrasting the evolution from near-source conditions, predominantly over polluted regions of continental Europe and the associated near-field and far-field outflow from it. Also shown are the background conditions encountered, which were predominantly encountered in the Baltic Sea region, for a contrast with the more polluted regimes. The near-urban points are not included as too few were sampled to yield a statistically robust summary.

The analysis indicates that under polluted and highly photochemically active conditions at near-source locations, ammonium nitrate and OM are the dominant chemical components. Concentrations range from 4.5–10.0 $\mu g\,sm^{-3}$ and 4.0–6.5 $\mu g\,sm^{-3}$ at the 50–95th percentile levels respectively. The upper percentile dominance of nitrate diminishes with increasing distance from source but it still maintains a significant fraction of the sub-micron mass, with concentrations comparable to sulphate. OM is the dominant component at all scales outside of the most polluted conditions, where nitrate is dominant. The estimated HOA mass fraction is typically between 5–15% at the 25–75th percentile levels across the range of conditions sampled. The composition of the OOA evolves strongly as a function of the O_3:NO_x ratio, with the LV-OOA fraction making up 50–65% of the OM at the 25–75th percentile levels close to source, through to 60–80% of the OM in the far-field outflow. In background conditions, LV-OOA makes up close to 90% of the OM at the 75th percentile and is at 100% at the 95th percentile. These features are reflected in the colouring of the Fig. 7c, with the LV-OOA increasing as a function of CO:NO_x and O_3:NO_x. The two apparent lines in the relationship are principally a consequence of the enhanced pollutant concentrations in LONGREX-1 (the lower line), during which NO_x and CO were enhanced thus the O_3:NO_x is shifted downwards relative to the other periods shown. The LV-OOA organic mass fraction captures this change as the LONGREX-1 OM is more dominated by SV-OOA (reduced LV-OOA fraction).

The results show that significant OM concentrations are rapidly formed under polluted conditions in continental Europe and that these concentrations are maintained upon advection downwind of the major sources in Europe. Much of the enhanced mass in Europe is associated with an increase in the SV-OOA fraction but a significant fraction is associated with LV-OOA, which is indicative of rapid photochemical processing of the OM on the regional scale. The median LV-OOA fraction is always greater than the SV-OOA fraction and the LV-OOA mass fraction steadily increases upon advection downwind.

OOA across Europe was frequently well correlated with ammonium nitrate and ammonium sulphate, both of which likely originate from anthropogenic sources. Furthermore, OOA is correlated with O_3:NO_x, again suggestive of an anthropogenic influence. Potentially this may point to the OOA sources being anthropogenic in origin also, although this contrasts with several previous studies in Europe which have identified that SOA is predominantly derived from biogenic sources (e.g. studies in Zurich, (Szidat et al., 2006), rural/remote areas, Gelencsér et al., 2007 and Göteborg, Szidat et al., 2009). A similar picture is presented for the United States by Bench et al. (2007), who demonstrated that modern

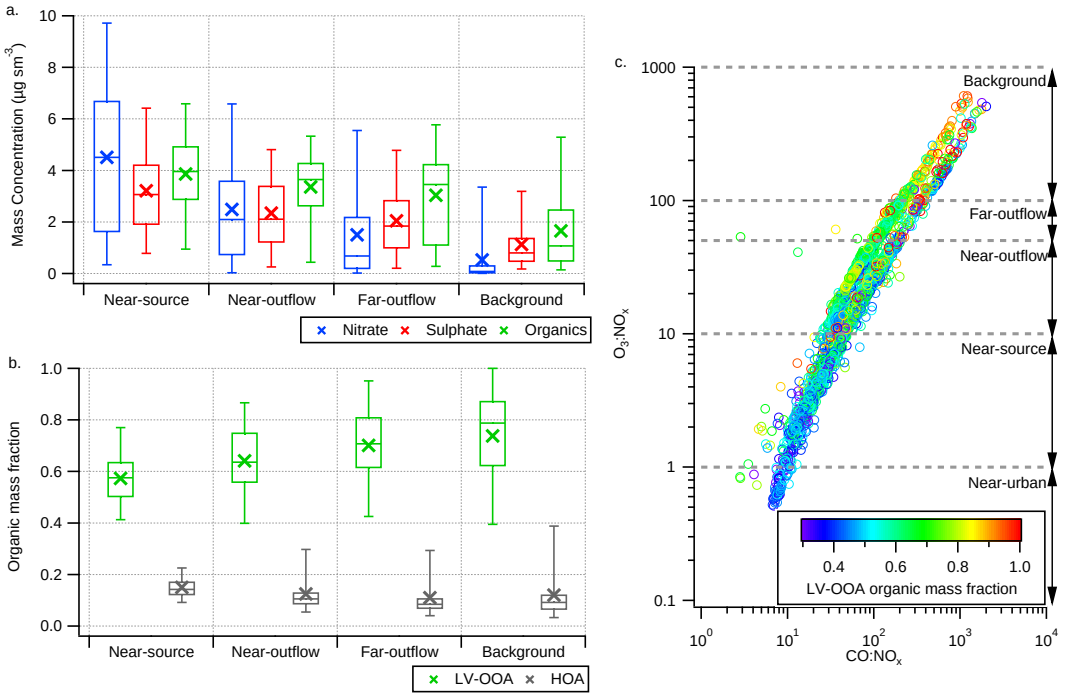

Fig. 7. Boxplot summary statistics of aerosol chemical composition as a function of proximity to source and photochemical processing. **(a)** Summarises the concentrations for nitrate, sulphate and organics, while **(b)** presents the organic mass fractions of LV-OOA and estimated HOA. Crosses represent the mean value, while horizontal lines represent the 25th, 50th and 75th percentiles. The whiskers represent the 5th and 95th percentiles. Values in (a) and (b) are for altitudes between 250–2500 m. **(c)** Summary of the relationship between the O_3:NO_x ratio and the CO:NO_x ratio for the dataset except for ADIENT-2 where no CO measurement was available. The grey horizontal lines designate the boundaries of the source proximities based upon the O_3:NO_x ratio which are used in (a) and (b). The points are coloured according to the LV-OOA organic mass fraction.

carbon dominated in rural areas, which suggests a biogenic source. However, measurements in urban plumes and closer to major anthropogenic sources have indicated that anthropogenic Volatile Organic Compounds (VOCs) are the main source of OM (e.g. de Gouw et al., 2005, 2008; Bahreini et al., 2009). Furthermore, the presence of both significant anthropogenic and biogenic sources in Northern Europe could mean that the OOA results from a mixture of both anthropogenic and biogenic sources and/or that enhanced biogenic SOA is formed in the presence of anthropogenic pollution, which has previously been identified in the south-eastern United States (Weber et al., 2007; Goldstein et al., 2009). However, the current study lacks suitable information regarding gas-phase organic precursors and/or additional OM chemical information to separate the different contributions of biogenic and anthropogenic to the total observed OM from the observations alone.

Enhanced SV-OOA concentrations in North-Western Europe are strongly coupled to ammonium nitrate concentrations, which are regularly observed to peak at the top of the boundary layer. This is prescribed to partitioning of semi-volatile gas phase precursors to the particle phase at reduced temperature and enhanced relative humidity (e.g. Morino et al., 2006; Morgan et al., 2009). These observations are discussed in Morgan et al. (2010) in the EUCAARI special issue.

6 Conclusions

The spatial distribution of sub-micron aerosol chemical composition has been characterised based upon airborne measurements in the planetary boundary layer across Europe, north of the Alpine regions. Organic Matter (OM) and ammonium nitrate are the largest components, typically contributing 20–50% each to the non-refractory mass. Ammonium nitrate dominates in North-Western Europe where the emissions of NO_x and ammonia reach their maximum. Ammonium nitrate dominates the infreqeunt but highly polluted periods sampled with concentrations ranging from 4–8 µg sm^{-3} at the 75–95th percentile levels. This is consistent with the dominance of ammonium nitrate in Western Europe during periods of high pollutant concentrations identified previously (Putaud et al., 2004; Morgan et al., 2009). OM generally dominates over sulphate over the whole of Europe, with OM concentrations typically 1.3–2.5 times greater than that of sulphate. Sulphate contributes 10–30% to the

regional non-refractory particulate mass burden. Consideration of OM and ammonium nitrate in modelling assessments of the impact of atmospheric aerosol in Europe is evidently required. The measurements presented here provide a useful test for regional and global aerosol models, due to the contrasting distributions of the OM components and inorganic components across the significant spatial and temporal scales sampled.

A positive matrix factorisation analysis of the OM component was conducted, revealing the dominance of Oxidised Organic Aerosol (OOA) over Hydrocarbon-like Organic Aerosol (HOA), which is consistent with previous literature (Zhang et al., 2007). This dominance meant that the HOA component was difficult to separate from the OOA in a robust manner across the dataset. An empirical estimate based upon previous research indicated that HOA contributes less than 15% to the OM burden. Two factor solutions were found to be the most robust characterisation of the OM burden. Two separate OOA components were identified; one representing an aged-more oxidised organic aerosol and another representing fresher-less oxidised organic aerosol. These factors closely resemble those derived in ground-based global AMS datasets (Jimenez et al., 2009; Ng et al., 2009) where the less oxidised factor is associated with Semi-Volatile OOA (SV-OOA) and the more oxidised factor is found in the Low-Volatility OOA (LV-OOA) fraction. The OM chemical composition and the associated OOA factors derived for each flight were highly variable in terms of their oxygen content, based upon normalised organic signal intensities at *m/z* 44 and 43. When combined, the OM data and factors can be viewed as a continuum with a progression from a less oxidised, more-volatile component to a highly oxidised, less-volatile component. This progression was observed to occur as a function of the distance from source, with more oxidised components dominating further downwind. During highly polluted conditions in North-Western Europe, the SV-OOA displayed strong coupling to ammonium nitrate, indicative of gas-to-particle partitioning of semi-volatile components. Highly active photochemical conditions encountered during the study meant that LV-OOA was the largest OM component at all locations and this dominance increased with distance from source. In background conditions, LV-OOA made up more than 80% of the OM burden. This evolution is consistent with the recent paradigm proposed by Jimenez et al. (2009).

The processes identified in this work result in the build up of significant amounts of anthropogenically influenced aerosol downwind of major source regions with total submicron mass loadings from the AMS exceeding 15 $\mu g\,sm^{-3}$ with OM and ammonium nitrate being the dominant chemical components. Such concentrations have the capacity to significantly perturb regional weather and climate.

Acknowledgements. This work is supported by NERC ADIENT project NE/E011101/1 and EUCAARI project 036833-2. W. T. Morgan was supported by a Natural Environment Research Council (NERC) studentship NER/S/A/2006/14040 and a CASE sponsorship from Aerodyne Research Inc. The NERC National Centre for Atmospheric Science (NCAS) Facility for Ground based Atmospheric Measurements (FGAM) supported the maintenance of the cToF-AMS. NCAS also supported the development of the data interpretation methods employed here through its Composition Directorate. Many thanks to Ingrid Ulbrich (University of Colorado at Boulder, USA) for providing and supporting the PMF toolkit. Thanks to the British Atmospheric Data Centre (BADC) for the calculation of trajectories and access to European Centre for Medium-Range Weather Forecasts (ECMWF) Operational Analysis data, available from http://badc.nerc.ac.uk/data/ecmwf-op/. We thank A. M. Middlebrook for the AMS collection efficiency algorithm. We also thank F. Abicht, C. L. McConnell, A. Minikin, T. Hamburger and A. Stohl for their major contributions to the project. We thank the FAAM, the Met Office, Avalon, DLR-Falcon and DirectFlight personnel for their contributions to the campaign. In memory of Keith Drummond, without whom the flying circus would never have got off the ground.

Edited by: O. Hov

References

Aiken, A. C., Decarlo, P. F., Kroll, J. H., Worsnop, D. R., Huffman, J. A., Docherty, K. S., Ulbrich, I. M., Mohr, C., Kimmel, J. R., Sueper, D., Sun, Y., Zhang, Q., Trimborn, A., Northway, M., Ziemann, P. J., Canagaratna, M. R., Onasch, T. B., Alfarra, M. R., Prevot, A. S. H., Dommen, J., Duplissy, J., Metzger, A., Baltensperger, U., and Jimenez, J. L.: O/C and OM/OC ratios of primary, secondary, and ambient organic aerosols with high-resolution time-of-flight aerosol mass spectrometry, Environ. Sci. Technol., 42, 4478–4485, 2008.

Aiken, A. C., Salcedo, D., Cubison, M. J., Huffman, J. A., DeCarlo, P. F., Ulbrich, I. M., Docherty, K. S., Sueper, D., Kimmel, J. R., Worsnop, D. R., Trimborn, A., Northway, M., Stone, E. A., Schauer, J. J., Volkamer, R. M., Fortner, E., de Foy, B., Wang, J., Laskin, A., Shutthanandan, V., Zheng, J., Zhang, R., Gaffney, J., Marley, N. A., Paredes-Miranda, G., Arnott, W. P., Molina, L. T., Sosa, G., and Jimenez, J. L.: Mexico City aerosol analysis during MILAGRO using high resolution aerosol mass spectrometry at the urban supersite (T0) – Part 1: Fine particle composition and organic source apportionment, Atmos. Chem. Phys., 9, 6633–6653, 2009, http://www.atmos-chem-phys.net/9/6633/2009/.

Alfarra, M. R., Coe, H., Allan, J. D., Bower, K. N., Boudries, H., Canagaratna, M. R., Jimenez, J. L., Jayne, J. T., Garforth, A. A., Li, S. M., and Worsnop, D. R.: Characterization of urban and rural organic particulate in the lower Fraser valley using two aerodyne aerosol mass spectrometers, Atmos. Environ., 38, 5745–5758, 2004.

Allan, J., Jimenez, J., Williams, P., Alfarra, M., Bower, K., Jayne, J., Coe, H., and Worsnop, D.: Quantitative sampling using an Aerodyne aerosol mass spectrometer: 1. Techniques of data interpretation and error analysis, J. Geophys. Res.-Atmos., 108, 4090, doi:10.1029/2003JD001607, 2003.

Allan, J. D., Delia, A. E., Coe, H., Bower, K. N., Alfarra, M. R., Jimenez, J. L., Middlebrook, A. M., Drewnick, F., Onasch, T. B., Canagaratna, M. R., Jayne, J. T., and Worsnop, D. R.: A generalised method for the extraction of chemically resolved mass spectra from aerodyne aerosol mass spectrometer data, J. Aerosol Sci., 35, 909–922, 2004.

Andreae, M. and Crutzen, P.: Atmospheric aerosols: Biogeochemical sources and role in atmospheric chemistry, Science, 276, 1052–1058, 1997.

Bahreini, R., Ervens, B., Middlebrook, A. M., Warneke, C., de Gouw, J. A., DeCarlo, P. F., Jimenez, J. L., Brock, C. A., Neuman, J. A., Ryerson, T. B., Stark, H., Atlas, E., Brioude, J., Fried, A., Holloway, J. S., Peischl, J., Richter, D., Walega, J., Weibring, P., Wollny, A. G., and Fehsenfeld, F. C.: Organic aerosol formation in urban and industrial plumes near Houston and Dallas, Texas, J. Geophys. Res., 114, D00F16, doi:10.1029/2008JD011493, 2009.

Bates, T. S., Quinn, P. K., Coffman, D. J., Johnson, J. E., and Middlebrook, A. M.: Dominance of organic aerosols in the marine boundary layer over the Gulf of Maine during NEAQS 2002 and their role in aerosol light scattering, J. Geophys. Res.-Atmos., 110, doi:10.1029/2005JD005797, d18202, 2005.

Baumgardner, D., Kok, G., and Raga, G.: Warming of the Arctic lower stratosphere by light absorbing particles, Geophys. Res. Lett., 31, l06117, doi:10.1029/2003GL018883, 2004.

Baumgardner, D., Grutter, M., Allan, J., Ochoa, C., Rappenglueck, B., Russell, L. M., and Arnott, P.: Physical and chemical properties of the regional mixed layer of Mexico's Megapolis, Atmos. Chem. Phys., 9, 5711–5727, 2009, http://www.atmos-chem-phys.net/9/5711/2009/.

Bench, G., Fallon, S., Schichtel, B., Malm, W., and McDade, C.: Relative contributions of fossil and contemporary carbon sources to $PM_{2.5}$ aerosols at nine Interagency Monitoring for Protection of Visual Environments (IMPROVE) network sites, J. Geophys. Res., 112, D10205, doi:10.1029/2006JD007708, 2007.

Brock, C. A., Sullivan, A. P., Peltier, R. E., Weber, R. J., Wollny, A., Gouw, J. A., Middlebrook, A. M., Atlas, E. L., Stohl, A., Trainer, M. K., Cooper, O. R., Fehsenfeld, F. C., Frost, G. J., Holloway, J. S., Hubler, G., Neuman, J. A., Ryerson, T. B., Warneke, C., and Wilson, J. C.: Sources of particulate matter in the northeastern United States in summer: 2. Evolution of chemical and microphysical properties, J. Geophys. Res.-Atmos., 113, d08302, doi:10.1029/2007JD009241, 2008.

Canagaratna, M. R., Jayne, J. T., Jimenez, J. L., Allan, J. D., Alfarra, M. R., Zhang, Q., Onasch, T. B., Drewnick, F., Coe, H., Middlebrook, A., Delia, A., Williams, L. R., Trimborn, A. M., Northway, M. J., DeCarlo, P. F., Kolb, C. E., Davidovits, P., and Worsnop, D. R.: Chemical and microphysical characterization of ambient aerosols with the aerodyne aerosol mass spectrometer, Mass Spectrometry Reviews, 26, 185–222, 2007.

Capes, G., Johnson, B., McFiggans, G., Williams, P. I., Haywood, J., and Coe, H.: Aging of biomass burning aerosols over West Africa: Aircraft measurements of chemical composition, microphysical properties, and emission ratios, J. Geophys. Res.-Atmos., 113, D00C15cro, doi:10.1029/2008JD009845, 2008.

Charlson, R. J., Schwartz, S. E., Hales, J. M., Cess, R. D., Coakley, J. A., Hansen, J. E., and Hofmann, D. J.: Climate Forcing by Anthropogenic Aerosols, Science, 255, 423–430, 1992.

Crosier, J., Allan, J. D., Coe, H., Bower, K. N., Formenti, P., and Williams, P. I.: Chemical composition of summertime aerosol in the Po Valley (Italy), northern Adriatic and Black Sea, Q. J. Roy. Meteorol. Soc., 133, 61–75, 2007.

Cross, E. S., Slowik, J. G., Davidovits, P., Allan, J. D., Worsnop, D. R., Jayne, J. T., Lewis, D. K., Canagaratna, M., and Onasch, T. B.: Laboratory and Ambient Particle Density Determinations using Light Scattering in Conjunction with Aerosol Mass Spectrometry, Aerosol Sci. Technol., 41, 343–359, 2007.

De Gouw, J. and Jimenez, J. L.: Organic Aerosols in the Earth's Atmosphere, Environ. Sci. Technol., 43, 7614–7618, doi:10.1021/es9006004, 2009.

de Gouw, J., Middlebrook, A., Warneke, C., Goldan, P., Kuster, W., Roberts, J., Fehsenfeld, F., Worsnop, D., Canagaratna, M., Pszenny, A., Keene, W., Marchewka, M., Bertman, S., and Bates, T.: Budget of organic carbon in a polluted atmosphere: Results from the New England Air Quality Study in 2002, J. Geophys. Res.-Atmos., 110, D16305, doi:10.1029/2004JD005623, 2005.

de Gouw, J. A., Brock, C. A., Atlas, E. L., Bates, T. S., Fehsenfeld, F. C., Goldan, P. D., Holloway, J. S., Kuster, W. C., Lerner, B. M., Matthew, B. M., Middlebrook, A. M., Onasch, T. B., Peltier, R. E., Quinn, P. K., Senff, C. J., Stohl, A., Sullivan, A. P., Trainer, M., Warneke, C., Weber, R. J., and Williams, E. J.: Sources of particulate matter in the northeastern United States in summer: 1. Direct emissions and secondary formation of organic matter in urban plumes, J. Geophys. Res.-Atmos., 113, D08301, doi:10.1029/2007JD009243, 2008.

DeCarlo, P. F., Kimmel, J. R., Trimborn, A., Northway, M. J., Jayne, J. T., Aiken, A. C., Gonin, M., Fuhrer, K., Horvath, T., Docherty, K. S., Worsnop, D. R., and Jimenez, J. L.: Field-deployable, high-resolution, time-of-flight aerosol mass spectrometer, Anal. Chem., 78, 8281–8289, 2006.

Denman, K., Brasseur, G., Chidthaisong, A., Ciais, P., Cox, P., Dickinson, R., Hauglustaine, D., Heinze, C., Holland, E., Jacob, D., Lohmann, U., Ramachandran, S., Dias, P. d. S., Wofsy, S., and Zhang, X.: Couplings Between Changes in the Climate System and Biogeochemistry, Climate Change 2007: The Physical Science Basis. Contribution of Working Group I to the Fourth Assessment Report of the Intergovernmental Panel on Climate Change, Cambridge University Press, Cambridge, United Kingdom and New York, NY, USA, 2007.

Docherty, K. S., Stone, E. A., Ulbrich, I. M., DeCarlo, P. F., Snyder, D. C., Schauer, J. J., Peltier, R. E., Weber, R. J., Murphy, S. N., Seinfeld, J. H., Grover, B. D., Eatough, D. J., and Jiimenez, J. L.: Apportionment of Primary and Secondary Organic Aerosols in Southern California during the 2005 Study of Organic Aerosols in Riverside (SOAR-1), Environ. Sci. Technol., 42, 7655–7662, 2008.

Donahue, N. M., Robinson, A. L., Stanier, C. O., and Pandis, S. N.: Coupled partitioning, dilution, and chemical aging of semivolatile organics, Environ. Sci. Technol., 40, 2635–2643, 2006.

Donahue, N. M., Robinson, A. L., and Pandis, S. N.: Atmospheric organic particulate matter: From smoke to secondary organic aerosol, Atmos. Environ., 43, 94–106, 2009.

Drewnick, F., Hings, S. S., DeCarlo, P., Jayne, J. T., Gonin, M., Fuhrer, K., Weimer, S., Jimenez, J. L., Demerjian, K. L., Borrmann, S., and Worsnop, D. R.: A new time-of-flight aerosol mass spectrometer (TOF-AMS) - Instrument description and first field deployment, Aerosol Sci. Technol., 39, 637–658, 2005.

Esselborn, M., Wirth, M., Fix, A., Tesche, M., and Ehret, G.: Airborne high spectral resolution lidar for measuring aerosol extinction and backscatter coefficients, Appl. Optics, 47, 346–358, 2008.

Fast, J., Aiken, A. C., Allan, J., Alexander, L., Campos, T., Canagaratna, M. R., Chapman, E., DeCarlo, P. F., de Foy, B., Gaffney, J., de Gouw, J., Doran, J. C., Emmons, L., Hodzic, A., Herndon, S. C., Huey, G., Jayne, J. T., Jimenez, J. L., Kleinman, L., Kuster, W., Marley, N., Russell, L., Ochoa, C., Onasch, T. B., Pekour, M., Song, C., Ulbrich, I. M., Warneke, C., Welsh-Bon, D., Wiedinmyer, C., Worsnop, D. R., Yu, X.-Y., and Zaveri, R.: Evaluating simulated primary anthropogenic and biomass burning organic aerosols during MILAGRO: implications for assessing treatments of secondary organic aerosols, Atmos. Chem. Phys., 9, 6191–6215, 2009, http://www.atmos-chem-phys.net/9/6191/2009/.

Foltescu, V. L., Selin, E., and Below, M.: Corrections for Particle Losses and Sizing Errors During Aircraft Aerosol Sampling Using a Rosemount Inlet and the Pms Las-X, Atmos. Environ., 29, 449–453, 1995.

Forster, P., Ramaswamy, V., Artaxo, P., Berntsen, T., Betts, R., W. Fahey, D., Haywood, J., Lean, J., Lowe, D., Myhre, G., Nganga, J., Prinn, R., Raga, G., Schulz, M., and Van Dorland, R.: Changes in Atmospheric Constituents and in Radiative Forcing, Climate Change 2007: The Physical Science Basis. Contribution of Working Group I to the Fourth Assessment Report of the Intergovernmental Panel on Climate Change, Cambridge University Press, Cambridge, United Kingdom and New York, NY, USA, 2007.

Gao, R. S., Schwarz, J. P., Kelly, K. K., Fahey, D. W., Watts, L. A., Thompson, T. L., Spackman, J. R., Slowik, J. G., Cross, E. S., Han, J. H., Davidovits, P., Onasch, T. B., and Worsnop, D. R.: A novel method for estimating light-scattering properties of soot aerosols using a modified single-particle soot photometer, Aerosol Sci. Technol., 41, 125–135, 2007.

Gelencsér, A., May, B., Simpson, D., Sánchez-Ochoa, A., Kasper-Giebl, A., Puxbaum, H., Caseiro, A., Pio, C., and Legrand, M.: Source apportionment of PM2.5 organic aerosol over Europe: Primary/secondary, natural/anthropogenic, and fossil/biogenic origin, J. Geophys. Res.-Atmos., 112, D23S04, doi:10.1029/2006JD008094, 2007.

Goldstein, A. H., Koven, C. D., Heald, C. L., and Fung, I. Y.: Biogenic carbon and anthropogenic pollutants combine to form a cooling haze over the southeastern United States, Proceedings of the National Academy of Sciences, 106, 8835–8840, 2009.

Hallar, A. G., Strawa, A. W., Schmid, B., Andrews, E., Ogren, J., Sheridan, P., Ferrare, R., Covert, D., Elleman, R., Jonsson, H., Bokarius, K., and Luu, A.: Atmospheric Radiation Measurements Aerosol Intensive Operating Period: Comparison of aerosol scattering during coordinated flights, J. Geophys. Res., 111, D05S09, doi:10.1029/2005JD006250, 2006.

Haywood, J. and Boucher, O.: Estimates of the direct and indirect radiative forcing due to tropospheric aerosols: A review, Rev. Geophys., 38, 513–543, 2000.

Huffman, J. A., Jayne, J. T., Drewnick, F., Aiken, A. C., Onasch, T., Worsnop, D. R., and Jimenez, J. L.: Design, modeling, optimization, and experimental tests of a particle beam width probe for the aerodyne aerosol mass spectrometer, Aerosol Sci. Technol., 39, 1143–1163, 2005.

Huffman, J. A., Docherty, K. S., Aiken, A. C., Cubison, M. J., Ulbrich, I. M., DeCarlo, P. F., Sueper, D., Jayne, J. T., Worsnop, D. R., Ziemann, P. J., and Jimenez, J. L.: Chemically-resolved aerosol volatility measurements from two megacity field studies, Atmos. Chem. Phys., 9, 7161–7182, 2009, http://www.atmos-chem-phys.net/9/7161/2009/.

Jayne, J. T., Leard, D. C., Zhang, X. F., Davidovits, P., Smith, K. A., Kolb, C. E., and Worsnop, D. R.: Development of an aerosol mass spectrometer for size and composition analysis of submicron particles, Aerosol Sci. Technol., 33, 49–70, 2000.

Jimenez, J. L., Canagaratna, M. R., Donahue, N. M., Prevot, A. S. H., Zhang, Q., Kroll, J. H., DeCarlo, P. F., Allan, J. D., Coe, H., Ng, N. L., Aiken, A. C., Docherty, K. S., Ulbrich, I. M., Grieshop, A. P., Robinson, A. L., Duplissy, J., Smith, J. D., Wilson, K. R., Lanz, V. A., Hueglin, C., Sun, Y. L., Tian, J., Laaksonen, A., Raatikainen, T., Rautiainen, J., Vaattovaara, P., Ehn, M., Kulmala, M., Tomlinson, J. M., Collins, D. R., Cubison, M. J., E., Dunlea, J., Huffman, J. A., Onasch, T. B., Alfarra, M. R., Williams, P. I., Bower, K., Kondo, Y., Schneider, J., Drewnick, F., Borrmann, S., Weimer, S., Demerjian, K., Salcedo, D., Cottrell, L., Griffin, R., Takami, A., Miyoshi, T., Hatakeyama, S., Shimono, A., Sun, J. Y., Zhang, Y. M., Dzepina, K., Kimmel, J. R., Sueper, D., Jayne, J. T., Herndon, S. C., Trimborn, A. M., Williams, L. R., Wood, E. C., Middlebrook, A. M., Kolb, C. E., Baltensperger, U., and Worsnop, D. R.: Evolution of Organic Aerosols in the Atmosphere, Science, 326, 1525–1529, doi:10.1126/science.1180353, 2009.

Kleinman, L. I., Daum, P. H., Lee, Y. N., Senum, G. I., Springston, S. R., Wang, J., Berkowitz, C., Hubbe, J., Zaveri, R. A., Brechtel, F. J., Jayne, J., Onasch, T. B., and Worsnop, D.: Aircraft observations of aerosol composition and ageing in New England and Mid-Atlantic States during the summer 2002 New England Air Quality Study field campaign, J. Geophys. Res.-Atmos., 112, D09310, doi:10.1029/2006JD007786, 2007.

Kleinman, L. I., Springston, S. R., Daum, P. H., Lee, Y.-N., Nunnermacker, L. J., Senum, G. I., Wang, J., Weinstein-Lloyd, J., Alexander, M. L., Hubbe, J., Ortega, J., Canagaratna, M. R., and Jayne, J.: The time evolution of aerosol composition over the Mexico City plateau, Atmos. Chem. Phys., 8, 1559–1575, 2008, http://www.atmos-chem-phys.net/8/1559/2008/.

Kulmala, M., Asmi, A., Lappalainen, H. K., Carslaw, K. S., Pöschl, U., Baltensperger, U., Hov, Ø., Brenquier, J.-L., Pandis, S. N., Facchini, M. C., Hansson, H.-C., Wiedensohler, A., and O'Dowd, C. D.: Introduction: European Integrated Project on Aerosol Cloud Climate and Air Quality interactions (EUCAARI) – integrating aerosol research from nano to global scales, Atmos. Chem. Phys., 9, 2825–2841, 2009, http://www.atmos-chem-phys.net/9/2825/2009/.

Lanz, V. A., Alfarra, M. R., Baltensperger, U., Buchmann, B., Hueglin, C., and Prévôt, A. S. H.: Source apportionment of submicron organic aerosols at an urban site by factor analytical modelling of aerosol mass spectra, Atmos. Chem. Phys., 7, 1503–1522, 2007, http://www.atmos-chem-phys.net/7/1503/2007/.

Lanz, V. A., Alfarra, M. R., Baltensperger, U., Buchmann, B., Hueglin, C., Szidat, S., Wehrli, M. N., Wacker, L., Weimer, S., Caseiro, A., Puxbaum, H., and Prevot, A. S. H.: Source attribution of submicron organic aerosols during wintertime inversions by advanced factor analysis of aerosol mass spectra, Environ.

Sci. Technol., 42, 214–220, 2008.

Liu, P. S. K., Leaitch, W. R., Strapp, J. W., and Wasey, M. A.: Response of Particle Measuring Systems Airborne ASASP and PCASP to Nacl and Latex-Particles, Aerosol Sci. Technol., 16, 83–95, 1992.

Matthew, B. M., Middlebrook, A. M., and Onasch, T. B.: Collection efficiencies in an Aerodyne Aerosol Mass Spectrometer as a function of particle phase for laboratory generated aerosols, Aerosol Sci. Technol., 42, 884–898, 2008.

McFiggans, G., Alfarra, M. R., Allan, J., Bower, K., Coe, H., Cubison, M., Topping, D., Williams, P., Decesari, S., Facchini, C., and Fuzzi, S.: Simplification of the representation of the organic component of atmospheric particulates, Faraday Discussions, 130, 341–362, 2005.

Mohr, C., Huffman, J. A., Cubison, M. J., Aiken, A. C., Docherty, K. S., Kimmel, J. R., Ulbrich, I. M., Hannigan, M., and Jimenez, J. L.: Characterization of Primary Organic Aerosol Emissions from Meat Cooking, Trash Burning, and Motor Vehicles with High-Resolution Aerosol Mass Spectrometry and Comparison with Ambient and Chamber Observations, Environ. Sci. Technol., 43, 2443–2449, 2009.

Moore, K. G., I., Clarke, A. D., Kapustin, V. N., McNaughton, C., Anderson, B. E., Winstead, E. L., Weber, R., Ma, Y., Lee, Y. N., Talbot, R., Dibb, J., Anderson, T., Doherty, S., Covert, D., and Rogers, D.: A comparison of similar aerosol measurements made on the NASA P3-B, DC-8, and NSF C-130 aircraft during TRACE-P and ACE-Asia, J. Geophys. Res., 109, D15S15, doi:10.1029/2003JD003543, 2004.

Morgan, W. T., Allan, J. D., Bower, K. N., Capes, G., Crosier, J., Williams, P. I., and Coe, H.: Vertical distribution of sub-micron aerosol chemical composition from North-Western Europe and the North-East Atlantic, Atmos. Chem. Phys., 9, 5389–5401, 2009,
http://www.atmos-chem-phys.net/9/5389/2009/.

Morgan, W. T., Allan, J. D., Bower, K. N., Esselborn, M., Harris, B., Henzing, J. S., Highwood, E. J., Kiendler-Scharr, A., McMeeking, G. R., Mensah, A. A., Northway, M. J., Osborne, S., Williams, P. I., Krejci, R., and Coe, H.: Enhancement of the aerosol direct radiative effect by semi-volatile aerosol components: airborne measurements in North-Western Europe, Atmos. Chem. Phys. Discuss., 10, 10653–10705, 2010,
http://www.atmos-chem-phys-discuss.net/10/10653/2010/.

Morino, Y., Kondo, Y., Takegawa, N., Miyazaki, Y., Kita, K., Komazaki, Y., Fukuda, M., Miyakawa, T., Moteki, N., and Worsnop, D. R.: Partitioning of HNO3 and particulate nitrate over Tokyo: Effect of vertical mixing, J. Geophys. Res.-Atmos., 111, D15215, doi:10.1029/2005JD006887, d15215, 2006.

Neuman, J. A., Nowak, J. B., Zheng, W., Flocke, F., Ryerson, T. B., Trainer, M., Holloway, J. S., Parrish, D. D., Frost, G. J., Peischl, J., Atlas, E. L., Bahreini, R., Wollny, A. G., and Fehsenfeld, F. C.: Relationship between photochemical ozone production and NOx oxidation in Houston, Texas, J. Geophys. Res., 114, D00F08, doi:10.1029/2008JD011688, 2009.

Ng, N. L., Canagaratna, M. R., Zhang, Q., Jimenez, J. L., Tian, J., Ulbrich, I. M., Kroll, J. H., Docherty, K. S., Chhabra, P. S., Bahreini, R., Murphy, S. M., Seinfeld, J. H., Hildebrandt, L., DeCarlo, P. F., Lanz, V. A., Prevot, A. S. H., Dinar, E., Rudich, Y., and Worsnop, D. R.: Organic aerosol components observed in worldwide datasets from aerosol mass spectrometry, Atmos. Chem. Phys. Discuss., 9, 27745–27789, 2009,
http://www.atmos-chem-phys-discuss.net/9/27745/2009/.

Osborne, S. R., Haywood, J. M., and Bellouin, N.: In situ and remote-sensing measurements of the mean microphysical and optical properties of industrial pollution aerosol during ADRIEX, Qu. J. Roy. Meteorol. Soc., 133, 17–32, 2007.

Paatero, P.: Least squares formulation of robust non-negative factor analysis, Chemometrics and Intelligent Laboratory Systems, 37, 23–35, 1997.

Paatero, P. and Tapper, U.: Positive Matrix Factorization – a Nonnegative Factor Model with Optimal Utilization of Error-Estimates of Data Values, Environmetrics, 5, 111–126, 1994.

Parrish, D. D., Allen, D. T., Bates, T. S., Estes, M., Fehsenfeld, F. C., Feingold, G., Ferrare, R., Hardesty, R. M., Meagher, J. F., Nielsen-Gammon, J. W., Pierce, R. B., Ryerson, T. B., Seinfeld, J. H., and Williams, E. J.: Overview of the Second Texas Air Quality Study (TexAQS II) and the Gulf of Mexico Atmospheric Composition and Climate Study (GoMACCS), J. Geophys. Res., 114, D00F13, doi:10.1029/2009JD011842, 2009.

Putaud, J.-P., Raes, F., Dingenen, R. V., Brüggemann, E., Facchini, M. C., Decesari, S., Fuzzi, S., Gehrig, R., Hüglin, C., Laj, P., Lorbeer, G., Maenhaut, W., Mihalopoulos, N., Müller, K., Querol, X., Rodriguez, S., Schneider, J., Spindler, G., ten Brink, H., Tørseth, K., and Wiedensohler, A.: A European aerosol phenomenology – 2: chemical characteristics of particulate matter at kerbside, urban, rural and background sites in Europe, Atmos. Environ., 38, 2579–2595, 2004.

Quinn, P. K., Bates, T. S., Coffman, D., Onasch, T. B., Worsnop, D., Baynard, T., de Gouw, J. A., Goldan, P. D., Kuster, W. C., Williams, E., Roberts, J. M., Lerner, B., Stohl, A., Pettersson, A., and Lovejoy, E. R.: Impacts of sources and aging on submicrometer aerosol properties in the marine boundary layer across the Gulf of Maine, J. Geophys. Res.-Atmos., 111, d23S36, doi:10.1029/2006JD007582, 2006.

Ramanathan, V., Crutzen, P. J., Lelieveld, J., Mitra, A. P., Althausen, D., Anderson, J., Andreae, M. O., Cantrell, W., Cass, G. R., Chung, C. E., Clarke, A. D., Coakley, J. A., Collins, W. D., Conant, W. C., Dulac, F., Heintzenberg, J., Heymsfield, A. J., Holben, B., Howell, S., Hudson, J., Jayaraman, A., Kiehl, J. T., Krishnamurti, T. N., Lubin, D., McFarquhar, G., Novakov, T., Ogren, J. A., Podgorny, I. A., Prather, K., Priestley, K., Prospero, J. M., Quinn, P. K., Rajeev, K., Rasch, P., Rupert, S., Sadourny, R., Satheesh, S. K., Shaw, G. E., Sheridan, P., and Valero, F. P. J.: Indian Ocean Experiment: An integrated analysis of the climate forcing and effects of the great Indo-Asian haze, J. Geophys. Res.-Atmos., 106, 28371–28398, 2001.

Reis, S., Pinder, R. W., Zhang, M., Lijie, G., and Sutton, M. A.: Reactive nitrogen in atmospheric emission inventories, Atmos. Chem. Phys., 9, 7657–7677, 2009,
http://www.atmos-chem-phys.net/9/7657/2009/.

Robinson, A. L., Donahue, N. M., Shrivastava, M. K., Weitkamp, E. A., Sage, A. M., Grieshop, A. P., Lane, T. E., Pierce, J. R., and Pandis, S. N.: Rethinking organic aerosols: Semivolatile emissions and photochemical aging, Science, 315, 1259–1262, 2007.

Rudich, Y., Donahue, N. M., and Mentel, T. F.: Aging of organic aerosol: Bridging the gap between laboratory and field studies, Ann. Rev. Phys. Chem., 58, 321–352, 2007.

Stephens, M., Turner, N., and Sandberg, J.: Particle identification by laser-induced incandescence in a solid-state laser cavity, Appl.

Optics, 42, 3726–3736, 2003.

Strapp, J. W., Leaitch, W. R., and Liu, P. S. K.: Hydrated and Dried Aerosol-Size-Distribution Measurements from the Particle Measuring Systems FSSP-300 Probe and the Deiced PCASP-100x Probe, J. Atmos. Oceanic Technol., 9, 548–555, 1992.

Szidat, S., Jenk, T. M., Synal, H.-A., Kalberer, M., Wacker, L., Hajdas, I., Kasper-Giebl, A., and Baltensperger, U.: Contributions of fossil fuel, biomass-burning, and biogenic emissions to carbonaceous aerosols in Zurich as traced by ^{14}C, J. Geophys. Res., 111, D07206, doi:10.1029/2005JD006590, 2006.

Szidat, S., Ruff, M., Perron, N., Wacker, L., Synal, H.-A., Hallquist, M., Shannigrahi, A. S., Yttri, K. E., Dye, C., and Simpson, D.: Fossil and non-fossil sources of organic carbon (OC) and elemental carbon (EC) in Gteborg, Sweden, Atmos. Chem. Phys., 9, 1521–1535, 2009, http://www.atmos-chem-phys.net/9/1521/2009/.

Ulbrich, I. M., Canagaratna, M. R., Zhang, Q., Worsnop, D. R., and Jimenez, J. L.: Interpretation of organic components from Positive Matrix Factorization of aerosol mass spectrometric data, Atmos. Chem. Phys., 9, 2891–2918, 2009, http://www.atmos-chem-phys.net/9/2891/2009/.

Volkamer, R., Jimenez, J. L., San Martini, F., Dzepina, K., Zhang, Q., Salcedo, D., Molina, L. T., Worsnop, D. R., and Molina, M. J.: Secondary organic aerosol formation from anthropogenic air pollution: Rapid and higher than expected, Geophys. Res. Lett., 33, L17811, doi:10.1029/2006GL026899, 2006.

Wang, W., Rood, M. J., Carrico, C. M., Covert, D. S., Quinn, P. K., and Bates, T. S.: Aerosol optical properties along the northeast coast of North America during the New England Air Quality Study – Intercontinental Transport and Chemical Transformation 2004 campaign and the influence of aerosol composition, J. Geophys. Res.-Atmos., 112, D10S23, doi:10.1029/2006JD007579, 2007.

Weber, R. J., Sullivan, A. P., Peltier, R. E., Russell, A., Yan, B., Zheng, M., de Gouw, J., Warneke, C., Brock, C., Holloway, J. S., Atlas, E. L., and Edgerton, E.: A study of secondary organic aerosol formation in the anthropogenic-influenced southeastern United States, J. Geophys. Res., 112, D13302, doi:10.1029/2007JD008408, 2007.

Williams, B. J., Goldstein, A. H., Millet, D. B., Holzinger, R., Kreisberg, N. M., Hering, S. V., White, A. B., Worsnop, D. R., Allan, J. D., and Jimenez, J. L.: Chemical speciation of organic aerosol during the International Consortium for Atmospheric Research on Transport and Transformation 2004: Results from in situ measurements, J. Geophys. Res.-Atmos., 112, D10S26, doi:10.1029/2006JD007601, 2007.

Zhang, Q., Alfarra, M. R., Worsnop, D. R., Allan, J. D., Coe, H., Canagaratna, M. R., and Jimenez, J. L.: Deconvolution and quantification of hydrocarbon-like and oxygenated organic aerosols based on aerosol mass spectrometry, Environ. Sci. Technol., 39, 4938–4952, doi:10.1029/2007GL029979,, 2005a.

Zhang, Q., Worsnop, D. R., Canagaratna, M. R., and Jimenez, J. L.: Hydrocarbon-like and oxygenated organic aerosols in Pittsburgh: insights into sources and processes of organic aerosols, Atmos. Chem. Phys., 5, 3289-3311, 2005b, http://www.atmos-chem-phys.net/5/3289/2005/.

Zhang, Q., Jimenez, J. L., Canagaratna, M. R., Allan, J. D., Coe, H., Ulbrich, I., Alfarra, M. R., Takami, A., Middlebrook, A. M., Sun, Y. L., Dzepina, K., Dunlea, E., Docherty, K., DeCarlo, P. F., Salcedo, D., Onasch, T., Jayne, J. T., Miyoshi, T., Shimono, A., Hatakeyama, S., Takegawa, N., Kondo, Y., Schneider, J., Drewnick, F., Borrmann, S., Weimer, S., Demerjian, K., Williams, P., Bower, K., Bahreini, R., Cottrell, L., Griffin, R. J., Rautiainen, J., Sun, J. Y., Zhang, Y. M., and Worsnop, D. R.: Ubiquity and dominance of oxygenated species in organic aerosols in anthropogenically-influenced Northern Hemisphere midlatitudes, Geophys. Res. Lett., 34, L13801, doi:10.1029/2007GL029979, 2007.

4.4 Paper III: Climate impact of semi-volatile aerosol components in North-Western Europe

Enhancement of the aerosol direct radiative effect by semi-volatile aerosol components: Airborne measurements in North-Western Europe

W.T. Morgan, J.D. Allan, K.N. Bower, M. Esselborn, B. Harris, J.S. Henzing, E.J. Highwood, A. Kiendler-Scharr, G.R. McMeeking, A.A. Mensah, M.J. Northway, S. Osborne, P.I. Williams, R. Krejci and H. Coe

Atmospheric Chemistry & Physics Discussions, 10 (4), 10653-10705, 2010
Revised and submitted to Atmospheric Chemistry & Physics

Submission date: 26 August 2010

Overview: This paper presents aerosol chemical composition and optical property measurements from two aircraft and one ground-based location in North-Western Europe. The vertical distribution of aerosol chemical composition in the atmospheric column above Cabauw is presented, which shows that ammonium nitrate and organic matter are significantly enhanced at the top of the boundary layer relative to the ground-based measurements. This is prescribed to partitioning of semi-volatile gas phase species to the particle phase at reduced temperature and enhanced relative humidity. Such increases strongly enhanced the ambient scattering potential of the aerosol burden. In polluted conditions, the aerosol optical depth was increased by 50-100% when the observed increase in secondary aerosol mass and associated water uptake was accounted for. Such enhancements conspired to increase the aerosol direct radiative forcing by more than a factor of 2. Such increases have major ramifications for regional climate predictions as semi-volatile components are often not included in aerosol models. Consequently, the observations indicate that failure to include the semi-volatile behavior of ammonium nitrate will result in significant errors in predicted aerosol direct radiative forcing. I led the AMS data collection, the data analysis and manuscript preparation.

Contributions from co-authors: Bower and Williams developed the cToF-AMS for use on-board the BAe-146. Allan, Esselborn, Henzing, Kiendler-Scharr, McMeeking, Mensah and Williams participated in the fieldwork. Bower, Highwood, Northway, Krejci and Coe were involved in flight planning for the flights. Allan, Esselborn, Harris, Henzing, Kiendler-Scharr, McMeeking, Mensah, Northway, Osborne, Krejci and Coe assisted in the data analysis. Allan, Harris, Henzing, Kiendler-Scharr, McMeeking, Osborne, Krejci and Coe assisted in manuscript preparation.

Manuscript prepared for Atmos. Chem. Phys.
with version 2.3 of the LaTeX class copernicus.cls.
Date: 26 August 2010

Enhancement of the aerosol direct radiative effect by semi-volatile aerosol components: Airborne measurements in North-Western Europe

W. T. Morgan[1], J. D. Allan[1,2], K. N. Bower[1], M. Esselborn[3+], B. Harris[4], J. S. Henzing[5], E.J. Highwood[4], A. Kiendler-Scharr[6], G. R. McMeeking[1], A. A. Mensah[6], M. J. Northway[4], S. Osborne[7*], P. I. Williams[1,2], R. Krejci[8], and H. Coe[1]

[1]Centre for Atmospheric Science, University of Manchester, Manchester, UK
[2]National Centre for Atmospheric Science, University of Manchester, Manchester, UK
[3]Institut für Physik der Atmosphäre, Deutsches Zentrum für Luft-und Raumfahrt (DLR), Oberpfaffenhofen, Germany
[4]Department of Meteorology, University of Reading, UK
[5]TNO, Utrecht, Netherlands
[6]Institute for Chemistry and Dynamics of the Geosphere, Institute 2: Troposphere, Research Centre Jülich, Jülich, Germany
[7]Met Office, Exeter, UK
[8]Department of Applied Environmental Science, Atmospheric Science Unit, Stockholm University, Sweden
[+]Now at European Southern Observatory (ESO), 85748 Garching bei München, Germany
[*]Now at Met Office, Cardington, UK

Correspondence to: W. T. Morgan (william.morgan@postgrad.manchester.ac.uk)

Abstract. A case study of atmospheric aerosol measurements exploring the impact of the vertical distribution of aerosol chemical composition upon the radiative budget in North-Western Europe is presented. Sub-micron aerosol chemical composition was measured by an Aerodyne Aerosol Mass Spectrometer (AMS) on both an airborne platform and a ground-based site at Cabauw in the Netherlands. The examined period in May 2008 was characterised by enhanced pollution loadings in North-Western Europe and was dominated by ammonium nitrate and Organic Matter (OM). Both ammonium nitrate and OM were observed to increase with altitude in the atmospheric boundary layer. This is primarily attributed to partitioning of semi-volatile gas phase species to the particle phase at reduced temperature and enhanced relative humidity. Increased ammonium nitrate concentrations in particular were found to strongly increase the ambient scattering potential of the aerosol burden, which was a consequence of the large amount of associated water as well as the enhanced mass. During particularly polluted conditions, increases in aerosol optical depth of 50-100% were estimated to occur due to the observed increase in secondary aerosol mass and associated water uptake. Furthermore, the single scattering albedo was also shown to increase with height in the boundary layer. These enhancements combined to increase the negative direct aerosol radiative forcing by close to a factor of two at the median percentile level. Such increases have major ramifications for regional climate predictions as semi-volatile components are often not included in aerosol models.

The results presented here provide an ideal opportunity to test regional and global representations of both the aerosol vertical distribution and subsequent impacts in North-Western Europe. North-Western Europe can be viewed as an analogue for the possible future air quality over other polluted regions of the Northern Hemisphere, where substantial reductions in sulphur dioxide emissions have yet to occur. Anticipated reductions in sulphur dioxide in polluted regions will result in an increase in the availability of ammonia to form ammonium nitrate as opposed to ammonium sulphate. This will be most important where intensive agricultural practises occur. Our observations over North-Western Europe, a region where sulphur dioxide emissions have already been reduced, indicate that failure to include the semi-volatile behaviour of ammonium nitrate will result in significant errors in predicted aerosol direct radiative forcing. Such errors will be particularly significant on regional scales.

1 Introduction

The radiative impact of anthropogenic aerosols is often most keenly felt upon regional scales due to its shorter life-time compared to greenhouse gases (e.g. Charlson et al., 1992). This is particularly evident over industrialized regions of the Northern Hemisphere such as North America, Europe and Asian countries such as India and China. Characterisation of aerosol chemical components and associated processes is paramount in order to assess the direct and indirect radiative forcing of atmospheric aerosol (e.g. Forster et al., 2007). Such assessments are traditionally undertaken via employment of global or regional scale models. However, these often produce wildly differing results due to the complexity of representing atmospheric aerosol (Kinne et al., 2006; Textor et al., 2006). One such complexity is the representation of semi-volatile compounds.

Traditionally, thermodynamical treatments of nitrate have not been included in global circulation models due to such difficulties (e.g. Myhre et al., 2006), although it has received more attention in global and regional chemical transport models (e.g. Schaap et al., 2004; Myhre et al., 2006). These intricacies also apply to representation of semi-volatile organic compounds. Ammonium nitrate and Organic Matter (OM) are two of the most abundant aerosol components in polluted regions of Europe (e.g. Putaud et al., 2004). Furthermore, the relative importance of such species to the aerosol burden in Europe is liable to further increase in the future due to the substantial reductions in sulphur dioxide that have occurred over the last 30 years (Monks et al., 2009). A key observation of previous studies in Western Europe is that nitrate is the dominant component during periods of high pollutant concentrations (Putaud et al., 2004; Morgan et al., 2009, 2010). Furthermore, ammonium nitrate has been shown to be a major contributor to aerosol light scattering in Western Europe based upon ground-based measurements (e.g. Diederen et al., 1985; Brink et al., 1996).

The vertical distribution of aerosol chemical components is a key parameter governing the radiative balance of the climate system (Textor et al., 2006). Deficiencies in its representation in

global aerosol models produce significant uncertainties in estimates of the aerosol direct effect (Textor et al., 2006). Vertical profiles of ammonium nitrate, a semi-volatile inorganic salt, indicate that concentrations regularly peak at the top of the boundary layer (Neuman et al., 2003; Morino et al., 2006; Crosier et al., 2007; Morgan et al., 2009). Such observations have been attributed to the equilibrium between gas phase nitric acid (HNO_3), ammonia (NH_3) and particulate ammonium nitrate (NH_4NO_3), which favours the particle phase at reduced temperature and enhanced relative humidity typical of the top of the boundary layer.

A growing body of evidence (Donahue et al., 2006; Robinson et al., 2007; Huffman et al., 2009; Jimenez et al., 2009) has recently highlighted the semi-volatile nature of the OM component of the atmospheric aerosol burden. Thus enhancement of the OM component could occur at the top of the boundary layer due to condensation to the particle phase in a similar manner to ammonium nitrate. Such a process could have major implications, as OM has been shown to dominate the sub-micron aerosol burden in many polluted locations across the Northern Hemisphere (Zhang et al., 2007). Furthermore, Zhang et al. (2007) indicated that the Secondary Organic Aerosol (SOA) component dominated on regional scales when compared to Primary Organic Aerosol (POA). Recent studies have shown that the more volatile fraction of the SOA dominates during the initial stages of oxidation, whereas lower volatility SOA is observed to be the largest fraction once the OM has aged appreciably (Morgan et al., 2010; Ng et al., 2010). Thus on continental scales such as North-Western Europe, the semi-volatile behaviour of OM may be highly important. Furthermore, the major contribution of OM and ammonium nitrate is not a situation specific to North-Western Europe. For example, the state of California in the USA is a region where both ammonium nitrate (e.g. White and Roberts, 1977; Neuman et al., 2003) and SOA (e.g. Docherty et al., 2008) are prevalent. Thus there is significant potential for perturbation of the radiative balance of the climate system on regional scales via addition of particulate mass by condensation of semi-volatile aerosol precursors.

Morgan et al. (2010) presented an overview of the aerosol chemical composition measurements from the UK Facility for Airborne Atmospheric Measurements (FAAM) BAe-146 research aircraft during the European Integrated Project on Aerosol Cloud Climate and Air Quality Interactions (EUCAARI, Kulmala et al., 2009) airborne intensive observation period. The study highlighted the ubiquity of OM across Europe and the dominance of ammonium nitrate during major pollution events in North-Western Europe. Two major OM components were identified; Low-Volatility Oxygenated Organic Aerosol (LV-OOA) and Semi-Volatile Oxygenated Organic Aerosol (SV-OOA), which correspond to more processed OM and fresher OM respectively (Jimenez et al., 2009). The spatial distribution of aerosol chemical composition indicated that the maximum pollution loading during a period dominated by anticyclonic conditions was located in North-Western Europe, specifically in the Netherlands region and the immediate outflow from it into the North Sea and English Channel. Such conditions were dominated by ammonium nitrate and the fractional contribution of the SV-OOA component to the OM was enhanced. This was a reflection of the proximity to major sources

in North-Western Europe, where the nitrogen oxide and ammonia source fields reach their maximum (Reis et al., 2009).

The focus of this manuscript is upon the identified enhanced pollution in North-Western Europe and its relationship with aerosol optical properties and the aerosol direct effect on climate. This is achieved via comparison of the coincident chemical composition measurements from the BAe-146 aircraft and a ground-based site at Cabauw, in the Netherlands. These measurements are complemented by remote sensing measurements from several ground-based locations in Western Europe. Particular focus is given to the vertical distribution of the chemical components and how this relates to the radiative impact of the aerosol burden.

2 Method

The EUCAARI airborne observation period included parallel studies known as the EUCAARI-LONG Range EXperiment (EUCAARI-LONGREX, henceforth referred to as LONGREX) and the Intensive Observation Period at Cabauw Tower (IMPACT). This analysis will focus upon flight missions conducted by the BAe-146 research aircraft when it operated in the vicinity of a ground-based measurement tower at Cabauw, in the western Netherlands. Cabauw served as the ground-based component and base of IMPACT, while the BAe-146 operated as a part of LONGREX. Flights in this area were characterised by high pollution loadings and predominantly cloud-free conditions. The selected flights are summarised in Table 1 and Fig. 1.

A suite of instrumentation capable of determining the chemical composition, microphysical, optical and hygroscopic properties of the atmospheric aerosol burden was utilised on the FAAM BAe-146 research aircraft during the LONGREX flying period. The BAe-146 flew in conjunction with the Deutsches Zentrum für Luft-und Raumfahrt (DLR) Falcon 20-E5 (e.g. Wandinger et al., 2002), which operated a LIDAR system that included a High Spectral Resolution LIDAR mode (HSRL, Esselborn et al., 2008). The HSRL measured aerosol backscatter and extinction coefficients in real time, which allowed identification of pollution plumes and subsequent sampling in-situ by the BAe-146. The Cabauw ground-based site is located in the western Netherlands (51° 58.223' N, 4° 55.575' E, shown in Fig. 1) in a predominantly agricultural setting, thus the site is largely representative of the wider region (Van Ulden and Wieringa, 1996). The aerosol instrumentation at the site sampled from a 60 m high inlet. Additionally, regular radiosonde launches from Cabauw were conducted during the study. An AErosol RObotic NETwork (AERONET, Holben et al., 1998) station is also located at Cabauw. Details of the relevant instrumentation utilised from the ground-based site at Cabauw and the BAe-146 are summarised in Table 2.

2.1 Aerosol chemical composition

A Droplet Measurement Technologies (DMT) Single Particle Soot Photometer (SP2, Stephens et al., 2003; Baumgardner et al., 2004) measured Black Carbon (BC) mass and the number of particles containing a BC core as a function of particle size over a diameter range of 55-400 nm assuming an ambient BC density of 1.8 $\mathrm{g cm^{-3}}$. The detection efficiency for BC particles at the smallest sizes may be less than 100% (Schwarz et al., 2010). In order to improve determination of the optical size of absorbing particles, the SP2 was modified to include a four-element avalanche photodiode (Gao et al., 2007).

Size-resolved chemical composition information of non-refractory particulate matter of widely varying volatility was measured by an Aerodyne compact Time-of-Flight Aerosol Mass Spectrometer (cToF-AMS, Drewnick et al., 2005; Canagaratna et al., 2007) onboard the BAe-146. Previous studies (Crosier et al., 2007; Morgan et al., 2009) have included detailed information regarding the sampling strategy of the AMS on the BAe-146. Morgan et al. (2010) included specific information regarding the quantification and analysis of the BAe-146 AMS data pertinent to this study. Details regarding the derivation of size-resolved chemical composition from the AMS on the BAe-146 is included in Appendix A. Additionally, a High-Resolution Time-of-Flight AMS (HR-ToF-AMS, DeCarlo et al., 2006; Canagaratna et al., 2007) was deployed at Cabauw during the study (Mensah, 2010), providing complementary chemical composition data to the airborne cToF-AMS. The AMS uses an aerodynamic lens system (Liu et al., 1995a,b) which has 100% transmission for 40–700 nm vacuum aerodynamic diameter (DeCarlo et al., 2004) particles. Mass concentration values are reported as micrograms per standard cubic metre ($\mathrm{\mu g\,sm^{-3}}$) i.e. at Standard Temperature and Pressure (STP) of 273.15 K and 1013.25 hPa respectively. The aerosol physical and optical properties detailed in the following section are also converted to STP in order to compare with the AMS measurements.

2.2 Aerosol physical and optical properties

A wing-mounted Particle Measurement Systems (PMS) Passive Cavity Aerosol Spectrometer Probe 100X (PCASP, Liu et al., 1992; Strapp et al., 1992) was used to measure dry number-size distributions of the aerosol burden. This is achieved via optical counting and sizing of particles across 15 channels across a diameter size range of 0.1-3 $\mu\mathrm{m}$. Particle size is determined via experimental calibrations using Di-Ethyl-Hexyl-Sebacate (DEHS), which is converted to a Polystyrene Latex Sphere (PSL) equivalent size.

The optical characteristics of the aerosol burden were determined using a TSI 3563 Nephelometer (Anderson et al., 1996) and a Radiance Research Particle Soot Absorption Photometer (PSAP, Bond et al., 1999). The operational procedures for these systems on the BAe-146 have been described previously (e.g. Osborne et al., 2007; Haywood et al., 2008), thus only a brief summary and specific

details pertinent to this study are described here.

The PSAP measures the absorption coefficient at 567 nm via monitoring the rate of decay of light transmission due to accumulation of absorbing particles upon a filter. Several corrections to the PSAP absorption coefficient are required (Bond et al., 1999). These include misinterpretation of scattering as absorption by purely scattering particles and overestimation of the absorption coefficient as a result of multiple scattering at the filter fibers. Furthermore, recent analyses (Cappa et al., 2008; Lack et al., 2008) have identified significant enhancement of the PSAP absorption signal that is correlated with high organic aerosol loadings, although no attempt is made in this study to account for any such enhancements.

The nephelometer system onboard the BAe-146 comprises two separate instruments operating in series. Scattering coefficients were corrected for angular truncation and non-lambertian light source errors assuming sub-micron aerosol dominated the scattering following the procedure presented by Anderson and Ogren (1998). The first nephelometer measures the sample aerosol in a 'dry' condition. The system does not use an active drying method, rather it relies on inlet ram heating and the increase in temperature in the cabin to reduce the humidity in the sample. This is usually sufficient to obtain 'dry' Relative Humidity (RH) values in the range of 20-40%. The aerosol sample is then passed through a controlled humidifier, which cycles between a 40-90% RH range prior to being sampled by the second instrument in order to measure the scattering coefficient as a function of RH. This allows derivation of the hygroscopic scattering enhancement, $f(RH)$, to be determined. The mean $f(RH)$ growth curve from each flight was used to calculate the ambient scattering coefficient by combining the dry nephelometer measurements with the measured ambient RH. Additional details regarding corrections to the nephelometer data are included in Appendix B.

At the Cabauw ground-based site, a single three-wavelength nephelometerl identical to the instruments operated on the BAe-146 sampled dry aerosol and was operated alongside a Thermo model 5012 Multi-Angle Absorption Photometer (MAAP Petzold et al., 2005), which measures the aerosol absorption coefficient at 670 nm. The nephelometer underwent the same corrections as the BAe-146 version for angular truncation and non-lambertian source errors. Both the MAAP and PSAP absorption coefficients were converted to the reference wavelengths of the nephelometer assuming a $1/\lambda$ wavelength dependence, which is consistent with urban derived aerosol where the absorption is dominated by black carbon (e.g. Kirchstetter et al., 2004; Bond and Bergstrom, 2006). Furthermore, no significant influence by biomass burning or mineral dust was present for these case studies, both of which are the major contributors to increased absorption wavelength dependence (i.e. exceeding the $1/\lambda$ wavelength dependence). These could then be combined with the nephelometer measurements to calculate the aerosol extinction coefficient and the single scattering albedo, ω_0.

2.3 Aerosol Mie scattering calculations

The experimental data alone cannot be used to separate the sensitivities of the aerosol scattering to changes in chemical composition and uptake of water vapour, so in order to estimate this, a Mie scattering model is employed to explore this sensitivity.

A Mie scattering code (Edwards and Slingo, 1996) was used to calculate the scattering due to aerosols at a wavelength of 550 nm based upon measured aerosol chemical and physical properties measured onboard the aircraft. The Mie code calculates scattering, absorption and phase function for a given aerosol mass based on its size distribution, bulk density and refractive index. In this case, the dry number-size distributions from the PCASP below 1 $\mu\mathrm{m}$ were used. Dry bulk density and refractive index were estimated using volume mixing of the component refractive indices and densities of the individual constituent aerosol components (summarised in Table 3) based upon the AMS and SP2 measurements. While such assumptions can prove quantitatively problematic (e.g. Oshima et al., 2009), we include the calculations in order to explore the sensitivity of atmospheric aerosol to changes in aerosol chemical composition, which includes the addition of water at high relative humidity.

In order to calculate the scattering coefficient in a fully humidified atmosphere, the contribution of hygroscopic water uptake to the bulk size distribution, refractive index and density of the aerosol must be calculated. The bulk hygroscopic growth factor of the aerosol mass was estimated by combining the individual growth factors of the constituent aerosol components at the required relative humidity using a ZSR mixing rule approach (Zdanovskii-Stokes-Robinson, Stokes and Robinson, 1966; Gysel et al., 2007; Swietlicki et al., 2008). The growth factors of the inorganic components (ammonium nitrate and ammonium sulphate) were parameterised based upon the work of Tang (1996), while BC was assumed to have a growth factor equal to unity. The hygroscopicity of the organic component was assumed to be consistent with that of Suwanee river fulvic acid using the treatment from Brooks et al. (2004). Fulvic acid was assumed to be representative of the relatively aged-oxidised nature of the OM encountered in this study, as it has chemical functionalities that are representative of aged OM (e.g. McFiggans et al., 2005). The volume of water taken up by the aerosol was then calculated based upon calculation of a humidified size distribution produced by applying the hygroscopic growth factor to the dry PCASP size distribution. Hygroscopic growth was assumed to occur uniformly across the entire size range, with no change in number density. A humidified bulk density and refractive index was then estimated by incorporating the physical and optical properties of water into the aerosol volume mixing calculation. Further details regarding this approach and its application to the entire LONGREX dataset will be included in a future manuscript in the EUCAARI Special Issue.

3 Overview of conditions in North-Western Europe during May 2008

In order to set the measurements over Cabauw in the context of the larger scale spatial distribution of Aerosol Optical Depth (AOD), data from several AERONET stations is shown in Fig. 2a from the high pressure period of LONGREX from the 06-14 May 2008. The latter days of the campaign i.e. when B379 took place are not shown as the temporal coverage was poor at some of the stations, particularly at Leipzig. The locations of the AERONET stations are approximately orientated west-to-east (shown in Fig. 1) in order to examine the impact of the large scale synoptic situation upon the AOD distribution. The AOD increased as a function of longitude from east-to-west, ranging from median values of 0.13 in Belsk to 0.30 at Chilbolton. The stations in North-Western Europe, Cabauw and Chilbolton, regularly exceeded the 95^{th} percentile value (0.32) observed at Leipzig, indicating that there was a significant gradient in the aerosol fields between these locations.

Fig. 2b displays a histogram of daily averaged AOD measurements for both May 2008 and all of 2008 at Cabauw. AOD values at Cabauw were typically below 0.2 on approximately 50% of the days with available measurements during all of 2008. The level 2.0 AERONET product is used which is cloud-screened, thus the meausurements are biased towards clearer sky periods and Spring/Summer (April-September). During May 2008, there were no AOD events below 0.1, with 16% of the days having daily averaged values from 0.1-0.2. The proportion of days where the AOD was between 0.2-0.3 (35%) was greatly enhanced compared with the long-term measurements (24%). Furthermore, there were a greater proportion of events at even larger AOD values compared with the annual statistics. These results indicate that May 2008 was a particularly polluted period compared with the rest of 2008.

For additional context in terms of the aerosol chemical composition, measurements from the HR-Tof-AMS at the ground-based site at Cabauw are shown in Fig. 3. The measurements presented correspond to the periods when the BAe-146 operated in the vicinity of Cabauw. A key feature of these periods is the dominance of the OM component over the nitrate component, particularly during daytime hours. A Positive Matrix Factorisation (PMF, Paatero, 1997; Paatero and Tapper, 1994) analysis of the organic mass spectra measured by the HR-ToF-AMS at Cabauw was conducted using the principles introduced by Ulbrich et al. (2009). The resolved PMF components were interpreted based upon their similarity to reference mass spectra and correlations with external time series (Mensah, 2010). The nomenclature used follows the framework adopted by Jimenez et al. (2009), which is consistent with the procedures used in Morgan et al. (2010). The PMF analysis revealed four major components; Hydrocarbon-like Organic Aerosol (HOA), SV-OOA and two LV-OOA type factors (Mensah, 2010). The SV-OOA time series shown in Fig. 3 displays similar trends to the nitrate time series, which is a common observation due to their semi-volatile nature. Furthermore, the SV-OOA component is typically less than the combined LV-OOA components.

Also shown are two radiosonde profiles of temperature and RH from days when the aircraft operated in the vicinity of Cabauw. These highlight the well-mixed nature of the atmospheric boundary

layer, with the ambient temperature profile closely following the adiabatic lapse rate and the RH profile peaking at the top of the boundary layer at approximately 2000 m. The well-mixed nature of the boundary layer over continental Europe was a key feature of the flights in this region.

The well-mixed nature of the boundary layer could also be determined from the aircraft operations. This is illustrated by Fig. 4 which shows the thermodynamic structure and its influence upon the aerosol concentration and composition from flight B362. The flight consisted of a sequence of Straight and Level Runs (SLRs) between 500-2000 m altitude heading north-westwards over continental Europe, followed by several lower level SLRs and profiles down to approximately 100 m over the North Sea off the eastern coast of the UK. Fig. 4b displays the relationship between the wet equivalent potential temperature and the total water content. A relatively linear relationship between these two properties indicates a water vapour-wet equivalent potential temperature mixing line, which was predominantly the case for most of the flight. The main divergence from this simple linear relationship corresponded to the low-level SLR-8 over the North Sea at approximately 100 m altitude, where a layer of much moister air was encountered. The mass-size distribution measured by the AMS during SLR-8 is shown in Fig. 4d, which shows that the aerosol was strongly enriched in ammonium nitrate and OM and that considerable amounts were present at large sizes (the largest particles are likely to be less efficiently transmitted through the aerodynamic lens, thus the concentrations reported in such instances are likely an underestimate). These shallow-moist layers over the ocean surface were consistently observed during the study, with associated enhancements in aerosol concentrations. The points are coloured according to the nitrate mass fraction, defined as the fractional contribution of nitrate to the total mass concentration derived from the AMS. Over continental Europe, enhanced nitrate mass fractions and increased sub-micron aerosol concentrations were associated with increases in potential temperature. This phenomenon is indicative of vertical mixing of air parcels within the boundary layer. During the flight, nitrate is either approximately equal to or enhanced relative to the OM, unlike the surface observations at Cabauw where the OM component is greater than the nitrate component.

4 Vertical distribution of aerosol chemical composition

The vertical variation in the aerosol chemical composition is presented in Fig. 5 from flights B366 and B379. Both flights consisted of SLRs between 600-2000 m altitude from east-to-west across Northern Germany and the Netherlands with short 'saw-tooth' profiles in order to probe the vertical variability. Both incorporated a series of SLRs at different altitudes upwind of the ground-site at Cabauw and are characterised by significant sub-micron aerosol loadings. These revealed a clear increasing gradient in total aerosol mass from east-to-west, which was predominantly driven by increasing OM and ammonium nitrate concentrations (see Morgan et al., 2010, for a more detailed discussion). Flight B366, whose flight track is shown in Fig. 5a, indicated that there is significant

variability in the concentrations of the OM and ammonium nitrate. Nitrate concentrations ranged from 2-12 $\mu g\,sm^{-3}$ in the vicinity of Cabauw, while OM concentration ranged from 2-5 $\mu g\,sm^{-3}$. Concentrations of nitrate and OM at the ground-site at Cabauw during this period were approximately 2–2.5 $\mu g\,sm^{-3}$ each. The second example is from B379, whose flight track is shown in Fig. 5c. The nitrate concentration exceeded that of the OM component on the aircraft, while at the surface the concentrations were approximately equal. The nitrate concentration at the surface was 3-4 $\mu g\,sm^{-3}$, while aloft the concentrations regularly exceeded 6 $\mu g\,sm^{-3}$. Additionally, the OM concentration was enhanced aloft compared with the ground-based measurements.

The vertical distribution of aerosol chemical composition from B366 during the SLRs in the vicinity of Cabauw is summarised in Fig. 6a. SLRs are used as the vertical profiles during the flights were relatively short compared to the AMS sampling frequency (30 s), thus if profiles were shown then very few data points would be included. B379 is not shown as the SLRs had reduced vertical coverage compared with B366. Comparison with the AMS measurements from the ground site indicated that the total mass concentration was enhanced aloft. The nitrate mass fraction increased with altitude and was the dominant chemical component, while at the ground, the OM component dominated. Furthermore, there was an increasing gradient in the OM concentration up to approximately 1500 m relative to the ground, while the absolute concentration exceeded the surface OM concentration up to approximately 2000 m. The LV-OOA mass concentration was relatively constant throughout the boundary layer and was very similar to the sulphate profile. Consequently, the increase in the OM was dominated by an increase in the SV-OOA component. The significant variability in the concentrations, as indicated by the large inter-quartile range at each altitude for nitrate and OM, was a consequence of vertical mixing. As the aircraft operated at a constant altitude over each SLR, the air mass sampled switched between surface originating air and mid-tropospheric air, modulating the aerosol concentrations accordingly. The SLRs typically range from at least 10-30 data points i.e. approximately 5-15 minutes sampling time. The SLR at 2100 m for example contained 11 data points. During B379, the mass concentrations for nitrate and OM were again elevated relative to the ground. Median nitrate concentrations of 6.9 $\mu g\,sm^{-3}$ and 7.3 $\mu g\,sm^{-3}$ at 500m and 1300m respectively were observed, while the OM median concentrations were 4.5 and 4.7 $\mu g\,sm^{-3}$. This compared with ground-based AMS measured values from 2.8-3.4 $\mu g\,sm^{-3}$ for nitrate and 2.7-3.2 $\mu g\,sm^{-3}$ for OM during this period.

Fig. 6b displays the strong association between the SV-OOA component and nitrate that existed in these polluted examples of flight operations in North-Western Europe. The markers in Fig. 6b are sized according to the longitude of the aircraft, which indicates that the association between SV-OOA and nitrate increases in Western Europe.

Fig. 7 displays the relationship between the aerosol chemical composition and the aerosol physical properties by comparing the AMS with the PCASP instrument during B379 (the PCASP was not functioning during B366). Fig. 7a shows that as the aerosol mass concentration increased, the

sub-micron number concentration measured by the PCASP increased, as does the mean geometric diameter of the aerosol. Thus the number concentration measured by the PCASP increases as more particles are present in the size range measured by the PCASP i.e. above 100 nm. This shift in the mean size displays an altitude dependence, which is shown in Fig. 7b, with a greater mean size towards the top of the boundary layer.

5 Aerosol optical properties

5.1 Aerosol scattering coefficient

Fig. 8 displays the relationship between the ambient scattering coefficient and total aerosol mass concentrations observed on the aircraft, which shows a strong coupling between them. The observed variability in the total mass concentration is driven predominantly by ammonium nitrate, with additional input from the SV-OOA in these cases.

To investigate the effect of the increase in semi-volatile components and the associated additional water on the optical properties as a function of height, we have compared the aircraft measurements made throughout the depth of the boundary layer, with the optical properties of the aerosol based upon the observations at the ground, extrapolated throughout the depth of the boundary layer. No additional particle mass was added to the ground based aerosol measurements with height but the aerosol were allowed to increase in size due to additional water condensation at higher humidities. This is accomplished using the following procedure:

1. Extract and average the scattering and absorption data that is coincident with the BAe-146 overpasses.
2. Assume that the number, mass and chemical composition of the particulate as measured at the ground are representative of the entire depth of the well-mixed boundary layer.
3. Calculate the ambient scattering vertical profile by assuming that this is equal to the scattering at the ground plus the additional water uptake as a function of increasing relative humidity, which is calculated from the $f(RH)$ measurements from the aircraft and the RH data from the radiosonde launches.
4. Assume that the absorption coefficient is not dependent upon RH and that the value is uniform throughout the boundary layer, which is consistent with the airborne and ground-based measurements.
5. Combine the estimated ambient scattering and absorption profiles to estimate the total extinction profile, which in turn can be used to estimate the AOD.
6. Calculate the average ambient ω_0 through the boundary layer column.

The above were estimated for boundary layer aerosol based upon the radiosonde data and the aerosol measurements from the BAe-146 during B366 and B379. The estimated ambient scattering profiles based upon the Cabauw data are shown in Fig. 9. Vertical profiles are used rather than SLRs as the nephelometer measurements from the aircraft have a time resolution of 1 s, which allows the vertical gradients to be more easily captured while minimising the impact of horizontal gradients upon the comparison with the ground. Also shown is the in-situ measured scattering from the aircraft when it operated in the vicinity of Cabauw. This shows that the scattering profile is entirely consistent with the chemical composition data, with strong enhancements relative to the ground-based measurements and an increasing gradient with height. This strong enhancement is particularly clear in Fig. 8, which demonstrates that the increased measured scattering is strongly associated with increased aerosol mass and that this is consistent with increased ammonium nitrate concentrations. The dry scattering coefficient measured by the nephelometer has an uncertainty estimate of 10% (Anderson et al., 1996). When comparing the dry scattering coefficient profile from the aircraft with the ground-based measurements, the airborne measurements are generally above this uncertainty and are consistent with the increased dry aerosol mass measured by the AMS. Some datapoints from B366 fall within the 10% band due to variability in the vertical domain closer to the surface and at the very top of the boundary layer.

The results indicate that there is a clear enhancement in the scattering coefficient when comparing between the in-situ measurements from the aircraft and those estimated based on the ground-based values. Also shown in Fig. 9a is the HSRL extinction profile observed from the DLR Falcon which took place shortly before the BAe-146 operations in the vicinity of Cabauw. The HSRL extinction profile follows the same general structure as the BAe-146, although the HSRL profile is averaged over a relatively short period in comparison to the BAe-146 measurements thus it does not exhibit the same variability. In Fig. 9b, the HSRL extinction profile shown is from several hours after the BAe-146 measurements. The HSRL extinction profile was approximately a factor of 2 greater than the measured profile from the BAe-146 earlier in the day. This is consistent with the advection of more polluted air over the ground site between the BAe-146 and HSRL measurement periods, which can be seen in Fig. 3. Nevertheless, the general vertical structure and main features are very similar. Also shown in Fig. 9b is the estimated scattering profile based on the Cabauw ground-based measurements during the HSRL measurements. Again there is considerable enhancement in the measured scattering profile versus the estimated scattering profile in this instance.

The relatively modest enhancement for B366 compared to B379 between 1500-2000 m is likely a result of differences in the thermodynamic structure observed by the aircraft and the radiosonde at the top of the boundary layer. The aircraft measurements indicate that the RH is beginning to reduce below 2000 m, which is consistent with the extinction profile from the HSRL, whereas for the radiosonde ascent, the RH does not begin to reduce until slightly above this level. For B379, the thermodynamic structure measured by the radiosonde ascent and the aircraft are in excellent

agreement, thus the scattering profiles display similar vertical structure.

5.2 Aerosol optical depth and single scattering albedo

The AOD and ω_0 values derived from the aircraft measurements were compared with the estimated values from the ground-based data assuming that the extinction below 500 m is equal to the estimated extinction based upon the ground-based in situ measurements, as the aircraft was unable to sample below that level. The results from B366 and B379 are summarised in Table 4.

For B366, the AOD calculated from the aircraft measurements was enhanced relative to the ground-based estimate above the 50^{th} percentile level, with increased AOD values of 14-21%. The AOD calculated from the airborne measurements is in good agreement with the HSRL, which measured average AOD values of 0.21 ± 0.05. At the lower percentile values, the aircraft values are comparable to the ground-based estimate. For B379, the AOD at the 50^{th} percentile level is enhanced by 80%, while at the 75^{th} percentile, the AOD measured on the aircraft was double that estimated from the ground. The increase in scattering aloft also caused a moderate change in ω_0 due to the enhanced scattering contribution to the total extinction.

The AOD from the aircraft measurements was also calculated at 450 nm in order to compare with corresponding AERONET measurements at 440 nm. The AOD for the entire vertical column was not estimated from the ground-based measurements as these only refer to the boundary layer contribution as the measurements do not reflect aerosol properties in the free troposphere. The AERONET AOD corresponds to the total vertical column, while the BAe-146 measurements refer to the aerosol profile below 7500 m and 8500 m for B366 and B379 respectively, as this was the maximum altitude achieved by the aircraft in the vicinity of Cabauw. The AOD contribution below the operating height of the aircraft was estimated from the ground-based measurements. The results of this comparison are shown in Table 5 and indicate that 70-80% of the observable extinction was located within the boundary layer. The results for the AERONET AOD values are within the range of values measured by the BAe-146, although the aircraft measurements are biased somewhat lower compared with the AERONET AOD. This could be a consequence of some upper layers which were not observed by the aircraft, which is potentially consistent with the HSRL data which indicated an increasing gradient with altitude at 8000 m. Furthermore, estimated ambient scattering based upon the airborne nephelometer measurements may be underestimated when more hygroscopic aerosol components, such as ammonium nitrate, contribute to the majority of the aerosol mass. This is a consequence of using the mean hygroscopic growth curve measured by the wet nephelometer. This would lead to an under-prediction of the ambient scattering and hence the AOD.

5.3 Aerosol water uptake

The Mie scattering code was used to investigate the importance of aerosol water uptake based upon measured size distributions and aerosol chemical composition, which was used to estimate aerosol

water uptake based upon ZSR calculations, from SLRs during B379. Experiments were also conducted for dry aerosols, with agreement to within 30% compared with the measured dry scattering coefficient values. Comparison between ambient scattering estimates based upon the nephelometer measurements and the Mie calculated values yielded typical agreement to within 50% for RH values below 75%. For run 5, where the average RH was 80%, the Mie scattering value was close to a factor of 2 greater than the estimate based upon the nephelometer measurements. Such a discrepancy could occur due to a multitude of reasons, which result from the assumptions applied to estimate both the ambient scattering from the nephelometer measurements and the Mie scattering calculations. As mentioned in Sect. 5.2, the water uptake by more hygroscopic aerosol components was likely underestimated, which would apply in this case as ammonium nitrate represented greater than 50% of the aerosol mass for run 5. The sampling efficiency of the nephelometer may also be reduced when larger particles (at enhanced relative humidity) are introduced. The simplified assumption of uniform hygroscopic growth across an internally mixed aerosol for the Mie calculations is liable to introduce some uncertainty in the Mie ambient scattering.

Mie calculations as a function of RH were used to explore the effect of water uptake by ambient aerosols by comparing the relative change in scattering with increasing ammonium nitrate and water content. The calculations are used to explore the theoretical sensitivity of the increase in scattering associated with enhanced ammonium nitrate content and the scattering due to additional water uptake. The apparent overestimation when comparing the Mie ambient scattering with the measured values suggests that the analysis will yield the maximum likely effect. Two experiments were undertaken; one where ammonium nitrate was assumed to have a growth factor of unity and a second where the literature values for ammonium nitrate detailed in Tang (1996) were used. By comparing these two experiments, the impact of additional scattering associated with water from the increasing ammonium nitrate mass could be estimated by examining the relative increase in scattering between the two experiments. Each SLR was used as input to the Mie code using a range of relative humidities. Fig. 10 summarises the percentage increase in scattering by water associated with ammonium nitrate by comparing the two experiments for each SLR. The SLRs are ordered by increasing ammonium nitrate mass concentration/fraction. At low concentrations and mass fractions of ammonium nitrate, the impact is slight. As the mass fraction and concentration increases, the scattering enhancement due to water uptake increases strongly. The relative increases are most dramatic at the greatest relative humidities. At 70% RH, increasing the ammonium nitrate mass fraction from 25% (SLR 1) to 50% (SLR 3) increases the enhancement from 16% to 36%. At 90% RH, the enhancement increases from 42% to 112%.

5.4 Aerosol radiative forcing

Aside from the nature of the underlying surface, the AOD, ω_0 and aerosol backscatter fraction terms govern the magnitude and sign of the direct radiative forcing by aerosols. This is shown in equation

1 from Haywood and Shine (1995), which defines the aerosol induced perturbation in the upward radiation flux at the Top-Of-Atmosphere (TOA) as:

$$\Delta_a F \uparrow = \frac{1}{2} F_T T^2 (1 - A_c) \times [\omega_0 \overline{\beta}_a (1 - \overline{R}_s)^2 - 2(1 - \omega_0)\overline{R}_s] AOD \quad (1)$$

The TOA forcing, $\Delta_a F \uparrow$, is estimated using the respective values from the aircraft and the ground site. The common terms for both scenarios in equation 1 are the solar constant, F_T, equal to 1366 Wm^{-2}, the atmospheric transmittance, T, equal to 0.76, the cloud fraction, A_c and the surface albedo, R_s. The solar constant value is weighted by the cosine of the solar zenith angle in order to account for the location of Cabauw and the time of day when the measurements took place. The surface albedo is assumed to be representative of grassland values with an albedo from 0.16-0.26. We calculated the aerosol backscatter fraction, β_a, using the nephelometer measurements. The average backscatter fraction at Cabauw was 0.14, while on the aircraft an average value of 0.16 was calculated for both B366 and B379. A value of 0.16 was applied for the radiative forcing calculations as the impact is small (less than 30% for greater R_s values) compared with changes in AOD and ω_0. The radiative forcing is estimated assuming cloud-free conditions, where A_c is zero, which results in a maximum forcing estimate.

The results are summarised in Table 4 and indicate that the direct radiative forcing is strongly enhanced when comparing the in-situ boundary layer airborne measurements with the ground-based derived values. For B366, the enhancement ranged from 21-33% at the 50^{th} percentile level depending upon the surface albedo. For B379, the radiative forcing estimate was always greater based on the aircraft estimate with an enhancement greater than a factor of two at the 50^{th} percentile level. Compared with the strong changes in the AOD, the ω_0 enhancements are relatively modest, thus the major changes in radiative forcing are dominated by changes in AOD rather than ω_0 for the case studies presented.

6 Discussion

6.1 Enhancement of semi-volatile material

The ground-based AMS data indicated that during the periods considered, significant pollution loadings were present in North-Western Europe, with sub-micron aerosol loadings largely exceeding 10 $\mu\mathrm{g\,sm}^{-3}$ in daytime conditions. A consistent feature of the results presented in Section 4 is the enhanced sub-micron particulate concentrations aloft measured on the BAe-146 compared to the ground-site at Cabauw. The increase was primarily a consequence of enhanced ammonium nitrate and OM concentrations. The median nitrate concentration increased by 2.0-3.4 times that of the ground based value, while the median OM concentration was increased by a factor of up to 1.6. The median sulphate concentration measured on the aircraft was between 1.3-1.7 times that of the surface concentration, while the lower range of values sampled by the aircraft were similar to the sulphate

concentrations on the ground. At the surface the OM component was generally either greater or equal to the nitrate concentration when the aircraft was operating close to the ground site. Furthermore, the aircraft data showed that the nitrate mass fraction had a positive gradient with increasing height within the boundary layer. The combined aircraft and ground-based data showed that the sulphate concentration was relatively uniform, with a slight enhancement observable in the aircraft data. Additionally, the PCASP data indicated that the mean diameter of the aerosol increased with altitude within the boundary layer. All of the observations were consistent with semi-volatile aerosol species condensing onto pre-existing aerosol, which results in an increase in the mean diameter of the aerosol.

The fact that the sulphate concentration measured on the aircraft is somewhat greater than the value measured at the ground was likely a consequence of imperfect vertical or horizontal mixing. In order to account for such potential inhomogeneities, the observed increase in the sulphate profile was used to calculate a normalised nitrate and organic profile by multiplying the ground-based values by the observed increase in sulphate. The results of this normalisation are shown on Fig. 6a, which indicates that the observed increase in the nitrate concentration is far in excess of the normalised nitrate profile. The median OM profile is very similar to the normalised OM profile, which suggests that the more modest increase in OM may be a result of imperfect mixing. However, the factor analysis indicates that the chemical nature of the OM changes with height, with the SV-OOA component increasing with altitude in the boundary layer. The results show that the observed increase in particle mass with altitude in the boundary layer was predominately driven by ammonium nitrate.

These comparisons between the ground-based and aircraft AMS instruments suggest that the increase in the mass of nitrate is well above the uncertainty limit for AMS mass concentrations measurements (approximately 25%, Canagaratna et al., 2007), while the median and 75^{th} percentile sulphate concentrations are within these bounds. The changes in OM are close to the uncertainty limit at the median level, although the concentrations exceed this limit at the 75^{th} percentile.

These chemical and physical observations of the aerosol vertical distribution are consistent with semi-volatile partitioning of gas-phase precursors to the particle phase. Ammonium nitrate and SV-OOA were strongly associated and increased with altitude, suggesting that semi-volatile partitioning predominantly drove the enhanced particulate mass aloft. In terms of the OM burden, this is consistent with recent frameworks which have proposed that the entire OM component should be treated as semi-volatile (Donahue et al., 2006; Robinson et al., 2007). Thus, adiabatic cooling and mixing of semi-volatile organic precursors could combine to produce enhanced SOA concentrations. Coincident with the reduction in temperature is the enhanced RH at the top of the boundary layer, which further favours partitioning to the particle phase. Such examples indicate the strong impact of the thermodynamic structure of the boundary layer upon both the concentration and composition of the aerosol burden.

6.2 Impact of semi-volatile aerosol components upon the radiative budget

The partitioning of semi-volatile components to the particle phase has significant implications for the radiative budget during the pollution episodes presented. Given that the partitioning behaviour occurs at elevated levels within the boundary layer, where the RH is increased, the aerosol extinction will be further enhanced due to additional water uptake. This is evident from the relationship between the ambient scattering coefficient and total aerosol mass concentrations discussed in section 5 and in Fig. 8. A key feature was that when the ammonium nitrate mass fraction was low, the total mass concentration was also reduced which in turn decreased the level of scattering by the aerosol burden. Thus the partitioning of semi-volatile aerosol precursors contributed significantly to the AOD during major pollution episodes where sub-micron aerosol concentrations were enhanced. While the SV-OOA concentration increased during such periods, such increases were generally smaller than the increases in ammonium nitrate concentration which was often 3-4 times that of SV-OOA. Thus the majority of the increased scattering and AOD was driven by changes in the ammonium nitrate concentration.

On the basis of the B379 case study, strong enhancements in scattering were associated with increased ammonium nitrate concentrations and mass fractions. Measured increases in the ammonium nitrate mass fraction from 25% to 50%, yielded a factor of two increase in dry scattering measured by the nephelometer. Compared with the estimated AOD based upon the ground-based measurements, enhancements of up to 100% at the 75^{th} percentile level were observed based upon the airborne measurements, which translated to a more than doubling of the associated radiative forcing when taking into account the increase in ω_0 also. On the basis of Mie calculations, increases in the ammonium nitrate mass fraction resulted in major increases in aerosol water uptake. This, in addition to the increased dry mass of the aerosol, dramatically increased the scattering coefficient higher in the boundary layer where the RH was greatest. The Mie calculations underline the importance of these observations, as they illustrate the importance of the enhancement of ammonium nitrate in an area of increased relative humidity.

An important observation when comparing the two case studies was that the scattering enhancement was greater for the B379 case study relative to the B366 case study. Examination of the temperature and RH profiles showed that the B379 case study was both colder and moister than the B366 case study, which is again consistent with an increased contribution from semi-volatile components aloft. This is similar to the modelling results presented by Morino et al. (2006), where a colder and moister atmosphere increased the particle mass higher in the boundary layer relative to the ground. Furthermore, the enhanced RH will increase the water uptake by the ammonium nitrate dominated aerosol mass, as shown by the Mie calculations.

Compared with the 2008 annual frequency distribution of AOD at Cabauw, May 2008 included 24% of the days where daily averaged AOD values exceeded 0.2. Consequently, the studies in May 2008 are representative of a significant pollution episode in North-Western Europe. Furthermore,

the observed increase in AOD from east-to-west was consistent with the spatial gradients in aerosol composition shown in Figs. 5 and 6 and the overview of aerosol concentration and composition presented in Morgan et al. (2010). These demonstrated that ammonium nitrate and OM concentrations reached a maximum in North-Western Europe during the period studied. We have demonstrated that such conditions are exacerbated by the partitioning of semi-volatile precursors to the particle phase, causing a large increase in the aerosol direct radiative forcing.

In terms of future climate scenarios and accompanying aerosol radiative forcing, North-Western Europe may represent an analogue for other highly polluted regions affected by substantial agricultural emissions. Significant reductions in SO_2 have occurred in recent years (Monks et al., 2009), which diminishes the role of sulphate aerosol but increases the availability of ammonia to form ammonium nitrate. Such reductions in SO_2 are also likely to occur in other polluted regions in future (e.g. Pinder et al., 2007). Thus an inability to accurately model semi-volatile compounds is likely to be a significant deficiency in attempts to constrain the direct radiative forcing by aerosols.

7 Conclusions

A case study comparing the aerosol chemical composition measured from two platforms operating during highly polluted conditions in North-Western Europe has been presented. This revealed an increase in secondary aerosol mass as a function of altitude in the boundary layer. Specifically, airborne in-situ measurements in the vicinity of a ground-based measurement site at Cabauw, Netherlands, showed that ammonium nitrate was the dominant chemical component aloft, while at the ground OM dominated. Furthermore, the fractional contribution to the sub-micron aerosol mass of ammonium nitrate increased with height in the boundary layer. This was primarily attributed to partitioning of semi-volatile gas phase precursors to the particle phase at reduced temperature and enhanced RH, a phenomenon which has been observed previously in California (Neuman et al., 2003), Tokyo (Morino et al., 2006) and the UK region (Morgan et al., 2009). In addition to the increase in ammonium nitrate, the OM component also increased with height in the boundary layer. The results of a factor analysis of the aircraft and ground-based AMS measurements show that the enhancement in the OM component was dominated by SV-OOA. This is consistent with gas-to-particle conversion of semi-volatile organic precursors, in a similar manner to the ammonium nitrate system. Consequently, partitioning of semi-volatile species can produce significant additional inorganic and organic particulate mass.

By comparing the optical properties measured on the aircraft with coincident measurements from the ground, a strong enhancement in the AOD was shown to occur. This was coupled with an increase in the single scattering albedo also. This directly translated to a significant perturbation of the radiative balance of the atmospheric column in the region. An enhancement of the direct radiative forcing by aerosols greater than 100% was observed when taking into account the additional mass, associ-

ated water uptake and hence scattering caused by the partitioning phenomenon. The hygroscopic properties of ammonium nitrate in particular were shown to cause significant increases in aerosol scattering based upon Mie calculations. Such increases in AOD and radiative forcing have major implications for regional weather and climate, particularly as semi-volatile compounds are often not included in global and regional aerosol models (e.g. Myhre et al., 2006). Consequently, the radiative impact of anthropogenic aerosols is likely to be severely underestimated in Northern Europe, where ammonium nitrate and OM are major components of the sub-micron aerosol burden. Such underestimations are liable to be greatest during major pollution episodes. The periods identified by this study present an ideal opportunity to test regional and global climate model representations of this anthropogenically perturbed region.

Appendix A: Size-resolved aerosol chemical composition

Morgan et al. (2010) did not include information regarding the derivation of size-resolved chemical composition from the AMS on the BAe-146, thus this is included here. The particle time-of-flight measurement through the AMS vacuum chamber is dependent upon the supersonic expansion of a particle as it enters the vacuum chamber. Particle diameter (D_{va}) is related to particle velocity (v_p) via application of the following equation from Allan et al. (2003):

$$v_p = \frac{L_c}{t_p} = \frac{v_g - v_l}{1 + (D_v a / D^*)^b} + v_l \tag{A1}$$

where L_c is the particle flight length, t_p is the particle time of flight, v_g is the gas velocity on exiting the nozzle, v_l is the gas velocity within the aerodynamic lens and D^* and b are experimentally determined calibration constants. The AMS on the BAe-146 did not use a constant pressure inlet system, thus a change in the ambient pressure will modulate the lens pressure, affecting the particle time-of-flight measurement. A reduction in ambient pressure will shift the transmission function of the lens to smaller sizes. Such a change will impact the mass measurement if the aerosol size distribution is markedly different to that of the lens transmission. In order to account for this, a pressure-dependent size calibration was performed following the principle detailed by Bahreini et al. (2003). This entailed varying the inlet pressure from 1000 hPa and 500 hPa, while Polystyrene Latex Spheres (PSLs) of known size, shape and density are introduced into the AMS in order to assess the affect of altitude upon the determined particle size. A pressure dependent form of equation A1 presented by Crosier et al. (2007) is then used to determine particle diameter:

$$v_p = \frac{(v_g^{'} + v_g^{''} P_l) - (v_l^{'} + v_l^{''} P_l)}{1 + (D_{va} / (D^{*\prime} + D^{*\prime\prime} P_l))^{(b^{\prime} + b^{\prime\prime} P_l)}} + (v_l^{'} + v_l^{''} P_l) \tag{A2}$$

where P_l is the line pressure of the AMS and $v_g^{'}$, $v_g^{''}$, $v_l^{'}$, $v_l^{''}$, $D^{*'}$, $D^{*''}$, $b^{'}$ and $b^{''}$ are experimentally determined coefficients. The predicted particle velocity was derived using a multivariate fit based on each particle size at each sample pressure and is shown in the supplementary material section.

The coefficients were as follows: $v_g^{'}$=106.22, $v_g^{''}$=0.36876, $v_l^{'}$=l51.236, $v_l^{''}$=-0.027345, $D^{*'}$=101.9, $D^{*''}$=-0.079133, $b^{'}$=0.9479 and $b^{''}$=-0.00045891.

Appendix B: Nephelometer corrections

On the BAe-146, the inlet system prior to the nephelometers and PSAP is not actively dried; instead the sample is dehydrated as a result of ram heating upon entering the inlet system. Consequently, the sample RH is known to vary as a function of the ambient RH, sometimes reaching more than 60% when the ambient RH exceeds approximately 95%. In order to account for these fluctuations, the following empirical formula from Carrico et al. (2003) was used to express the hygroscopic response of the aerosol sample:

$$f(RH) = 1 + a\left(\frac{RH_{wet}}{100}\right)^{b} \tag{B1}$$

where $f(RH)$ refers to the ratio of the 'wet' scattering coefficient, σ_w and the 'dry' scattering coefficient, σ_d, RH_{wet} refers to the RH of the 'wet' nephelometer and a and b are fit coefficients. Only data from Straight and Level Runs (SLRs) when the 'dry' nephelometer's RH was less than 40% was used, which eliminates erroneous $f(RH)$ measurements due to a change in the RH of the 'dry' nephelometer. Fits were derived for each flight in order to account for any variations in size and composition. This information was then applied to the 'dry' nephelometer data above 40% RH in order to generate corrected nephelometer data, σ_{cd} at a reference RH of 40% using the following equation:

$$\sigma_{cd} = \sigma_d\left(1 + a\left(\frac{RH_{dry}}{100}\right)^{b}\right) \tag{B2}$$

where RH_{dry} is the desired reference RH for the corrected nephelometer data. The $f(RH)$ curves can then be recalculated using a consistent reference RH across all of the data. The calculated fit coefficients, a and b, are then used to approximate the ambient scattering coefficient, σ_{amb}, using the following modified form of equation B2:

$$\sigma_{amb} = \sigma_{cd}\left(1 + a\left(\frac{RH_{amb}}{100}\right)^{b}\right) \tag{B3}$$

where RH_{amb} is the measured ambient RH.

Further potential uncertainties in the nephelometer scattering coefficients may arise due to water uptake at high relative humidity e.g. at values above 85%. Larger particles may grow above 1 μm at sufficient RH, which would invalidate the correction coefficients applied to the 'wet' nephelometer. The $f(RH)$ response was also tested by comparing the ratio of the uncorrected 'dry' and 'wet' nephelometers and negligible differences were found at high RH values. Water uptake will also lower the refractive index of the aerosol sample (Massoli et al., 2009) and introduce an error in the $f(RH)$ determination when using the Anderson and Ogren (1998) truncation corrections as they are

sensitive to the assumed refractive index. Massoli et al. (2009) estimate a 2% error, which is within the experimental error for the system. Consequently, we have not included a correction for changes in the refractive index.

Acknowledgements. This work is supported by Natural Environment Research Council (NERC) ADIENT project NE/E011101/1, EUCAARI project 036833-2 and EUSAAR contract 026140. W. T. Morgan was supported by NERC studentship NER/S/A/2006/14040 and a CASE sponsorship from Aerodyne Research Inc. The NERC National Centre for Atmospheric Science (NCAS) Facility for Ground based Atmospheric Measurements (FGAM) supported the maintenance of the cToF-AMS. NCAS also supported the development of the data interpretation methods employed here through its Composition Directorate. Thanks to the Cabauw IMPACT team for provision of the radiosonde data. We thank G. de Leeuw, the principal investigator at the AERONET station at Cabauw for the provision of the AOD data and the principal investigators at the other AERONET sites used. We also thank F. Abicht, A. Minikin, T. Hamburger and A. Stohl for their major contributions to the project. We thank the FAAM, the Met Office, Avalon, DLR-Falcon and DirectFlight personnel for their contributions to the campaign.

References

Alfarra, M. R., Paulsen, D., Gysel, M., Garforth, A. A., Dommen, J., Prevot, A. S. H., Worsnop, D. R., Baltensperger, U., and Coe, H.: A mass spectrometric study of secondary organic aerosols formed from the photooxidation of anthropogenic and biogenic precursors in a reaction chamber, Atmospheric Chemistry and Physics, 6, 5279–5293, 2006.

Allan, J. D., Jimenez, J. L., Williams, P. I., Alfarra, M. R., Bower, K. N., Jayne, J. T., Coe, H., and Worsnop, D. R.: Quantitative sampling using an Aerodyne aerosol mass spectrometer: 1. Techniques of data interpretation and error analysis, Journal of Geophysical Research, 108 (D9), 4090, doi:10.1029/2003JD001607, 2003.

Anderson, T. L. and Ogren, J. A.: Determining aerosol radiative properties using the TSI 3563 integrating nephelometer, Aerosol Science & Technology, 29, 57–69, doi:10.1080/02786829808965551, 1998.

Anderson, T. L., Covert, D. S., Marshall, S. F., Laucks, M. L., Charlson, R. J., Waggoner, A. P., Ogren, J. A., Caldow, R., Holm, R. L., Quant, F. R., Sem, G. J., Wiedensohler, A., Ahlquist, N. A., and Bates, T. S.: Performance characteristics of a high-sensitivity, three-wavelength, total scatter/backscatter nephelometer, Journal of Atmospheric and Oceanic Technology, 13, 967–986, 1996.

Bahreini, R., Jimenez, J. L., Wang, J., Flagan, R. C., Seinfeld, J. H., Jayne, J. T., and Worsnop, D. R.: Aircraft-based aerosol size and composition measurements during ACE-Asia using an Aerodyne aerosol mass spectrometer, Journal of Geophysical Research, 108 (D23), 8645, doi:10.1029/2002JD003226, 2003.

Baumgardner, D., Kok, G., and Raga, G.: Warming of the Arctic lower stratosphere by light absorbing particles, Geophysical Research Letters, 31, L06 117, doi:10.1029/2003GL018883, 2004.

Bond, T. C. and Bergstrom, R. W.: Light Absorption by Carbonaceous Particles: An Investigative Review, Aerosol Science & Technology, 40 (1), 27–67, doi:10.1080/02786820500421521, 2006.

Bond, T. C., Anderson, T. L., and Campbell, D.: Calibration and intercomparison of filter-based measurements of visible light absorption by aerosols, Aerosol Science & Technology, 30, 582–600, doi:10.1080/027868299304435, 1999.

Brink, H. M. T., Veefkind, J. P., Waijers-Ijpelaan, A., and van Der Hage, J. C.: Aerosol light-scattering in The Netherlands, Atmospheric Environment, 30 (24), 4251–4261, doi:10.1016/1352-2310(96)00091-X, 1996.

Brooks, S. D., DeMott, P. J., and Kreidenweis, S. M.: Water uptake by particles containing humic materials and mixtures of humic materials with ammonium sulfate, Atmospheric Environment, 38, 1859–1868, doi:10.1016/j.atmosenv.2004.01.009, 2004.

Canagaratna, M. R., Jayne, J. T., Jimenez, J. L., Allan, J. D., Alfarra, M. R., Zhang, Q., Onasch, T. B., Drewnick, F., Coe, H., Middlebrook, A., Delia, A. E., Williams, L. R., Trimborn, A. M., Northway, M. J., Decarlo, P. F., Kolb, C. E., Davidovits, P., and Worsnop, D. R.: Chemical and microphysical characterization of ambient aerosols with the aerodyne aerosol mass spectrometer, Mass Spectrometry Reviews, 26, 185–222, doi:10.1002/mas.20115, 2007.

Cappa, C. D., Lack, D. A., Burkhardt, J., and Ravishankara, A. R.: Bias in Filter-Based Aerosol Light Absorption Measurements Due to Organic Aerosol Loading: Evidence from Laboratory Measurements, Aerosol Science & Technology, 42, 1022–1032, 2008.

Carrico, C. M., Kus, P., Rood, M. J., Quinn, P. K., and Bates, T. S.: Mixtures of pollution, dust, sea salt, and volcanic aerosol during ACE-Asia: Radiative properties as a function of relative humidity, Journal of

Geophysical Research, 108 (D23), 8650, doi:10.1029/2003JD003405, 2003.

Charlson, R. J., Schwartz, S. E., Hales, J. M., Cess, R. D., Coakley, J. A., Hansen, J. E., and Hofmann, D. J.: Climate Forcing by Anthropogenic Aerosols, Science, 255, 423–430, doi:10.1126/science.255.5043.423, 1992.

Crosier, J., Allan, J. D., Coe, H., Bower, K. N., Formenti, P., and Williams, P. I.: Chemical composition of summertime aerosol in the Po Valley (Italy), northern Adriatic and Black Sea, Quarterly Journal of the Royal Meteorological Society, 133 (S1), 61–75, doi:10.1002/qj.88, 2007.

DeCarlo, P. F., Slowik, J. G., Worsnop, D. R., Davidovits, P., and Jimenez, J. L.: Particle morphology and density characterization by combined mobility and aerodynamic diameter measurements. Part 1: Theory, Aerosol Science & Technology, 38, 1185–1205, doi:10.1080/027868290903907, 2004.

DeCarlo, P. F., Kimmel, J. R., Trimborn, A., Northway, M. J., Jayne, J. T., Aiken, A. C., Gonin, M., Fuhrer, K., Horvath, T., Docherty, K. S., Worsnop, D. R., and Jimenez, J. L.: Field-deployable, high-resolution, time-of-flight aerosol mass spectrometer, Analytical Chemistry, 78, 8281–8289, doi:10.1021/ac061249n, 2006.

Diederen, H. S. M. A., Guicherit, R., and HolLonder, J. C. T.: Visibility reduction by air pollution in The Netherlands, Atmospheric Environment, 19, 377–383, doi:10.1016/0004-6981(85)90105-2, http://www.sciencedirect.com/science/article/B757C-48C7CSJ-BK/2/965e32c77c288595fcb02b4b39a38818, 1985.

Dinar, E., Riziq, A. A., Spindler, C., Erlick, C., Kiss, G., and Rudich, Y.: The complex refractive index of atmospheric and model humic-like substances (HULIS) retrieved by a cavity ring down aerosol spectrometer (CRD-AS), Faraday Discussions, 137, 279–295, 2008.

Docherty, K. S., Stone, E. A., Ulbrich, I. M., Decarlo, P. F., Snyder, D. C., Schauer, J. J., Peltier, R. E., Weber, R. J., Murphy, S. N., Seinfeld, J. H., Grover, B. D., Eatough, D. J., and Jimenez, J. L.: Apportionment of Primary and Secondary Organic Aerosols in Southern California during the 2005 Study of Organic Aerosols in Riverside (SOAR-1), Environmental Science & Technology, 42, 7655–7662, 2008.

Donahue, N. M., Robinson, A. L., Stanier, C. O., and Pandis, S. N.: Coupled partitioning, dilution, and chemical aging of semivolatile organics, Environmental Science & Technology, 40, 2635–2643, doi:10.1021/es052297c, 2006.

Drewnick, F., Hings, S. S., Decarlo, P. F., Jayne, J. T., Gonin, M., Fuhrer, K., Weimer, S., Jimenez, J. L., Demerjian, K. L., Borrmann, S., and Worsnop, D. R.: A new time-of-flight aerosol mass spectrometer (TOF-AMS) - Instrument description and first field deployment, Aerosol Science & Technology, 39, 637–658, doi:10.1080/02786820500182040, 2005.

Edwards, J. M. and Slingo, A.: Studies with a flexible new radiation code. 1: Choosing a configuration for a large-scale model, Quarterly Journal Of The Royal Meteorological Society, 122, 689–719, 1996.

Esselborn, M., Wirth, M., Fix, A., Tesche, M., and Ehret, G.: Airborne high spectral resolution lidar for measuring aerosol extinction and backscatter coefficients, Applied Optics, 47, 346–358, 2008.

Forster, P., Ramaswamy, V., Artaxo, P., Berntsen, T. K., Betts, R., W. Fahey, D. W., Haywood, J., Lean, J., Lowe, D. C., Myhre, G., Nganga, J., Prinn, R., Raga, G., Schulz, M., and Van Dorland, R.: Changes in Atmospheric Constituents and in Radiative Forcing, Climate Change 2007: The Physical Science Basis. Contribution of Working Group I to the Fourth Assessment Report of the Intergovernmental Panel on Climate Change, Cambridge University Press, Cambridge, United Kingdom and New York, NY, USA, 2007.

Gao, R. S., Schwarz, J. P., Kelly, K. K., Fahey, D. W., Watts, L. A., Thompson, T. L., Spackman, J. R.,

Slowik, J. G., Cross, E. S., Han, J. H., Davidovits, P., Onasch, T. B., and Worsnop, D. R.: A novel method for estimating light-scattering properties of soot aerosols using a modified single-particle soot photometer, Aerosol Science & Technology, 41 (2), 125–135, doi:10.1080/02786820601118398, 2007.

Gysel, M., Crosier, J., Topping, D. O., Whitehead, J. D., Bower, K. N., Cubison, M. J., Williams, P. I., Flynn, M. J., McFiggans, G. B., and Coe, H.: Closure study between chemical composition and hygroscopic growth of aerosol particles during TORCH2, Atmospheric Chemistry and Physics, 7, 6131–6144, http://www.atmos-chem-phys.net/7/6131/2007/, 2007.

Haywood, J., Bush, M., Abel, S., Claxton, B., Coe, H., Crosier, J., Harrison, M., Macpherson, B., Naylor, M., and Osborne, S.: Prediction of visibility and aerosol within the operational Met Office Unified Model. II: Validation of model performance using observational data, Quarterly Journal of the Royal Meteorological Society, 134, 1817–1832, doi:10.1002/qj.275, 2008.

Haywood, J. M. and Shine, K. P.: The Effect of Anthropogenic Sulfate and Soot Aerosol on the Clear-Sky Planetary Radiation Budget, Geophysical Research Letters, 22, 603–606, 1995.

Holben, B. N., Eck, T. F., Slutsker, I., Tanre, D., Buis, J. P., Setzer, A., Vermote, E., Reagan, J. A., Kaufman, Y. J., Nakajima, T., Lavenu, F., Jankowiak, I., and Smirnov, A.: AERONET - A federated instrument network and data archive for aerosol characterization, Remote Sensing of Environment, 66, 1–16, 1998.

Huffman, J. A., Docherty, K. S., Aiken, A. C., Cubison, M. J., Ulbrich, I. M., Decarlo, P. F., Sueper, D., Jayne, J. T., Worsnop, D. R., Ziemann, P. J., and Jimenez, J. L.: Chemically-resolved aerosol volatility measurements from two megacity field studies, Atmospheric Chemistry and Physics, 9, 7161–7182, http://www.atmos-chem-phys.net/9/7161/2009/, 2009.

Jimenez, J. L., Canagaratna, M. R., Donahue, N. M., Prevot, A. S. H., Zhang, Q., Kroll, J. H., Decarlo, P. F., Allan, J. D., Coe, H., Ng, N. L., Aiken, A. C., Docherty, K. S., Ulbrich, I. M., Grieshop, A. P., Robinson, A. L., Duplissy, J., Smith, J. D., Wilson, K. R., Lanz, V. A., Hueglin, C., Sun, Y. L., Tian, J., Laaksonen, A., Raatikainen, T., Rautiainen, J., Vaattovaara, P., Ehn, M., Kulmala, M., Tomlinson, J. M., Collins, D. R., Cubison, M. J., E., Dunlea, E. J., Huffman, J. A., Onasch, T. B., Alfarra, M. R., Williams, P. I., Bower, K. N., Kondo, Y., Schneider, J., Drewnick, F., Borrmann, S., Weimer, S., Demerjian, K. L., Salcedo, D., Cottrell, L., Griffin, R., Takami, A., Miyoshi, T., Hatakeyama, S., Shimono, A., Sun, J. Y., Zhang, Y. M., Dzepina, K., Kimmel, J. R., Sueper, D., Jayne, J. T., Herndon, S. C., Trimborn, A. M., Williams, L. R., Wood, E. C., Middlebrook, A. M., Kolb, C. E., Baltensperger, U., and Worsnop, D. R.: Evolution of Organic Aerosols in the Atmosphere, Science, 326, 1525–1529, doi:10.1126/science.1180353, 2009.

Kinne, S., Schulz, M., Textor, C., Guibert, S., Balkanski, Y., Bauer, S. E., Berntsen, T. K., Berglen, T. F., Boucher, O., Chin, M., Collins, W. D., Dentener, F. J., Diehl, T., Easter, R. C., Feichter, J., Fillmore, D., Ghan, S., Ginoux, P., Gong, S., Grini, A., Hendricks, J. E., Herzog, M., Horowitz, L., Isaksen, L., Iversen, T., Kirkavag, A., Kloster, S., Koch, D., Kristjansson, J. E., Krol, M., Lauer, A., Lamarque, J. F., Lesins, G., Liu, X., Lohmann, U., Montanaro, V., Myhre, G., Penner, J. E., Pitari, G., Reddy, S., Seland, O., Stier, P., Takemura, T., and Tie, X.: An AeroCom initial assessment - optical properties in aerosol component modules of global models, Atmospheric Chemistry and Physics, 6, 1815–1834, www.atmos-chem-phys.net/6/1815/2006/, 2006.

Kirchstetter, T. W., Novakov, T., and Hobbs, P. V.: Evidence that the spectral dependence of light absorption by aerosols is affected by organic carbon, Journal of Geophysical Research, 109, D21 208, doi:10.1029/

2004JD004999, 2004.

Kulmala, M., Asmi, A., Lappalainen, H. K., Carslaw, K. S., Pöschl, U., Baltensperger, U., Hov, A., Brenguier, J. L., Pandis, S. N., Facchini, M. C., Hansson, H. C., Wiedensohler, A., and O'Dowd, C. D.: Introduction: European Integrated Project on Aerosol Cloud Climate and Air Quality interactions (EUCAARI) integrating aerosol research from nano to global scales, Atmospheric Chemistry and Physics, 9, 2825–2841, www.atmos-chem-phys.net/9/2825/2009/, 2009.

Lack, D. A., Cappa, C. D., Covert, D. S., Baynard, T., Massoli, P., Sierau, B., Bates, T. S., Quinn, P. K., Lovejoy, E. R., and Ravishankara, A. R.: Bias in Filter-Based Aerosol Light Absorption Measurements Due to Organic Aerosol Loading: Evidence from Ambient Measurements, Aerosol Science & Technology, 42, 1033–1041, 2008.

Liu, P., Ziemann, P. J., Kittelson, D. B., and McMurry, P. H.: Generating Particle Beams of Controlled Dimensions and Divergence .1. Theory of Particle Motion in Aerodynamic Lenses and Nozzle Expansions, Aerosol Science & Technology, 22, 293–313, doi:10.1080/02786829408959748, 1995a.

Liu, P., Ziemann, P. J., Kittelson, D. B., and McMurry, P. H.: Generating Particle Beams of Controlled Dimensions and Divergence .2. Experimental Evaluation of Particle Motion in Aerodynamic Lenses and Nozzle Expansions, Aerosol Science & Technology, 22, 314–324, doi:10.1080/02786829408959749, 1995b.

Liu, P. S. K., Leaitch, W. R., Strapp, J. W., and Wasey, M. A.: Response of Particle Measuring Systems Airborne ASASP and PCASP to Nacl and Latex-Particles, Aerosol Science & Technology, 16, 83–95, doi:10.1080/02786829208959539, 1992.

Massoli, P., Murphy, D. M., Lack, D. A., Baynard, T., Brock, C. A., and Lovejoy, E. R.: Uncertainty in Light Scattering Measurements by TSI Nephelometer: Results from Laboratory Studies and Implications for Ambient Measurements, Aerosol Science & Technology, 43, 1064–1074, doi:10.1080/02786820903156542, 2009.

McFiggans, G. B., Alfarra, M. R., Allan, J. D., Bower, K. N., Coe, H., Cubison, M. J., Topping, D., Williams, P., Decesari, S., Facchini, C., and Fuzzi, S.: Simplification of the representation of the organic component of atmospheric particulates, Faraday Discussions, 130, 341–362, doi:10.1039/b419435g, 2005.

Mensah, A. A.: Water and Organic Nitrate Detection in an AMS: Laboratory Characterization and Application to Ambient Measurements, Inaugural-dissertation, Universitaet zu Koeln, Cologne, Germany, 2010.

Monks, P. S., Granier, C., Fuzzi, S., Stohl, A., Williams, M. L., Akimoto, H., Amann, M., Baklanov, A., Baltensperger, U., Bey, I., Blake, N., Blake, R. S., Carslaw, K. S., Cooper, O. R., Dentener, F. J., Fowler, D., Fragkou, E., Frost, G. J., Generoso, S., Ginoux, P., Grewe, V., Guenther, A., Hansson, H. C., Henne, S., Hjorth, J., Hofzumahaus, A., Huntrieser, H., Isaksen, I. S. A., Jenkin, M. E., Kaiser, J., Kanakidou, M., Klimont, Z., Kulmala, M., Laj, P., Lawrence, M. G., Lee, J. D., Liousse, C., Maione, M., McFiggans, G. B., Metzger, A., Mieville, A., Moussiopoulos, N., Orlando, J. J., O'Dowd, C. D., Palmer, P. I., Parrish, D. D., Petzold, A., Platt, U., Pöschl, U., Prévôt, A. S. H., Reeves, C. E., Reimann, S., Rudich, Y., Sellegri, K., Steinbrecher, R., Simpson, D., ten Brink, H., Theloke, J., van Der Werf, G. R., Vautard, R., Vestreng, V., Vlachokostas, C., and von Glasow, R.: Atmospheric composition change - global and regional air quality, Atmospheric Environment, 43, 5268–5350, doi:10.1016/j.atmosenv.2009.08.021, 2009.

Morgan, W. T., Allan, J. D., Bower, K. N., Capes, G., Crosier, J., Williams, P. I., and Coe, H.: Vertical distribution of sub-micron aerosol chemical composition from North-Western Europe and the North-East Atlantic,

Atmospheric Chemistry and Physics, 9, 5389–5401, http://www.atmos-chem-phys.net/9/5389/2009/, 2009.

Morgan, W. T., Allan, J. D., Bower, K. N., Highwood, E. J., Liu, D., McMeeking, G. R., Northway, M. J., Williams, P. I., Krejci, R., and Coe, H.: Airborne measurements of the spatial distribution of aerosol chemical composition across Europe and evolution of the organic fraction, Atmospheric Chemistry and Physics, 10, 4065–4083, doi:10.5194/acp-10-4065-2010, http://www.atmos-chem-phys.net/10/4065/2010/, 2010.

Morino, Y., Kondo, Y., Takegawa, N., Miyazaki, Y., Kita, K., Komazaki, Y., Fukuda, M., Miyakawa, T., Moteki, N., and Worsnop, D. R.: Partitioning of HNO3 and particulate nitrate over Tokyo: Effect of vertical mixing, Journal of Geophysical Research, 111, D15 215, doi:10.1029/2005JD006887, 2006.

Myhre, G., Grini, A., and Metzger, S.: Modelling of nitrate and ammonium-containing aerosols in presence of sea salt, Atmospheric Chemistry and Physics, 6, 4809–4821, http://www.atmos-chem-phys.net/6/4809/2006/, 2006.

Neuman, J. A., Nowak, J. B., Brock, C. A., Trainer, M., Fehsenfeld, F. C., Holloway, J. S., Hubler, G., Hudson, P. K., Murphy, D. M., Nicks, D. K., Orsini, D., Parrish, D. D., Ryerson, T. B., Sueper, D. T., Sullivan, A., and Weber, R.: Variability in ammonium nitrate formation and nitric acid depletion with altitude and location over California, Journal of Geophysical Research, 108, D17, doi:10.1029/2003JD003616, 2003.

Ng, N. L., Canagaratna, M. R., Zhang, Q., Jimenez, J. L., Tian, J., Ulbrich, I. M., Kroll, J. H., Docherty, K. S., Chhabra, P. S., Bahreini, R., Murphy, S. M., Seinfeld, J. H., Hildebrandt, L., Donahue, N. M., DeCarlo, P. F., Lanz, V. A., Prévôt, A. S. H., Dinar, E., Rudich, Y., and Worsnop, D. R.: Organic aerosol components observed in Northern Hemispheric datasets from Aerosol Mass Spectrometry, Atmospheric Chemistry and Physics, 10, 4625–4641, doi:10.5194/acp-10-4625-2010, 2010.

Osborne, S. R., Haywood, J. M., and Bellouin, N.: In situ and remote-sensing measurements of the mean microphysical and optical properties of industrial pollution aerosol during ADRIEX, Quarterly Journal of the Royal Meteorological Society, 133 (S1), 17–32, doi:10.1002/qj.92, 2007.

Oshima, N., Koike, M., Zhang, Y., and Kondo, Y.: Aging of black carbon in outflow from anthropogenic sources using a mixing state resolved model: 2. Aerosol optical properties and cloud condensation nuclei activities, Journal of Geophysical Research, 114, doi:10.1029/2008JD011681, http://www.agu.org/pubs/crossref/2009/2008JD011681.shtml, 2009.

Paatero, P.: Least squares formulation of robust non-negative factor analysis, Chemometrics and Intelligent Laboratory Systems, 37, 23–35, 1997.

Paatero, P. and Tapper, U.: Positive Matrix Factorization - a Nonnegative Factor Model with Optimal Utilization of Error-Estimates of Data Values, Environmetrics, 5, 111–126, 1994.

Penner, J. E., Chuang, C. C., and Grant, K.: Climate forcing by carbonaceous and sulfate aerosols, Climate Dynamics, 14, 839–851, 1998.

Petzold, A., Schloesser, H., Sheridan, P. J., Arnott, W. P., Ogren, J. A., and Virkkula, A.: Evaluation of Multi-angle Absorption Photometry for Measuring Aerosol Light Absorption, Aerosol Science & Technology, 39, 40–51, http://www.informaworld.com/10.1080/027868290901945, 2005.

Pinder, R. W., Adams, P. J., and Pandis, S. N.: Ammonia Emission Controls as a Cost-Effective Strategy for Reducing Atmospheric Particulate Matter in the Eastern United States, Environmental Science & Technology, 41, 380–386, doi:10.1021/es060379a, 2007.

Putaud, J.-P., Raes, F., Dingenen, R. V., Brüggemann, E., Facchini, M. C., Decesari, S., Fuzzi, S., Gehrig,

R., Hüglin, C., Laj, P., Lorbeer, G., Maenhaut, W., Mihalopoulos, N., Müller, K., Querol, X., Rodriguez, S., Schneider, J., Spindler, G., ten Brink, H., Tørseth, K., and Wiedensohler, A.: A European aerosol phenomenology–2: chemical characteristics of particulate matter at kerbside, urban, rural and background sites in Europe, Atmospheric Environment, 38, 2579–2595, doi:10.1016/j.atmosenv.2004.01.041, 2004.

Reis, S., Pinder, R. W., Zhang, M., Lijie, G., and Sutton, M. A.: Reactive nitrogen in atmospheric emission inventories, Atmospheric Chemistry and Physics, 9, 7657–7677, http://www.atmos-chem-phys.net/9/7657/2009/, 2009.

Robinson, A. L., Donahue, N. M., Shrivastava, M. K., Weitkamp, E. A., Sage, A. M., Grieshop, A. P., Lane, T. E., Pierce, J. R., and Pandis, S. N.: Rethinking organic aerosols: Semivolatile emissions and photochemical aging, Science, 315, 1259–1262, doi:10.1126/science.1133061, 2007.

Schaap, M., van Loon, M., ten Brink, H. M., Dentener, F. J., and Builtjes, P. J. H.: Secondary inorganic aerosol simulations for Europe with special attention to nitrate, Atmospheric Chemistry and Physics, 4, 857–874, http://www.atmos-chem-phys.net/4/857/2004/, 2004.

Schwarz, J. P., Spackman, J. R., Gao, R. S., Perring, A. E., Cross, E., Onasch, T. B., Ahern, A., Wrobel, W., Davidovits, P., Olfert, J., Dubey, M. K., Mazzoleni, C., and Fahey, D. W.: The Detection Efficiency of the Single Particle Soot Photometer, Aerosol Science & Technology, 44, 612–628, doi:10.1080/02786826.2010.481298, 2010.

Stephens, M., Turner, N., and Sandberg, J.: Particle Identification by Laser-Induced Incandescence in a Solid-State Laser Cavity, Applied Optics, 42, 3726, doi:10.1364/AO.42.003726, 2003.

Stokes, R. H. and Robinson, R. A.: Interactions in Aqueous Nonelectrolyte Solutions. I. Solute-Solvent Equilibria, The Journal of Physical Chemistry, 70, 2126–2131, doi:10.1021/j100879a010, 1966.

Strapp, J. W., Leaitch, W. R., and Liu, P. S. K.: Hydrated and Dried Aerosol-Size-Distribution Measurements from the Particle Measuring Systems FSSP-300 Probe and the Deiced PCASP-100x Probe, Journal of Atmospheric and Oceanic Technology, 9, 548–555, 1992.

Swietlicki, E., Hansson, H. C., Hameri, K., Svenningsson, B., Massling, A., McFiggans, G. B., McMurry, P. H., Petaja, T., Tunved, P., Gysel, M., Topping, D., Weingartner, E., Baltensperger, U., Rissler, J., Wiedensohler, A., and Kulmala, M.: Hygroscopic properties of submicrometer atmospheric aerosol particles measured with H-TDMA instruments in various environments - a review, Tellus Series B-Chemical and Physical Meteorology, 60, 432–469, 2008.

Tang, I. N.: Chemical and size effects of hygroscopic aerosols on light scattering coefficients, Journal of Geophysical Research, 101, 19 245–19 250, doi:10.1029/96JD03003, 1996.

Textor, C., Schulz, M., Guibert, S., Kinne, S., Balkanski, Y., Bauer, S. E., Berntsen, T. K., Berglen, T. F., Boucher, O., Chin, M., Dentener, F. J., Diehl, T., Easter, R. C., Feichter, H., Fillmore, D., Ghan, S., Ginoux, P., Gong, S., Kristjansson, J. E., Krol, M., Lauer, A., Lamarque, J. F., Liu, X., Montanaro, V., Myhre, G., Penner, J., Pitari, G., Reddy, S., Seland, O., Stier, P., Takemura, T., and Tie, X.: Analysis and quantification of the diversities of aerosol life cycles within AeroCom, Atmospheric Chemistry and Physics, 6, 1777–1813, doi:www.atmos-chem-phys.net/6/1777/2006/, 2006.

Toon, O. B., Pollack, J. B., and Khare, B. N.: Optical-Constants Of Several Atmospheric Aerosol Species - Ammonium-Sulfate, Aluminum-Oxide, And Sodium-Chloride, Journal of Geophysical Research, 81, 5733–5748, 1976.

Ulbrich, I. M., Canagaratna, M. R., Zhang, Q., Worsnop, D. R., and Jimenez, J. L.: Interpretation of organic components from Positive Matrix Factorization of aerosol mass spectrometric data, Atmospheric Chemistry and Physics, 9, 2891–2918, doi:www.atmos-chem-phys.net/9/2891/2009/, 2009.

Van Ulden, A. P. and Wieringa, J.: Atmospheric boundary layer research at Cabauw, Boundary-Layer Meteorology, 78, 39–69, 1996.

Wandinger, U., Müller, D., Böckmann, C., Althausen, D., Matthias, V., Bösenberg, J., Weiß, V., Fiebig, M., Wendisch, M., Stohl, A., and Ansmann, A.: Optical and microphysical characterization of biomass-burning and industrial-pollution aerosols from multiwavelength lidar and aircraft measurements, Journal of Geophysical Research, 107, D21, doi:10.1029/2000JD000202, 2002.

Weast, R. C.: Handbook of Chemistry and Physics, 66th edition, CRC Press: Florida, 1985.

White, W. H. and Roberts, P. T.: Nature and Origins of Visibility-Reducing Aerosols in Los Angeles Air Basin, Atmospheric Environment, 11, 803–812, doi:10.1016/0004-6981(77)90042-7, 1977.

Zhang, Q., Jimenez, J. L., Canagaratna, M. R., Allan, J. D., Coe, H., Ulbrich, I., Alfarra, M. R., Takami, A., Middlebrook, A. M., Sun, Y. L., Dzepina, K., Dunlea, E. J., Docherty, K. S., Decarlo, P. F., Salcedo, D., Onasch, T., Jayne, J. T., Miyoshi, T., Shimono, A., Hatakeyama, S., Takegawa, N., Kondo, Y., Schneider, J., Drewnick, F., Borrmann, S., Weimer, S., Demerjian, K. L., Williams, P., Bower, K. N., Bahreini, R., Cottrell, L., Griffin, R. J., Rautiainen, J., Sun, J. Y., Zhang, Y. M., and Worsnop, D. R.: Ubiquity and dominance of oxygenated species in organic aerosols in anthropogenically-influenced Northern Hemisphere midlatitudes, Geophysical Research Letters, 34, L13 801, doi:10.1029/2007GL029979, 2007.

Table 1. Flight summary of the operations included in this study. All flights were conducted during 2008. Also included are the times when the BAe-146 operated in the vicinity of Cabauw

Flight	Date	Start	End	Sortie Objectives
B362	06 May	11:03	11:23	Map pollution outflow from Central Europe towards UK and North Sea.
B366	08 May	15:04	16:04	Survey Northern Germany and Netherlands to probe pollution gradient extending from east to west.
B379	21 May	11:16	12:22	Survey Northern Germany and Netherlands to probe pollution gradient extending from east to west.

Table 2. Summary of instrumentation from the ground-based site at Cabauw and the BAe-146 aircraft used in this study. Acronyms used are as follows: cToF-AMS (compact Time-of-Flight Aerosol Mass Spectrometer, HR-ToF-AMS (High-Resolution Time-of-Flight Aerosol Mass Spectrometer), Single Particle Soot Photometer (SP2), PSAP (Particle Soot Absorption Photometer), MAAP (Multi-Angle Absorption Photometer) and PCASP (Passive Cavity Aerosol Spectrometer Probe). The wavelengths and size ranges applicable to the optical and physical property measurements are given in brackets.

Measurement	Cabauw	BAe-146
Composition	HR-ToF-AMS	cToF-AMS, SP2
Scattering coefficient	Nephelometer (450, 550, 700 nm)	Nephelometer (450, 550, 700 nm)
Absorption coefficient	MAAP (670 nm)	PSAP (567 nm)
Size distribution	N/A	PCASP (0.1-3 µm)

Table 3. Summary of the individual component densities and refractive indices used in this study. The numbers in brackets refer to the study referenced for the associated parameter value, which are as follows: [1] Weast (1985), [2] Penner et al. (1998), [3] Alfarra et al. (2006), [4] Bond and Bergstrom (2006), [5] Toon et al. (1976) and [6] Dinar et al. (2008).

Aerosol component	Density (kgm^{-3})	Refractive index
Ammonium nitrate	1725 [1]	1.60 - 0i [1]
Ammonium sulphate	1769 [2]	1.53 - 0i [5]
Organic matter	1400 [3]	1.63 - 0.021i [6]
Black carbon	1800 [4]	1.95 - 0.79i [4]

Table 4. Summary of optical properties for flight B366 and B379 when comparing between the measurements from the BAe-146 and estimated values based upon the ground-based measurements from Cabauw. The Aerosol Optical Depth (AOD) is calculated using the ambient scattering coefficient and the corresponding absorption value from 0-2 km. ω_0 refers to the average single scattering albedo for the vertical column from 0-2 km. RF refers to the calculated negative radiative forcing based upon the AOD, ω_0 and the surface albedo (R_s) values used. The solar constant is normalised by the cosine of the solar zenith angle (56°during this period for B366 and 32°for B379) in order to account for the sun's location not being directly overhead.

Flight	Parameter	Cabauw (550 nm)	BAe-146 (550 nm)				
		Mean	5^{th}	25^{th}	50^{th}	75^{th}	95^{th}
B366	AOD	0.14	0.13	0.14	0.16	0.16	0.17
	ω_0	0.92	0.91	0.92	0.93	0.93	0.93
	RF (R_s=0.16)	1.35	1.19	1.35	1.63	1.63	1.73
	RF (R_s=0.26)	0.67	0.53	0.67	0.89	0.89	0.95
B379	AOD	0.10	0.14	0.17	0.18	0.20	0.21
	ω_0	0.93	0.94	0.95	0.95	0.96	0.96
	RF (R_s=0.16)	2.34	3.45	4.40	4.66	5.42	5.69
	RF (R_s=0.26)	1.28	2.03	2.76	2.92	3.59	3.77

Table 5. Summary of Aerosol Optical Depth (AOD) values for flights B366 and B379. The values derived from the column integrated measurements from the BAe-146 and AERONET are compared. The BAe-146 data corresponds to the vertical column above Cabauw up to 7500 m for B366 and 8500 m for B379. The percentage values reported in brackets below the BAe-146 values represent the approximate fraction of the AOD located below 2000 m. The AERONET values are the total column integrated values.

Flight	BAe-146 (450 nm)			AERONET (440 nm)
	5^{th}	50^{th}	95^{th}	Mean
B366	0.20	0.26	0.34	0.35
	(95%)	(85%)	(74%)	
B379	0.23	0.33	0.44	0.44
	(83%)	(76%)	(68%)	

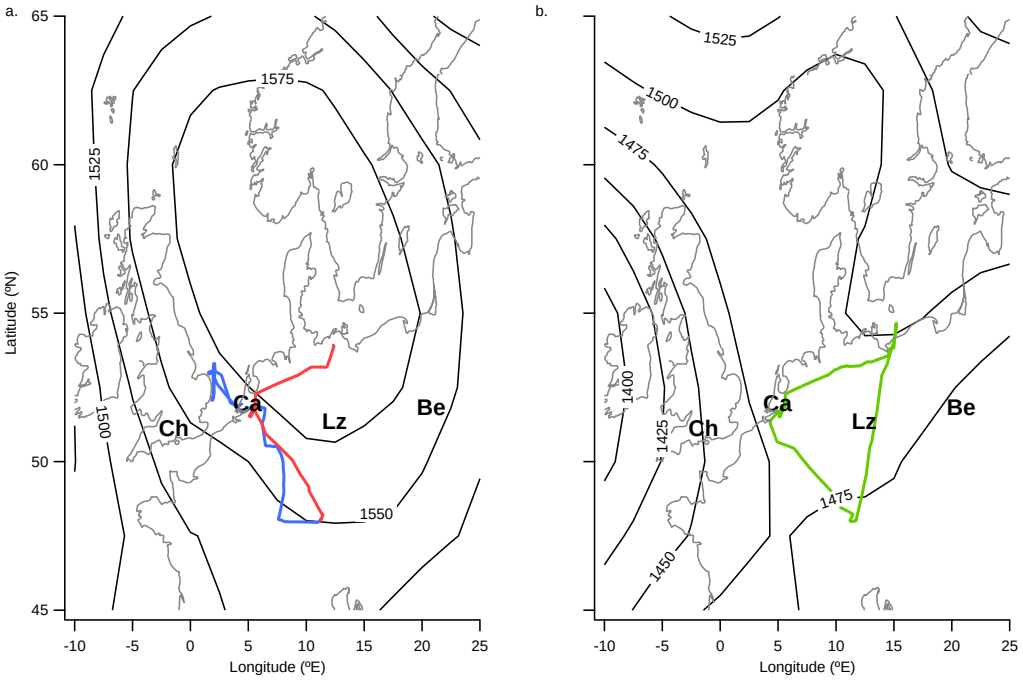

Fig. 1. Flight tracks of the BAe-146 considered by this analysis. Also shown are ECMWF 850 hPa geopotential height fields. Panel (a) displays the flight tracks for B362 (06 May 2008, blue track) and B366 (08 May 2008, red track) and the geopotential height field is from 12 UTC on 06 May 2008. Panel (b) displays the flight track for B379 (21 May 2008, green track) and the geopotential height field is from the same date at 12 UTC. AERONET stations relevant to this study are marked, including Chilbolton (Ch), Cabauw (Ca), IFT-Leipzig (Lz) and Belsk (Be).

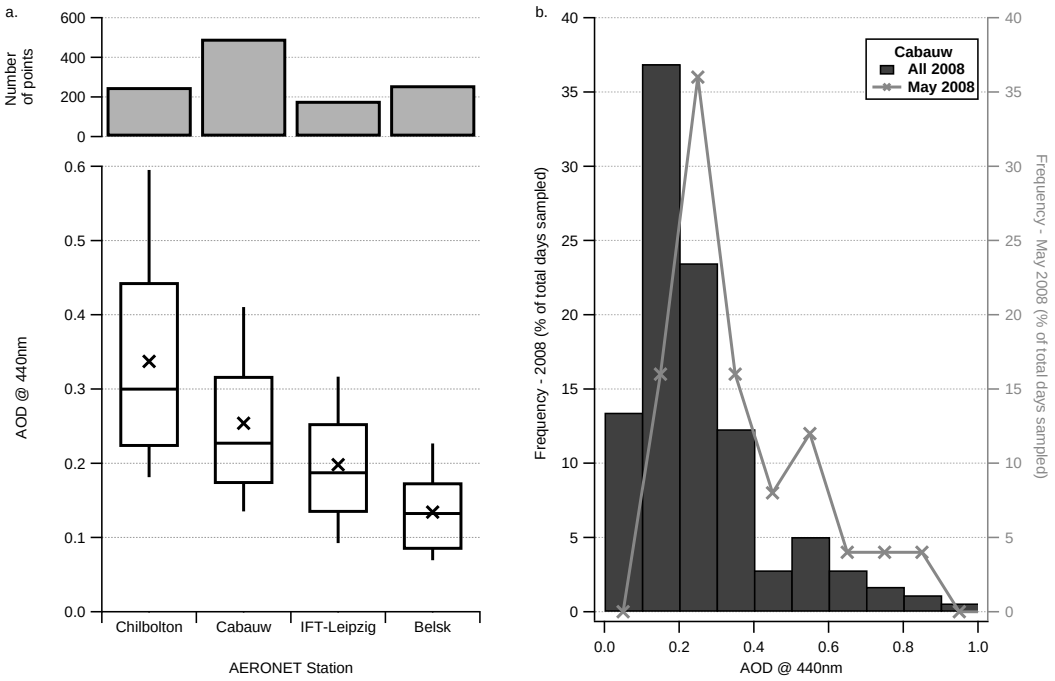

Fig. 2. Panel (a) displays boxplot summary statistics for AOD derived from AERONET stations in Northern Europe during the LONGREX high pressure period (06-14 May 2008). Crosses represent the mean value, while horizontal lines represent the 25^{th}, 50^{th} and 75^{th} percentiles. The whiskers represent the 5^{th} and 95^{th} percentiles. Panel (b) displays a histogram of daily mean AOD at Cabauw for the year 2008 (left axis) and May 2008 (right axis). The values are normalised to the total number of days sampled in each case, which equaled 179 for the year 2008 and 25 for May 2008.

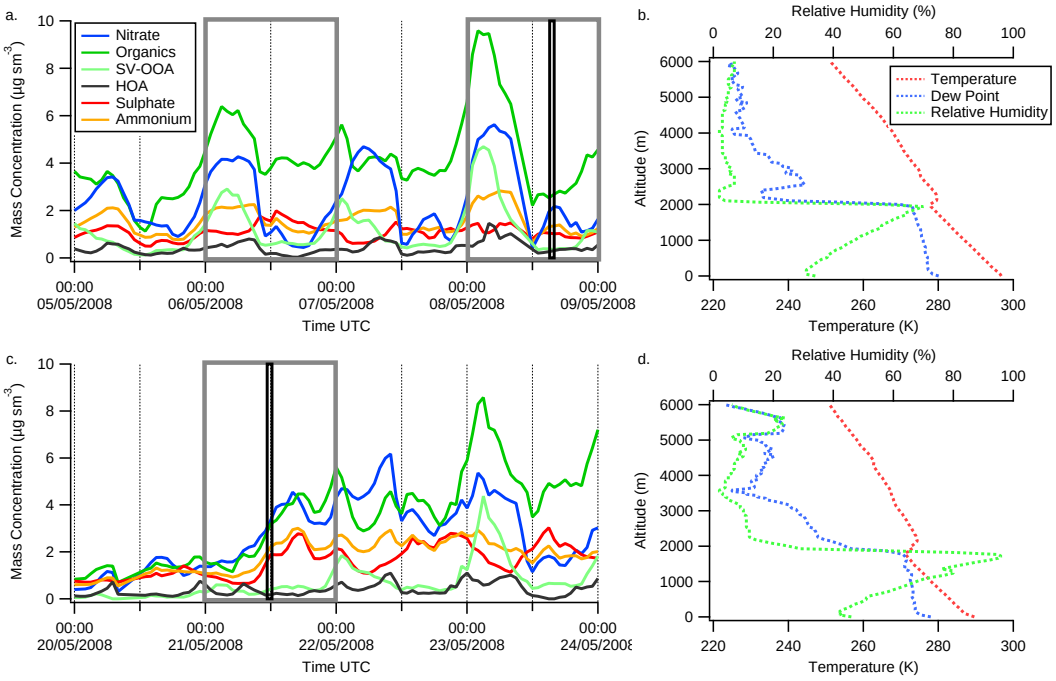

Fig. 3. Panels (a) and (c) display time series of AMS mass concentrations from Cabauw from 05-09 May 2008 and 20-24 May 2008 respectively. The Semi-Volatile Oxygenated Organic Aerosol (SV-OOA) and Hydrocarbon-like Organic Aerosol (HOA) components are also shown. The grey boxes indicate days when the BAe-146 conducted flight operations in the vicinity of Cabauw, while the black boxes indicate the time periods when the BAe-146 was within 50 km of Cabauw during B366 and B379. Panels (b) and (d) display the temperature and relative humidity profiles derived from radiosonde launches from Cabauw at 1604 UTC on 08 May 2008 and 1201 UTC on 21 May 2008 respectively.

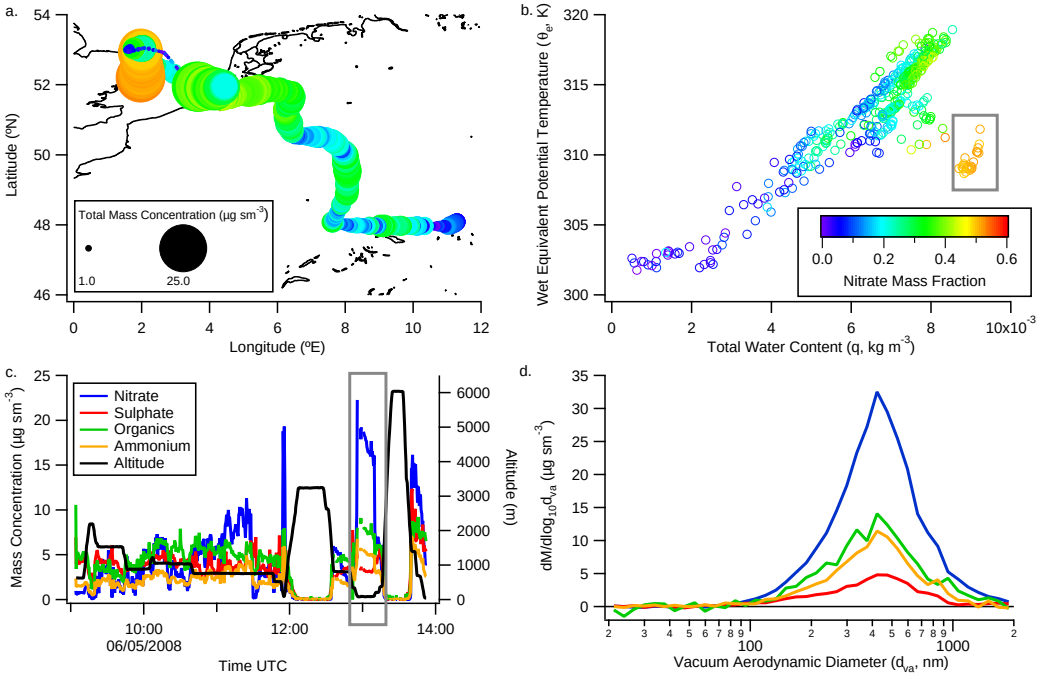

Fig. 4. Case study example of the vertical mixing of atmospheric aerosol during flight B362. (a) displays the aircraft's flight track coloured according to the nitrate mass fraction, while the markers are sized according to the AMS total mass concentration. (b) shows the relationship between the wet equivalent potential temperature, θ_e, and the total water content, q. The relationship is coloured according to the nitrate mass fraction, while the grey box indicates the data corresponding to SLR-8 during B362. (c) shows the AMS mass concentration time series and the altitude of the aircraft during the flight. (d) shows the mass-size distribution from the AMS for SLR-8.

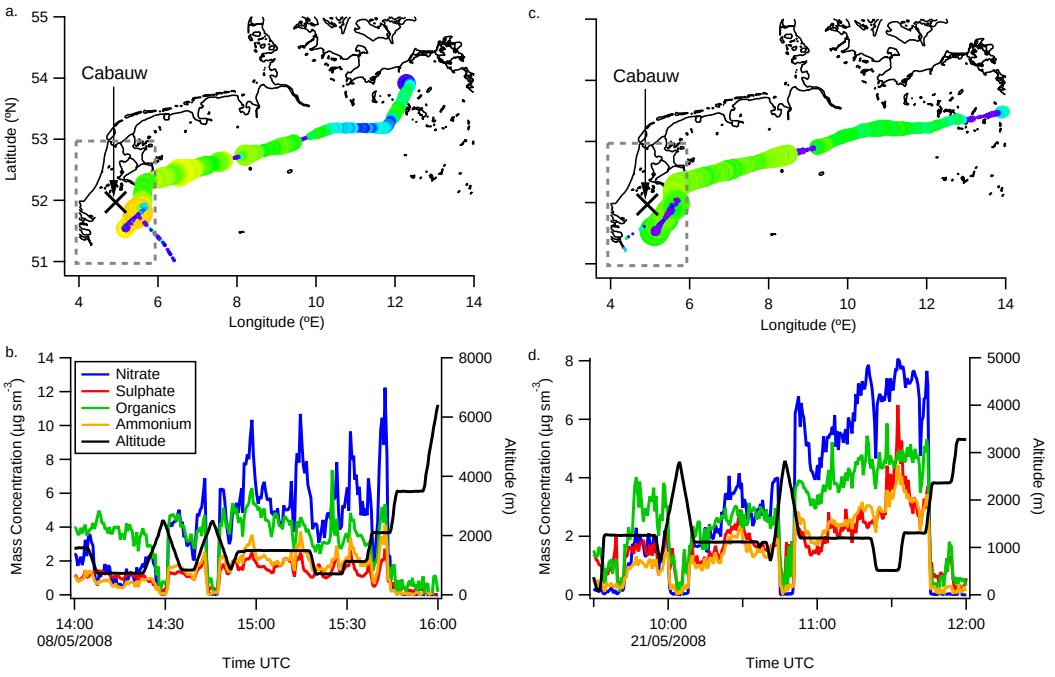

Fig. 5. Case study example of the distribution of aerosol chemical composition from B366 and B379. Panel (a) displays the B366 flight track coloured according to the nitrate mass fraction, while the markers are sized according to the AMS total mass concentration. The same colourscale and marker size is used as Fig. 4. Panel (b) shows the B366 AMS mass concentration time series and the altitude of the aircraft during the flight. Panel (c) shows the flight track for B379. Panel (d) shows the B379 AMS mass concentration time series and the altitude track of the BAe-146. The grey boxes in panels (a) and (c) mark out the boundaries of the defined proximity to Cabauw in the main text.

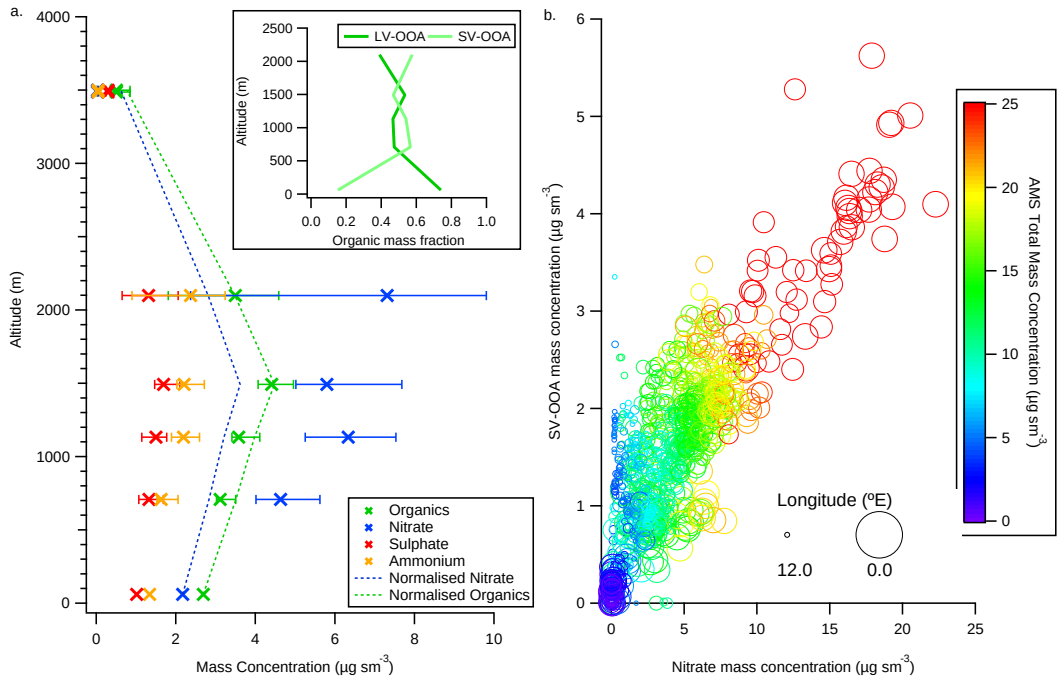

Fig. 6. Case study example of the vertical distribution of aerosol chemical composition. Panel (a) displays the AMS mass concentrations as a function of height from SLRs in the vicinity of Cabauw during flight B366, where the markers indicate the median concentration and the horizontal bars represent the 25^{th} and 75^{th} percentiles. The points at the lowest altitude correspond to the concentrations from a ground-based AMS at Cabauw. The hashed lines represent the normalised nitrate and organic profiles when they are scaled to the change in sulphate with height relative to the ground-based measurement. The inset panel displays the altitude dependence of the Low-Volatility Oxygenated Organic Aerosol (LV-OOA) and the Semi-Volatile Oxygenated Organic Aerosol (SV-OOA) organic mass fractions. Panel (b) displays the relationship between the SV-OOA component and nitrate for B362, B366 and B379. The markers are coloured according to the AMS total mass concentration and sized by longitude.

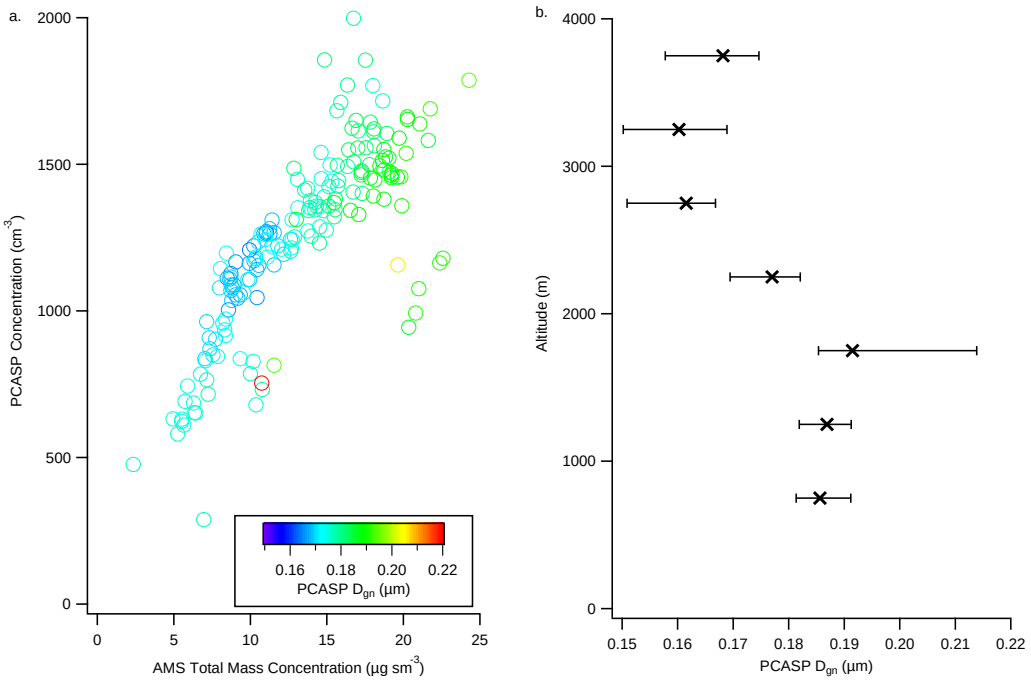

Fig. 7. Relationship between aerosol microphysical properties and total mass concentration from the AMS. Panel (a) displays the relationship between the sub-micron aerosol number concentration from the PCASP instrument with total AMS mass concentration. The points are coloured according to the sub-micron geometric mean diameter. Panel (b) shows the sub-micron geometric mean diameter derived from the PCASP measurements as a function of height when averaged over SLRs. The crosses refer to the median geometric diameter, while the horizontal bars represent the 25^{th} and 75^{th} percentiles.

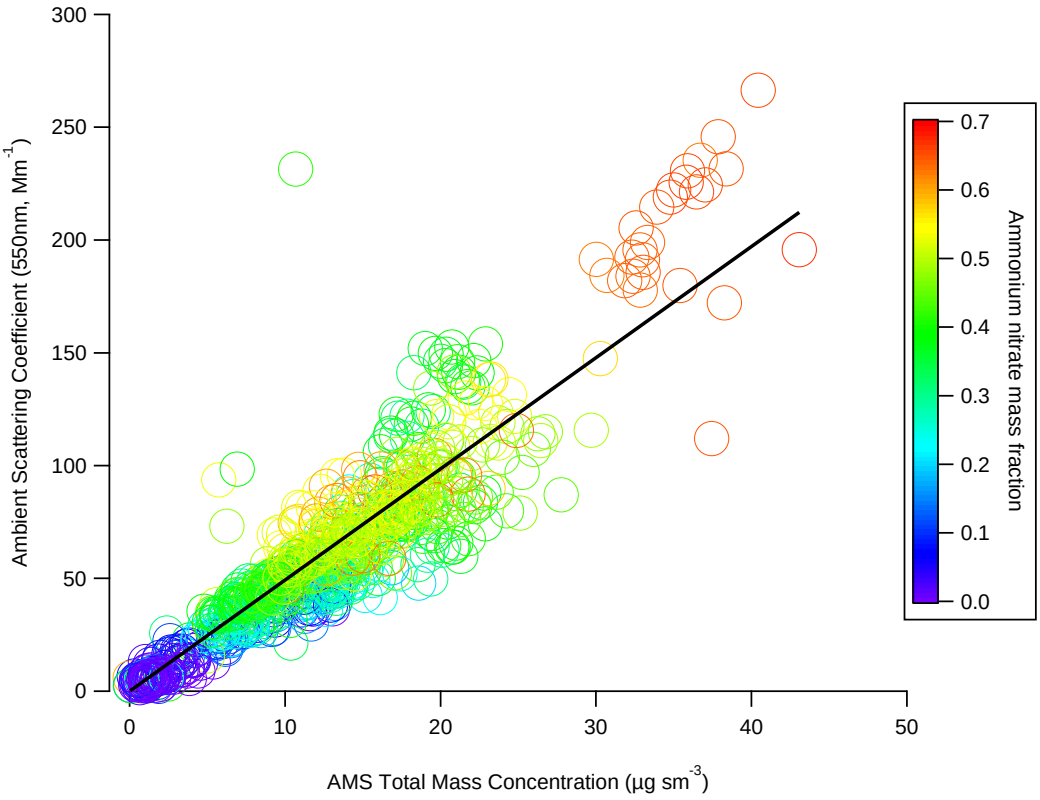

Fig. 8. Relationship between ambient light scattering and the total mass concentration derived from the AMS on the BAe-146. The solid black line indicates the slope of the linear regression analysis, which corresponds to an ambient mass scattering efficiency of 4.93 $\mathrm{m^2 g^{-1}}$. The points are coloured according to the ammonium nitrate mass fraction.

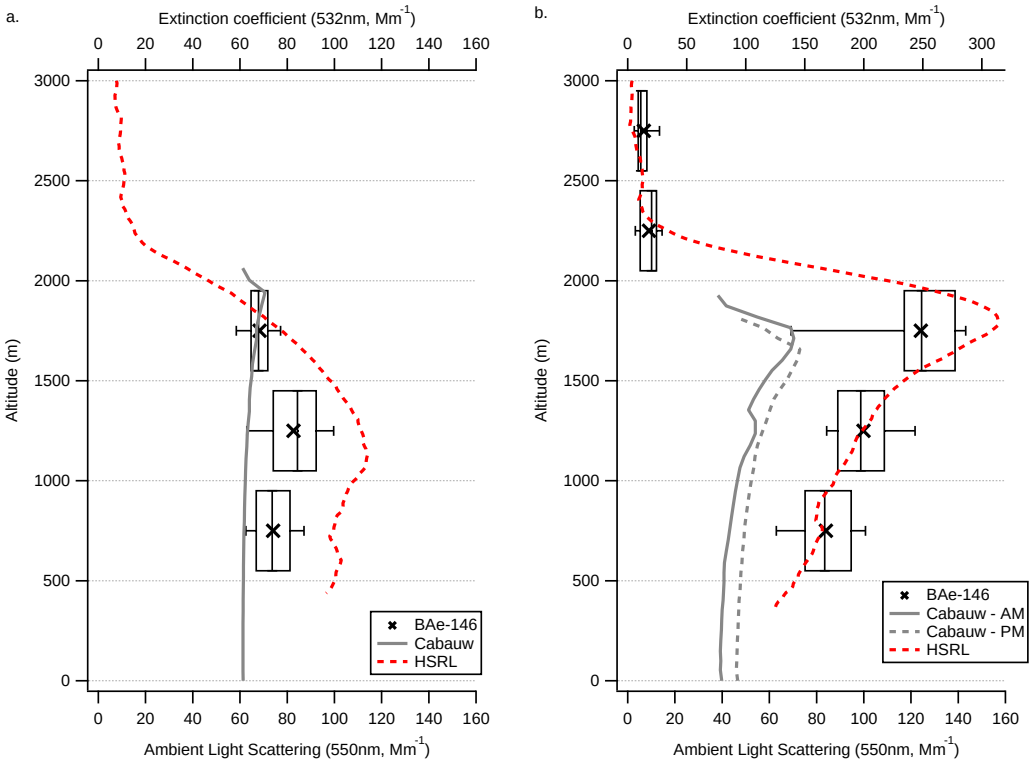

Fig. 9. Boxplot summary statistics for the measured ambient scattering profile from the BAe-146 in the vicinity of Cabauw for (a) B366 and (b) B379. Crosses represent the mean value, while horizontal lines represent the 25^{th}, 50^{th} and 75^{th} percentiles. The whiskers represent the 5^{th} and 95^{th} percentiles. Also shown is the measured ambient scattering from the ground site at Cabauw, which is extrapolated to derive an estimated scattering profile based upon the method described in Sect. 5.1. In (a) the extinction profile from the HSRL onboard the DLR Falcon is also shown from 14:44-14:56 UTC. In (b) the extinction profile from the HSRL is shown for 13:46-13:54 UTC. Note that the scale for the nephelometer measurements and the HSRL are different in (b).

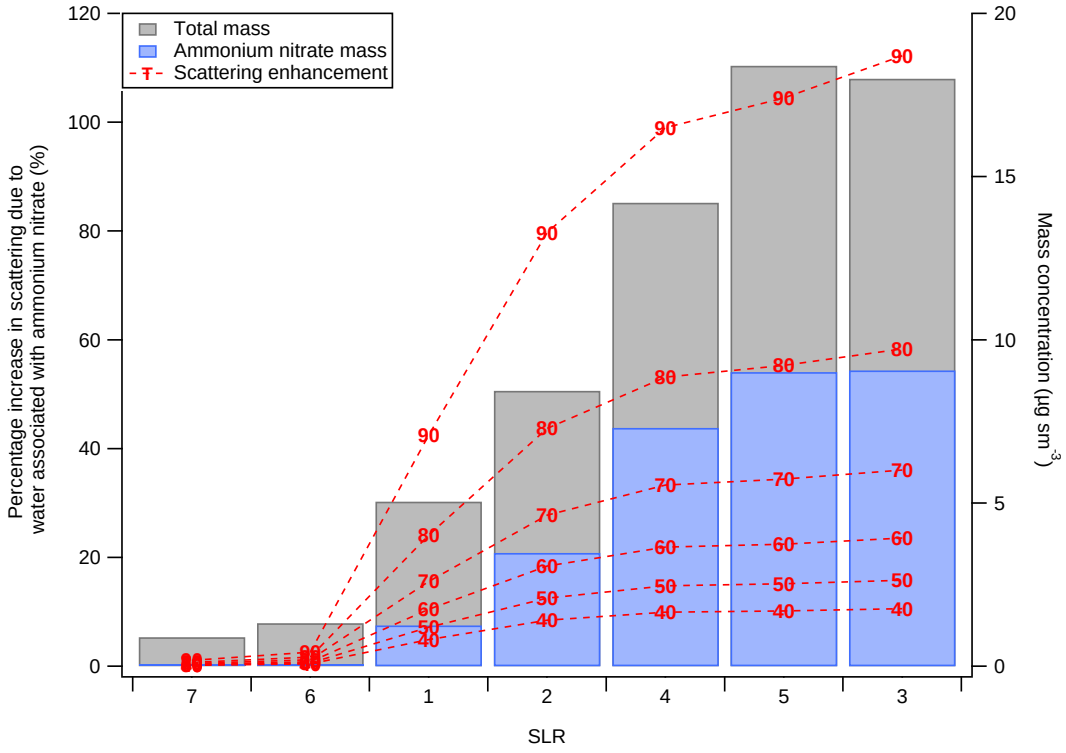

Fig. 10. Summary of the enhancement in aerosol scattering due to water uptake by ammonium nitrate aerosol derived from the Mie calculations. The text markers and hashed line refer to the percentage increase in scattering by water associated with ammonium nitrate over a relative humidity range from 40-90%. The Straight and Level Runs (SLRs) are from B379 and are ordered by increasing ammonium nitrate mass concentration or mass fraction. Also shown is the average total mass and ammonium nitrate concentrations for each of the SLRs.

Chapter 5

Conclusions

Europe represents a highly dynamic region, both in terms of its meteorology and emission footprint. Significant uncertainties exist regarding the atmospheric aerosol burden at the regional scale in Europe. Such deficiencies complicate assessments of the impact of atmospheric aerosol upon regional ecosystems, air quality and climate. Greater knowledge of the life cycle of atmospheric aerosol on the regional scale is required, which will facilitate our understanding of such impacts, both now and in the future. The analyses presented in this thesis represent a concentrated effort to characterise the properties, processing and associated impacts of atmospheric aerosol across Northern Europe. A suite of in-situ instrumentation was used to constrain the spatial distribution of atmospheric aerosol, with particular emphasis on the chemical composition of the sub-micron component and its effects upon regional climate.

The following chapter will summarise the research findings, discuss their implications and focus upon future work pertinent to the issues raised in this thesis.

5.1 Summary of research findings

A statistical examination of the vertical distribution of aerosol chemical composition in North-Western Europe was presented in Section 4.2, for a range of meteorological conditions. Both the absolute sub-micron aerosol concentration and its relative composition were found to be significantly modulated by the dominant meteorological conditions. Low concentrations of aerosol mass, composed of primarily ammonium sulphate and Organic Matter (OM), were associated with long-range air mass transport across the Atlantic Ocean. Increased mass concentrations were coincident with outflow from Western Europe and periods of stagnant/recirculating air masses. Such conditions were strongly driven by an increase in the absolute concentration and relative contribution of ammonium nitrate to the aerosol burden. The vertical distribution of ammonium nitrate was determined by the thermodynamic structure of the lower atmosphere. Enhanced

concentrations occurred at reduced temperatures and increased relative humidity at the top of the boundary layer.

The EUCAARI-LONGREX and ADIENT campaigns provided an opportunity to comprehensively study the conditions associated with enhanced pollution in Northern Europe, which were identified in Section 4.2. The spatial gradients in the aerosol chemical composition across Northern Europe was investigated in Section 4.3, along with specific attention to the evolution of the OM component. The distribution of aerosol chemical composition was sampled across a range of conditions, stretching from relatively clean background conditions in the Baltic Sea, polluted conditions over North-Western Europe and far-field outflow from such conditions in the Eastern Atlantic Ocean. Ammonium nitrate was found to be an important constituent, with typical contributions of 20-50%. In North-Western Europe during periods associated with enhanced pollution loadings, ammonium nitrate was found to dominate. This was attributed to the enhanced NO_x and ammonia sources in this region. OM was found to be ubiquitous across Europe, with mass fractions ranging from 20-50%. Furthermore, concentrations generally exceeded those of sulphate by 30-160%. OM was identified as being largely secondary in its nature and found to dynamically and continuously evolve, as a function of its distance from source and level of photochemical processing. The propensity for substantial concentrations of atmospheric aerosol on the regional scale was demonstrated by the advection of continental European pollution far downwind, with significant concentrations extending into the Eastern Atlantic region.

The radiative impact of the enhanced pollution in North-Western Europe, which was a major theme of the findings in Sections 4.2 and 4.3, was investigated in Section 4.4. The vertical structure of aerosol chemical composition was investigated by comparing the in-situ measurements from the Aerosol Mass Spectrometer (AMS) on the BAe-146 with those from a ground-based AMS at Cabauw in the Netherlands during May 2008. This comparison revealed that ammonium nitrate and OM increased with altitude in the atmospheric boundary layer. Such increases were hypothesised to be the result of partitioning of semi-volatile gas phase species to the particle phase at the reduced temperatures and enhanced relative humidity at the top of the boundary layer. The increased ammonium nitrate concentrations, in particular, were found to significantly increase the scattering potential of the aerosol burden. This was caused by the large amount of associated water and the enhanced particulate mass coincident with this increase. In the most polluted conditions, increases in Aerosol Optical Depth (AOD) of 50-100% were estimated to occur. Such increases in AOD were accompanied by increases in the single scattering albedo, which yielded close to a factor of two increase in the median negative direct aerosol radiative forcing.

5.2 Implications

Taken as a whole, the research findings present two main strands in relation to the chemical composition of the aerosol burden in Europe; the properties and evolution of Secondary Organic Aerosol (SOA) upon the regional scale and the importance of ammonium nitrate to the aerosol burden and its resultant impact. The implications of these findings will be discussed in the following section.

5.2.1 Evolution of secondary organic aerosol

The research presented in this thesis supplements previous observations (e.g. Zhang et al., 2007; Jimenez et al., 2009; Ng et al., 2010) regarding the ubiquity and evolution of SOA at a range of spatial scales. Crucially, the present research explores the transformation of OM across Northern Europe, a region that had previously received less attention than other industrial and continental environments.

A ground-based network of AMS instruments were deployed during month long intensives in May 2008, October 2008 and March 2009 across Europe; these results add to the body of measurements from the airborne experiments. The AMS instruments were also complemented by measurements of the aerosol size distribution, optical properties and hygroscopic properties in many locations. This dataset will be used to probe the chemical composition of the European aerosol burden, with specific attention to the OM component. The datasets are to being examined using various factor analysis techniques e.g. PMF, which will allow further categorisation of the temporal and spatial scales involved in the evolution of OM component on the regional scale.

The results presented in Section 4.3 illustrated that the evolution of SOA can be viewed as a dynamic continuum of oxidation, from Semi Volatile-Oxygenated Organic Aerosol (SV-OOA) through to Low Volatility-Oxygenated Organic Aerosol (LV-OOA). This is a consequence of photochemical processing as the air mass is advected downwind of its major sources. Similar behaviour was noted by Ng et al. (2010) when comparing multiple ground-based measurements. The aircraft measurements were consistent with rapid formation of SOA close to major sources, which is processed substantially upon advection downwind. The measurements across Europe demonstrated that in environments sufficiently downwind from major source regions, the OM component was almost exclusively dominated by the LV-OOA component. An area that was not explored in this study was the relative roles of anthropogenic and biogenic precursors to the formation of SOA over Northern Europe. Several studies in Europe (e.g. Szidat et al., 2006; Gelencsér et al., 2007; Szidat et al., 2009) have suggested that biogenic precursors play the dominant role in SOA formation. However, studies in North America have suggested that SOA is derived from biogenic sources (e.g. Bench et al., 2007), anthropogenic sources (e.g. de Gouw et al., 2005, 2008; Bahreini et al., 2009) and to

complicate matters further, a mixture of both (e.g. Weber et al., 2007; Goldstein et al., 2009). Consequently, characterisation of this fundamental aspect of SOA formation in polluted environments is vital. This is especially true in a highly diverse environment such as Northern Europe, where large biogenic sources are situated in close proximity to major urban and industrial locations.

The observations of the vertical distribution of OM underlined the importance of considering the chemical make-up of SOA in the atmosphere. Little evidence for significant changes with altitude within the boundary layer was observed in the statistical overview in Section 4.2. However, the observations in Sections 4.3 and 4.4 suggested that significant changes in composition could occur because of changes in temperature and relative humidity with altitude. SV-OOA was shown to be enhanced at the top of the boundary layer relative to ground-based measurements and airborne measurements at lower altitude in the vicinity of Cabauw. Furthermore, strong increases in SV-OOA concentrations were noted above the sea surface in areas of enhanced relative humidity. This was attributed to partitioning of semi-volatile species to the particle phase. This is consistent with recent frameworks that have proposed that the entire OM component should be treated as semi-volatile (Donahue et al., 2006; Robinson et al., 2007). Conceptually, adiabatic cooling and mixing of semi-volatile OM precursors could combine to inflate SOA concentrations, as a function of the thermodynamic structure of the boundary layer. The ubiquity of SOA across vast areas of the globe suggest that such a phenomenon could have major impacts on both the transformation of the aerosol burden and the radiative impact and cycling of atmospheric aerosols. Further work relating to SOA measurements should attempt to quantify the processing and impact of partitioning to the particle phase, as such a phenomenon could significantly alter the aerosol burden both vertically and temporally/diurnally.

The research in this thesis demonstrated that OM exhibits comparable concentrations to sulphate across Northern Europe. In many areas, its concentration significantly exceeds that of sulphate. Sulphate has historically received more attention than OM in terms of its contribution to the anthropogenic aerosol burden (e.g. Forster et al., 2007). Sulphate has been shown to exert a large net negative radiative forcing since the industrial revolution (e.g. Forster et al., 2007). Aerosol models have historically been unable to replicate the concentration, chemical make-up and evolution of OM (e.g. Heald et al., 2005; Volkamer et al., 2006; Goldstein and Galbally, 2007; Hallquist et al., 2009), which introduces significant uncertainties into assessments of the impact of atmospheric aerosols.

A major area of future work regarding atmospheric aerosol is the replication of the observed ambient properties of OM in both laboratory experiments and numerical models. Ng et al. (2010) demonstrated conclusively that the majority of chamber measurements of SOA do not resemble the often highly oxidised nature of ambient SOA. Numerical models across both regional and global scales have historically been

unable to replicate the concentration and dominance of SOA over Primary Organic Aerosol (POA). Recent modelling studies (e.g. Dzepina et al., 2009; Hodzic et al., 2010; Tsimpidi et al., 2010) of the Mexico City region have attempted to reconcile measurements of SOA by considering its formation from non-traditional sources, such as primary semi-volatile and intermediate volatility species (Donahue et al., 2006; Robinson et al., 2007). Such analyses have improved absolute concentration comparisons between models and measurements of ambient SOA, although further work is required to evaluate the properties of SOA such as the O:C ratio and volatility distribution. Such analyses should be extended to other regions. A recent global SOA modelling study (Farina et al., 2010), incorporated these non-traditional species and found that global anthropogenic SOA concentrations were markedly increased and compared favourably with measurements.

The ultimate fate of SOA dictates that it is either removed via deposition or oxidation to CO or CO_2, or recycled back to the gas-phase in the form of Volatile Organic Compounds (VOCs, e.g. Goldstein and Galbally, 2007). The observations presented in this thesis supplement current evidence (e.g. Jimenez et al., 2009; Heald et al., 2010; Ng et al., 2010) that atmospheric aging of OM results in the formation of an increasingly oxidised aerosol. Future experiments will likely employ more complete instrumentation packages. This will allow us to characterise both the gas and particle phase components involved in the formation and processing of SOA. Ultimately, this will improve our understanding of the precursors to ambient SOA and the processes involved in its evolution.

5.2.2 Ammonium nitrate in North-Western Europe

The research presented in this thesis demonstrates the importance of ammonium nitrate to the aerosol burden in Northern Europe, with particular emphasis upon the role of its vertical distribution. Several previous studies have highlighted the role of ammonium nitrate in Europe (e.g. Brink et al., 1996; Schaap et al., 2002; Putaud et al., 2004; Abdalmogith and Harrison, 2005; Crosier et al., 2007a), with specific regard for its significant contribution to episodes of enhanced pollution loadings. The analyses presented in this thesis reinforce such conclusions, as ammonium nitrate was shown to be a major driver of enhanced pollution episodes, particularly in North-Western Europe. During such conditions, ammonium nitrate concentrations were found to exceed the concentrations of both ammonium sulphate and OM.

Air mass history was found to exhibit a significant role in determining the concentration of ammonium nitrate in North-Western Europe. This was a consequence of the availability of ammonium nitrate precursors, in particular ammonia, which along with NO_x, tends to peak in North-Western Europe (e.g. Reis et al., 2009). Air masses that had previously been advected across this region exhibited enhanced ammonium nitrate

concentrations and mass fractions. An important observation was that during the high pressure phase of the LONGREX study, significant concentrations of aerosol were observed far downwind of the major sources in Western Europe. Such conditions, where precipitation in the region was low, meant that enhanced concentrations of atmospheric aerosol were present across the regional scale. Total sub-micron aerosol concentrations exceeding 15 $\mu g\,sm^{-3}$ were measured, with ammonium nitrate contributing comparable concentrations to OM and also exceeding the ammonium sulphate concentration. Such observations illustrate how ammonium nitrate can maintain a significant contribution to the atmospheric aerosol burden on the regional scale, in areas far removed from its emission sources.

As SO_2 emissions in North-Western Europe are relatively low in comparison to NO_x, the main limiting terms regarding ammonium nitrate formation will be the conversion of NO_x to HNO_3 and the availability of ammonia. A key observation when analysing the ammonium nitrate spatial distribution across Europe, is that concentrations typically peaked in North-Western Europe. This was in the vicinity of the Netherlands and the East Anglian coast of the UK, areas which exhibit enhanced ammonia concentrations (e.g. Monks et al., 2009). The aerosol burden was typically observed to be neutralised, thus increases in ammonia are liable to result in increased condensation to the particle phase and the formation of ammonium nitrate. These spatial patterns in both the emission sources and the observed particulate concentrations point to the importance of ammonia when considering aerosol in Europe. The importance of ammonia in North America has also been highlighted (e.g. Makar et al., 2009). Consequently, knowledge of the emission and cycling of ammonia in the atmosphere should be a major area of future research when considering the impact of atmospheric aerosols. This is especially pertinent when such research focuses on regional impacts based upon both measurements and models. A significant advance for the FAAM research aircraft will be the recent deployment of a Chemical Ionisation Mass Spectrometer (CIMS), which will measure both ammonia and nitric acid. These measurements will be combined with the AMS during the upcoming RONOCO project (ROle of Night-time chemistry in controlling the Oxidising Capacity of the atmOsphere), which will examine the processes and pathways involved in night-time nitrogen chemistry.

Another important parameter that controlled the distribution of ammonium nitrate, was the thermodynamic structure of the boundary layer; a phenomenon that has been observed previously in a range of locations (e.g. Neuman et al., 2003; Morino et al., 2006; Crosier et al., 2007a). This was demonstrated to be a significant feature in both Sections 4.2 and 4.4. Comparison of aerosol mass concentrations with light scattering measurements revealed that ammonium nitrate was a major driver of the optical impact of the aerosol burden. The increase in ammonium nitrate concentrations led to dramatic increases in AOD and associated radiative forcing. Ammonium nitrate is highly hygroscopic, thus such enhancements were strongly driven by water uptake, as

the increase in ammonium nitrate mass occurred in areas of greater relative humidity.

While the impact of partitioning of semi-volatile precursors to the particle phase at the top of the boundary layer was assessed in this thesis, the impact of such changes upon the indirect effect has yet to be quantified. Increases in Cloud Condensation Nuclei (CCN) were observed with altitude for the case studies in the vicinity of Cabauw. This was not associated with an increase in the overall aerosol number concentration i.e. the fraction of CCN active particles increased with height in the boundary layer. This is unsurprising as ammonium nitrate serves as a highly effective CCN. Furthermore, the changes in mean size of the aerosol particles observed would further promote activation to form CCN. Such increases in CCN with altitude are highly pertinent, as clouds form at the top of the boundary layer and entrain aerosol particles from beneath them. This increases the cloud droplet number concentration within them. Future assessments of the climate impact of ammonium nitrate should seek to quantify this effect. It could potentially significantly increase the CCN burden in a portion of the atmosphere which is directly coupled to cloud formation and subsequent processing.

Ammonium nitrate is often not included in global aerosol models (e.g. Textor et al., 2006; Forster et al., 2007), although it has received more attention in regional chemical transport models (e.g. Schaap et al., 2004; Myhre et al., 2006). Failure to include ammonium nitrate in assessments of the impact of atmospheric aerosols is liable to lead to significant deficiencies, especially when examining the vertical distribution. Such deficiencies may be exacerbated in future, as SO_2 emissions reduce in polluted regions of the globe (e.g. Pinder et al., 2007; Monks et al., 2009). This will diminish the role of sulphate aerosol and increase the availability of ammonia to form ammonium nitrate.

5.3 Closing remarks

As discussed in Section 4.4, Northern Europe can be seen as an analogue for other polluted regions of the globe in terms of its changing emission footprint. This is a key concept, as reductions in SO_2 emissions may result in the increased importance of ammonium nitrate and OM in terms of aerosol radiative forcing and regional air quality. Consequently, the research highlighted in this thesis points towards several challenges to be tackled.

The apparent schism between measured and modelled concentrations of SOA requires rectification, as future assessments of OM will be highly challenging until this is achieved. Recent paradigms considering the volatility of OM point towards potential avenues of future research. Control strategies pertaining to OM will be dependent upon understanding its life cycle, which includes its emission precursors, formation and evolution in the atmosphere. The lack of detailed knowledge regarding whether SOA is derived from anthropogenic sources, biogenic sources or a mixture of both presents

a major difficulty to control strategies e.g. is it more effective to target anthropogenic emissions of VOCs or NO_x? If the VOC precursors to SOA are predominantly biogenic in origin, then efforts to curtail anthropogenic VOC emissions will result in minimal impact upon SOA concentrations. Alternatively, NO_x emissions could be targeted, which would have the co-benefits of reducing SOA concentrations and ammonium nitrate concentrations, as NO_x is the precursor to HNO_3. Thus, greater knowledge of the formation pathways of OM are necessary. This will likely involve application of new instrumental techniques and coordination of multi-scale experimental and modelling programmes. Such studies should focus upon the formation and evolution of SOA in the atmosphere.

The lack of consideration of ammonium nitrate by many global and regional aerosol models presents a major deficiency in attempts to constrain uncertainties of the impact of atmospheric aerosol upon the Earth's climate. Ammonium nitrate also represents a key constituent when examining regional air quality and environmental degradation of regional ecosystems, due to acidification and eutrophication. Adams et al. (2001) represents one of the few global modelling studies to investigate the role of ammonium nitrate in relation to radiative forcing in the 21^{st} century. They predicted that by the year 2100, nitrate radiative forcing would exceed both the present day sulphate forcing and the 2100 sulphate forcing. Such studies should be repeated with current state-of-the-art climate models with specific consideration of the regional impact of ammonium nitrate on both present day and future climate regimes. Ammonium nitrate was not included in the previous AEROCOM assessment (Kinne et al., 2006; Schulz et al., 2006; Textor et al., 2006). It is hoped that this will be rectified for the forthcoming AEROCOM analyses, which will contribute significantly to the next IPCC report.

Future studies should compare measurements in Northern Europe, such as this study, with other polluted continental regions. There are significant differences in meteorology and emission fields in both Eastern Europe and Southern Europe. Undoubtedly this will result in differences between the observed composition of the aerosol burden in such locations, when compared with Northern Europe. Differences in SO_2 and NH_3 emissions will be particularly important based upon the findings of this study. The photochemical environment in Southern Europe is also distinct from that in Northern Europe, which could play a role in determining the time scales for evolution of both the inorganic and organic components. The anticipated strong future reductions in SO_2 in other polluted regions should also be assessed. This should include changes in OM and ammonium nitrate precursors, as these components may become more important than sulphate aerosol.

Significant questions have been posed by the research highlighted in this thesis. Future analysis should investigate how the emission fields will evolve under different climate and economic scenarios. For example, if biogenic VOCs play a dominant role in SOA formation, how will future predicted increases in temperature affect their emis-

sions and the subsequent formation of SOA? Ammonia has been shown to be a key ingredient in determining the make-up of the Northern European aerosol burden. Future changes in agricultural practices are therefore likely to play an important role. The differing time lines for emission reductions in SO_2, NO_x and VOCs will be highly vital when assessing future climate scenarios, especially as energy and fuel usage is modified in response to climate change mitigation and prevention strategies. Consequently, detailed knowledge of the life cycle of atmospheric aerosol is required. This is necessary for constraint of the uncertainties associated with anthropogenic perturbation of the Earth's climate, both now and in the future.

Chapter 6

Appendices

6.1 Supplementary material for Paper I

The following supplementary material supports the analyses conducted as part of Paper I in Section 4.2. The supplementary material includes a meteorological overview of the back trajectory clusters identified and summary statistics of the vertical profiles for each of the chemical components measured.

Vertical distribution of sub-micron aerosol chemical composition from North-Western Europe and the North-East Atlantic

W.T. Morgan[1], J.D. Allan[1,2], K.N. Bower[1], G. Capes[1], J. Crosier[1,2], P.I. Williams[1,2] and H. Coe[1]

1. Centre for Atmospheric Science, University of Manchester, Manchester, UK
2. National Centre for Atmospheric Science, University of Manchester, UK

Correspondance to: W. T. Morgan (william.morgan@postgrad.manchester.ac.uk)

Supplementary material for the maunscript published in ACP.

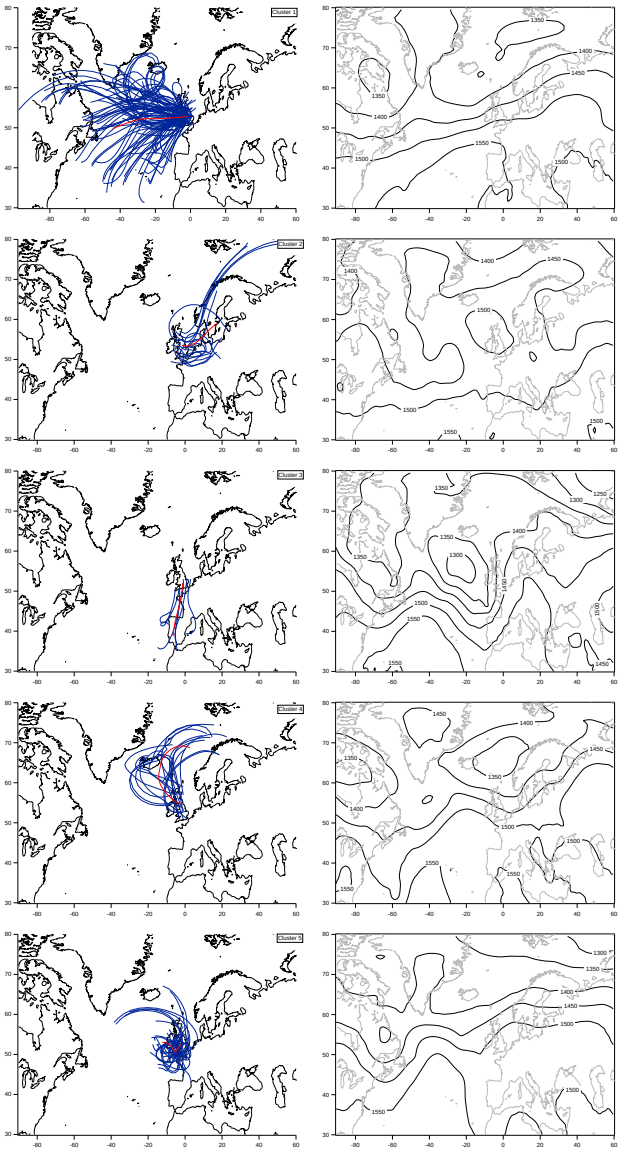

Figure S1: Maps of all back trajectories for each cluster along with the mean trajectory (red line). Also shown are average ECMWF* 850hPa geopotential height fields based on a 2.5 by 2.5 horizontal grid. *European Centre for Medium-Range Weather Forecasts. ECMWF Operational Analysis data, [Internet]. BADC, .2006-2008.
Available from http://badc.nerc.ac.uk/data/ecmwf-op/

		Altitude (km)										
Species	Statistic	0.0-0.5	0.5-1.0	1.0-1.5	1.5-2.0	2.0-2.5	2.5-3.0	3.0-3.5	3.5-4.0	4.0-4.5	4.5-5.0	5.0-5.5
Organics	25thpercentile	0.066	-0.121	-0.201	-0.280	-0.218	-0.348	-0.378	-0.609	-1.067	-0.846	-1.420
	50thpercentile	0.768	0.558	0.535	0.415	0.441	0.333	0.228	0.033	-0.013	-0.070	-0.309
	75thpercentile	1.632	1.470	1.445	1.323	1.383	0.904	1.081	1.037	1.048	1.075	0.731
	Mean	1.052	0.801	0.799	0.716	0.610	0.446	0.382	0.264	0.206	0.199	-0.188
	$MAE/\sqrt{n}$	0.049	0.047	0.054	0.060	0.083	0.084	0.067	0.146	0.175	0.191	0.208
Sulphate	25thpercentile	0.302	0.200	0.203	0.142	0.107	0.075	0.053	0.030	-0.042	-0.030	-0.041
	50thpercentile	0.800	0.678	0.663	0.482	0.450	0.254	0.311	0.189	0.117	0.185	0.148
	75thpercentile	1.504	1.365	1.358	1.103	0.925	0.687	0.532	0.512	0.412	0.374	0.524
	Mean	1.093	1.029	0.964	0.782	0.642	0.409	0.341	0.330	0.176	0.182	0.254
	$MAE/\sqrt{n}$	0.032	0.031	0.032	0.028	0.035	0.030	0.026	0.049	0.035	0.049	0.047
Nitrate	25thpercentile	0.027	0.014	0.017	-0.004	-0.009	-0.015	-0.017	-0.030	-0.032	-0.082	-0.030
	50thpercentile	0.140	0.099	0.079	0.045	0.049	0.027	0.033	0.017	0.020	0.005	0.028
	75thpercentile	0.619	0.516	0.623	0.170	0.178	0.119	0.090	0.076	0.136	0.115	0.151
	Mean	0.911	0.696	0.657	0.328	0.310	0.099	0.052	0.022	0.038	0.017	0.052
	$MAE/\sqrt{n}$	0.033	0.025	0.026	0.015	0.019	0.012	0.007	0.012	0.016	0.019	0.019
Ammonium	25thpercentile	-0.028	-0.072	-0.110	-0.176	-0.220	-0.186	-0.348	-0.470	-0.464	-0.402	-0.418
	50thpercentile	0.375	0.306	0.352	0.274	0.262	0.157	0.045	0.106	0.092	0.197	0.180
	75thpercentile	0.910	0.879	0.935	0.782	0.729	0.593	0.564	0.548	0.725	0.596	0.640
	Mean	0.646	0.550	0.514	0.384	0.303	0.234	0.062	0.001	0.100	0.137	0.156
	$MAE/\sqrt{n}$	0.030	0.028	0.033	0.034	0.051	0.046	0.043	0.115	0.101	0.127	0.119

Table S1a: Profile statistics summary for the full dataset from 0.0-5.5km. MAE refers to the Mean Absolute Error and *n* refers to the number of points.

		Altitude (km)										
Species	Statistic	5.5-6.0	6.0-6.5	6.5-7.0	7.0-7.5	7.5-8.0	8.0-8.5	8.5-9.0	9.0-9.5	9.5-10.0	10.0-10.5	10.5-11.0
Organics	25^{th}percentile	-1.400	-1.392	-1.118	-0.931	-1.629	-1.262	-1.568	-1.322	-2.032	-2.160	-1.857
	50^{th}percentile	0.275	0.139	0.535	0.661	-0.031	0.563	-0.109	0.958	0.026	-0.351	0.079
	75^{th}percentile	1.514	1.130	1.878	2.059	1.542	2.307	2.532	3.458	2.246	2.349	2.012
	Mean	0.227	-0.039	0.566	0.812	0.181	0.762	0.666	1.687	0.062	-0.301	0.498
	$MAE/\sqrt{n}$	0.327	0.301	0.342	0.261	0.320	0.338	0.301	0.381	0.514	0.458	0.561
Sulphate	25^{th}percentile	-0.063	-0.130	-0.168	-0.081	-0.212	-0.175	-0.060	-0.106	-0.424	-0.057	0.184
	50^{th}percentile	0.222	0.177	0.242	0.228	0.206	0.227	0.263	0.348	0.460	0.271	0.715
	75^{th}percentile	0.542	0.552	0.523	0.665	0.659	0.850	0.693	0.834	0.891	0.778	1.023
	Mean	0.2123	0.162	0.188	0.264	0.216	0.321	0.315	0.301	0.409	0.423	0.603
	$MAE/\sqrt{n}$	0.0589	0.075	0.083	0.063	0.080	0.100	0.072	0.090	0.165	0.089	0.146
Nitrate	25^{th}percentile	-0.096	-0.112	-0.169	-0.063	-0.124	-0.067	-0.093	-0.195	-0.186	-0.252	-0.198
	50^{th}percentile	0.003	0.007	0.024	0.033	0.011	0.014	0.023	-0.007	0.100	0.048	0.031
	75^{th}percentile	0.173	0.099	0.121	0.217	0.160	0.168	0.192	0.130	0.324	0.229	0.281
	Mean	0.031	-0.020	-0.0312	0.042	0.024	0.012	0.020	-0.035	0.094	0.048	0.101
	$MAE/\sqrt{n}$	0.026	0.048	0.080	0.031	0.030	0.034	0.036	0.046	0.070	0.060	0.056
Ammonium	25^{th}percentile	-0.595	-0.499	-0.612	-0.832	-0.726	-0.724	-1.023	-1.338	-1.294	-0.706	-0.860
	50^{th}percentile	0.146	0.176	0.148	0.204	0.364	0.008	0.253	0.016	0.334	0.159	-0.042
	75^{th}percentile	0.902	1.012	0.832	0.883	0.972	0.947	1.247	1.334	1.384	1.288	0.735
	Mean	0.093	0.185	0.090	0.011	0.332	0.135	0.068	-0.083	-0.050	0.194	0.056
	$MAE/\sqrt{n}$	0.145	0.150	0.179	0.187	0.166	0.161	0.225	0.217	0.403	0.206	0.269

Table S1b: Profile statistics summary for the full dataset from 5.5-11.0km.

		Altitude (km)										
Species	Statistic	0.0-0.5	0.5-1.0	1.0-1.5	1.5-2.0	2.0-2.5	2.5-3.0	3.0-3.5	3.5-4.0	4.0-4.5	4.5-5.0	5.0-5.5
Organics	25^{th}percentile	-0.009	-0.150	-0.239	-0.379	-0.433	-0.360	-0.429	-0.257	-0.660	-1.063	-0.852
	50^{th}percentile	0.624	0.442	0.243	0.210	0.233	0.258	0.107	0.909	0.420	0.116	0.007
	75^{th}percentile	1.264	1.145	0.934	0.861	0.837	0.730	0.832	1.862	2.018	1.777	1.905
	Mean	0.673	0.479	0.336	0.287	0.281	0.3067	0.314	0.830	0.963	0.748	0.633
	$MAE/\sqrt{n}$	0.058	0.054	0.053	0.072	0.108	0.119	0.088	0.381	0.371	0.323	0.313
Sulphate	25^{th}percentile	0.299	0.243	0.193	0.189	0.105	0.087	0.095	-0.088	-0.117	-0.173	-0.011
	50^{th}percentile	0.764	0.583	0.485	0.434	0.3547	0.241	0.366	0.184	0.107	0.266	0.120
	75^{th}percentile	1.282	1.112	1.164	0.864	0.731	0.617	0.583	0.772	0.329	0.471	0.499
	Mean	0.933	0.782	0.775	0.642	0.527	0.338	0.385	0.384	0.119	0.189	0.276
	$MAE/\sqrt{n}$	0.035	0.031	0.035	0.033	0.043	0.034	0.042	0.118	0.060	0.112	0.067
Nitrate	25^{th}percentile	0.030	0.013	0.016	-0.002	-0.005	-0.021	-0.010	-0.032	-0.071	-0.059	-0.170
	50^{th}percentile	0.150	0.089	0.060	0.036	0.025	0.0054	0.032	0.022	0.035	0.098	0.017
	75^{th}percentile	0.495	0.392	0.329	0.091	0.086	0.043	0.090	0.079	0.167	0.196	0.161
	Mean	0.489	0.375	0.278	0.127	0.142	-0.014	0.055	0.018	0.030	0.043	0.010
	$MAE/\sqrt{n}$	0.024	0.019	0.016	0.009	0.014	0.038	0.010	0.022	0.035	0.071	0.052
Ammonium	25^{th}percentile	0.012	-0.118	-0.186	-0.119	-0.301	-0.336	-0.346	-0.733	-0.521	-0.920	-0.408
	50^{th}percentile	0.379	0.282	0.296	0.239	0.202	0.086	0.082	0.122	0.021	-0.003	0.062
	75^{th}percentile	0.802	0.696	0.743	0.686	0.651	0.449	0.564	0.449	0.305	0.410	0.389
	Mean	0.452	0.344	0.347	0.333	0.199	0.112	0.066	-0.098	-0.052	-0.209	0.095
	$MAE/\sqrt{n}$	0.034	0.033	0.043	0.041	0.079	0.068	0.070	0.192	0.167	0.327	0.109

Table S2a: Profile statistics summary for the Atlantic cluster from 0.0-5.5km.

		Altitude (km)										
Species	Statistic	5.5-6.0	6.0-6.5	6.5-7.0	7.0-7.5	7.5-8.0	8.0-8.5	8.5-9.0	9.0-9.5	9.5-10.0	10.0-10.5	10.5-11.0
Organics	25^{th}percentile	-1.218	-1.056	-1.439	-0.876	-1.813	-1.197	-0.909	0.006	-1.249	-1.880	-1.754
	50^{th}percentile	0.055	0.519	0.299	0.725	-0.116	0.538	0.630	1.654	0.026	-0.293	0.206
	75^{th}percentile	1.335	1.430	1.778	1.964	1.376	1.818	3.711	4.336	2.062	2.349	2.207
	Mean	0.115	0.243	0.344	1.086	-0.010	0.837	1.621	2.229	0.478	-0.118	0.856
	$MAE/\sqrt{n}$	0.316	0.419	0.381	0.292	0.377	0.364	0.430	0.408	0.5118	0.441	0.915
Sulphate	25^{th}percentile	-0.129	-0.147	-0.038	0.069	-0.260	-0.346	-0.191	-0.143	-0.433	-0.158	-0.065
	50^{th}percentile	0.129	0.111	0.279	0.293	0.251	0.184	0.217	0.235	0.505	0.2267	0.587
	75^{th}percentile	0.368	0.461	0.526	0.683	0.659	0.794	0.636	0.6591	1.095	0.750	0.887
	Mean	0.115	0.093	0.240	0.338	0.166	0.308	0.253	0.270	0.492	0.394	0.3989
	$MAE/\sqrt{n}$	0.075	0.093	0.096	0.078	0.120	0.145	0.090	0.108	0.235	0.097	0.213
Nitrate	25^{th}percentile	-0.091	-0.074	-0.020	-0.040	-0.057	-0.047	-0.059	-0.080	-0.207	-0.102	-0.211
	50^{th}percentile	-0.015	0.021	0.066	0.027	0.003	0.014	0.021	0.014	0.077	0.071	0.002
	75^{th}percentile	0.154	0.107	0.189	0.121	0.101	0.117	0.123	0.114	0.240	0.222	0.101
	Mean	0.011	-0.005	0.060	0.048	0.035	0.036	0.037	0.023	0.037	0.106	0.029
	$MAE/\sqrt{n}$	0.033	0.060	0.038	0.029	0.027	0.019	0.024	0.031	0.084	0.040	0.050
Ammonium	25^{th}percentile	-0.706	-0.572	-0.623	-0.911	-0.418	-0.717	-1.027	-1.021	-1.267	-0.7056	-1.172
	50^{th}percentile	0.0923	0.176	-0.099	0.204	0.384	-0.001	0.0256	-0.043	0.177	0.159	-0.091
	75^{th}percentile	0.672	0.928	0.812	0.883	0.981	0.7489	0.739	1.260	1.748	1.288	0.626
	Mean	-0.018	0.075	-0.032	-0.025	0.439	0.082	-0.177	-0.055	0.231	0.165	-0.101
	$MAE/\sqrt{n}$	0.198	0.269	0.179	0.249	0.204	0.194	0.235	0.240	0.393	0.239	0.438

Table S2b: Profile statistics summary for the Atlantic cluster from 5.5-11.0km.

		Altitude (km)										
Species	Statistic	0.0-0.5	0.5-1.0	1.0-1.5	1.5-2.0	2.0-2.5	2.5-3.0	3.0-3.5	3.5-4.0	4.0-4.5	4.5-5.0	5.0-5.5
Organics	25^{th}percentile	0.632	0.275	0.593	0.029	0.538	-0.033	-0.036	-2.268	-0.617	-1.000	-3.025
	50^{th}percentile	1.171	1.135	1.591	0.796	1.358	0.843	0.296	-1.125	0.404	-0.437	-1.464
	75^{th}percentile	2.228	2.497	2.793	2.038	1.994	1.612	1.206	-0.152	0.589	1.771	0.341
	Mean	1.481	1.480	1.758	1.068	1.399	0.933	0.473	-1.245	0.061	0.067	-1.481
	$MAE/\sqrt{n}$	0.112	0.121	0.153	0.121	0.171	0.194	0.180	0.690	0.654	0.461	0.853
Sulphate	25^{th}percentile	0.570	0.179	0.588	0.331	0.619	0.294	0.157	0.314	0.243	-0.347	-0.354
	50^{th}percentile	1.037	0.985	1.074	0.801	1.030	0.713	0.319	0.417	0.743	-0.035	0.272
	75^{th}percentile	1.724	2.297	1.783	1.299	1.509	1.277	0.752	0.781	1.001	0.154	0.492
	Mean	1.308	1.429	1.315	0.975	1.100	0.960	0.485	0.663	0.656	-0.081	0.139
	$MAE/\sqrt{n}$	0.077	0.108	0.068	0.072	0.099	0.124	0.073	0.139	0.180	0.118	0.355
Nitrate	25^{th}percentile	0.079	0.029	0.077	0.0467	0.091	0.064	0.033	-0.027	-0.007	-0.072	0.002
	50^{th}percentile	0.440	0.354	0.737	0.125	0.256	0.261	0.061	0.017	0.010	-0.045	0.026
	75^{th}percentile	1.255	2.323	2.708	0.815	1.194	0.560	0.141	0.038	0.027	-0.005	0.096
	Mean	1.898	1.588	1.827	0.753	1.006	0.508	0.105	0.004	0.013	-0.044	0.042
	$MAE/\sqrt{n}$	0.166	0.137	0.143	0.072	0.135	0.066	0.014	0.021	0.010	0.019	0.014
Ammonium	25^{th}percentile	0.096	0.052	0.213	-0.030	0.090	-0.006	-0.479	-0.198	-0.789	-0.847	-0.949
	50^{th}percentile	0.677	0.482	0.891	0.378	0.669	0.248	-0.007	0.266	1.245	0.093	0.277
	75^{th}percentile	1.713	1.611	1.328	1.239	1.444	0.992	0.760	0.923	1.917	1.106	1.386
	Mean	1.294	1.044	1.034	0.633	0.896	0.436	-0.013	0.233	0.761	0.156	0.226
	$MAE/\sqrt{n}$	0.112	0.090	0.094	0.082	0.152	0.143	0.160	0.495	1.202	0.622	0.476

Table S3a: Profile statistics summary for the easterly cluster from 0.0-5.5km.

		Altitude (km)										
Species	Statistic	5.5-6.0	6.0-6.5	6.5-7.0	7.0-7.5	7.5-8.0	8.0-8.5	8.5-9.0	9.0-9.5	9.5-10.0	10.0-10.5	10.5-11.0
Organics	25^{th}percentile	-3.329	-1.816	N/A	N/A	N/A	N/A	N/A	N/A	N/A	N/A	N/A
	50^{th}percentile	0.100	-0.282	N/A	N/A	N/A	N/A	N/A	N/A	N/A	N/A	N/A
	75^{th}percentile	2.060	0.454	N/A	N/A	N/A	N/A	N/A	N/A	N/A	N/A	N/A
	Mean	-0.670	-0.601	N/A	N/A	N/A	N/A	N/A	N/A	N/A	N/A	N/A
	$MAE/\sqrt{n}$	1.545	0.859	N/A	N/A	N/A	N/A	N/A	N/A	N/A	N/A	N/A
Sulphate	25^{th}percentile	-0.114	0.123	N/A	N/A	N/A	N/A	N/A	N/A	N/A	N/A	N/A
	50^{th}percentile	0.202	0.521	N/A	N/A	N/A	N/A	N/A	N/A	N/A	N/A	N/A
	75^{th}percentile	0.609	0.786	N/A	N/A	N/A	N/A	N/A	N/A	N/A	N/A	N/A
	Mean	0.225	0.468	N/A	N/A	N/A	N/A	N/A	N/A	N/A	N/A	N/A
	$MAE/\sqrt{n}$	0.164	0.244	N/A	N/A	N/A	N/A	N/A	N/A	N/A	N/A	N/A
Nitrate	25^{th}percentile	-0.067	-0.084	N/A	N/A	N/A	N/A	N/A	N/A	N/A	N/A	N/A
	50^{th}percentile	-0.014	-0.007	N/A	N/A	N/A	N/A	N/A	N/A	N/A	N/A	N/A
	75^{th}percentile	0.059	0.018	N/A	N/A	N/A	N/A	N/A	N/A	N/A	N/A	N/A
	Mean	0.006	-0.028	N/A	N/A	N/A	N/A	N/A	N/A	N/A	N/A	N/A
	$MAE/\sqrt{n}$	0.038	0.040	N/A	N/A	N/A	N/A	N/A	N/A	N/A	N/A	N/A
Ammonium	25^{th}percentile	-0.190	-0.640	N/A	N/A	N/A	N/A	N/A	N/A	N/A	N/A	N/A
	50^{th}percentile	0.499	-0.156	N/A	N/A	N/A	N/A	N/A	N/A	N/A	N/A	N/A
	75^{th}percentile	1.737	1.529	N/A	N/A	N/A	N/A	N/A	N/A	N/A	N/A	N/A
	Mean	0.580	0.324	N/A	N/A	N/A	N/A	N/A	N/A	N/A	N/A	N/A
	$MAE/\sqrt{n}$	0.483	0.464	N/A	N/A	N/A	N/A	N/A	N/A	N/A	N/A	N/A

Table S3b: Profile statistics summary for the easterly cluster from 5.5-11.0km.

		Altitude (km)										
Species	Statistic	0.0-0.5	0.5-1.0	1.0-1.5	1.5-2.0	2.0-2.5	2.5-3.0	3.0-3.5	3.5-4.0	4.0-4.5	4.5-5.0	5.0-5.5
Organics	25^{th}percentile	0.470	0.063	0.108	-0.242	-0.036	0.0109	-0.380	-1.026	-1.427	-0.673	-2.011
	50^{th}percentile	1.555	0.678	1.255	0.681	0.959	0.424	0.424	-0.100	-0.145	0.465	-0.567
	75^{th}percentile	2.312	2.280	2.337	1.861	1.883	1.568	1.285	0.306	0.803	1.527	0.741
	Mean	1.927	1.419	1.385	1.253	1.035	0.689	0.505	-0.2156	-0.289	0.220	-0.519
	$MAE/\sqrt{n}$	0.208	0.174	0.248	0.204	0.282	0.218	0.180	0.376	0.451	0.538	0.349
Sulphate	25^{th}percentile	0.314	0.342	0.302	0.031	0.250	0.030	-0.111	0.058	-0.098	-0.054	-0.174
	50^{th}percentile	1.251	1.035	0.894	0.399	0.637	0.418	0.139	0.253	0.031	0.104	0.082
	75^{th}percentile	2.454	1.748	1.548	1.482	1.071	0.810	0.386	0.374	0.406	0.375	0.528
	Mean	1.740	1.431	1.089	1.052	0.860	0.440	0.156	0.227	0.089	0.150	0.216
	$MAE/\sqrt{n}$	0.165	0.125	0.114	0.135	0.100	0.105	0.045	0.065	0.073	0.079	0.109
Nitrate	25^{th}percentile	0.019	0.022	0.019	-0.008	-0.005	-0.016	-0.029	-0.027	0.009	-0.116	-0.058
	50^{th}percentile	0.108	0.115	0.086	0.026	0.061	0.072	0.019	0.060	0.057	-0.007	0.026
	75^{th}percentile	0.910	1.036	0.642	0.323	0.416	0.227	0.053	0.118	0.172	0.022	0.180
	Mean	2.124	1.394	0.855	0.848	0.423	0.164	0.032	0.053	0.086	-0.021	0.065
	$MAE/\sqrt{n}$	0.283	0.156	0.101	0.115	0.074	0.032	0.010	0.047	0.038	0.050	0.037
Ammonium	25^{th}percentile	-0.070	-0.034	-0.135	-0.342	-0.419	-0.187	-0.279	-0.778	-0.897	-0.402	-0.697
	50^{th}percentile	0.241	0.334	0.320	0.198	0.281	0.237	0.011	0.144	0.104	0.409	-0.054
	75^{th}percentile	1.117	1.031	1.015	1.029	0.737	0.705	0.521	0.745	0.778	1.040	1.046
	Mean	1.034	0.876	0.513	0.541	0.239	0.258	0.104	-0.044	-0.035	0.451	0.001
	$MAE/\sqrt{n}$	0.134	0.116	0.102	0.110	0.184	0.108	0.069	0.370	0.335	0.157	0.240

Table S4a: Profile statistics summary for the stagnant air mass cluster from 0.0-5.5km.

		Altitude (km)										
Species	Statistic	5.5-6.0	6.0-6.5	6.5-7.0	7.0-7.5	7.5-8.0	8.0-8.5	8.5-9.0	9.0-9.5	9.5-10.0	10.0-10.5	10.5-11.0
Organics	25^{th}percentile	-1.351	-1.701	-1.172	-1.702	-1.045	-1.644	-1.945	-2.274	-3.905	-2.822	-2.215
	50^{th}percentile	0.826	0.003	0.525	0.320	0.119	0.969	-0.639	-0.148	-0.476	-0.651	-0.850
	75^{th}percentile	2.894	0.675	2.715	2.338	2.551	2.874	1.237	2.573	2.444	3.081	1.585
	Mean	0.874	-0.321	0.792	0.306	0.386	0.624	-0.420	1.076	-0.622	-0.745	-0.025
	$MAE/\sqrt{n}$	0.716	0.608	0.626	0.510	0.633	0.705	0.398	0.605	1.020	1.365	0.743
Sulphate	25^{th}percentile	0.169	-0.320	-0.289	-0.318	-0.216	-0.151	-0.047	-0.105	-0.426	-0.025	0.5156
	50^{th}percentile	0.388	0.182	-0.049	0.082	0.203	0.260	0.424	0.454	0.429	0.462	0.865
	75^{th}percentile	0.651	0.612	0.488	0.660	0.598	1.039	0.715	0.909	0.832	0.991	1.255
	Mean	0.373	0.188	0.067	0.130	0.236	0.346	0.386	0.337	0.273	0.495	0.901
	$MAE/\sqrt{n}$	0.132	0.136	0.130	0.121	0.096	0.138	0.115	0.144	0.279	0.206	0.145
Nitrate	25^{th}percentile	-0.173	-0.275	-0.516	-0.310	-0.239	-0.275	-0.346	-0.445	-0.174	-0.474	-0.194
	50^{th}percentile	0.141	-0.005	-0.241	0.167	-0.006	0.051	0.094	-0.150	0.206	-0.264	0.239
	75^{th}percentile	0.305	0.262	0.107	0.287	0.231	0.318	0.322	0.163	0.471	0.336	0.551
	Mean	0.105	-0.038	-0.210	0.032	-0.008	-0.031	0.001	-0.010	0.188	-0.095	0.205
	$MAE/\sqrt{n}$	0.082	0.087	0.117	0.086	0.075	0.109	0.087	0.073	0.122	0.108	0.152
Ammonium	25^{th}percentile	-0.576	-0.350	-0.748	-0.656	-0.862	-0.733	-1.032	-1.596	-2.976	-0.697	-0.790
	50^{th}percentile	0.364	0.502	0.448	0.169	0.364	0.227	0.519	0.186	0.404	0.147	0.129
	75^{th}percentile	1.051	1.216	1.124	0.955	0.972	1.280	1.547	1.512	1.090	1.637	0.7856
	Mean	0.231	0.417	0.305	0.047	0.224	0.231	0.347	-0.114	-0.510	0.267	0.286
	$MAE/\sqrt{n}$	0.254	0.276	0.599	0.319	0.315	0.287	0.331	0.393	1.127	0.340	0.375

Table S4b: Profile statistics summary for the stagnant air mass cluster from 5.5-11.0km.

		Altitude (km)										
Species	Statistic	0.0-0.5	0.5-1.0	1.0-1.5	1.5-2.0	2.0-2.5	2.5-3.0	3.0-3.5	3.5-4.0	4.0-4.5	4.5-5.0	5.0-5.5
Organics	25^{th}percentile	1.274	-1.415	-1.214	0.032	-0.468	-1.238	-0.782	-0.180	-1.400	-2.032	-1.919
	50^{th}percentile	2.588	0.915	0.401	1.100	0.620	0.465	-0.277	0.291	-0.228	-0.669	-0.344
	75^{th}percentile	5.263	2.101	2.231	2.268	1.276	2.133	1.080	1.448	1.089	0.275	0.999
	Mean	3.290	0.884	0.810	1.153	0.722	0.713	0.734	0.438	-0.231	-1.018	-0.555
	$MAE/\sqrt{n}$	0.420	0.459	0.395	0.313	0.415	0.745	0.530	0.246	0.426	0.693	0.993
Sulphate	25^{th}percentile	1.393	0.847	0.491	0.652	0.124	-0.285	0.164	-0.044	0.012	0.159	0.044
	50^{th}percentile	1.740	1.740	1.133	1.225	0.620	0.323	0.315	0.527	0.090	0.317	0.455
	75^{th}percentile	2.643	2.418	2.440	1.982	1.105	0.488	0.459	0.583	0.396	0.448	0.798
	Mean	2.068	2.176	1.903	1.443	0.681	0.060	0.302	0.383	0.156	0.289	0.379
	$MAE/\sqrt{n}$	0.145	0.181	0.220	0.138	0.131	0.284	0.059	0.226	0.055	0.092	0.188
Nitrate	25^{th}percentile	0.167	-0.155	-0.145	-0.073	-0.083	-0.056	0.020	-0.027	-0.112	-0.013	-0.049
	50^{th}percentile	0.575	0.047	0.032	0.088	0.037	0.109	0.089	0.027	0.001	0.073	0.058
	75^{th}percentile	2.947	0.204	0.174	0.342	0.209	0.394	0.135	0.100	0.061	0.171	0.245
	Mean	1.867	0.361	0.150	0.185	0.210	0.121	0.092	0.031	-0.013	0.072	0.113
	$MAE/\sqrt{n}$	0.281	0.064	0.046	0.041	0.045	0.110	0.026	0.025	0.048	0.042	0.067
Ammonium	25^{th}percentile	0.290	0.069	-0.110	0.091	-0.217	-0.159	-0.429	-0.429	0.027	-0.322	0.342
	50^{th}percentile	1.051	0.490	0.444	0.637	0.262	0.300	0.373	0.414	0.462	0.167	0.543
	75^{th}percentile	2.177	1.160	1.064	1.244	0.832	1.229	0.637	0.623	0.985	0.699	1.270
	Mean	1.237	0.760	0.635	0.635	0.215	0.673	0.166	0.212	0.455	0.092	0.797
	$MAE/\sqrt{n}$	0.155	0.164	0.162	0.126	0.151	0.312	0.258	0.353	0.235	0.241	0.177

Table S5a: Profile statistics summary for the southerley air mass cluster from 0.0-5.5km.

		Altitude (km)										
Species	Statistic	5.5-6.0	6.0-6.5	6.5-7.0	7.0-7.5	7.5-8.0	8.0-8.5	8.5-9.0	9.0-9.5	9.5-10.0	10.0-10.5	10.5-11.0
Organics	25^{th}percentile	-3.059	N/A	N/A	N/A	N/A	N/A	N/A	N/A	N/A	N/A	N/A
	50^{th}percentile	-0.344	N/A	N/A	N/A	N/A	N/A	N/A	N/A	N/A	N/A	N/A
	75^{th}percentile	-1.489	N/A	N/A	N/A	N/A	N/A	N/A	N/A	N/A	N/A	N/A
	Mean	-2.274	N/A	N/A	N/A	N/A	N/A	N/A	N/A	N/A	N/A	N/A
	$MAE/\sqrt{n}$	0.785	N/A	N/A	N/A	N/A	N/A	N/A	N/A	N/A	N/A	N/A
Sulphate	25^{th}percentile	-0.006	N/A	N/A	N/A	N/A	N/A	N/A	N/A	N/A	N/A	N/A
	50^{th}percentile	0.455	N/A	N/A	N/A	N/A	N/A	N/A	N/A	N/A	N/A	N/A
	75^{th}percentile	1.403	N/A	N/A	N/A	N/A	N/A	N/A	N/A	N/A	N/A	N/A
	Mean	0.698	N/A	N/A	N/A	N/A	N/A	N/A	N/A	N/A	N/A	N/A
	$MAE/\sqrt{n}$	0.704	N/A	N/A	N/A	N/A	N/A	N/A	N/A	N/A	N/A	N/A
Nitrate	25^{th}percentile	-0.009	N/A	N/A	N/A	N/A	N/A	N/A	N/A	N/A	N/A	N/A
	50^{th}percentile	0.058	N/A	N/A	N/A	N/A	N/A	N/A	N/A	N/A	N/A	N/A
	75^{th}percentile	0.117	N/A	N/A	N/A	N/A	N/A	N/A	N/A	N/A	N/A	N/A
	Mean	0.054	N/A	N/A	N/A	N/A	N/A	N/A	N/A	N/A	N/A	N/A
	$MAE/\sqrt{n}$	0.063	N/A	N/A	N/A	N/A	N/A	N/A	N/A	N/A	N/A	N/A
Ammonium	25^{th}percentile	-0.535	N/A	N/A	N/A	N/A	N/A	N/A	N/A	N/A	N/A	N/A
	50^{th}percentile	0.543	N/A	N/A	N/A	N/A	N/A	N/A	N/A	N/A	N/A	N/A
	75^{th}percentile	0.146	N/A	N/A	N/A	N/A	N/A	N/A	N/A	N/A	N/A	N/A
	Mean	-0.194	N/A	N/A	N/A	N/A	N/A	N/A	N/A	N/A	N/A	N/A
	$MAE/\sqrt{n}$	0.341	N/A	N/A	N/A	N/A	N/A	N/A	N/A	N/A	N/A	N/A

Table S5b: Profile statistics summary for the southerley air mass cluster from 5.5-11.0km.

		Altitude (km)										
Species	Statistic	0.0-0.5	0.5-1.0	1.0-1.5	1.5-2.0	2.0-2.5	2.5-3.0	3.0-3.5	3.5-4.0	4.0-4.5	4.5-5.0	5.0-5.5
Organics	25^{th}percentile	-0.403	-0.498	-0.226	-0.547	-0.416	-0.531	-0.293	-0.565	-1.231	-0.472	-0.818
	50^{th}percentile	0.034	0.078	0.308	0.278	0.037	-0.243	0.134	-0.251	-0.380	-0.227	-0.265
	75^{th}percentile	0.706	0.860	1.198	1.692	0.456	0.311	1.179	1.037	0.513	0.832	0.420
	Mean	0.253	0.483	0.652	0.761	0.166	0.082	0.235	0.253	-0.369	0.114	-0.271
	$MAE/\sqrt{n}$	0.102	0.125	0.162	0.149	0.165	0.154	0.193	0.218	0.296	0.248	0.321
Sulphate	25^{th}percentile	0.014	-0.019	-0.043	-0.106	0.009	-0.015	-0.025	0.041	0.051	0.123	0.001
	50^{th}percentile	0.147	0.130	0.043	0.106	0.104	0.094	0.241	0.100	0.197	0.215	0.194
	75^{th}percentile	0.538	0.597	0.378	0.361	0.324	0.236	0.522	0.257	0.489	0.303	0.380
	Mean	0.500	0.470	0.494	0.266	0.235	0.256	0.332	0.177	0.287	0.252	0.275
	$MAE/\sqrt{n}$	0.054	0.065	0.075	0.039	0.044	0.040	0.064	0.034	0.081	0.052	0.065
Nitrate	25^{th}percentile	-0.016	-0.016	-0.046	-0.079	-0.077	-0.018	-0.105	-0.046	-0.059	-0.093	0.021
	50^{th}percentile	0.020	0.036	0.051	0.018	-0.013	0.036	-0.011	0.002	0.020	0.003	0.053
	75^{th}percentile	0.070	0.153	0.153	0.099	0.060	0.079	0.084	0.047	0.111	0.111	0.106
	Mean	0.064	0.203	0.383	0.106	-0.004	0.042	0.005	0.001	0.027	0.019	0.075
	$MAE/\sqrt{n}$	0.010	0.026	0.058	0.018	0.017	0.021	0.029	0.022	0.036	0.033	0.017
Ammonium	25^{th}percentile	-0.230	-0.183	-0.201	-0.635	-0.244	-0.066	-0.241	-0.323	-0.165	0.003	-0.027
	50^{th}percentile	0.014	0.186	0.078	0.012	0.066	0.138	0.045	-0.121	0.029	0.519	0.238
	75^{th}percentile	0.368	0.839	0.430	0.510	0.480	0.599	0.550	0.256	0.475	0.641	0.464
	Mean	0.071	0.243	0.220	-0.070	0.070	0.266	0.013	0.051	0.133	0.276	0.199
	$MAE/\sqrt{n}$	0.057	0.087	0.071	0.118	0.099	0.080	0.117	0.108	0.137	0.186	0.132

Table S6a: Profile statistics summary for the northerley air mass cluster from 0.0-5.5km.

		Altitude (km)										
Species	Statistic	5.5-6.0	6.0-6.5	6.5-7.0	7.0-7.5	7.5-8.0	8.0-8.5	8.5-9.0	9.0-9.5	9.5-10.0	10.0-10.5	10.5-11.0
Organics	25^{th}percentile	0.281	-1.212	0.759	0.014	-0.838	N/A	N/A	N/A	N/A	N/A	N/A
	50^{th}percentile	0.390	-0.047	1.835	1.094	1.069	N/A	N/A	N/A	N/A	N/A	N/A
	75^{th}percentile	1.270	0.935	2.596	1.862	1.445	N/A	N/A	N/A	N/A	N/A	N/A
	Mean	0.699	-0.108	1.730	0.990	0.559	N/A	N/A	N/A	N/A	N/A	N/A
	$MAE/\sqrt{n}$	0.220	0.589	0.971	1.330	1.396	N/A	N/A	N/A	N/A	N/A	N/A
Sulphate	25^{th}percentile	0.028	0.079	0.018	0.223	0.102	N/A	N/A	N/A	N/A	N/A	N/A
	50^{th}percentile	0.133	0.261	0.161	0.302	0.721	N/A	N/A	N/A	N/A	N/A	N/A
	75^{th}percentile	0.456	0.390	0.831	0.333	1.058	N/A	N/A	N/A	N/A	N/A	N/A
	Mean	0.220	0.243	0.336	0.286	0.627	N/A	N/A	N/A	N/A	N/A	N/A
	$MAE/\sqrt{n}$	0.091	0.098	0.175	0.085	0.525	N/A	N/A	N/A	N/A	N/A	N/A
Nitrate	25^{th}percentile	-0.176	-0.103	-0.084	-0.040	0.066	N/A	N/A	N/A	N/A	N/A	N/A
	50^{th}percentile	-0.125	-0.037	0.034	0.039	0.185	N/A	N/A	N/A	N/A	N/A	N/A
	75^{th}percentile	0.071	0.027	0.061	0.092	0.355	N/A	N/A	N/A	N/A	N/A	N/A
	Mean	-0.067	-0.038	0.004	0.030	0.202	N/A	N/A	N/A	N/A	N/A	N/A
	$MAE/\sqrt{n}$	0.053	0.044	0.088	0.033	0.054	N/A	N/A	N/A	N/A	N/A	N/A
Ammonium	25^{th}percentile	-0.449	-0.544	-0.162	-0.699	-1.036	N/A	N/A	N/A	N/A	N/A	N/A
	50^{th}percentile	0.057	-0.464	0.192	0.349	-0.120	N/A	N/A	N/A	N/A	N/A	N/A
	75^{th}percentile	0.547	-0.366	0.508	0.942	1.301	N/A	N/A	N/A	N/A	N/A	N/A
	Mean	0.051	-0.458	0.179	0.198	0.048	N/A	N/A	N/A	N/A	N/A	N/A
	$MAE/\sqrt{n}$	0.353	0.051	0.341	0.456	0.443	N/A	N/A	N/A	N/A	N/A	N/A

Table S6b: Profile statistics summary for the northerley air mass cluster from 5.5-11.0km.

6.2 Supplementary material for Paper II

The following supplementary material supoorts the analyses conducted as part of Paper II in Section 4.3. The supplementary material provides additional information regarding the meteorological situation associated with the study, AMS data quantification and the photochemical context. Further information regarding the factor analysis methods and results is also included.

Airborne measurements of the spatial distribution of aerosol chemical composition across Europe and evolution of the organic fraction: Supplementary material

W. T. Morgan[1], J. D. Allan[1,2], K. N. Bower[1], E.J. Highwood[3], D. Liu[1], G. R. McMeeking[1], M. J. Northway[3], P. I. Williams[1,2], R. Krejci[4] and H. Coe[1]

1. *Centre for Atmospheric Science, University of Manchester, Manchester, UK*
2. *National Centre for Atmospheric Science, University of Manchester, UK*
3. *Department of Meteorology, University of Reading, UK*
4. *Department of Applied Environmental Science, Atmospheric Science Unit, Stockholm University, Sweden*

1 Scope

The supplementary material outlined in this document is provided in order to present the meteorological context of the flight operations and support the analysis techniques and data quantification steps outlined in the main paper. The meteorological fields corresponding to each flying period are presented and further information regarding the photochemical context of the operations is presented. Further details regarding the volume closure between the Aerosol Mass Spectrometer (AMS) and the Passive Cavity Aerosol Spectrometer Probe (PCASP) are discussed. Comparison of the estimated HOA with primary combustion tracers is included. The relationship between the fractional contribution of Low-Volatility Oxygenated Organic Aerosol (LV-OOA) to the organic mass and the normalised organic signal at m/z 44 is also shown. Further information is provided regarding the Positive Matrix Factorisation (PMF) analysis examples from the main text, as well as a summary of some PMF diagnostics for the whole dataset. The PMF analysis was performed using the tools presented by Ulbrich et al. (2009).

2 Meteorological summary

Figs. S1 and S2 display the typical meteorological conditions prevalent during each period considered by the analysis. The periods are relatively consistent in terms of their transport patterns, with the air masses transporting pollution from continental Europe downwind to either the UK region or into the Eastern Atlantic Ocean. Thus the flights are predominantly focused upon either sampling such pollution over continental Europe itself or at a range of scales downwind.

The evolution of the aerosol chemical composition during the LONGREX-2 period was examined based upon the relatively consistent transport patterns prevalent during the period. Fig. S3a displays the back trajectories for each flight during this period based upon Straight and Level Runs (SLRs) during each flight. The trajectories display highly consistent behaviour during the period, which is unsurprising given the relative stability of the high pressure system located over Northern Europe during this period. Fig. S3b highlights the back trajectory from the 14 May 2008, which was initialised from a SLR during B374 in the Eastern Atlantic Ocean. B374 represented the end-point in our operations during this period both in terms of the geographical location of the missions and also the distance from continental European sources i.e. the most aged polluted air mass. The back trajectory indicates that the spatial coverage of the flight operations closely matches the air mass transport during the period leading up to the 14 May 2008. Specifically, flights B370-B374 took place across Northern Europe during this period covering close to 5 days of air mass transport.

3 AMS versus PCASP comparison

Validation of the collection efficiency treatment applied to the dataset following the principles developed by Matthew et al. (2008) is accomplished by comparing the AMS data with the volume estimated concentrations from the PCASP instrument. The AMS total mass concentrations were converted to total volume concentrations using the densities reported by Cross et al. (2007), which correspond to 1.27 $\mathrm{g\,cm^{-3}}$ for organics and 1.77 $\mathrm{g\,cm^{-3}}$ for inorganics. A comparison of the estimated volume from the AMS and PCASP is shown for SLRs below 3000 m in Fig. S4. Over all of the considered flights, the estimated AMS volume concentrations were 26% higher than the estimated PCASP volumes. This average agreement is predominantly determined by the LONGREX flights, which were quite consistent in terms of the agreement from flight-to-flight. The ADIENT flying periods sit on either side of the overall regression slope, with the ADIENT-2 flying indicating that the PCASP volume was 48% of the AMS volume. These discrepancies are considered tolerable given the large uncertainties previously reported in the literature for PCASP volume estimates (e.g. Moore et al., 2004; Hallar et al., 2006) and the uncertainties in the AMS volume estimates.

For B357, the PCASP volume estimate was more than two times greater than the AMS volume estimate, which is outside of the bounds of uncertainty for the two instruments. The reason for this discrepancy is unknown but could reflect an artifact in either instrument or the presence of material that is not detected by the AMS. The discrepancy between the two instruments is also reflected in the calculated volume-scattering

relationship when comparing the measurements with a nephelometer system. The main difference between B357 and the other flights in the dataset is the sampling altitude of the aircraft, where in B357, the aircraft operated at a constant altitude of 200 m for the majority of the flight. The other flights in the dataset operated at altitudes higher in the boundary layer. Potentially, the nephelometer and PCASP measurements could be perturbed by the constant low-level flying in a humid environment as the aerosol sampled may not be sufficiently dried in the inlet lines and by the heater respectively. The AMS volume estimates do not include water, so this could potentially cause the discrepancy. Additionally, the PCASP and nephelometer may be measuring refractory material or particles above the cut off of the AMS aerodynamic lens. This would also lead to the AMS underestimating the volume relative to the PCASP.

4 Photochemical context

The relationship between O_3 and CO with the O_3:NO_x ratio discussed in the main paper is presented in Fig. S5. The results indicate that O_3 increases and CO decreases steadily in the 1-100 O_3:NO_x range, which is a reflection of photochemistry and dilution respectively. Beyond an O_3:NO_x ratio of 100, the concentrations decrease with CO returning to background levels and O_3 remaining relatively constant in the 40-60 ppb range.

5 Positive Matrix Factorisation

Potentially, the most challenging and subjective aspect of PMF analysis is the selection of the appropriate number of factors. For AMS datasets, this is usually accomplished using internal PMF diagnostics, similarity to reference mass spectra and external measurement parameters. An example of an internal diagnostic is the parameter $Q/Q_{expected}$, which is defined as the total sum of the scaled residuals, divided by its expected value. This expected value is derived based upon the error estimates for the data matrix (Ulbrich et al., 2009). A value of unity for the $Q/Q_{expected}$ parameter indicates that the expected variance associated with random errors can be explained by the solution set. Values greater than unity indicate that there is additional variance not accounted for by the solution set. The suite of aerosol and gas phase instrumentation available on the aircraft provides several necessary external parameters to facilitate validation of the solution. Reference spectra utilised in this study are taken from the AMS spectral database (`http://cires.colorado.edu/jimenez-group/AMSsd/`) described in Ulbrich et al. (2009). The factor solutions are interpreted based upon comparisons with external parameters and reference mass spectra. Comparisons between mass spectra are accomplished using the Uncentered Correlation (UC, Ulbrich et al., 2009) coefficient, while the comparisons with external parameters use the Pearson's R coefficient.

Here we include additional information regarding the PMF solutions used in the main manuscript. This includes example PMF solutions from a range of flights in different conditions, a summary of the results for the whole dataset and further details

regarding the estimation of HOA from our data.

5.1 Example PMF solutions

Several PMF solutions will be illustrated in the following section based upon some example flights from the dataset. The flights chosen are B357 (16 April 2008), B362 (6 May 2008), B369 (10 May 2008) and B406 (25 September 2008) as these broadly represent the range of operations conducted in terms of their proximity to pollution sources. B357 was conducted primarily downwind of the major conurbations of Manchester and Liverpool, in the North-West of England. B362 was conducted on a South-North transect originating from Oberpfaffenhofen in southern Germany, culminating in a sequence of Straight-and-Level Runs (SLRs) in the North Sea in the outflow from continental Europe. B406 was conducted in the outflow from continental Europe along the southern coast of the UK. B369 was conducted in the Baltic Sea region and reflects background conditions for comparison with the more polluted examples.

The results for B357 are shown in Fig. S6, for B362 in Fig. S7, for B369 in Fig. S8 and B406 in Fig, S9. All the examples show excellent agreement between the measured and reconstructed organic mass concentrations.

5.1.1 Close to source case study – B357

For B357, a 2-factor solution was deemed most appropriate as increasing the number of factors led to a phenomenon known as "splitting". This leads to multiple factors being assigned with numerically similar factor profiles and time series. In this case, the additional factors merely represented variability within the factors identified in the 2-factor solution. Consequently, the 2-factor solution was retained for analysis. The $Q/Q_{expected}$ was equal to 1.38. Reconstructed OM concentrations made up 98% of the measured OM concentrations. Factor 1 (OOA-1) exhibits a correlation coefficient of 0.89 and 0.98 when compared to reference spectra for an ambient rural case (from Canada) and laboratory generated fulvic acid respectively, which has chemical functionalities that are representative of aged OM (e.g. McFiggans et al., 2005) and hence is indicative of an LV-OOA type factor. Factor 2 (OOA-2) is interpreted as HOA as it exhibits a high correlation (0.91) with the derived HOA mass spectrum from Pittsburgh (Zhang et al., 2005a). Additionally, it has a correlation coefficient of 0.87 when compared to diesel exhaust from a chase study in New York (Canagaratna et al., 2004). The factor 2 time series correlates with NO_x (r=0.65), CO (r=0.73) and BC (r=0.79), with the strong gradients in the time series coincident with large increases in NO_x, CO and BC. Cororally, factor 1 exhibits low correlation (r<0.35) with these combustion tracers. Comparison of the emission ratio of POA to NO_x from B357, which is equal to 29.9 $\mu g\,sm^{-3}$ ppm^{-1}, with the previous studies summarised in Table S1 yields good agreement. Furthermore, the emission ratio relative to CO of 8.0 $\mu g\,sm^{-3}$ ppm^{-1} falls within the literature values summarised in Table S1. Therefore, it appears that factor 2 in this case is likely attributable to primary sources of OM in the form of HOA.

5.1.2 Continental European scale case studies – B362 and B406

While B357 presented a relatively straight forward 2-factor solution, B362 and B406 present highly complex examples of the factor analysis. When more than 3 factors were examined, the "splitting" phenomenon was observed. The 3-factor solutions contained a factor profile strongly resembling LV-OOA, with *m/z* 44 dominating the mass spectrum and a high correlation with the reference spectra for fulvic acid and the ambient rural case. The second factor is characterised by a mass spectrum with similar intensities at m/z43 and 44 and an enhanced base peak at *m/z* 55. Such a spectrum is fairly typical of a SV-OOA type component (Ulbrich et al., 2009; Jimenez et al., 2009). The remaining factor appeared to represent a second SV-OOA mass spectrum but with enhanced mass peaks associated with commonly resolved hydrocarbon peaks (*m/z*'s 27, 29, 41, 43, 55, 57, 69, 71, ...), indicating a contribution of HOA. This third factor was correlated with NO_x, CO and BC but for B362 the slope was found to be approximately a factor of 2 greater than the range of literature values cited in Table S1. A regression for the same factor from B406 with NO_x and BC also yielded a similar discrepancy although a CO measurement was not available during the flight so a comparison with CO was not possible. Enhanced signal is not identified at *m/z* 60 or 73 during either flight. These are typical mass spectral markers for wood burning emissions (Alfarra et al., 2007), therefore solid fuel burning is not considered to be a potential source of the enhanced mass. Consequently, it appears that the 3-factor solution is "blending" more than one distinct organic component into a single factor. This is likely a consequence of there being more chemical variability in the SV-OOA component (arising from evaporation/condensation, aging etc.) than in the HOA component. Thus the PMF solution identifies a factor which represents a 'mathematical mixing' of the more recently formed OOA with a HOA component. This arises due to the commonality between some of the major peaks in their respective mass spectra e.g. *m/z* 29 and 43.

The number of factors was increased under the supposition that an increase beyond 3-factors would reveal a more realistic contribution of HOA to the OM by separating it from the more volatile, fresher OOA fraction. While OOA factor profiles generally display significant variability as a result of differing processes such as aging and partitioning, HOA factor profiles are far more chemically distinct. Additionally, the largely linear association between HOA concentrations and urban primary emission markers makes source identification more straightforward than for OOA. Based upon these criteria, the number of factors was increased and inspected at each step until a single factor was present that most resembled HOA. For B362, this occurred for a 6-factor solution while for B406, a 7-factor solution was chosen. These factors were chosen due to their strong resemblance to HOA based upon their mass spectra and comparisons with combustion tracers. The comparison with the combustion tracers for B362 is shown in Fig. S14b, which indicates that increasing the number of factors does appear to bring the HOA-type component closer to the literature emission ratio. The main deviation from the relationship is from a low-level SLR in a highly moist layer (RH>95%) where total mass concentrations exceeded 50 $\mu g\,sm^{-3}$ and ammonium nitrate was the dominant chemical component. The layer is likely characteristic of freshly formed secondary material and it appears that some of the freshest-OOA mass has been apportioned to the HOA profile. The number of factors was increased

to 15 but this did not significantly alter the mass apportionment during this event.

5.2 Bootstrapping analysis

The numerical stability of the factor solutions was quantitatively evaluated using a bootstrapping analysis (Ulbrich et al., 2009, and references therein), where random resampling of the data matrix is performed in the time dimension. This analysis was performed using 20 iterations, with the results being grouped according to the UC coefficient between mass spectral profiles. The results of this analysis are summarised in Fig. S14a for B362 by comparing the contribution to total mass versus *m/z* 44 for each factor as the solutions are stepped through an increasing number of factors. The derived mean and standard deviations from the bootstrapping analysis are compared with the base solutions. The analysis indicates that by increasing the number of factors, the solutions become increasingly unstable in a numerical sense. This is a consequence of the aforementioned chemical variability inherent in the air masses sampled during the flight operations, which results in large scope for different factor solutions for larger numbers of factors. The bootstrapping analysis suggests that the 2-factor solution is the most appropriate solution, especially as the OOA-1 component is highly robust with a close match between the base solution and the bootstrapping solution. The enhanced standard deviation in the *m/z* 44 for the OOA-2 component is likely a consequence of the variability in the chemical nature of the OM. Very similar results were derived for B406, with the 2-factor solution being more numerically robust than subsequent solutions.

Further results from the bootstrapping analysis are shown for B357 in Fig. S13, for B362 in Fig. S14, for B369 in Fig. S15 and for B406 in Fig. S16. The bootstrapping results for all the flights are summarised in Table S2. The variance of the solutions in both the time series and factor profile dimensions is evaluated using suitable metrics. The time series diagnostic is the mean of the standard deviation for each factor, reported as a percentage of the overall mean mass concentration. For the mass spectra, the greatest standard deviation for each factor profile from the bootstrapping analysis is reported. A mean is not deemed appropriate to evaluate the stability of the mass spectra as the chemical assignment of factors is performed based on a limited number of peaks (i.e. less than 10).

The OOA-1 (LV-OOA) factor profiles are highly robust with little deviation between the average mass spectrum from the bootstrapping analysis and the base solution. Furthermore, the standard deviations are typically low. This is a consistent result throughout the dataset, which is shown by the low scores for the diagnostics in Table S2. The OOA-2 factor profiles are more variable for B362, B369 and B406, with less stability in the signal intensity at m/z 44. This reflects the continuum nature of the OM discussed in the main text, whereby there is significant variability on a given flight in the level of oxidation. Thus by randomly resampling the dataset in the time dimension using the bootstrapping procedure, conditions with either enhanced or diminished m/z 44 in the OOA-2 may be encountered and this is reflected by enhanced standard deviations in both the time series and mass spectra. The normalised standard deviation for the time series of OOA-2 for B369 is much greater than the other flights in the dataset. This is predominantly a result of the low concentrations encountered during the flight,

coupled with large standard deviations which are associated with large changes in the composition of the OOA-2 component in this instance. For much of the flight, signal at m/z 57 is close to zero indicating that HOA makes a minimal contribution to the OOA-2 component. However, during the peak OM event at 15:47 UTC, signal at m/z 57 is enhanced and thus the contribution of HOA is likely elevated. This event coincides with the maximum in the NO_x concentration and is associated with potential sampling of low-level urban outflow from Stockholm into the Baltic Sea. During this period, the standard deviations for the OOA-2 factor increase. Thus such changes in the OOA-2 composition from SV-OOA dominated to HOA dominated are reflected by large increases in the standard deviation values from the bootstrapping analysis. The much lower normalised standard deviation values associated with the time series of the OOA-2 components for the rest of the dataset suggest this feature to be atypical. This is a reflection of the regional nature of the measurements, with few instances of prolonged exposure to intense urban signatures.

The results presented here demonstrate the robustness of the chosen 2-factor solutions in terms of both the mass spectra and time series of the components. The OOA-1 (LV-OOA) components are highly numerically stable, while the decreased numerical stability of the OOA-2 (SV-OOA and HOA) components is entirely consistent with the continuum of oxidation/aging discussed in the main text.

5.3 Application to the entire dataset

The remaining flights in the dataset were analysed in an identical manner to the framework established in the previous section. This resulted in broadly similar behaviour in terms of the inability to accurately and quantitatively resolve HOA. A consistent theme was that increasing the number of factors in order to attempt to separate the HOA contribution led to a numerically unstable solution. Thus we chose to use the 2-factor solutions as these consistently represented a more quantitative solution set.

A summary of the $Q/Q_{expected}$ parameter is shown in Fig. S12, which indicates that the parameter is generally less than 2. Four flights had $Q/Q_{expected}$ values greater than 2, with the largest value being 5.01 (B374). Such values are greater than is generally considered optimal if attempting to produce a perfect characterisation of the dataset but given the difficulty in deriving robust results when more than 2 factors are chosen, it is not possible to reduce Q further. Consequently, the additional Q contribution prevalent in the dataset is considered as 'model error'.

The available solutions include some rotational ambiguity, which is explored by varying a parameter known as "fPeak" (Ulbrich et al., 2009, and references therein). An fPeak range from from -2.5 to 2.5 is investigated in order to explore the numerical variability in factor profiles and time series for small changes in $Q/Q_{expected}$. Investigation of the rotational freedom in the solutions using fPeak was accomplished by inspecting the mass spectra and time series in relation to external tracers for a subset of fPeak values from -2.5 to 2.5. The most appropriate value was then chosen, which for this dataset was determined to be zero in all cases. A test of the numerical uniqueness of the solution sets is the dependence upon the initiation seed, which is described by Ulbrich et al. (2009). Each of the 2-factor solutions was examined using this technique and little variation was exhibited for a range of different seeds.

5.3.1 Estimation of HOA and comparison with OOA components

Included in Fig. S11a are correlations of the estimated HOA concentration with Black Carbon (BC), NO_x and CO. These indicate that for 8 of the flights, the correlations of the estimated HOA with these primary emission tracers are greater than 0.5. Correlations lower than 0.5 are generally encountered on flights where these tracers and the estimated HOA are very low, thus the correlations break down at values when the relationships exhibit enhanced noise due to low signal. This is demonstrated in Fig. S11b and c, where at low concentrations the relationships are relatively flat but at enhanced concentrations, the correlation is greater. Given the simple nature of the HOA estimate, these correlations and relationships do provide some confidence that the estimated HOA provides a qualitative indicator of the contribution of HOA to the OM burden. The HOA estimate using this approach is likely an upper limit as the contribution of any oxidised fragments at *m/z* 57 has not been removed.

Also shown in Fig. S11a are the correlations between the Low-Volatility Oxidised Organic Aerosol (LV-OOA) organic mass fraction and the m/z 44:OM ratio described in the main paper.

References

Alfarra, M. R., Prevot, A. S. H., Szidat, S., Sandradewi, J., Weimer, S., Lanz, V. A., Schreiber, D., Mohr, M., and Baltensperger, U.: Identification of the mass spectral signature of organic aerosols from wood burning emissions, Environmental Science & Technology, 41, 5770–5777, 2007.

Allan, J. D., Williams, P. I., Morgan, W. T., Martin, C. L., Flynn, M. J., Lee, J., Nemitz, E., Phillips, G. J., Gallagher, M. W., and Coe, H.: Contributions from transport, solid fuel burning and cooking to primary organic aerosols in two UK cities, Atmospheric Chemistry and Physics, 10, 647–668, 2010.

Canagaratna, M. R., Jayne, J. T., Ghertner, D. A., Herndon, S., Shi, Q., Jimenez, J. L., Silva, P. J., Williams, P., Lanni, T., Drewnick, F., Demerjian, K. L., Kolb, C. E., and Worsnop, D. R.: Chase studies of particulate emissions from in-use New York City vehicles, Aerosol Science and Technology, 38, 555–573, 2004.

Cross, E. S., Slowik, J. G., Davidovits, P., Allan, J. D., Worsnop, D. R., Jayne, J. T., Lewis, D. K., Canagaratna, M., and Onasch, T. B.: Laboratory and Ambient Particle Density Determinations using Light Scattering in Conjunction with Aerosol Mass Spectrometry, Aerosol Science and Technology, 41, 343–359, URL http://www.informaworld.com/10.1080/02786820701199736, 2007.

de Gouw, J., Middlebrook, A., Warneke, C., Goldan, P., Kuster, W., Roberts, J., Fehsenfeld, F., Worsnop, D., Canagaratna, M., Pszenny, A., Keene, W., Marchewka, M., Bertman, S., and Bates, T.: Budget of organic carbon in a polluted atmosphere: Results from the New England Air Quality Study in 2002, Journal of Geophysical Research-Atmospheres, 110, doi:10.1029/2004JD005623, 2005.

Hallar, A. G., Strawa, A. W., Schmid, B., Andrews, E., Ogren, J., Sheridan, P., Ferrare, R., Covert, D., Elleman, R., Jonsson, H., Bokarius, K., and Luu, A.: Atmospheric Radiation Measurements Aerosol Intensive Operating Period: Comparison of aerosol scattering during coordinated flights, J. Geophys. Res., 111, D05S09, doi:10.1029/2005JD006250, 2006.

Jimenez, J. L., Canagaratna, M. R., Donahue, N. M., Prevot, A. S. H., Zhang, Q., Kroll, J. H., DeCarlo, P. F., Allan, J. D., Coe, H., Ng, N. L., Aiken, A. C., Docherty, K. S., Ulbrich, I. M., Grieshop, A. P., Robinson, A. L., Duplissy, J., Smith, J. D., Wilson, K. R., Lanz, V. A., Hueglin, C., Sun, Y. L., Tian, J., Laaksonen, A., Raatikainen, T., Rautiainen, J., Vaattovaara, P., Ehn, M., Kulmala, M., Tomlinson, J. M., Collins, D. R., Cubison, M. J., E., Dunlea, J., Huffman, J. A., Onasch, T. B., Alfarra, M. R., Williams, P. I., Bower, K., Kondo, Y., Schneider, J., Drewnick, F., Borrmann, S., Weimer, S., Demerjian, K., Salcedo, D., Cottrell, L., Griffin, R., Takami, A., Miyoshi, T., Hatakeyama, S., Shimono, A., Sun, J. Y., Zhang, Y. M., Dzepina, K., Kimmel, J. R., Sueper, D., Jayne, J. T., Herndon, S. C., Trimborn, A. M., Williams, L. R., Wood, E. C., Middlebrook, A. M., Kolb, C. E., Baltensperger, U., and Worsnop, D. R.: Evolution of Organic Aerosols in the Atmosphere, Science, 326, 1525–1529, doi:10.1126/science.1180353, 2009.

Kirchstetter, T. W., Harley, R. A., Kreisberg, N. M., Stolzenburg, M. R., and Hering, S. V.: On-road measurement of fine particle and nitrogen oxide emissions from light- and heavy-duty motor vehicles, Atmospheric Environment, 33, 2955–2968, 1999.

Lanz, V. A., Alfarra, M. R., Baltensperger, U., Buchmann, B., Hueglin, C., and Prevot, A. S. H.: Source apportionment of submicron organic aerosols at an urban site by factor analytical modelling of aerosol mass spectra, Atmospheric Chemistry and Physics, 7, 1503–1522, 2007.

Matthew, B. M., Middlebrook, A. M., and Onasch, T. B.: Collection efficiencies in an Aerodyne Aerosol Mass Spectrometer as a function of particle phase for laboratory generated aerosols, Aerosol Science and Technology, 42, 884–898, 2008.

McFiggans, G., Alfarra, M. R., Allan, J., Bower, K., Coe, H., Cubison, M., Topping, D., Williams, P., Decesari, S., Facchini, C., and Fuzzi, S.: Simplification of the representation of the organic component of atmospheric particulates, Faraday Discussions, 130, 341–362, 2005.

Moore, K. G., I., Clarke, A. D., Kapustin, V. N., McNaughton, C., Anderson, B. E., Winstead, E. L., Weber, R., Ma, Y., Lee, Y. N., Talbot, R., Dibb, J., Anderson, T., Doherty, S., Covert, D., and Rogers, D.: A comparison of similar aerosol measurements made on the NASA P3-B, DC-8, and NSF C-130 aircraft during TRACE-P and ACE-Asia, J. Geophys. Res., 109, D15S15, doi:10.1029/2003JD003543, 2004.

Ulbrich, I. M., Canagaratna, M. R., Zhang, Q., Worsnop, D. R., and Jimenez, J. L.: Interpretation of organic components from Positive Matrix Factorization of aerosol mass spectrometric data, Atmospheric Chemistry and Physics, 9, 2891–2918, 2009.

Zhang, Q., Alfarra, M. R., Worsnop, D. R., Allan, J. D., Coe, H., Canagaratna, M. R., and Jimenez, J. L.: Deconvolution and quantification of hydrocarbon-like and oxygenated organic aerosols based on aerosol mass spectrometry, Environmental Science & Technology, 39, 4938–4952, doi:10.1029/2007GL029979,, 2005a.

Zhang, Q., Worsnop, D. R., Canagaratna, M. R., and Jimenez, J. L.: Hydrocarbon-like and oxygenated organic aerosols in Pittsburgh: insights into sources and processes of organic aerosols, Atmospheric Chemistry and Physics, 5, 3289–3311, 2005b.

Table S1: Summary of POA:NO_x and POA:CO emission ratios used in this study. Emission ratios are given in μg sm^{-3} ppm^{-1}.

Study	Location	POA:NO_x	POA:CO
Allan et al. (2010)	London, UK	31.6	N/A
Allan et al. (2010)	Manchester, UK	N/A	20.5
de Gouw et al. (2005)	Northeastern USA	N/A	9.4
Kirchstetter et al. (1999)	Tunnel study, USA	11.0	N/A
Lanz et al. (2007)	Zurich, Switzerland	15.9	20.4
Zhang et al. (2005b)	Pittsburgh, USA	N/A	4.3

Table S2: Summary of the diagnostics relating to the bootstrapping analysis from the dataset for each flight.

Flight	SD_{ts}/TS (%)		Max (SD_{ms}) (%)	
	OOA-1	OOA-2	OOA-1	OOA-2
B357	2.0	2.5	0.77	0.85
B362	5.6	9.7	1.00	2.44
B365	2.8	3.0	0.62	1.31
B366	13.4	11.8	1.66	1.46
B369	19.1	45.9	2.23	1.66
B370	2.9	3.6	0.52	0.46
B371	4.8	8.0	0.41	1.82
B373	2.3	3.9	1.06	0.86
B374	1.1	1.7	0.44	0.68
B379	6.6	9.3	0.61	1.63
B380	1.4	2.4	0.36	0.37
B401	11.1	13.3	0.24	0.32
B402	5.5	14.9	0.76	1.23
B406	1.4	1.8	1.06	0.79

Table S3: Summary statistics regarding the AMS chemical composition for each zone referred to the main paper. Concentrations are reported in μg sm^{-3}t at the 25^{th}, 50^{th} and 75^{th} percentiles.

Species	Statistic	Zones						
		1	2	3	4	5	6	7
Organics	25^{th}	3.69	0.57	3.21	3.49	2.65	2.84	0.66
	50^{th}	4.13	0.91	3.69	4.13	3.63	3.68	1.40
	75^{th}	4.55	1.29	4.40	4.83	4.96	4.39	3.40
Nitrate	25^{th}	3.04	0.58	1.15	2.10	0.24	0.33	0.05
	50^{th}	3.51	2.11	2.92	4.84	1.24	1.00	0.14
	75^{th}	4.40	3.02	4.98	6.85	2.72	3.16	1.45
Sulphate	25^{th}	2.78	0.83	2.88	1.99	0.98	1.13	0.49
	50^{th}	3.25	1.20	3.82	3.02	1.93	1.44	0.92
	75^{th}	3.65	1.78	4.89	3.65	4.12	1.93	2.12
Ammonium	25^{th}	2.60	0.55	1.48	1.67	0.51	0.61	0.17
	50^{th}	2.87	1.14	2.06	2.25	1.11	1.23	0.45
	75^{th}	3.06	1.47	3.06	3.36	2.03	1.77	1.46

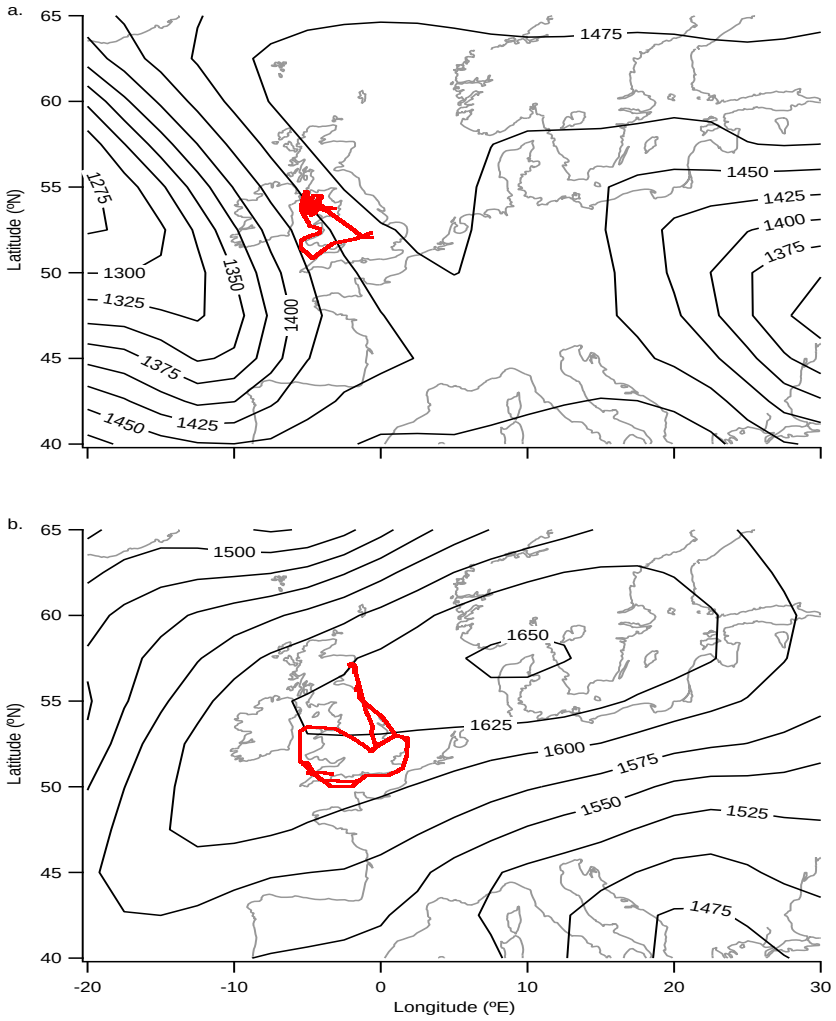

Figure S1: Flight tracks of the BAe-146 considered by this analysis for the ADIENT periods. Also shown are ECMWF 850 hPa geopotential height fields for each period considered by the analysis, where the field is either pertinent to a particular flight or is representative of the overall meteorological regime of the period. All geopotential height fields are for 12UTC. (a) summarises the flights for the UK-based ADIENT flying in April 2008 and the geopotential height field is from 16 April 2008 (B357). (b) summarises the flights for the UK-based ADIENT flying in September 2008 and the geopotential height field is from 25 September 2008 (B406).

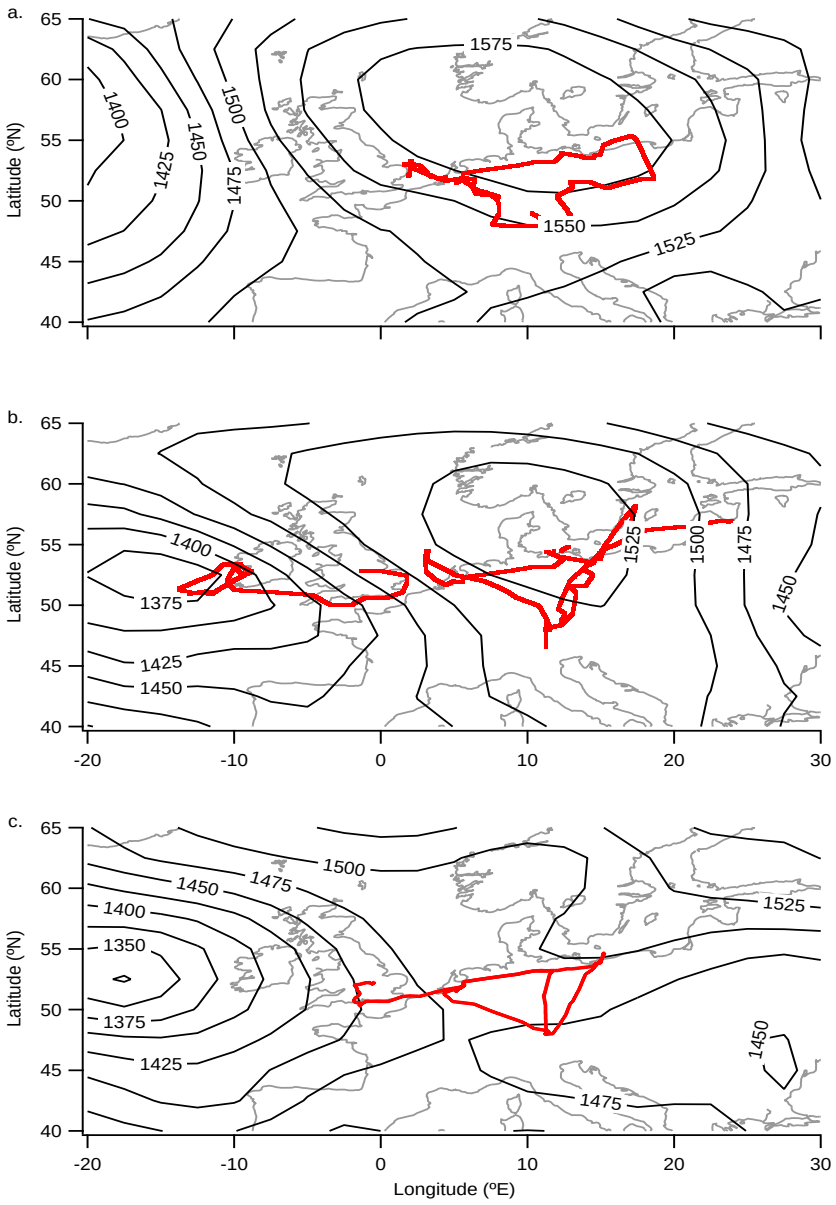

Figure S2: Same plots as Fig. S1 but now for the LONGREX flying period. (a) summarises the flights for the LONGREX-1 period with a geopotential height field for the 06 May 2008. (b) summarises the flights for the LONGREX-2 period with a geopotential height field for the 14 May 2008. (c) summarises the flights for the LONGREX-3 period with a geopotential height field for the 22 May 2008.

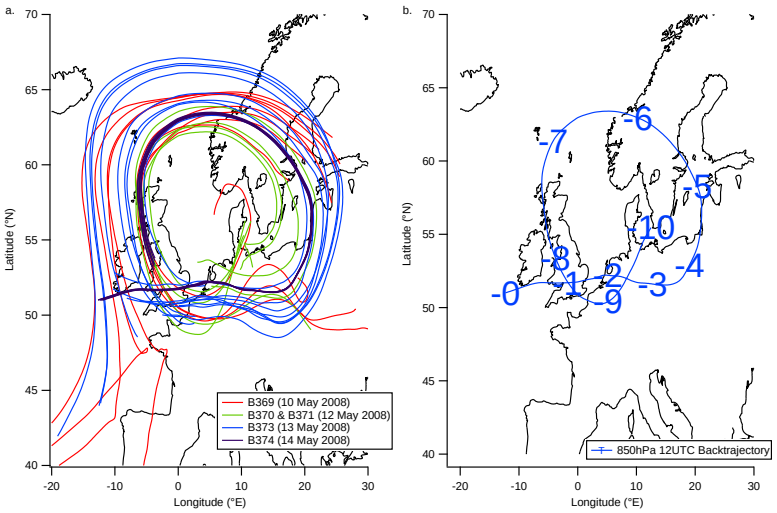

Figure S3: (a) Back trajectories at 850 hPa initialised from 1200 UTC on each flight day from the LONGREX-2 period. The initialisation points correspond to several SLRs during each flight. (b) Air mass back trajectory initialised from 1200 UTC on 14 May 2008 at 850 hPa. The numbered points relate to the number of days passed since the air mass was in that location.

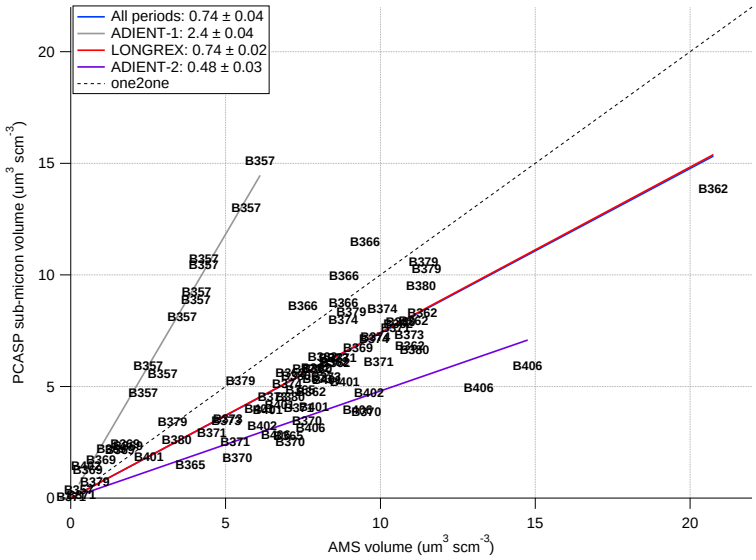

Figure S4: Comparison of inferred volume from the AMS with estimated sub-micron volume derived from the PCASP. The markers refer to SLRs below 3000 m i.e. within the boundary layer. The text markers refer to the flight which the point is from. Linear regression lines are shown for both individual flying periods and the study as a whole.

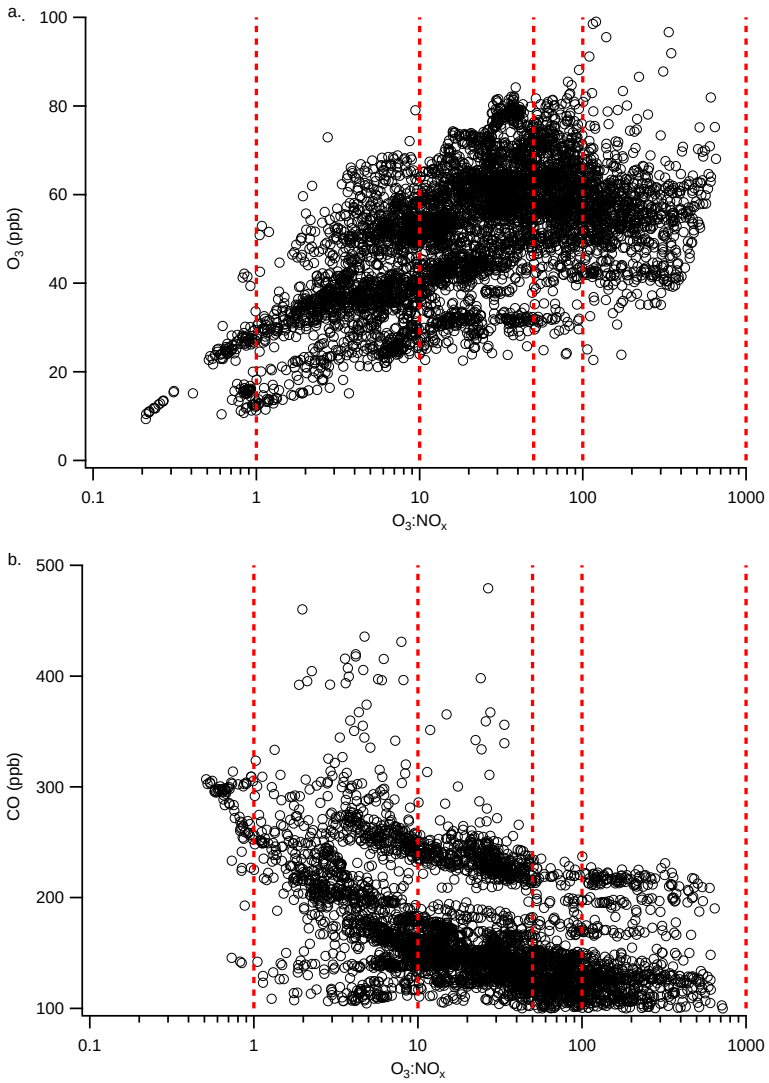

Figure S5: (a) Relationship between O_3 and O_3:NO_x for all flights. (b) Relationship between CO and O_3:NO_x for all flights expect for ADIENT-2. The red dashed lines refer to the distance from source boundaries discussed in the main paper.

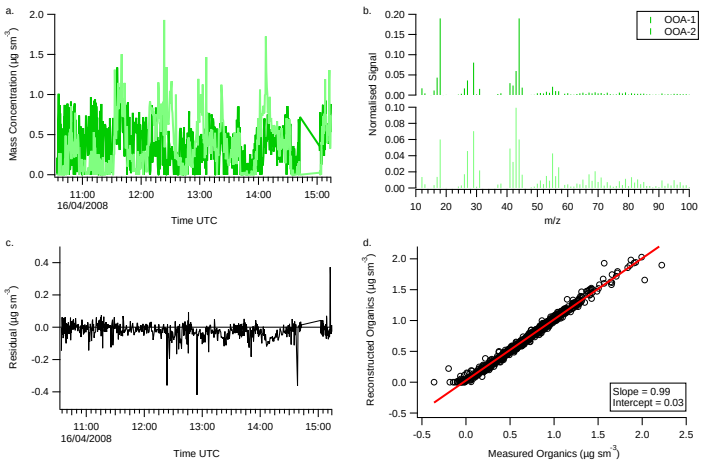

Figure S6: PMF solution for the two factor case from flight B357 including factor component time series (a) and mass spectra (b). The absolute residual is also shown in (c), whilst a comparison between the factor analysis reconstructed mass and measured organic signal is displayed in (d).

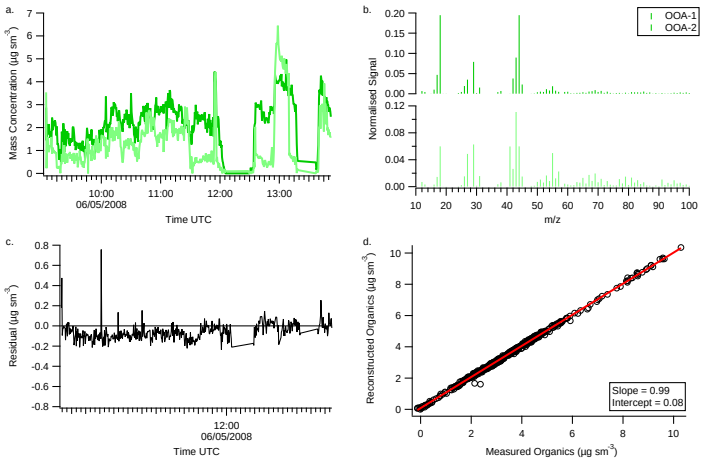

Figure S7: PMF solution for the two factor case from flight B362 including factor component time series (a) and mass spectra (b). The absolute residual is also shown in (c), whilst a comparison between the factor analysis reconstructed mass and measured organic signal is displayed in (d).

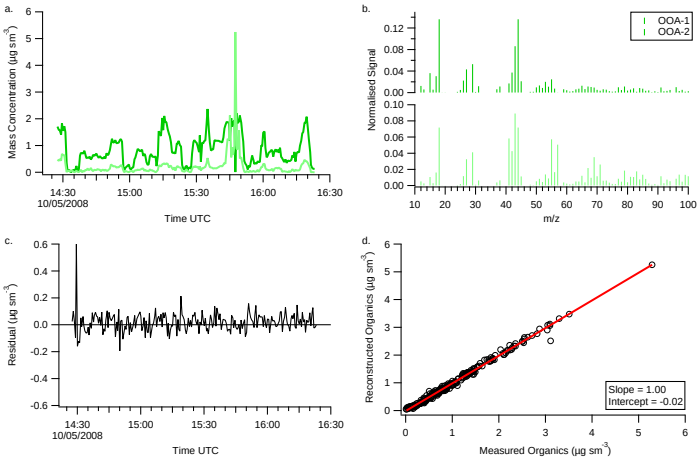

Figure S8: PMF solution for the two factor case from flight B369 including factor component time series (a) and mass spectra (b). The absolute residual is also shown in (c), whilst a comparison between the factor analysis reconstructed mass and measured organic signal is displayed in (d).

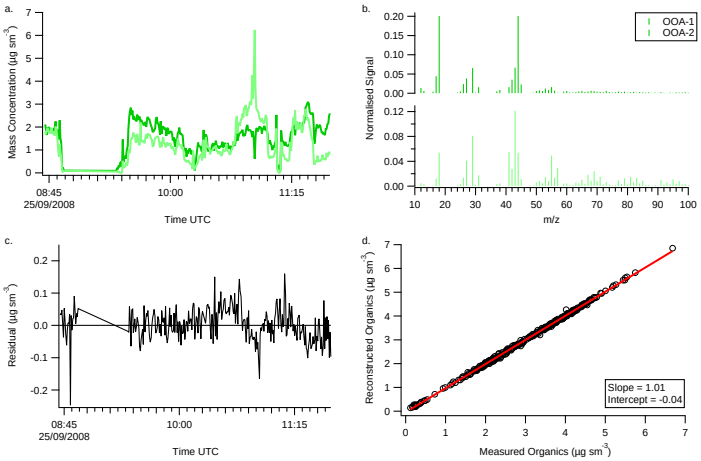

Figure S9: PMF solution for the two factor case from flight B406 including factor component time series (a) and mass spectra (b). The absolute residual is also shown in (c), whilst a comparison between the factor analysis reconstructed mass and measured organic signal is displayed in (d).

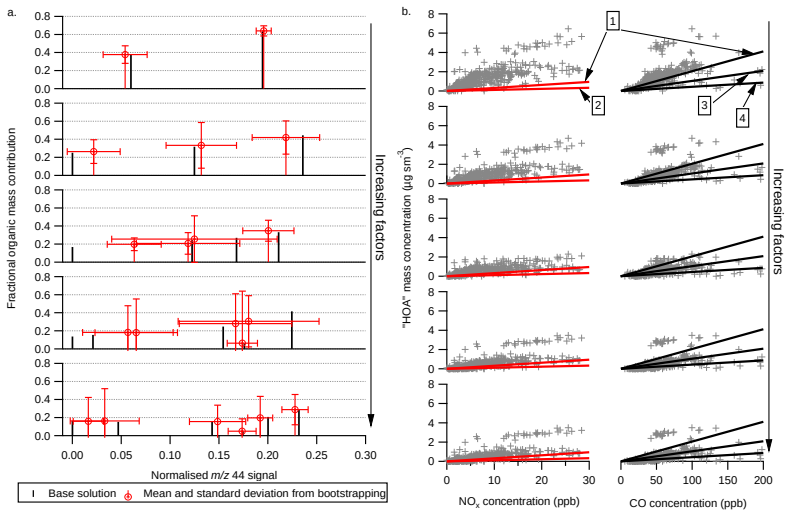

Figure S10: **(a)** Example from flight B362 of the relationship between the fractional mass contribution of a given factor to its normalised signal at *m/z* 44 for PMF solutions from two through seven factors. The black vertical bars refer to the base solution, while the red vertical and horizontal bars are the results from a resampling analysis known as bootstrapping. Increased standard deviations and mismatching between the base and bootstrapping solutions suggest a numerical unstable solution. **(b)** Relationship between the most HOA like factor profile with NO_x (red line) and CO (black line) for the factor solutions in (a). Solid red and black lines refer to literature emission ratios where (1) is from Allan et al. (2010), (2) is from Kirchstetter et al. (1999), (3) is from Lanz et al. (2007) and (4) is from Zhang et al. (2005b).

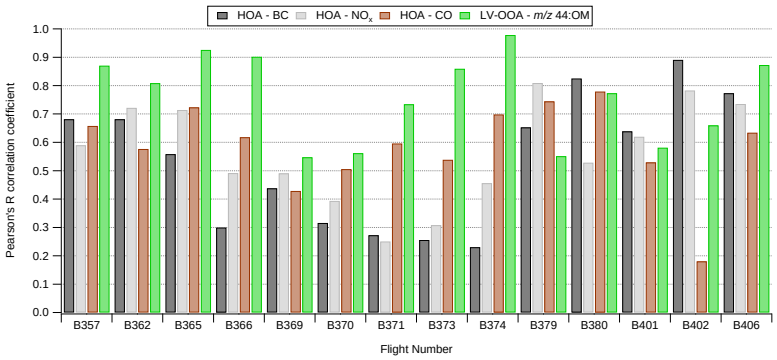

Figure S11: Summary of correlations for estimated HOA with Black Carbon (BC), NO_x and CO. Also shown are the correlations for LV-OOA organic mass fractions with the normalised organic signal at m/z 44.

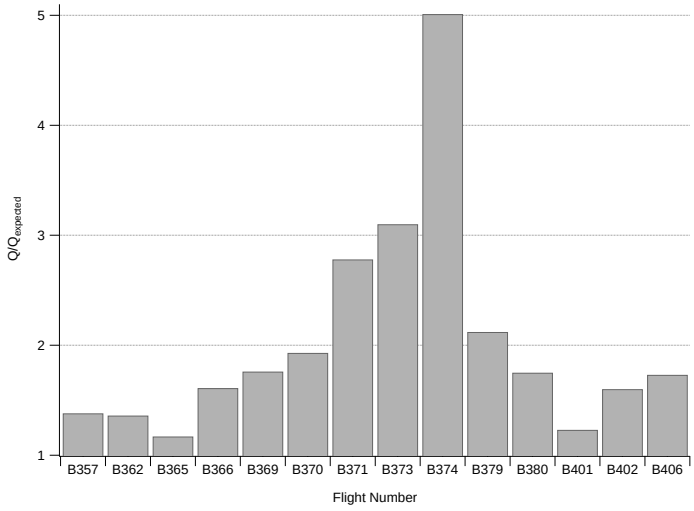

Figure S12: Summary of the $Q/Q_{expected}$ parameter for each flight in the dataset. All values are for the two-factor solutions with an fPeak of zero.

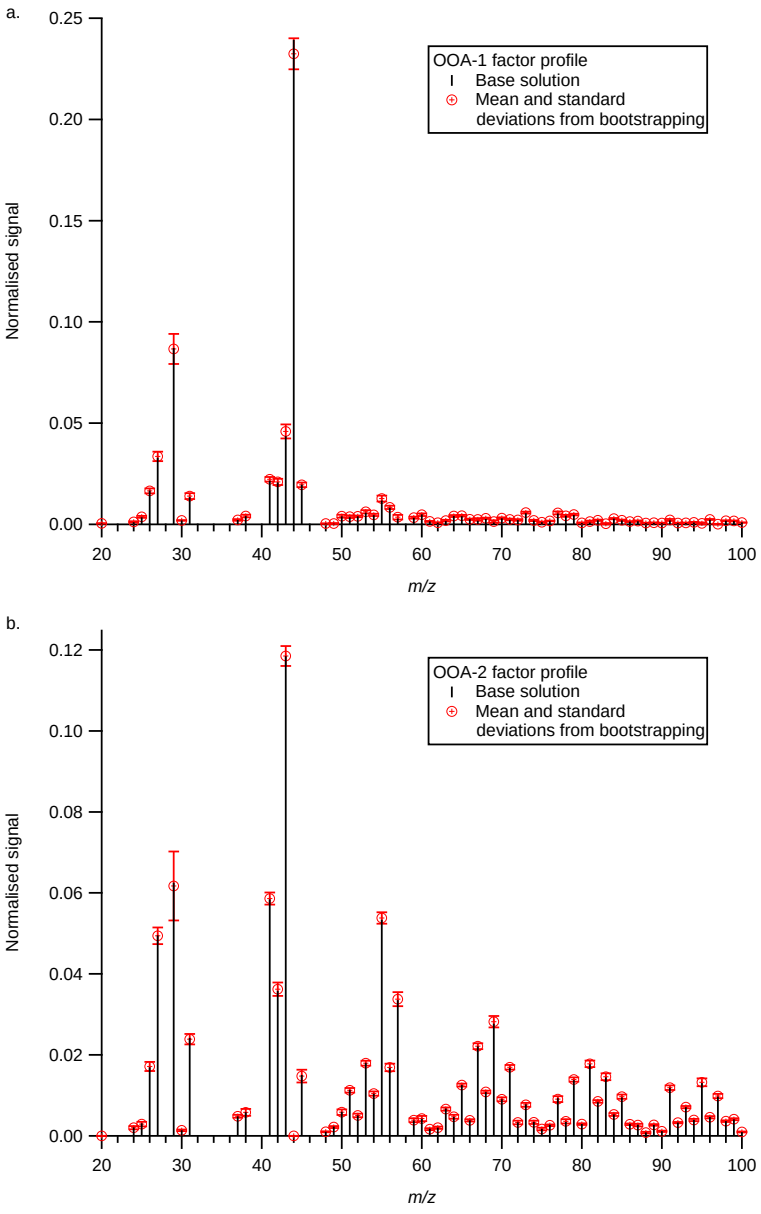

Figure S13: Results of the bootstrapping analysis for the two factor solution mass spectra for flight B357. (a) displays the mass spectrum for OOA-1, while (b) displays the mass spectrum for OOA-2.

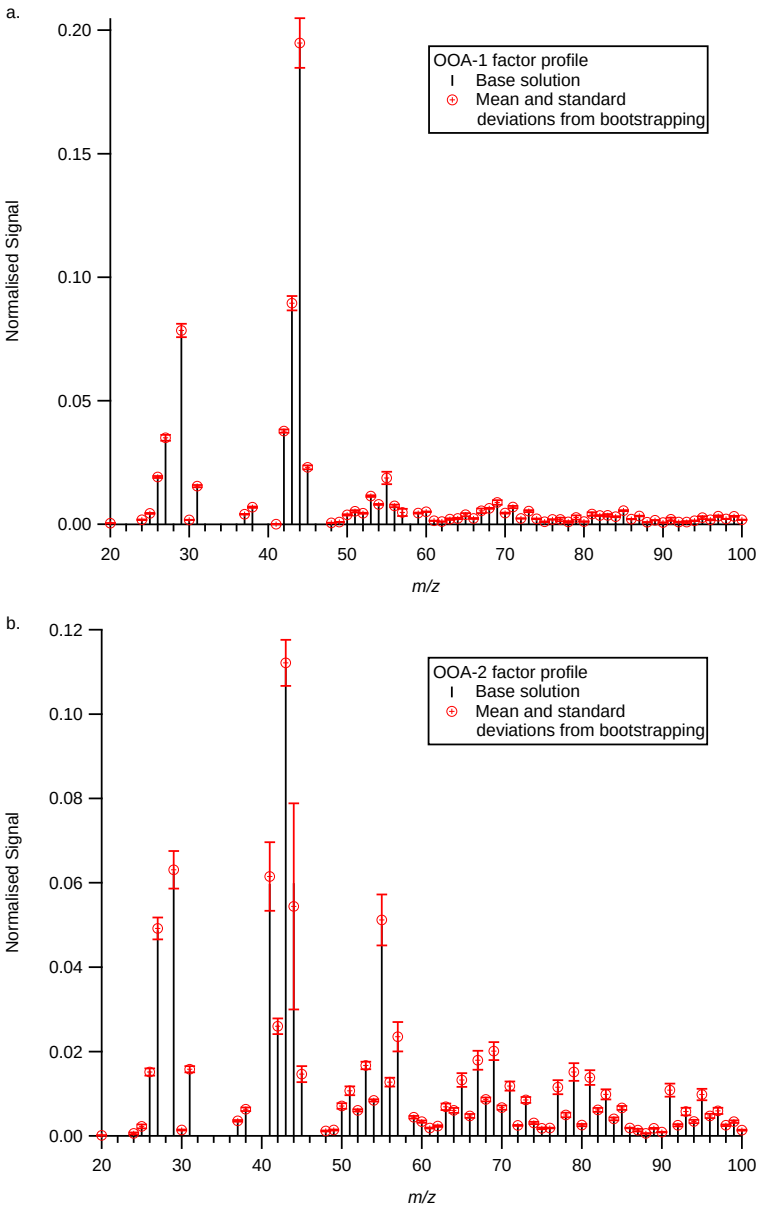

Figure S14: Results of the bootstrapping analysis for the two factor solution mass spectra for flight B362. (a) displays the mass spectrum for OOA-1, while (b) displays the mass spectrum for OOA-2.

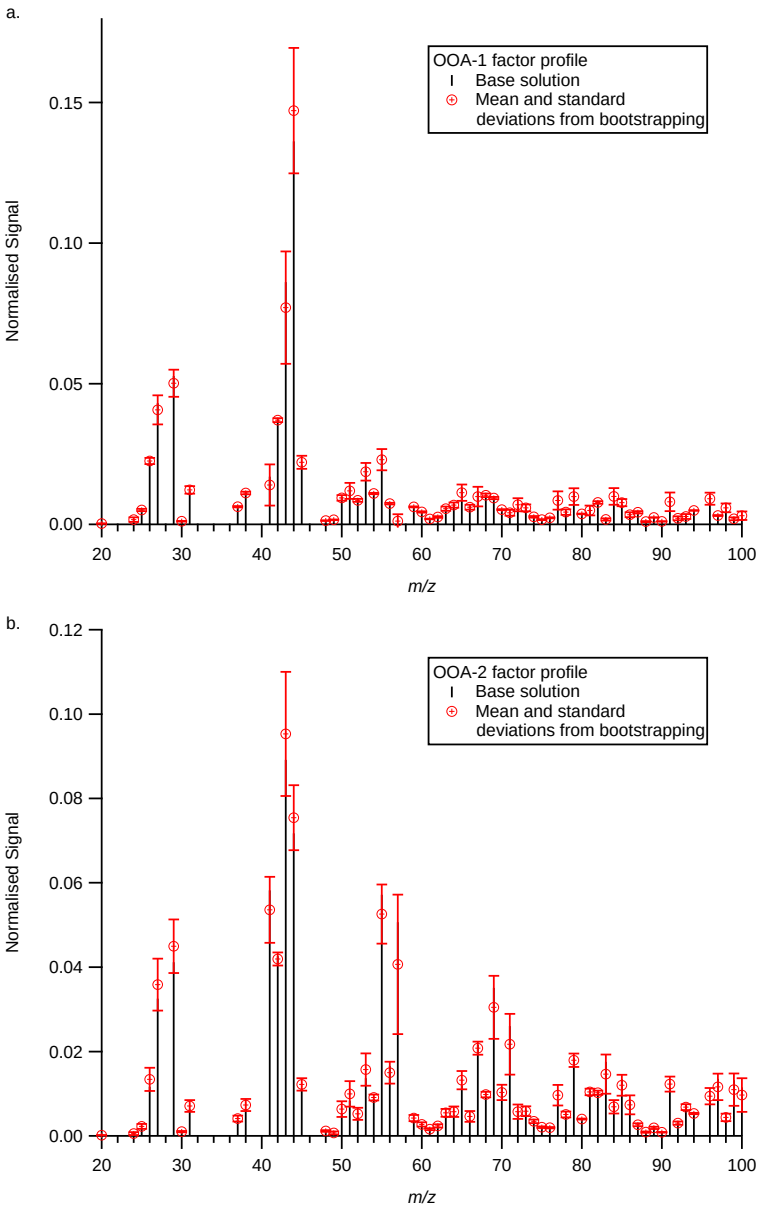

Figure S15: Results of the bootstrapping analysis for the two factor solution mass spectra for flight B369. (a) displays the mass spectrum for OOA-1, while (b) displays the mass spectrum for OOA-2.

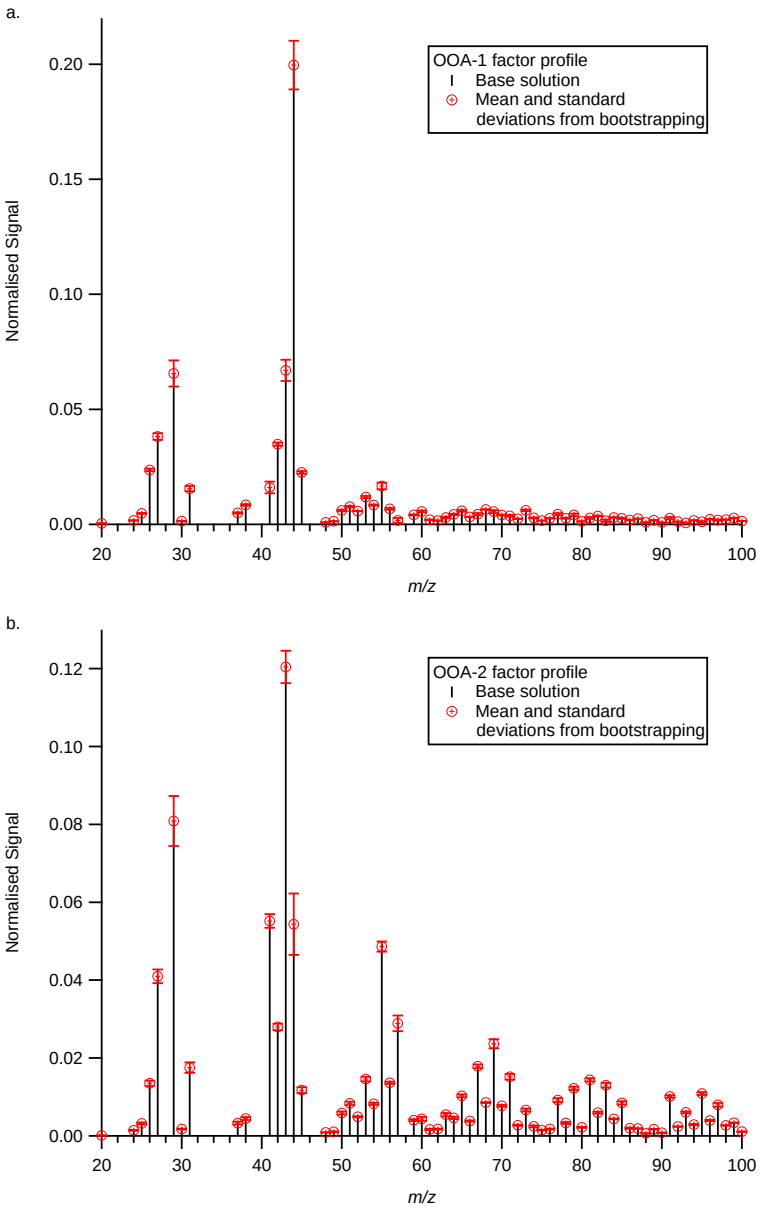

Figure S16: Results of the bootstrapping analysis for the two factor solution mass spectra for flight B406. (a) displays the mass spectrum for OOA-1, while (b) displays the mass spectrum for OOA-2.

References

Abdalmogith, S. S. and Harrison, R. M.: The use of trajectory cluster analysis to examine the long-range transport of secondary inorganic aerosol in the UK, Atmospheric Environment, 39, 6686–6695, doi:10.1016/j.atmosenv.2005.07.059, 2005.

Abel, S. J., Haywood, J. M., Highwood, E. J., Li, J., and Buseck, P. R.: Evolution of biomass burning aerosol properties from an agricultural fire in southern Africa, Geophysical Research Letters, 30 (15), 1783, doi:10.1029/2003GL017342, 2003.

Ackerman, A. S., Toon, O. B., Stevens, D. E., Heymsfield, A. J., Ramanathan, V., and Welton, E. J.: Reduction of tropical cloudiness by soot, Science, 288, 1042–1047, doi:10.1126/science.288.5468.1042, 2000.

Adams, P. J., Seinfeld, J. H., and Koch, D. M.: Global concentrations of tropospheric sulfate, nitrate, and ammonium aerosol simulated in a general circulation model, Journal of Geophysical Research, 104 (D11), 13,791–13,823, doi:10.1029/1999JD900083, 1999.

Adams, P. J., Seinfeld, J. H., Koch, D., Mickley, L., and Jacob, D.: General circulation model assessment of direct radiative forcing by the sulfate-nitrate-ammonium-water inorganic aerosol system, Journal of Geophysical Research, 106 (D1), 1097–1111, doi:10.1029/2000JD900512, 2001.

Aiken, A. C., Salcedo, D., Cubison, M. J., Huffman, J. A., Decarlo, P. F., Ulbrich, I. M., Docherty, K. S., Sueper, D., Kimmel, J. R., Worsnop, D. R., Trimborn, A., Northway, M., Stone, E. A., Schauer, J. J., Volkamer, R. M., Fortner, E., de Foy, B., Wang, J., Laskin, A., Shutthanandan, V., Zheng, J., Zhang, R., Gaffney, J., Marley, N. A., Paredes-Miranda, G., Arnott, W. P., Molina, L. T., Sosa, G., and Jimenez, J. L.: Mexico City aerosol analysis during MILAGRO using high resolution aerosol mass spectrometry at the urban supersite (T0) - Part 1: Fine particle composition and organic source apportionment, Atmospheric Chemistry and Physics, 9, 6633–6653, `http://www.atmos-chem-phys.net/9/6633/2009/`, 2009.

Alfarra, M. R.: Insights into atmospheric organic aerosols using an aerosol mass spectrometer., Ph.D. thesis, Unversity of Manchester, UK, 2004.

Alfarra, M. R., Coe, H., Allan, J. D., Bower, K. N., Boudries, H., Canagaratna, M. R., Jimenez, J. L., Jayne, J. T., Garforth, A. A., Li, S. M., and Worsnop, D. R.: Characterization of urban and rural organic particulate in the lower Fraser valley using two aerodyne aerosol mass spectrometers, Atmospheric Environment, 38, 5745–5758, doi:10.1016/j.atmosenv.2004.01.054, 2004.

Alfarra, M. R., Prevot, A. S. H., Szidat, S., Sandradewi, J., Weimer, S., Lanz, V. A., Schreiber, D., Mohr, M., and Baltensperger, U.: Identification of the mass spectral signature of organic aerosols from wood burning emissions, Environmental Science & Technology, 41, 5770–5777, doi:10.1021/es062289b, 2007.

Allan, J. D., Alfarra, M. R., Bower, K. N., Williams, P. I., Gallagher, M. W., Jimenez, J. L., McDonald, A. G., Nemitz, E., Canagaratna, M. R., Jayne, J. T., Coe, H., and Worsnop, D. R.: Quantitative sampling using an Aerodyne aerosol mass spectrometer - 2. Measurements of fine particulate chemical composition in two U.K. cities, Journal of Geophysical Research, 108 (D3), 4091, doi:10.1029/2002JD002359, 2003a.

Allan, J. D., Jimenez, J. L., Williams, P. I., Alfarra, M. R., Bower, K. N., Jayne, J. T., Coe, H., and Worsnop, D. R.: Quantitative sampling using an Aerodyne aerosol mass spectrometer: 1. Techniques of data interpretation and error analysis, Journal of Geophysical Research, 108 (D9), 4090, doi:10.1029/2003JD001607, 2003b.

Allan, J. D., Bower, K. N., Coe, H., Boudries, H., Jayne, J. T., Canagaratna, M. R., Millet, D. B., Goldstein, A. H., Quinn, P. K., Weber, R. J., and Worsnop, D. R.: Submicron aerosol composition at Trinidad Head, California, during ITCT 2K2: Its relationship with gas phase volatile organic carbon and assessment of instrument performance, Journal of Geophysical Research, 109 (D23S2, 10.1029/2003JD004208, 2004a.

Allan, J. D., Delia, A. E., Coe, H., Bower, K. N., Alfarra, M. R., Jimenez, J. L., Middlebrook, A. M., Drewnick, F., Onasch, T. B., Canagaratna, M. R., Jayne, J. T., and Worsnop, D. R.: A generalised method for the extraction of chemically resolved mass spectra from aerodyne aerosol mass spectrometer data, Journal of Aerosol Science, 35, 909–922, doi:10.1016/j.jaerosci.2004.02.007, 2004b.

Allan, J. D., Williams, P. I., Morgan, W. T., Martin, C. L., Flynn, M. J., Lee, J., Nemitz, E., Phillips, G. J., Gallagher, M. W., and Coe, H.: Contributions from transport, solid fuel burning and cooking to primary organic aerosols in two UK cities, Atmospheric Chemistry and Physics, 10, 647–668, www.atmos-chem-phys.net/10/647/2010/, 2010.

Anderson, T. L. and Ogren, J. A.: Determining aerosol radiative properties using the TSI 3563 integrating nephelometer, Aerosol Science & Technology, 29, 57–69, doi: 10.1080/02786829808965551, 1998.

Anderson, T. L., Covert, D. S., Marshall, S. F., Laucks, M. L., Charlson, R. J., Waggoner, A. P., Ogren, J. A., Caldow, R., Holm, R. L., Quant, F. R., Sem, G. J., Wiedensohler, A., Ahlquist, N. A., and Bates, T. S.: Performance characteristics of a high-sensitivity, three-wavelength, total scatter/backscatter nephelometer, Journal of Atmospheric and Oceanic Technology, 13, 967–986, 1996.

Andreae, M. O. and Crutzen, P. J.: Atmospheric aerosols: Biogeochemical sources and role in atmospheric chemistry, Science, 276, 1052–1058, doi:10.1126/science.276.5315.1052, 1997.

Andreae, M. O. and Rosenfeld, D.: Aerosol-cloud-precipitation interactions. Part 1. The nature and sources of cloud-active aerosols, Earth-Science Reviews, 89, 13–41, doi:10.1016/j.earscirev.2008.03.001, 2008.

Bahreini, R., Jimenez, J. L., Wang, J., Flagan, R. C., Seinfeld, J. H., Jayne, J. T., and Worsnop, D. R.: Aircraft-based aerosol size and composition measurements during ACE-Asia using an Aerodyne aerosol mass spectrometer, Journal of Geophysical Research, 108 (D23), 8645, doi:10.1029/2002JD003226, 2003.

Bahreini, R., Ervens, B., Middlebrook, A. M., Warneke, C., de Gouw, J. A., Decarlo, P. F., Jimenez, J. L., Brock, C. A., Neuman, J. A., Ryerson, T. B., Stark, H., Atlas, E. L., Brioude, J., Fried, A., Holloway, J. S., Peischl, J., Richter, D., Walega, J., Weibring, P., Wollny, A. G., and Fehsenfeld, F. C.: Organic aerosol formation in urban and industrial plumes near Houston and Dallas, Texas, Journal of Geophysical Research, 114, D00F16, doi:10.1029/2008JD011493, 2009.

Bates, T. S., Quinn, P. K., Coffman, D. J., Johnson, J. E., and Middlebrook, A. M.: Dominance of organic aerosols in the marine boundary layer over the Gulf of Maine during NEAQS 2002 and their role in aerosol light scattering, Journal of Geophysical Research, 110, D18 202, doi:10.1029/2005JD005797, 2005.

Bates, T. S., Anderson, T. L., Baynard, T., Bond, T. C., Boucher, O., Carmichael, G. R., Clarke, A. D., Erlick, C., Guo, H., Horowitz, L., Howell, S., Kulkarni, S., Maring, H., McComiskey, A., Middlebrook, A., Noone, K., O'Dowd, C. D., Ogren, J., Penner, J., Quinn, P. K., Ravishankara, A. R., Savoie, D. L., Schwartz, S. E., Shinozuka, Y., Tang, Y., Weber, R. J., and Wu, Y.: Aerosol direct radiative effects over the northwest Atlantic, northwest Pacific, and North Indian Oceans: estimates based on in-situ chemical and optical measurements and chemical transport modeling, Atmospheric Chemistry and Physics, 6, 1657–1732, www.atmos-chem-phys.net/6/1657/2006/, 2006.

Bauer, S. E., Koch, D., Unger, N., Metzger, S. M., Shindell, D. T., and Streets, D. G.: Nitrate aerosols today and in 2030: a global simulation including aerosols and tropospheric ozone, Atmospheric Chemistry and Physics, 7, 5043–5059, www.atmos-chem-phys.net/7/5043/2007/, 2007.

Baumgardner, D., Kok, G., and Raga, G.: Warming of the Arctic lower stratosphere by light absorbing particles, Geophysical Research Letters, 31, L06 117, doi:10.1029/2003GL018883, 2004.

Baumgardner, D., Grutter, M., Allan, J. D., Ochoa, C., Rappenglueck, B., Russell, L. M., and Arnott, W. P.: Physical and chemical properties of the regional mixed layer of Mexico's Megapolis, Atmospheric Chemistry and Physics, 9, 5711–5727, http://www.atmos-chem-phys.net/9/5711/2009/, 2009.

Bellouin, N., Boucher, O., Haywood, J., and Reddy, M. S.: Global estimate of aerosol direct radiative forcing from satellite measurements, Nature, 438, 1138–1141, doi:10.1038/nature04348, 2005.

Bench, G., Fallon, S., Schichtel, B., Malm, W., and McDade, C.: Relative contributions of fossil and contemporary carbon sources to PM 2.5 aerosols at nine Interagency Monitoring for Protection of Visual Environments (IMPROVE) network sites, Journal of Geophysical Research, 112, D10 205, doi:10.1029/2006JD007708, 2007.

Bond, T. C. and Bergstrom, R. W.: Light Absorption by Carbonaceous Particles: An Investigative Review, Aerosol Science & Technology, 40 (1), 27–67, doi:10.1080/02786820500421521, 2006.

Bond, T. C., Anderson, T. L., and Campbell, D.: Calibration and intercomparison of filter-based measurements of visible light absorption by aerosols, Aerosol Science & Technology, 30, 582–600, doi:10.1080/027868299304435, 1999.

Bond, T. C., Habib, G., and Bergstrom, R. W.: Limitations in the enhancement of visible light absorption due to mixing state, Journal of Geophysical Research, 111, D20 211, doi:10.1029/2006JD007315, 2006.

Brink, H. M. T., Veefkind, J. P., Waijers-Ijpelaan, A., and van Der Hage, J. C.: Aerosol light-scattering in The Netherlands, Atmospheric Environment, 30 (24), 4251–4261, doi:10.1016/1352-2310(96)00091-X, 1996.

Brock, C. A., Sullivan, A. P., Peltier, R. E., Weber, R. J., Wollny, A., Gouw, J. A., Middlebrook, A. M., Atlas, E. L., Stohl, A., Trainer, M. K., Cooper, O. R., Fehsenfeld, F. C., Frost, G. J., Holloway, J. S., Hubler, G., Neuman, J. A., Ryerson, T. B., Warneke, C., and Wilson, J. C.: Sources of particulate matter in the northeastern United States in summer: 2. Evolution of chemical and microphysical properties, Journal of Geophysical Research, 113, D8, doi:10.1029/2007JD009241, 2008.

Canagaratna, M. R., Jayne, J. T., Jimenez, J. L., Allan, J. D., Alfarra, M. R., Zhang, Q., Onasch, T. B., Drewnick, F., Coe, H., Middlebrook, A., Delia, A. E., Williams, L. R., Trimborn, A. M., Northway, M. J., Decarlo, P. F., Kolb, C. E., Davidovits, P., and Worsnop, D. R.: Chemical and microphysical characterization of ambient aerosols with the aerodyne aerosol mass spectrometer, Mass Spectrometry Reviews, 26, 185–222, doi:10.1002/mas.20115, 2007.

Carrico, C. M., Kus, P., Rood, M. J., Quinn, P. K., and Bates, T. S.: Mixtures of pollution, dust, sea salt, and volcanic aerosol during ACE-Asia: Radiative properties as a function of relative humidity, Journal of Geophysical Research, 108 (D23), 8650, doi:10.1029/2003JD003405, 2003.

Charlson, R. J., Schwartz, S. E., Hales, J. M., Cess, R. D., Coakley, J. A., Hansen, J. E., and Hofmann, D. J.: Climate Forcing by Anthropogenic Aerosols, Science, 255, 423–430, doi:10.1126/science.255.5043.423, 1992.

Chuang, P. Y.: Measurement of the timescale of hygroscopic growth for atmospheric aerosols, Journal of Geophysical Research, 108 (D9), 4282, doi:10.1029/2002JD002757, 2003.

Chung, C. E., Ramanathan, V., Kim, D., and Podgorny, I. A.: Global anthropogenic aerosol direct forcing derived from satellite and ground-based observations, Journal of Geophysical Research, 110, doi:10.1029/2005JD006356, 2005.

Chylek, P., Videen, G., Ngo, D., Pinnick, R. G., and Klett, J. D.: Effect of Black Carbon on the Optical-Properties and Climate Forcing of Sulfate Aerosols, Journal of Geophysical Research, 100, 16 325–16 332, doi:10.1029/95JD01465, 1995.

Cook, J. and Highwood, E. J.: Climate response to tropospheric absorbing aerosols in an intermediate general-circulation model, Quarterly Journal of the Royal Meteorological Society, 130 (596), 175–191, doi:10.1256/qj.03.64, 2004.

Crosier, J., Allan, J. D., Coe, H., Bower, K. N., Formenti, P., and Williams, P. I.: Chemical composition of summertime aerosol in the Po Valley (Italy), northern Adriatic and Black Sea, Quarterly Journal of the Royal Meteorological Society, 133 (S1), 61–75, doi:10.1002/qj.88, 2007a.

Crosier, J., Jimenez, J. L., Allan, J. D., Bower, K. N., Williams, P. I., Alfarra, M. R., Canagaratna, M. R., Jayne, J. T., Worsnop, D. R., and Coe, H.: Technical Note: Description and Use of the New Jump Mass Spectrum Mode of Operation for the Aerodyne Quadrupole Aerosol Mass Spectrometers (Q-AMS), Aerosol Science & Technology, 41, 865–872, doi:10.1080/02786820701501899, 2007b.

de Gouw, J. A., Middlebrook, A. M., Warneke, C., Goldan, P. D., Kuster, W. C., Roberts, J. M., Fehsenfeld, F. C., Worsnop, D. R., Canagaratna, M. R., Pszenny,

A. A. P., Keene, W. C., Marchewka, M., Bertman, S. B., and Bates, T. S.: Budget of organic carbon in a polluted atmosphere: Results from the New England Air Quality Study in 2002, Journal of Geophysical Research, 110, D16 305, doi: 10.1029/2004JD005623, 2005.

de Gouw, J. A., Brock, C. A., Atlas, E. L., Bates, T. S., Fehsenfeld, F. C., Goldan, P. D., Holloway, J. S., Kuster, W. C., Lerner, B. M., Matthew, B. M., Middlebrook, A. M., Onasch, T. B., Peltier, R. E., Quinn, P. K., Senff, C. J., Stohl, A., Sullivan, A. P., Trainer, M., Warneke, C., Weber, R. J., and Williams, E. J.: Sources of particulate matter in the northeastern United States in summer: 1. Direct emissions and secondary formation of organic matter in urban plumes, Journal of Geophysical Research, 113, D08 301, doi:10.1029/2007JD009243, 2008.

de Gouw, J. A., Welsh-Bon, D., Warneke, C., Kuster, W. C., Alexander, L., Baker, A. K., Beyersdorf, A. J., Blake, D. R., Canagaratna, M. R., Celada, A. T., Huey, L. G., Junkermann, W., Onasch, T. B., Salcido, A., Sjostedt, S. J., Sullivan, A. P., Tanner, D. J., Vargas, O., Weber, R. J., Worsnop, D. R., Yu, X. Y., and Zaveri, R.: Emission and chemistry of organic carbon in the gas and aerosol phase at a sub-urban site near Mexico City in March 2006 during the MILAGRO study, Atmospheric Chemistry and Physics, 9, 3425–3442, http://www.atmos-chem-phys.net/9/3425/2009/, 2009.

DeCarlo, P. F., Slowik, J. G., Worsnop, D. R., Davidovits, P., and Jimenez, J. L.: Particle morphology and density characterization by combined mobility and aerodynamic diameter measurements. Part 1: Theory, Aerosol Science & Technology, 38, 1185–1205, doi:10.1080/027868290903907, 2004.

DeCarlo, P. F., Kimmel, J. R., Trimborn, A., Northway, M. J., Jayne, J. T., Aiken, A. C., Gonin, M., Fuhrer, K., Horvath, T., Docherty, K. S., Worsnop, D. R., and Jimenez, J. L.: Field-deployable, high-resolution, time-of-flight aerosol mass spectrometer, Analytical Chemistry, 78, 8281–8289, doi:10.1021/ac061249n, 2006.

DeCarlo, P. F., Dunlea, E. J., Kimmel, J. R., Aiken, A. C., Sueper, D., Crounse, J. D., Wennberg, P. O., Emmons, L., Shinozuka, Y., Clarke, A. D., Zhou, J., Tomlinson, J., Collins, D. R., Knapp, D., Weinheimer, A. J., Montzka, D. D., Campos, T. L., and Jimenez, J. L.: Fast airborne aerosol size and chemistry measurements above Mexico City and Central Mexico during the MILAGRO campaign, Atmospheric Chemistry and Physics, 8, 4027–4048, www.atmos-chem-phys.net/8/4027/2008/, 2008.

Denman, K. L., Brasseur, G., Chidthaisong, A., Ciais, P., Cox, P. M., Dickinson, R. E., Hauglustaine, D., Heinze, C., Holland, E., Jacob, D., Lohmann, U., Ramachandran, S., Dias, P. L. d. S., Wofsy, S. C., and Zhang, X.: Couplings Between Changes in the Climate System and Biogeochemistry, Climate Change 2007: The Physical

Science Basis. Contribution of Working Group I to the Fourth Assessment Report of the Intergovernmental Panel on Climate Change, Cambridge University Press, Cambridge, United Kingdom and New York, NY, USA, 2007.

Dockery, D. W., Pope, C. A., Xu, X. P., Spengler, J. D., Ware, J. H., Fay, M. E., Ferris, B. G., and Speizer, F. E.: An Association between Air-Pollution and Mortality in 6 United-States Cities, New England Journal of Medicine, 329 (24), 1753–1759, 1993.

Doherty, S. J., Quinn, P. K., Jefferson, A., Carrico, C. M., Anderson, T. L., and Hegg, D.: A comparison and summary of aerosol optical properties as observed in situ from aircraft, ship, and land during ACE-Asia, Journal of Geophysical Research, 110, doi:10.1029/2004JD004964, 2005.

Donahue, N. M., Robinson, A. L., Stanier, C. O., and Pandis, S. N.: Coupled partitioning, dilution, and chemical aging of semivolatile organics, Environmental Science & Technology, 40, 2635–2643, doi:10.1021/es052297c, 2006.

Donahue, N. M., Robinson, A. L., and Pandis, S. N.: Atmospheric organic particulate matter: From smoke to secondary organic aerosol, Atmospheric Environment, 43, 94–106, doi:10.1016/j.atmosenv.2008.09.055, 2009.

Drewnick, F., Schwab, J. J., Hogrefe, O., Peters, S., Husain, L., Diamond, D., Weber, R., and Demerjian, K. L.: Intercomparison and evaluation of four semi-continuous PM2.5 sulfate instruments, Atmospheric Environment, 37, 3335–3350, doi:10.1016/S1352-2310(03)00351-0, 2003.

Drewnick, F., Hings, S. S., Decarlo, P. F., Jayne, J. T., Gonin, M., Fuhrer, K., Weimer, S., Jimenez, J. L., Demerjian, K. L., Borrmann, S., and Worsnop, D. R.: A new time-of-flight aerosol mass spectrometer (TOF-AMS) - Instrument description and first field deployment, Aerosol Science & Technology, 39, 637–658, doi:10.1080/02786820500182040, 2005.

Drewnick, F., Hings, S. S., Alfarra, M. R., Prevot, A. S. H., and Borrmann, S.: Aerosol quantification with the Aerodyne Aerosol Mass Spectrometer: detection limits and ionizer background effects, Atmospheric Measurement Techniques, 2, 33–46, `http://www.atmos-meas-tech.net/2/33/2009/`, 2009.

Dubovik, O. and King, M. D.: A flexible inversion algorithm for retrieval of aerosol optical properties from Sun and sky radiance measurements, Journal of Geophysical Research, 105, 20 673–20 696, doi:10.1029/2000JD900282, 2000.

Dzepina, K., Volkamer, R. M., Madronich, S., Tulet, P., Ulbrich, I. M., Zhang, Q., Cappa, C. D., Ziemann, P. J., and Jimenez, J. L.: Evaluation of recently-proposed secondary organic aerosol models for a case study in Mexico City, Atmospheric

Chemistry and Physics, 9, 5681–5709, http://www.atmos-chem-phys.net/9/5681/2009/, 2009.

Easter, R. C., Ghan, S. J., Zhang, Y., Saylor, R. D., Chapman, E. G., Laulainen, N. S., Abdul-Razzak, H., Leung, L. R., Bian, X. D., and Zaveri, R. A.: MIRAGE: Model description and evaluation of aerosols and trace gases, Journal of Geophysical Research, 109, D20 210, doi:10.1029/2004JD004571, 2004.

Farina, S. C., Adams, P. J., and Pandis, S. N.: Modeling global secondary organic aerosol formation and processing with the volatility basis set: Implications for anthropogenic secondary organic aerosol, Journal of Geophysical Research, 115, D09 202, doi:10.1029/2009JD013046, 2010.

Foltescu, V. L., Selin, E., and Below, M.: Corrections for Particle Losses and Sizing Errors During Aircraft Aerosol Sampling Using a Rosemount Inlet and the Pms Las-X, Atmospheric Environment, 29, 449–453, 1995.

Forster, P., Ramaswamy, V., Artaxo, P., Berntsen, T. K., Betts, R., W. Fahey, D. W., Haywood, J., Lean, J., Lowe, D. C., Myhre, G., Nganga, J., Prinn, R., Raga, G., Schulz, M., and Van Dorland, R.: Changes in Atmospheric Constituents and in Radiative Forcing, Climate Change 2007: The Physical Science Basis. Contribution of Working Group I to the Fourth Assessment Report of the Intergovernmental Panel on Climate Change, Cambridge University Press, Cambridge, United Kingdom and New York, NY, USA, 2007.

Gao, R. S., Schwarz, J. P., Kelly, K. K., Fahey, D. W., Watts, L. A., Thompson, T. L., Spackman, J. R., Slowik, J. G., Cross, E. S., Han, J. H., Davidovits, P., Onasch, T. B., and Worsnop, D. R.: A novel method for estimating light-scattering properties of soot aerosols using a modified single-particle soot photometer, Aerosol Science & Technology, 41 (2), 125–135, doi:10.1080/02786820601118398, 2007.

Gelencsér, A., May, B., Simpson, D., Sánchez-Ochoa, A., Kasper-Giebl, A., Puxbaum, H., Caseiro, A., Pio, C., and Legrand, M.: Source apportionment of PM2.5 organic aerosol over Europe: Primary/secondary, natural/anthropogenic, and fossil/biogenic origin, Journal of Geophysical Research, 112, D23, doi:10.1029/2006JD008094, 2007.

Goldstein, A. H. and Galbally, I. E.: Known and Unexplored Organic Constituents in the Earth's Atmosphere, Environmental Science & Technology, 41, 1514–1521, doi:10.1021/es072476p, 2007.

Goldstein, A. H., Koven, C. D., Heald, C. L., and Fung, I. Y.: Biogenic carbon and anthropogenic pollutants combine to form a cooling haze over the southeastern

United States, Proceedings of the National Academy of Sciences, 106, 8835–8840, www.pnas.org/cgi/doi/10.1073/pnas.0904128106, 2009.

Grieshop, A. P., Logue, J. M., Donahue, N. M., and Robinson, A. L.: Laboratory investigation of photochemical oxidation of organic aerosol from wood fires 1: measurement and simulation of organic aerosol evolution, Atmospheric Chemistry and Physics, 9, 1263–1277, http://www.atmos-chem-phys.net/9/1263/2009/, 2009.

Grossi, C. M. and Brimblecombe, P.: The effect of atmospheric pollution on building materials, Journal De Physique Iv, 12, 197–210, doi:10.1051/jp4:20020460, 2002.

Hallquist, M., Wenger, J. C., Baltensperger, U., Rudich, Y., Simpson, D., Claeys, M., Dommen, J., Donahue, N. M., George, C., Goldstein, A. H., Hamilton, J. F., Herrmann, H., Hoffmann, T., Iinuma, Y., Jang, M., Jenkin, M. E., Jimenez, J. L., Kiendler-Scharr, A., Maenhaut, W., McFiggans, G. B., Mentel, T. F., Monod, A., Prevot, A. S. H., Seinfeld, J. H., Surratt, J. D., Szmigielski, R., and Wildt, J.: The formation, properties and impact of secondary organic aerosol: current and emerging issues, Atmospheric Chemistry and Physics, 9, 5155–5235, 2009.

Hamilton, J. F., Webb, P. J., Lewis, A. C., Hopkins, J. R., Smith, S., and Davy, P.: Partially oxidised organic components in urban aerosol using GCXGC-TOF/MS, Atmospheric Chemistry and Physics, 4, 1279–1290, www.atmos-chem-phys.net/4/1279/2004/, 2004.

Hansen, J., Sato, M., and Ruedy, R.: Radiative forcing and climate response, Journal of Geophysical Research, 102 (D6), 6831–6864, doi:10.1029/96JD03436, 1997.

Hansen, J., Sato, M., Ruedy, R., Nazarenko, L., Lacis, A., Schmidt, G. A., Russell, G., Aleinov, I., Bauer, M., Bauer, S. E., Bell, N., Cairns, B., Canuto, V., Chandler, M., Cheng, Y., Del Genio, A. D., Faluvegi, G., Fleming, E., Friend, A., Hall, T., Jackman, C., Kelley, M., Kiang, N., Koch, D., Lean, J., Lerner, J., Lo, K., Menon, S., Miller, R., Minnis, P., Novakov, T., Oinas, V., Perlwitz, J., Rind, D., Romanou, A., Shindell, D., Stone, P., Sun, S., Tausnev, N., Thresher, D., Wielicki, B., Wong, T., Yao, M., and Zhang, S.: Efficacy of climate forcings, Journal of Geophysical Research, 110, D18 104, doi:10.1029/2005JD005776, 2005.

Haywood, J. and Boucher, O.: Estimates of the direct and indirect radiative forcing due to tropospheric aerosols: A review, Reviews of Geophysics, 38, 513–543, doi:10.1029/1999RG000078, 2000.

Haywood, J., Bush, M., Abel, S., Claxton, B., Coe, H., Crosier, J., Harrison, M., Macpherson, B., Naylor, M., and Osborne, S.: Prediction of visibility and aerosol

within the operational Met Office Unified Model. II: Validation of model performance using observational data, Quarterly Journal of the Royal Meteorological Society, 134, 1817–1832, doi:10.1002/qj.275, 2008.

Heald, C. L., Jacob, D. J., Park, R. J., Russell, L. M., Huebert, B. J., Seinfeld, J. H., Liao, H., and Weber, R. J.: A large organic aerosol source in the free troposphere missing from current models, Geophysical Research Letters, 32, L18 809, doi:10.1029/2005GL023831, 2005.

Heald, C. L., Goldstein, A. H., Allan, J. D., Aiken, A. C., Apel, E., Atlas, E. L., Baker, A. K., Bates, T. S., Beyersdorf, A. J., Blake, D. R., Campos, T. L., Coe, H., Crounse, J. D., Decarlo, P. F., de Gouw, J. A., Dunlea, E. J., Flocke, F. M., Fried, A., Goldan, P., Griffin, R. J., Herndon, S. C., Holloway, J. S., Holzinger, R., Jimenez, J. L., Junkermann, W., Kuster, W. C., Lewis, A. C., Meinardi, S., Millet, D. B., Onasch, T., Polidori, A., Quinn, P. K., Riemer, D. D., Roberts, J. M., Salcedo, D., Sive, B., Swanson, A. L., Talbot, R., Warneke, C., Weber, R. J., Weibring, P., Wennberg, P. O., Worsnop, D. R., Wittig, A. E., Zhang, R., Zheng, J., and Zheng, W.: Total observed organic carbon (TOOC) in the atmosphere: a synthesis of North American observations, Atmospheric Chemistry and Physics, 8, 2007–2025, www.atmos-chem-phys.net/8/2007/2008/, 2008.

Heald, C. L., Kroll, J. H., Jimenez, J. L., Docherty, K. S., Decarlo, P. F., Aiken, A. C., Chen, Q., Martin, S. T., Farmer, D. K., and Artaxo, P.: A simplified description of the evolution of organic aerosol composition in the atmosphere, Geophysical Research Letters, 37, L08 803, doi:10.1029/2010GL042737, 2010.

Hering, S. V., Stolzenburg, M. R., Quant, F. R., Oberreit, D. R., and Keady, P. B.: A Laminar-Flow, Water-Based Condensation Particle Counter (WCPC), Aerosol Science & Technology, 39 (7), 659–672, doi:10.1080/02786820500182123, 2005.

Highwood, E. J., Haywood, J. M., Coe, H., Cook, J., Osborne, S., Williams, P., Crosier, J., Bower, K. N., Formenti, P., McQuaid, J., Brooks, B., Thomas, G., Grainger, R., Barnaba, F., Gobbi, P., de Leeuw, G., and Hopkins, J.: Aerosol direct radiative impact experiment (ADRIEX) overview, Quarterly Journal of the Royal Meteorological Society, 133 (S1), 3–15, doi:10.1002/qj.89, 2007.

Hings, S. S., Walter, S., Schneider, J., Borrmann, S., and Drewnick, F.: Comparison of a Quadrupole and a Time-of-Flight Aerosol Mass Spectrometer during the Feldberg Aerosol Characterization Experiment 2004, Aerosol Science & Technology, 41, 679–691, doi:10.1080/02786820701408483, 2007.

Hodzic, A., Jimenez, J. L., Madronich, S., Canagaratna, M. R., Decarlo, P. F., Kleinman, L., and Fast, J.: Potential contribution of semi-volatile and intermediate

volatility primary organic compounds to secondary organic aerosol in the Mexico City region, Atmospheric Chemistry and Physics Discussions, 10, 657–710, http://www.atmos-chem-phys-discuss.net/10/657/2010/, 2010.

Hogrefe, O., Schwab, J. J., Drewnick, F., Lala, G. G., Peters, S., Demerjian, K. L., Rhoads, K., Felton, H. D., Rattigan, O. V., Husain, L., and Dutkiewicz, V. A.: Semicontinuous PM2.5 sulfate and nitrate measurements at an urban and a rural location in New York: PMTACS-NY summer 2001 and 2002 campaigns, Journal of the Air & Waste Management Association, 54, 1040–1060, 2004.

Holben, B. N., Eck, T. F., Slutsker, I., Tanre, D., Buis, J. P., Setzer, A., Vermote, E., Reagan, J. A., Kaufman, Y. J., Nakajima, T., Lavenu, F., Jankowiak, I., and Smirnov, A.: AERONET - A federated instrument network and data archive for aerosol characterization, Remote Sensing of Environment, 66, 1–16, 1998.

Hoyle, C. R., Berntsen, T. K., Myhre, G., and Isaksen, I. S. A.: Secondary organic aerosol in the global aerosol - chemical transport model Oslo CTM2, Atmospheric Chemistry and Physics, 7, 5675–5694, www.atmos-chem-phys.net/7/5675/2007/, 2007.

Huebert, B. J., Bates, T. S., Russell, P. B., Shi, G. Y., Kim, Y. J., Kawamura, K., Carmichael, G. R., and Nakajima, T.: An overview of ACE-Asia: Strategies for quantifying the relationships between Asian aerosols and their climatic impacts, Journal of Geophysical Research, 108 (D23), 8633, doi:10.1029/2003JD003550, 2003.

Huffman, J. A., Jayne, J. T., Drewnick, F., Aiken, A. C., Onasch, T., Worsnop, D. R., and Jimenez, J. L.: Design, modeling, optimization, and experimental tests of a particle beam width probe for the aerodyne aerosol mass spectrometer, Aerosol Science & Technology, 39, 1143–1163, doi:10.1080/02786820500423782, 2005.

Huffman, J. A., Docherty, K. S., Aiken, A. C., Cubison, M. J., Ulbrich, I. M., Decarlo, P. F., Sueper, D., Jayne, J. T., Worsnop, D. R., Ziemann, P. J., and Jimenez, J. L.: Chemically-resolved aerosol volatility measurements from two megacity field studies, Atmospheric Chemistry and Physics, 9, 7161–7182, http://www.atmos-chem-phys.net/9/7161/2009/, 2009.

Isaksen, I. S. A., Granier, C., Myhre, G., Berntsen, T. K., Dalsøren, S. B., Gauss, M., Klimont, Z., Benestad, R., Bousquet, P., Collins, W. D., Cox, T., Eyring, V., Fowler, D., Fuzzi, S., Jöckel, P., Laj, P., Lohmann, U., Maione, M., Monks, P., Prevot, A. S. H., Raes, F., Richter, A., Rognerud, B., Schulz, M., Shindell, D., Stevenson, D. S., Storelvmo, T., Wang, W.-C., van Weele, M., Wild, M., and Wuebbles, D.: Atmospheric composition change: Climate-Chemistry interactions, Atmospheric Environment, 43, 5138–5192, doi:DOI:10.1016/j.atmosenv.2009.08.003, 2009.

Jacobson, M. Z.: Global direct radiative forcing due to multicomponent anthropogenic and natural aerosols, Journal of Geophysical Research, 106 (D2), 1551–1568, doi: 10.1029/2000JD900514, 2001.

Jacobson, M. Z.: Control of fossil-fuel particulate black carbon and organic matter, possibly the most effective method of slowing global warming, Journal of Geophysical Research, 107 (D19), 4410, doi:10.1029/2001JD001376, 2002.

Jayne, J. T., Leard, D. C., Zhang, X. F., Davidovits, P., Smith, K. A., Kolb, C. E., and Worsnop, D. R.: Development of an aerosol mass spectrometer for size and composition analysis of submicron particles, Aerosol Science & Technology, 33 (1-2), 49–70, doi:10.1080/027868200410840, 2000.

Jimenez, J. L., Jayne, J. T., Shi, Q., Kolb, C. E., Worsnop, D. R., Yourshaw, I., Seinfeld, J. H., Flagan, R. C., Zhang, X. F., Smith, K. A., Morris, J. W., and Davidovits, P.: Ambient aerosol sampling using the Aerodyne Aerosol Mass Spectrometer, Journal of Geophysical Research, 108 (D7), 8425, doi:doi:10.1029/2001JD001213, 2003.

Jimenez, J. L., Canagaratna, M. R., Donahue, N. M., Prevot, A. S. H., Zhang, Q., Kroll, J. H., Decarlo, P. F., Allan, J. D., Coe, H., Ng, N. L., Aiken, A. C., Docherty, K. S., Ulbrich, I. M., Grieshop, A. P., Robinson, A. L., Duplissy, J., Smith, J. D., Wilson, K. R., Lanz, V. A., Hueglin, C., Sun, Y. L., Tian, J., Laaksonen, A., Raatikainen, T., Rautiainen, J., Vaattovaara, P., Ehn, M., Kulmala, M., Tomlinson, J. M., Collins, D. R., Cubison, M. J., E., Dunlea, E. J., Huffman, J. A., Onasch, T. B., Alfarra, M. R., Williams, P. I., Bower, K. N., Kondo, Y., Schneider, J., Drewnick, F., Borrmann, S., Weimer, S., Demerjian, K. L., Salcedo, D., Cottrell, L., Griffin, R., Takami, A., Miyoshi, T., Hatakeyama, S., Shimono, A., Sun, J. Y., Zhang, Y. M., Dzepina, K., Kimmel, J. R., Sueper, D., Jayne, J. T., Herndon, S. C., Trimborn, A. M., Williams, L. R., Wood, E. C., Middlebrook, A. M., Kolb, C. E., Baltensperger, U., and Worsnop, D. R.: Evolution of Organic Aerosols in the Atmosphere, Science, 326, 1525–1529, doi:10.1126/science.1180353, 2009.

Johnson, B. T., Shine, K. P., and Forster, P. M.: The semi-direct aerosol effect: Impact of absorbing aerosols on marine stratocumulus, Quarterly Journal of the Royal Meteorological Society, 130, 1407–1422, doi:10.1256/qj.03.61, 2004.

Kanakidou, M., Seinfeld, J. H., Pandis, S. N., Barnes, I., Dentener, F. J., Facchini, M. C., Van Dingenen, R., Ervens, B., Nenes, A., Nielsen, C. J., Swietlicki, E., Putaud, J. P., Balkanski, Y., Fuzzi, S., Horth, J., Moortgat, G. K., Winterhalter, R., Myhre, C. E. L., Tsigaridis, K., Vignati, E., Stephanou, E. G., and Wilson, J.: Organic aerosol and global climate modelling: a review, Atmospheric Chemistry and Physics, 5, 1053–1123, www.atmos-chem-phys.org/acp/5/1053/, 2005.

Kinne, S., Schulz, M., Textor, C., Guibert, S., Balkanski, Y., Bauer, S. E., Berntsen, T. K., Berglen, T. F., Boucher, O., Chin, M., Collins, W. D., Dentener, F. J., Diehl, T., Easter, R. C., Feichter, J., Fillmore, D., Ghan, S., Ginoux, P., Gong, S., Grini, A., Hendricks, J. E., Herzog, M., Horowitz, L., Isaksen, L., Iversen, T., Kirkavag, A., Kloster, S., Koch, D., Kristjansson, J. E., Krol, M., Lauer, A., Lamarque, J. F., Lesins, G., Liu, X., Lohmann, U., Montanaro, V., Myhre, G., Penner, J. E., Pitari, G., Reddy, S., Seland, O., Stier, P., Takemura, T., and Tie, X.: An AeroCom initial assessment - optical properties in aerosol component modules of global models, Atmospheric Chemistry and Physics, 6, 1815–1834, www.atmos-chem-phys.net/6/1815/2006/, 2006.

Kirkevag, A. and Iversen, T.: Global direct radiative forcing by process-parameterized aerosol optical properties, Journal of Geophysical Research, 107, 4433, doi:10.1029/2001JD000886, 2002.

Kleinman, L. I., Daum, P. H., Lee, Y. N., Senum, G. I., Springston, S. R., Wang, J., Berkowitz, C., Hubbe, J., Zaveri, R. A., Brechtel, F. J., Jayne, J. T., Onasch, T. B., and Worsnop, D. R.: Aircraft observations of aerosol composition and ageing in New England and Mid-Atlantic States during the summer 2002 New England Air Quality Study field campaign, Journal of Geophysical Research, 112, D09 310, doi:10.1029/2006JD007786, 2007.

Kleinman, L. I., Springston, S. R., Daum, P. H., Lee, Y. N., Nunnermacker, L. J., Senum, G. I., Wang, J., Weinstein-Lloyd, J., Alexander, M. L., Hubbe, J., Ortega, J., Canagaratna, M. R., and Jayne, J. T.: The time evolution of aerosol composition over the Mexico City plateau, Atmospheric Chemistry and Physics, 8, 1559–1575, www.atmos-chem-phys.net/8/1559/2008/, 2008.

Koch, D.: Transport and direct radiative forcing of carbonaceous and sulfate aerosols in the GISS GCM, Journal of Geophysical Research, 106 (D17), 20,311–20,332, doi:10.1029/2001JD900038, 2001.

Koelemeijer, R. B. A., Homan, C. D., and Matthijsen, J.: Comparison of spatial and temporal variations of aerosol optical thickness and particulate matter over Europe, Atmospheric Environment, 40, 5304–5315, doi:10.1016/j.atmosenv.2006.04.044, 2006.

Kotchenruther, R. A. and Hobbs, P. V.: Humidification factors of aerosols from biomass burning in Brazil, Journal of Geophysical Research, 103 (D24), 32 081–32 089, doi:10.1029/98JD00340, 1998.

Kotchenruther, R. A., Hobbs, P. V., and Hegg, D. A.: Humidification factors for atmospheric aerosols off the mid-Atlantic coast of the United States, Journal of Geophysical Research, 104 (D2), 2239–2251, doi:10.1029/98JD01751, 1999.

Kroll, J. H. and Seinfeld, J. H.: Chemistry of secondary organic aerosol: Formation and evolution of low-volatility organics in the atmosphere, Atmospheric Environment, 42, 3593–3624, doi:10.1016/j.atmosenv.2008.01.003, 2008.

Kulmala, M.: How particles nucleate and grow, Science, 302 (5647), 1000–1001, doi: 10.1126/science.1090848, 2003.

Kulmala, M., Vehkamaki, H., Petajda, T., Dal Maso, M., Lauri, A., Kerminen, V. M., Birmili, W., and McMurry, P. H.: Formation and growth rates of ultrafine atmospheric particles: a review of observations, Journal of Aerosol Science, 35, 143–176, doi:10.1016/j.jaerosci.2003.10.003, 2004.

Kulmala, M., Asmi, A., Lappalainen, H. K., Carslaw, K. S., Pöschl, U., Baltensperger, U., Hov, A., Brenguier, J. L., Pandis, S. N., Facchini, M. C., Hansson, H. C., Wiedensohler, A., and O'Dowd, C. D.: Introduction: European Integrated Project on Aerosol Cloud Climate and Air Quality interactions (EUCAARI) integrating aerosol research from nano to global scales, Atmospheric Chemistry and Physics, 9, 2825–2841, www.atmos-chem-phys.net/9/2825/2009/, 2009.

Lanz, V. A., Alfarra, M. R., Baltensperger, U., Buchmann, B., Hueglin, C., and Prevot, A. S. H.: Source apportionment of submicron organic aerosols at an urban site by factor analytical modelling of aerosol mass spectra, Atmospheric Chemistry and Physics, 7, 1503–1522, www.atmos-chem-phys.net/7/1503/2007/, 2007.

Lanz, V. A., Alfarra, M. R., Baltensperger, U., Buchmann, B., Hueglin, C., Szidat, S., Wehrli, M. N., Wacker, L., Weimer, S., Caseiro, A., Puxbaum, H., and Prevot, A. S. H.: Source attribution of submicron organic aerosols during wintertime inversions by advanced factor analysis of aerosol mass spectra, Environmental Science & Technology, 42, 214–220, doi:10.1021/es0707207, 2008.

Lauer, A., Hendricks, J., Ackermann, I., Schell, B., Hass, H., and Metzger, S.: Simulating aerosol microphysics with the ECHAM/MADE GCM - Part I: Model description and comparison with observations, Atmospheric Chemistry and Physics, 5, 3251–3276, 2005.

Lelieveld, J., Crutzen, P. J., Ramanathan, V., Andreae, M. O., Brenninkmeijer, C. A. M., Campos, T. L., Cass, G. R., Dickerson, R. R., Fischer, H., de Gouw, J. A., Hansel, A., Jefferson, A., Kley, D., de Laat, A. T. J., Lal, S., Lawrence, M. G., Lobert, J. M., Mayol-Bracero, O. L., Mitra, A. P., Novakov, T., Oltmans, S. J., Prather, K. A., Reiner, T., Rodhe, H., Scheeren, H. A., Sikka, D., and Williams, J.: The Indian Ocean Experiment: Widespread air pollution from South and Southeast Asia, Science, 291, 1031–1036, doi:10.1126/science.1057103, 2001.

Liao, H. and Seinfeld, J. H.: Global impacts of gas-phase chemistry-aerosol interactions on direct radiative forcing by anthropogenic aerosols and ozone, Journal of Geophysical Research, 110, D18 208, doi:10.1029/2005JD005907, 2005.

Linstrom, P. J. and Mallard, W. G.: The NIST Chemistry WebBook: A chemical data resource on the internet, Journal of Chemical Engineering, 46, 1059–1063, 2001.

Liu, P., Ziemann, P. J., Kittelson, D. B., and McMurry, P. H.: Generating Particle Beams of Controlled Dimensions and Divergence .1. Theory of Particle Motion in Aerodynamic Lenses and Nozzle Expansions, Aerosol Science & Technology, 22, 293–313, doi:10.1080/02786829408959748, 1995a.

Liu, P., Ziemann, P. J., Kittelson, D. B., and McMurry, P. H.: Generating Particle Beams of Controlled Dimensions and Divergence .2. Experimental Evaluation of Particle Motion in Aerodynamic Lenses and Nozzle Expansions, Aerosol Science & Technology, 22, 314–324, doi:10.1080/02786829408959749, 1995b.

Liu, P. S. K., Leaitch, W. R., Strapp, J. W., and Wasey, M. A.: Response of Particle Measuring Systems Airborne ASASP and PCASP to Nacl and Latex-Particles, Aerosol Science & Technology, 16, 83–95, doi:10.1080/02786829208959539, 1992.

Makar, P. A., Moran, M. D., Zheng, Q., Cousineau, S., Sassi, M., Duhamel, A., Besner, M., Davignon, D., Crevier, L. P., and Bouchet, V. S.: Modelling the impacts of ammonia emissions reductions on North American air quality, Atmospheric Chemistry and Physics, 9, 7183–7212, http://www.atmos-chem-phys.net/9/7183/2009/, 2009.

Malm, W. C., Schichtel, B. A., Ames, R. B., and Gebhart, K. A.: A 10-year spatial and temporal trend of sulfate across the United States, Journal of Geophysical Research, 107 (D22), 4627, doi:10.1029/2002JD002107, 2002.

Markowicz, K. M., Flatau, P. J., Quinn, P. K., Carrico, C. M., Flatau, M. K., Vogelmann, A. M., Bates, D., Liu, M., and Rood, M. J.: Influence of relative humidity on aerosol radiative forcing: An ACE-Asia experiment perspective, Journal of Geophysical Research, 108 (D23), 8662, doi:10.1029/2002JD003066, 2003.

Matthew, B. M., Middlebrook, A. M., and Onasch, T. B.: Collection efficiencies in an Aerodyne Aerosol Mass Spectrometer as a function of particle phase for laboratory generated aerosols, Aerosol Science & Technology, 42, 884–898, doi:10.1080/02786820802356797, 2008.

Matthias, V., Balis, D., Bösenberg, J., Eixmann, R., Iarlori, M., Komguem, L., Mattis, I., Papayannis, A., Pappalardo, G., Perrone, M. R., and Wang, X.: Vertical aerosol distribution over Europe: Statistical analysis of Raman lidar data from 10 European

Aerosol Research Lidar Network (EARLINET) stations, Journal of Geophysical Research, 109, D18 201, doi:10.1029/2004JD004638, 2004.

McFiggans, G. B., Alfarra, M. R., Allan, J. D., Bower, K. N., Coe, H., Cubison, M. J., Topping, D., Williams, P., Decesari, S., Facchini, C., and Fuzzi, S.: Simplification of the representation of the organic component of atmospheric particulates, Faraday Discussions, 130, 341–362, doi:10.1039/b419435g, 2005.

McLafferty, F. W. and Turecek, F.: Interpretation of mass spectra, Mill Valley, California: University Science Books, 1993.

Metzger, S., Dentener, F. J., Krol, M., Jeuken, A., and Lelieveld, J.: Gas/aerosol partitioning - 2. Global modeling results, Journal of Geophysical Research, 107 (D16), 4313, doi:10.1029/2001JD001103, 2002.

Monks, P. S., Granier, C., Fuzzi, S., Stohl, A., Williams, M. L., Akimoto, H., Amann, M., Baklanov, A., Baltensperger, U., Bey, I., Blake, N., Blake, R. S., Carslaw, K. S., Cooper, O. R., Dentener, F. J., Fowler, D., Fragkou, E., Frost, G. J., Generoso, S., Ginoux, P., Grewe, V., Guenther, A., Hansson, H. C., Henne, S., Hjorth, J., Hofzumahaus, A., Huntrieser, H., Isaksen, I. S. A., Jenkin, M. E., Kaiser, J., Kanakidou, M., Klimont, Z., Kulmala, M., Laj, P., Lawrence, M. G., Lee, J. D., Liousse, C., Maione, M., McFiggans, G. B., Metzger, A., Mieville, A., Moussiopoulos, N., Orlando, J. J., O'Dowd, C. D., Palmer, P. I., Parrish, D. D., Petzold, A., Platt, U., Pöschl, U., Prévôt, A. S. H., Reeves, C. E., Reimann, S., Rudich, Y., Sellegri, K., Steinbrecher, R., Simpson, D., ten Brink, H., Theloke, J., van Der Werf, G. R., Vautard, R., Vestreng, V., Vlachokostas, C., and von Glasow, R.: Atmospheric composition change - global and regional air quality, Atmospheric Environment, 43, 5268–5350, doi:10.1016/j.atmosenv.2009.08.021, 2009.

Morino, Y., Kondo, Y., Takegawa, N., Miyazaki, Y., Kita, K., Komazaki, Y., Fukuda, M., Miyakawa, T., Moteki, N., and Worsnop, D. R.: Partitioning of HNO3 and particulate nitrate over Tokyo: Effect of vertical mixing, Journal of Geophysical Research, 111, D15 215, doi:10.1029/2005JD006887, 2006.

Mozurkewich, M.: The Dissociation-Constant of Ammonium-Nitrate and Its Dependence on Temperature, Relative-Humidity and Particle-Size, Atmospheric Environment, 27 (2), 261–270, doi:10.1016/0960-1686(93)90356-4, 1993.

Murayama, T., Sugimoto, N., Uno, I., Kinoshita, K., Aoki, K., Hagiwara, N., Liu, Z. Y., Matsui, I., Sakai, T., Shibata, T., Arao, K., Sohn, B. J., Won, J. G., Yoon, S. C., Li, T., Zhou, J., Hu, H. L., Abo, M., Iokibe, K., Koga, R., and Iwasaka, Y.: Ground-based network observation of Asian dust events of April 1998 in east Asia, Journal of Geophysical Research, 106 (D16), 18 345–18 359, doi:10.1029/2000JD900554, 2001.

Murphy, D. M.: Something in the air, Science, 307, 1888–1890, doi:10.1126/science.1108160, 2005.

Murphy, D. M., Solomon, S., Portmann, R. W., Rosenlof, K. H., Forster, P. M., and Wong, T.: An observationally based energy balance for the Earth since 1950, Journal of Geophysical Research, 114, D17 107, doi:10.1029/2009JD012105, 2009.

Myhre, G., Stordal, F., Johnsrud, M., Diner, D. J., Geogdzhayev, I. V., Haywood, J. M., Holben, B. N., Holzer-Popp, T., Ignatov, A., Kahn, R. A., Kaufman, Y. J., Loeb, N., Martonchik, J. V., Mishchenko, M. I., Nalli, N. R., Remer, L. A., Schroedter-Homscheidt, M., Tanre, D., Torres, O., and Wang, M.: Intercomparison of satellite retrieved aerosol optical depth over ocean during the period September 1997 to December 2000, Atmospheric Chemistry and Physics, 5, 1697–1719, www.atmos-chem-phys.org/acp/5/1697/, 2005.

Myhre, G., Grini, A., and Metzger, S.: Modelling of nitrate and ammonium-containing aerosols in presence of sea salt, Atmospheric Chemistry and Physics, 6, 4809–4821, http://www.atmos-chem-phys.net/6/4809/2006/, 2006.

Myhre, G., Berglen, T. F., Hoyle, C. R., Christopher, S. A., Coe, H., Crosier, J., Formenti, P., Haywood, J. M., Johnsrud, M., Jones, T. A., Loeb, N., Osborne, S., and Remer, L. A.: Modelling of chemical and physical aerosol properties during the ADRIEX aerosol campaign, Quarterly Journal of the Royal Meteorological Society, 135, 53–66, doi:10.1002/qj.350, 2009.

Neuman, J. A., Nowak, J. B., Brock, C. A., Trainer, M., Fehsenfeld, F. C., Holloway, J. S., Hubler, G., Hudson, P. K., Murphy, D. M., Nicks, D. K., Orsini, D., Parrish, D. D., Ryerson, T. B., Sueper, D. T., Sullivan, A., and Weber, R.: Variability in ammonium nitrate formation and nitric acid depletion with altitude and location over California, Journal of Geophysical Research, 108, D17, doi:10.1029/2003JD003616, 2003.

Ng, N. L., Canagaratna, M. R., Zhang, Q., Jimenez, J. L., Tian, J., Ulbrich, I. M., Kroll, J. H., Docherty, K. S., Chhabra, P. S., Bahreini, R., Murphy, S. M., Seinfeld, J. H., Hildebrandt, L., Donahue, N. M., DeCarlo, P. F., Lanz, V. A., Prévôt, A. S. H., Dinar, E., Rudich, Y., and Worsnop, D. R.: Organic aerosol components observed in Northern Hemispheric datasets from Aerosol Mass Spectrometry, Atmospheric Chemistry and Physics, 10, 4625–4641, doi:10.5194/acp-10-4625-2010, 2010.

Osborne, S. R., Haywood, J. M., and Bellouin, N.: In situ and remote-sensing measurements of the mean microphysical and optical properties of industrial pollution aerosol during ADRIEX, Quarterly Journal of the Royal Meteorological Society, 133 (S1), 17–32, doi:10.1002/qj.92, 2007.

Paatero, P.: Least squares formulation of robust non-negative factor analysis, Chemometrics and Intelligent Laboratory Systems, 37, 23–35, 1997.

Paatero, P. and Tapper, U.: Positive Matrix Factorization - a Nonnegative Factor Model with Optimal Utilization of Error-Estimates of Data Values, Environmetrics, 5, 111–126, 1994.

Pandis, S. N., Wexler, A. S., and Seinfeld, J. H.: Dynamics of Tropospheric Aerosols, Journal of Physical Chemistry, 99, 9646–9659, doi:10.1021/j100024a003, 1995.

Penner, J. E., Andreae, M. O., Annegarn, H., Barrie, L., Feichter, J., Hegg, D., Jayaraman, A., Leaitch, R., Murphy, D., Nganga, J., and Pitari, G.: Aerosols, their Direct and Indirect Effects, Climate Change 2001: The Scientific Basis. Contribution of Working Group I to the Third Assessment Report of the Intergovernmental Panel on Climate Change, Cambridge University Press, Cambridge, United Kingdom and New York, NY, USA, 2001.

Pinder, R. W., Adams, P. J., and Pandis, S. N.: Ammonia Emission Controls as a Cost-Effective Strategy for Reducing Atmospheric Particulate Matter in the Eastern United States, Environmental Science & Technology, 41, 380–386, doi:10.1021/es060379a, 2007.

Posfai, M., Simonics, R., Li, J., Hobbs, P. V., and Buseck, P. R.: Individual aerosol particles from biomass burning in southern Africa: 1. Compositions and size distributions of carbonaceous particles, Journal of Geophysical Research, 108 (D13), 8483, doi:10.1029/2002JD002291, 2003.

Putaud, J.-P., Raes, F., Dingenen, R. V., Brüggemann, E., Facchini, M. C., Decesari, S., Fuzzi, S., Gehrig, R., Hüglin, C., Laj, P., Lorbeer, G., Maenhaut, W., Mihalopoulos, N., Müller, K., Querol, X., Rodriguez, S., Schneider, J., Spindler, G., ten Brink, H., Tørseth, K., and Wiedensohler, A.: A European aerosol phenomenology–2: chemical characteristics of particulate matter at kerbside, urban, rural and background sites in Europe, Atmospheric Environment, 38, 2579–2595, doi:10.1016/j.atmosenv.2004.01.041, 2004.

Quinn, P. K. and Bates, T. S.: Regional aerosol properties: Comparisons of boundary layer measurements from ACE 1, ACE 2, aerosols99, INDOEX, ACE asia, TARFOX, and NEAQS, Journal of Geophysical Research, 110, D14 202, doi:10.1029/2004JD004755, 2005.

Quinn, P. K., Coffman, D. J., Bates, T. S., Welton, E. J., Covert, D. S., Miller, T. L., Johnson, J. E., Maria, S., Russell, L., Arimoto, R., Carrico, C. M., Rood, M. J., and Anderson, J.: Aerosol optical properties measured on board the Ronald H. Brown

during ACE-Asia as a function of aerosol chemical composition and source region, Journal of Geophysical Research, 109, D19, doi:10.1029/2004JD004755, 2004.

Quinn, P. K., Bates, T. S., Baynard, T., Clarke, A. D., Onasch, T. B., Wang, W., Rood, M. J., Andrews, E., Allan, J. D., Carrico, C. M., Coffman, D. J., and Worsnop, D. R.: Impact of particulate organic matter on the relative humidity dependence of light scattering: A simplified parameterization, Geophysical Research Letters, 32, L22 809, doi:10.1029/2005GL024322, 2005.

Quinn, P. K., Bates, T. S., Coffman, D. J., Onasch, T. B., Worsnop, D. R., Baynard, T., de Gouw, J. A., Goldan, P. D., Kuster, W. C., Williams, E., Roberts, J. M., Lerner, B., Stohl, A., Pettersson, A., and Lovejoy, E. R.: Impacts of sources and aging on submicrometer aerosol properties in the marine boundary layer across the Gulf of Maine, Journal of Geophysical Research, 111, D23, doi:10.1029/2006JD007582, 2006.

Raes, F., Van Dingenen, R., Vignati, E., Wilson, J., Putaud, J. P., Seinfeld, J. H., and Adams, P. J.: Formation and cycling of aerosols in the global troposphere, Atmospheric Environment, 34, 4215–4240, doi:10.1016/S1352-2310(00)00239-9, 2000.

Ramanathan, V., Crutzen, P. J., Lelieveld, J., Mitra, A. P., Althausen, D., Anderson, J., Andreae, M. O., Cantrell, W., Cass, G. R., Chung, C. E., Clarke, A. D., Coakley, J. A., Collins, W. D., Conant, W. C., Dulac, F., Heintzenberg, J., Heymsfield, A. J., Holben, B., Howell, S., Hudson, J., Jayaraman, A., Kiehl, J. T., Krishnamurti, T. N., Lubin, D., McFarquhar, G., Novakov, T., Ogren, J. A., Podgorny, I. A., Prather, K., Priestley, K., Prospero, J. M., Quinn, P. K., Rajeev, K., Rasch, P., Rupert, S., Sadourny, R., Satheesh, S. K., Shaw, G. E., Sheridan, P., and Valero, F. P. J.: Indian Ocean Experiment: An integrated analysis of the climate forcing and effects of the great Indo-Asian haze, Journal of Geophysical Research, 106 (D22), 28 371–28 398, doi:10.1029/2001JD900133, 2001.

Ramaswamy, V., Boucher, O., Haigh, J., Hauglustaine, D., Haywood, J., Myhre, G., Nakajima, T., Shi, G. Y., and Solomon, S.: Radiative forcing of climate change, Cambridge University Press, Cambridge, United Kingdom and New York, NY, USA, 2001.

Reddy, M. S. and Boucher, O.: A study of the global cycle of carbonaceous aerosols in the LMDZT general circulation model, Journal of Geophysical Research, 109, D14 202, doi:10.1029/2003JD004048, 2004.

Reis, S., Pinder, R. W., Zhang, M., Lijie, G., and Sutton, M. A.: Reactive nitrogen in atmospheric emission inventories, Atmospheric Chemistry and Physics, 9, 7657–7677, http://www.atmos-chem-phys.net/9/7657/2009/, 2009.

Roberts, G. C. and Nenes, A.: A continuous-flow streamwise thermal-gradient CCN chamber for atmospheric measurements, Aerosol Science & Technology, 39, 206–221, doi:10.1080/027868290913988, 2005.

Robinson, A. L., Donahue, N. M., Shrivastava, M. K., Weitkamp, E. A., Sage, A. M., Grieshop, A. P., Lane, T. E., Pierce, J. R., and Pandis, S. N.: Rethinking organic aerosols: Semivolatile emissions and photochemical aging, Science, 315, 1259–1262, doi:10.1126/science.1133061, 2007.

Robles González, C., Schaap, M., de Leeuw, G., Builtjes, P. J. H., and van Loon, M.: Spatial variation of aerosol properties over Europe derived from satellite observations and comparison with model calculations, Atmospheric Chemistry and Physics, 3, 521–533, http://www.atmos-chem-phys.net/3/521/2003/, 2003.

Sage, A. M., Weitkamp, E. A., Robinson, A. L., and Donahue, N. M.: Evolving mass spectra of the oxidized component of organic aerosol: results from aerosol mass spectrometer analyses of aged diesel emissions, Atmospheric Chemistry and Physics, 8, 1139–1152, http://www.atmos-chem-phys.net/8/1139/2008/, 2008.

Salcedo, D., Onasch, T. B., Dzepina, K., Canagaratna, M. R., Zhang, Q., Huffman, J. A., Decarlo, P. F., Jayne, J. T., Mortimer, P., Worsnop, D. R., Kolb, C. E., Johnson, K. S., Zuberi, B., Marr, L. C., Volkamer, R., Molina, L. T., Molina, M. J., Cardenas, B., Bernabé, R. M., Márquez, C., Gaffney, J. S., Marley, N. A., Laskin, A., Shutthanandan, V., Xie, Y., Brune, W., Lesher, R., Shirley, T., and Jimenez, J. L.: Characterization of ambient aerosols in Mexico City during the MCMA-2003 campaign with Aerosol Mass Spectrometry: results from the CENICA Supersite, Atmospheric Chemistry and Physics, 6, 925–946, http://www.atmos-chem-phys.net/6/925/2006/, 2006.

Schaap, M., Muller, K., and ten Brink, H. M.: Constructing the European aerosol nitrate concentration field from quality analysed data, Atmospheric Environment, 36, 1323–1335, doi:10.1016/S1352-2310(01)00556-8, 2002.

Schaap, M., van Loon, M., ten Brink, H. M., Dentener, F. J., and Builtjes, P. J. H.: Secondary inorganic aerosol simulations for Europe with special attention to nitrate, Atmospheric Chemistry and Physics, 4, 857–874, http://www.atmos-chem-phys.net/4/857/2004/, 2004.

Schnaiter, M., Linke, C., Mohler, O., Naumann, K. H., Saathoff, H., Wagner, R., Schurath, U., and Wehner, B.: Absorption amplification of black carbon internally mixed with secondary organic aerosol, Journal of Geophysical Research, 110, D19 204, doi:10.1029/2005JD006046, 2005.

Schneider, J., Weimer, S., Drewnick, F., Borrmann, S., Helas, G., Gwaze, P., Schmid, O., Andreae, M. O., and Kirchner, U.: Mass spectrometric analysis and aerodynamic properties of various types of combustion-related aerosol particles, International Journal of Mass Spectrometry, 258, 37–49, doi:10.1016/j.ijms.2006.07.008, 2006.

Schulz, M., Textor, C., Kinne, S., Balkanski, Y., Bauer, S. E., Berntsen, T. K., Berglen, T. F., Boucher, O., Dentener, F. J., Guibert, S., Isaksen, I. S. A., Iversen, T., Koch, D., Kirkevag, A., Liu, X., Montanaro, V., Myhre, G., Penner, J. E., Pitari, G., Reddy, S., Seland, O., Stier, P., and Takemura, T.: Radiative forcing by aerosols as derived from the AeroCom present-day and pre-industrial simulations, Atmospheric Chemistry and Physics, 6, 5225–5246, www.atmos-chem-phys.net/6/5225/2006/, 2006.

Schuster, G. L., Dubovik, O., Holben, B. N., and Clothiaux, E. E.: Inferring black carbon content and specific absorption from Aerosol Robotic Network (AERONET) aerosol retrievals, Journal of Geophysical Research, 110, D10S17, doi:10.1029/2004JD004548, 2005.

Seinfeld, J. H. and Pandis, S. N.: Atmospheric chemistry and physics: from air pollution to climate change, John Wiley & Sons, New York, 1998.

Shinozuka, Y., Clarke, A. D., Howell, S. G., Kapustin, V. N., McNaughton, C. S., Zhou, J., and Anderson, B. E.: Aircraft profiles of aerosol microphysics and optical properties over North America: Aerosol optical depth and its association with PM2.5 and water uptake, Journal of Geophysical Research, 112, D12, doi:10.1029/2006JD007918, 2007.

Shiraiwa, M., Kondo, Y., Moteki, N., Takegawa, N., Sahu, L. K., Takami, A., Hatakeyama, S., Yonemura, S., and Blake, D. R.: Radiative impact of mixing state of black carbon aerosol in Asian outflow, Journal of Geophysical Research, 113, D24 210, doi:10.1029/2008JD010546, 2008.

Steiner, W. E., Clowers, B. H., Fuhrer, K., Gonin, M., Matz, L. M., Siems, W. F., Schultz, A. J., and Hill, H. H.: Electrospray ionization with ambient pressure ion mobility separation and mass analysis by orthogonal time-of-flight mass spectrometry, Rapid Communications in Mass Spectrometry, 15, 2221–2226, doi:10.1002/rcm.495, 2001.

Stelson, A. and Seinfeld, J.: Relative humidity and temperature dependence of the ammonium nitrate dissociation constant, Atmospheric Environment, 16, 983–992, doi:10.1016/j.atmosenv.2007.10.063, 1982a.

Stelson, A. W. and Seinfeld, J. H.: Relative-Humidity and pH Dependence of the Vapor Pressure of Ammonium Nitrate-Nitric Acid Solutions at 25 °C, Atmospheric Environment, 16, 993–1000, doi:10.1016/0004-6981(82)90185-8, 1982b.

Stephens, M., Turner, N., and Sandberg, J.: Particle Identification by Laser-Induced Incandescence in a Solid-State Laser Cavity, Applied Optics, 42, 3726, doi:10.1364/AO.42.003726, 2003.

Strapp, J. W., Leaitch, W. R., and Liu, P. S. K.: Hydrated and Dried Aerosol-Size-Distribution Measurements from the Particle Measuring Systems FSSP-300 Probe and the Deiced PCASP-100x Probe, Journal of Atmospheric and Oceanic Technology, 9, 548–555, 1992.

Subramanian, R., Kok, G. L., Baumgardner, D., Clarke, A. D., Shinozuka, Y., Campos, T. L., Heizer, C. G., Stephens, B. B., de Foy, B., Voss, P. B., and Zaveri, R. A.: Black carbon over Mexico: the effect of atmospheric transport on mixing state, mass absorption cross-section, and BC/CO ratios, Atmospheric Chemistry and Physics, 10, 219–237, http://www.atmos-chem-phys.net/10/219/2010/, 2010.

Szidat, S., Jenk, T. M., Synal, H.-A., Kalberer, M., Wacker, L., Hajdas, I., Kasper-Giebl, A., and Baltensperger, U.: Contributions of fossil fuel, biomass-burning, and biogenic emissions to carbonaceous aerosols in Zurich as traced by ^{14}C, Journal of Geophysical Research, 111, D07 206, doi:10.1029/2005JD006590, 2006.

Szidat, S., Ruff, M., Perron, N., Wacker, L., Synal, H.-A., Hallquist, M., Shannigrahi, A. S., Yttri, K. E., Dye, C., and Simpson, D.: Fossil and non-fossil sources of organic carbon (OC) and elemental carbon (EC) in Göteborg, Sweden, Atmospheric Chemistry and Physics, 9, 1521–1535, doi:www.atmos-chem-phys.net/9/1521/2009/, 2009.

Takami, A., Miyoshi, T., Shimono, A., and Hatakeyama, S.: Chemical composition of fine aerosol measured by AMS at Fukue Island, Japan during APEX period, Atmospheric Environment, 39, 4913–4924, doi:DOI:10.1016/j.atmosenv.2005.04.038, 2005.

Takegawa, N., Miyazaki, Y., Kondo, Y., Komazaki, Y., Miyakawa, T., Jimenez, J. L., Jayne, J. T., Worsnop, D. R., Allan, J. D., and Weber, R. J.: Characterization of an Aerodyne Aerosol Mass Spectrometer (AMS): Intercomparison with other aerosol instruments, Aerosol Science & Technology, 39, 760–770, doi:10.1080/02786820500243404, 2005.

Takemura, T., Nozawa, T., Emori, S., and Nakajima, T.: Simulation of climate response to aerosol direct and indirect effects with aerosol transport-radiation model, Journal of Geophysical Research, 110, D2202, doi:10.1029/2004JD005029, 2005.

Tang, I. N.: Chemical and size effects of hygroscopic aerosols on light scattering coefficients, Journal of Geophysical Research, 101, 19 245–19 250, doi:10.1029/96JD03003, 1996.

Textor, C., Schulz, M., Guibert, S., Kinne, S., Balkanski, Y., Bauer, S. E., Berntsen, T. K., Berglen, T. F., Boucher, O., Chin, M., Dentener, F. J., Diehl, T., Easter, R. C., Feichter, H., Fillmore, D., Ghan, S., Ginoux, P., Gong, S., Kristjansson, J. E., Krol, M., Lauer, A., Lamarque, J. F., Liu, X., Montanaro, V., Myhre, G., Penner, J., Pitari, G., Reddy, S., Seland, O., Stier, P., Takemura, T., and Tie, X.: Analysis and quantification of the diversities of aerosol life cycles within AeroCom, Atmospheric Chemistry and Physics, 6, 1777–1813, doi:www.atmos-chem-phys.net/6/1777/2006/, 2006.

Topping, D., Coe, H., McFiggans, G. B., Burgess, R., Allan, J. D., Alfarra, M. R., Bower, K. N., Choularton, T. W., Decesari, S., and Facchini, M. C.: Aerosol chemical characteristics from sampling conducted on the Island of Jeju, Korea during ACE Asia, Atmospheric Environment, 38, 2111–2123, doi:10.1016/j.atmosenv.2004.01.022, 2004.

Tsigaridis, K. and Kanakidou, M.: Global modelling of secondary organic aerosol in the troposphere: a sensitivity analysis, Atmospheric Chemistry and Physics, 3, 1849–1869, http://www.atmos-chem-phys.net/3/1849/2003/, 2003.

Tsimpidi, A. P., Karydis, V. A., Zavala, M., Lei, W., Molina, L., Ulbrich, I. M., Jimenez, J. L., and Pandis, S. N.: Evaluation of the volatility basis-set approach for the simulation of organic aerosol formation in the Mexico City metropolitan area, Atmospheric Chemistry and Physics, 10, 525–546, http://www.atmos-chem-phys.net/10/525/2010/, 2010.

Ulbrich, I. M., Canagaratna, M. R., Zhang, Q., Worsnop, D. R., and Jimenez, J. L.: Interpretation of organic components from Positive Matrix Factorization of aerosol mass spectrometric data, Atmospheric Chemistry and Physics, 9, 2891–2918, doi:www.atmos-chem-phys.net/9/2891/2009/, 2009.

Volkamer, R., Jimenez, J. L., San Martini, F., Dzepina, K., Zhang, Q., Salcedo, D., Molina, L. T., Worsnop, D. R., and Molina, M. J.: Secondary organic aerosol formation from anthropogenic air pollution: Rapid and higher than expected, Geophysical Research Letters, 33, L17 811, doi:10.1029/2006GL026899, 2006.

Wandinger, U., Müller, D., Böckmann, C., Althausen, D., Matthias, V., Bösenberg, J., Weiß, V., Fiebig, M., Wendisch, M., Stohl, A., and Ansmann, A.: Optical and microphysical characterization of biomass-burning and industrial-pollution aerosols from multiwavelength lidar and aircraft measurements, Journal of Geophysical Research, 107, D21, doi:10.1029/2000JD000202, 2002.

Wang, S. C. and Flagan, R. C.: Scanning Electrical Mobility Spectrometer, Aerosol Science & Technology, 13, 230–240, doi:10.1080/02786829008959441, 1990.

Wang, W., Rood, M. J., Carrico, C. M., Covert, D. S., Quinn, P. K., and Bates, T. S.: Aerosol optical properties along the northeast coast of North America during the New England Air Quality Study - Intercontinental Transport and Chemical Transformation 2004 campaign and the influence of aerosol composition, Journal of Geophysical Research, 112, D10S23, doi:10.1029/2006JD007579, 2007.

Weber, R. J., Sullivan, A. P., Peltier, R. E., Russell, A., Yan, B., Zheng, M., de Gouw, J. A., Warneke, C., Brock, C. A., Holloway, J. S., Atlas, E. L., and Edgerton, E.: A study of secondary organic aerosol formation in the anthropogenic-influenced southeastern United States, Journal of Geophysical Research, 112, D13 302, doi: 10.1029/2007JD008408, 2007.

Weimer, S., Drewnick, F., Hogrefe, O., Schwab, J. J., Rhoads, K., Orsini, D., Canagaratna, M. R., Worsnop, D. R., and Demerjian, K. L.: Size-selective nonrefractory ambient aerosol measurements during the Particulate Matter Technology Assessment and Characterization Study - New York 2004 Winter Intensive in New York City, Journal of Geophysical Research, 111, D18 305, doi:10.1029/2006JD007215, 2006.

Welton, E. J., Campbell, J. R., Spinhirne, J. D., and Scott, V. S.: Global monitoring of clouds and aerosols using a network of micro-pulse lidar systems, vol. 4153, SPIE, Bellingham, WA, 2001.

White, W. H. and Roberts, P. T.: Nature and Origins of Visibility-Reducing Aerosols in Los Angeles Air Basin, Atmospheric Environment, 11, 803–812, doi:10.1016/0004-6981(77)90042-7, 1977.

Williams, B. J., Goldstein, A. H., Kreisberg, N. M., and Hering, S. V.: An In-Situ Instrument for Speciated Organic Composition of Atmospheric Aerosols: Thermal Desorption Aerosol GC/MS-FID (TAG), Aerosol Science & Technology, 40 (8), 627–638, doi:10.1080/02786820600754631, 2006.

Williams, B. J., Goldstein, A. H., Millet, D. B., Holzinger, R., Kreisberg, N. M., Hering, S. V., White, A. B., Worsnop, D. R., Allan, J. D., and Jimenez, J. L.: Chemical speciation of organic aerosol during the International Consortium for Atmospheric Research on Transport and Transformation 2004: Results from in situ measurements, Journal of Geophysical Research, 112, D10S26, doi:10.1029/2006JD007601, 2007.

Xiong, J. Q., Zhong, M. H., Fang, C. P., Chen, L. C., and Lippmann, M.: Influence of organic films on the hygroscopicity of ultrafine sulfuric acid aerosol, Environmental Science & Technology, 32, 3536–3541, doi:10.1021/es980019q, 1998.

Yu, H., Kaufman, Y. J., Chin, M., Feingold, G., Remer, L. A., Anderson, T. L., Balkanski, Y., Bellouin, N., Boucher, O., Christopher, S. A., DeCola, P., Kahn, R., Koch,

D., Loeb, N., Reddy, M. S., Schulz, M., Takemura, T., and Zhou, M.: A review of measurement-based assessments of the aerosol direct radiative effect and forcing, Atmospheric Chemistry and Physics, 6, 613–666, doi:www.atmos-chem-phys.net/6/613/2006/, 2006.

Zhang, Q., Alfarra, M. R., Worsnop, D. R., Allan, J. D., Coe, H., Canagaratna, M. R., and Jimenez, J. L.: Deconvolution and quantification of hydrocarbon-like and oxygenated organic aerosols based on aerosol mass spectrometry, Environmental Science & Technology, 39, 4938–4952, doi:10.1029/2007GL029979, 2005a.

Zhang, Q., Canagaratna, M. R., Jayne, J. T., Worsnop, D. R., and Jimenez, J. L.: Time- and size-resolved chemical composition of submicron particles in Pittsburgh: Implications for aerosol sources and processes, Journal of Geophysical Research, 110, doi:10.1029/2004JD004649, 2005b.

Zhang, Q., Jimenez, J. L., Canagaratna, M. R., Allan, J. D., Coe, H., Ulbrich, I., Alfarra, M. R., Takami, A., Middlebrook, A. M., Sun, Y. L., Dzepina, K., Dunlea, E. J., Docherty, K. S., Decarlo, P. F., Salcedo, D., Onasch, T., Jayne, J. T., Miyoshi, T., Shimono, A., Hatakeyama, S., Takegawa, N., Kondo, Y., Schneider, J., Drewnick, F., Borrmann, S., Weimer, S., Demerjian, K. L., Williams, P., Bower, K. N., Bahreini, R., Cottrell, L., Griffin, R. J., Rautiainen, J., Sun, J. Y., Zhang, Y. M., and Worsnop, D. R.: Ubiquity and dominance of oxygenated species in organic aerosols in anthropogenically-influenced Northern Hemisphere midlatitudes, Geophysical Research Letters, 34, L13 801, doi:10.1029/2007GL029979, 2007.

Zhang, X. F., Smith, K. A., Worsnop, D. R., Jimenez, J. L., Jayne, J. T., and Kolb, C. E.: A numerical characterization of particle beam collimation by an aerodynamic lens-nozzle system: Part I. An individual lens or nozzle, Aerosol Science & Technology, 36, 617–631, doi:10.1080/02786820252883856, 2002.

Zhang, X. F., Smith, K. A., Worsnop, D. R., Jimenez, J. L., Jayne, J. T., Kolb, C. E., Morris, J., and Davidovits, P.: Numerical characterization of particle beam collimation: Part II - Integrated aerodynamic-lens-nozzle system, Aerosol Science & Technology, 38, 619–638, doi:10.1080/02786820490479833, 2004.